Sachdev-Ye-Kitaev models and beyond:
Window into non-Fermi liquids

Debanjan Chowdhury[*]

Department of Physics, Cornell University, Ithaca, New York 14853, USA

Antoine Georges[†]

Collège de France, 11 place Marcelin Berthelot, 75005 Paris, France,
Center for Computational Quantum Physics, Flatiron Institute,
New York, New York 10010, USA,
CPHT, CNRS, Ecole Polytechnique, IP Paris, F-91128 Palaiseau, France,
and DQMP, Université de Genève, 24 quai Ernest Ansermet, CH-1211 Genève, Suisse

Olivier Parcollet[‡]

Center for Computational Quantum Physics, Flatiron Institute,
New York, New York, 10010, USA
and Université Paris–Saclay, CNRS, CEA, Institut de Physique Théorique,
91191 Gif-sur-Yvette, France

Subir Sachdev[§]

Department of Physics, Harvard University, Cambridge, Massachusetts 02138, USA
and School of Natural Sciences, Institute for Advanced Study,
Princeton, New Jersey 08540, USA

This is a review of the Sachdev-Ye-Kitaev (SYK) model of compressible quantum many-body systems without quasiparticle excitations, and its connections to various theoretical studies of non-Fermi liquids in condensed matter physics. The review is placed in the context of numerous experimental observations on correlated electron materials. Strong correlations in metals are often associated with their proximity to a Mott transition to an insulator created by the local Coulomb repulsion between the electrons. The phase diagrams of a number of models of such a local electronic correlation are explored, employing a dynamical mean-field theory in the presence of random spin exchange interactions. Numerical analyses and analytical solutions, using renormalization group methods and expansions in large spin degeneracy, lead to critical regions that display SYK physics. The models studied include the single-band Hubbard model, the *t-J* model, and the two-band Kondo-Heisenberg model in the presence of random spin exchange interactions. Also examined are non-Fermi liquids obtained by considering each SYK model with random four-fermion interactions to be a multiorbital atom, with the SYK atoms arranged in an infinite lattice. Connections are made to theories of sharp Fermi surfaces without any low-energy quasiparticles in the absence of spatial disorder, obtained by coupling a Fermi liquid to a gapless boson; a systematic large-N theory of such a critical Fermi surface, with SYK characteristics, is obtained by averaging over an ensemble of theories with random boson-fermion couplings. Finally, an overview of the links between the SYK model and quantum gravity is presented, and the review ends with an outlook on open questions.

CONTENTS

[*]debanjanchowdhury@cornell.edu
[†]ageorges@flatironinstitute.org
[‡]oparcollet@flatironinstitute.org
[§]sachdev@g.harvard.edu

I. INTRODUCTION

The discovery of high-temperature superconductivity in the cuprate compounds in 1986 posed numerous challenges to quantum theories of electronic matter. The greatest mystery, as became evident early on, was the unusual metallic state of these materials above the superconducting critical temperature. This "strange metal," as it has since come to be called, displayed unusual temperature and frequency dependencies in its properties, which indicated that the strange metal was an entangled many-body quantum state without "quasiparticles." Almost all of quantum condensed matter physics is built on the idea of quasiparticles: this allows us to account for the Coulomb interactions between electrons by assuming that their main effect is to renormalize each electron with a cloud of electron-hole pairs, after which we can treat each electron as a nearly independent quasiparticle. This decomposition of the excitations of a many-body system into a composite of simple quasiparticle excitations is an assumption so deeply engrained in the theoretical framework that it is usually left unstated.

The aim of this review is to present some recent advances in describing quantum phases of matter that do not host any quasiparticle excitations. Much has been understood theoretically in recent years about the properties of a solvable model of a many-body quantum system without quasiparticle excitations in the regime of strong interactions: the Sachdev-Ye-Kitaev (SYK) model. We discuss some of these advances in this review, along with a discussion of the application of these advances to more realistic models of quantum matter without quasiparticles.

The idea of employing a quasiparticle description of a macroscopic many-particle system can be traced back to Boltzmann (1872). Boltzmann was thinking of a *dilute classical* gas of molecules, as that found in the atmosphere. In 1872, he introduced an equation that described the time evolution of the observable properties of a dilute gas in response to external forces. He applied Newton's laws of motion to individual molecules and obtained an equation for $f_{\boldsymbol{p}}$, the density of particles with momentum $\boldsymbol{p}$. In a spatially uniform situation, Boltzmann's equation takes the following form:

$$\frac{\partial f_{\boldsymbol{p}}}{\partial t} + \boldsymbol{F} \cdot \boldsymbol{\nabla}_{\boldsymbol{p}} f_{\boldsymbol{p}} = \mathcal{C}[f], \qquad (1.1)$$

where t is the time and $\boldsymbol{F}$ is the external force. The left-hand side of Eq. (1.1) is simply a restatement of Newton's laws for

individual molecules. Boltzmann's innovation was the right-hand side, which describes collisions between the molecules. Boltzmann introduced the concept of "molecular chaos," which asserted that in a sufficiently dilute gas successive collisions were statistically independent. With this assumption, Boltzmann showed that

$$\mathcal{C}[f] \propto - \int_{\boldsymbol{p}_{1,2,3}} \cdots [f_{\boldsymbol{p}} f_{\boldsymbol{p}_1} - f_{\boldsymbol{p}_2} f_{\boldsymbol{p}_3}] \qquad (1.2)$$

for molecules with momenta $\boldsymbol{p}, \boldsymbol{p}_1$ colliding to momenta $\boldsymbol{p}_2, \boldsymbol{p}_3$. The statistical independence of collisions is reflected in the products of the densities in Eq. (1.2), and the second term represents the time-reversed collision.

The notable fact is that Boltzmann's equation also applies, with relatively minor modifications, to the *dense quantum* gas of electrons found in ordinary metals, as was argued in Landau's Fermi-liquid theory (Landau, 1957). Individual electrons move in Bloch waves (Bloch, 1929) characterized by a crystal momentum $\boldsymbol{p}$. Now collisions become rare because of Pauli's exclusion principle, and the statistical independence of collisions is assumed to continue to apply. The main modification is that the collision term in Eq. (1.2) is replaced by

$$\mathcal{C}[f] \propto - \int_{\boldsymbol{p}_{1,2,3}} \cdots [f_{\boldsymbol{p}} f_{\boldsymbol{p}_1} (1 - f_{\boldsymbol{p}_2})(1 - f_{\boldsymbol{p}_3})$$
$$- f_{\boldsymbol{p}_2} f_{\boldsymbol{p}_3} (1 - f_{\boldsymbol{p}})(1 - f_{\boldsymbol{p}_1})], \qquad (1.3)$$

where the additional $(1 - f)$ factors ensure that the final states of collisions are not occupied. Now the $f_{\boldsymbol{p}}$ measure the distribution of electronic quasiparticles, and a cloud of particle-hole pairs around each electron renormalizes only the microscopic scattering cross section. Such a quantum Boltzmann equation is the foundation of the quasiparticle theory of the electron gas in metals, superconductors, semiconductors, and insulators, and indeed almost all of condensed matter physics before the 1980s.

Our interest here is in quantum materials in which the description in terms of a quasiparticle distribution function $f_{\boldsymbol{p}}$ obeying a quantum Boltzmann equation breaks down. The time between collisions becomes so short that the quantum interference between successive collisions cannot be ignored, and the collisions cannot be treated as statistically independent. Landau's Fermi-liquid theory has the feature that the quasiparticles are essentially dressed electrons, but there are situations in which the quasiparticles are emergent excitations of the many-body system with no simple relation to the bare electrons; such systems can be treated by extensions of Landau's approach, and these will also not be of interest to us.

Given a quantum many-body system, how do we ascertain the absence of low-energy quasiparticles in any basis and the associated universal diagnostics (if any)? The simplest diagnostic we might consider for detecting the presence of electronic quasiparticles is via poles in the single-particle Green's function (sharp peaks in the spectral function). However, the existence of a broad electron spectral function

is, by itself, not sufficient to conclude that there are no quasiparticle excitations. After all, interacting electrons in one dimension have broad electron spectral functions (Giamarchi, 2003). This is understood in Luttinger-liquid theory using a description in terms of a different set of quasiparticles: linearly dispersing bosons associated with collective excitations. The electron operator is an exponential of the boson operator, and this leads to the broad spectral functions. The bosonic quasiparticles describe all the many-body eigenstates, but the electron operator has a complicated form in this representation. Similarly, while the electron spectral function in certain fractional quantum Hall phases and paramagnetic Mott insulators (Broholm *et al.*, 2020) can be complicated, at low energies they might host *emergent* quasiparticle excitations that are well defined but impossible to diagnose using a two-point spectral function, as the latter quantity is not even a gauge-invariant observable. These examples illustrate that the electron spectral function is not a universal diagnostic for detecting quasiparticles; it is useful when the overlap between the wave function of the low-energy quasiparticle and the physical electron is nonzero [as in a Landau-Fermi liquid (Abrikosov, Gorkov, and Dzyaloshinskii, 1963)]. On the other hand, when the two are orthogonal, as in the previously highlighted examples, the diagnostic fails and the spectral function is ill equipped to analyze the fate of the quasiparticles. A further weakness in the spectral function diagnostic is apparent when we consider disordered systems (such as even a disordered Fermi liquid). Electronic quasiparticles are well defined in such systems (Abrahams *et al.*, 1981), but they are not apparent in electronic spectral functions unless the spatial form of the quasiparticle wave function is already known: they are not plane waves, as in Fermi liquids in clean crystals.

These considerations make it clear that a system with quasiparticle excitations is best characterized by an extension of the original Landau perspective (Landau, 1957): the low-energy states of a many-body system can be decomposed into composites of single-quasiparticle states, and the energies of these states are functionals of the densities of individual quasiparticle states. In other words, quasiparticles are *additive* excitations of a many-body system. Analyzing the spectrum of low-lying eigenstates of a many-body quantum system for a large but finite volume therefore provides a useful diagnostic of the validity of a quasiparticle description or of its failure. We use this "spectral fingerprint" in several places in this review; see Sec. IV.B.

With this perspective, in a many-body quantum system without quasiparticle excitations it is not possible to decompose the low-lying states into any basis of quasiparticle excitations. This is, however, a practical definition only when the full low-lying spectrum is available. Furthermore, it may be possible to exclude a candidate quasiparticle basis, but it is often difficult to exclude them all. For a more positive and practical definition, we consider the approach of a quantum many-body system to local thermal equilibrium at a temperature T after the action of a local perturbation. In a system with quasiparticle excitations such as a Fermi liquid, the solution of the quantum Boltzmann equation shows that this will happen in a time that is at least as long as $\sim 1/T^2$ as $T \to 0$. This long span of time is required for individual quasiparticles to collide with each other. In a system

without quasiparticles, we expect the length of time to be much shorter. But how short can the local equilibration time get as $T \to 0$? Studies of numerous model systems without quasiparticle excitations, some of which are described in this review, show that the time is never shorter than a time of the order of the "Planckian time" $\hbar/k_B T$, i.e., the minimum time associated with an energy of the order of $k_B T$ according to the Heisenberg uncertainty principle. On the other hand, it is clear from a study of systems with quasiparticles that such systems can never equilibrate as quickly as the Planckian time as long as quasiparticles are well defined. Thus, we reach the proposal that many-body quantum systems without quasiparticles are those that locally equilibrate in a time of the order of $\hbar/k_B T$, and no system can equilibrate any faster (Sachdev, 1999; Hartnoll, Lucas, and Sachdev, 2016).

Our focus in this review is primarily on metallic quantum many-body systems without quasiparticle excitations, i.e., non-Fermi liquids. Section II presents a general perspective on non-Fermi liquids, with a summary of some of their experimental signatures and an overview of some theoretical ideas and their relationship to the SYK models presented in this review. An outline of the perspective of this review appears in Sec. II.C. Readers wanting to focus on the SYK viewpoint can skip directly ahead to Sec. II.C and then to Sec. IV. In Sec. III, we qualitatively discuss the properties of "bad metals" and "Planckian metals," two forms of unconventional transport often encountered in non-Fermi liquids. In Sec. IV, we first review the random-matrix model for noninteracting fermions that realizes a Fermi liquid with quasiparticles. The SYK model system is introduced and reviewed in Sec. V. The insights gained from this study are then applied to several extensions thereof in Secs. VI, VII, VIII, X, and XI, with an eye toward capturing certain universal phenomenological aspects of quantum materials with strong electronic correlations. There are also noteworthy connections between the SYK model and quantum theories of Einstein gravity in black holes, and these are reviewed in Sec. XII. In recent years, precise diagnostics of a class of nonquasiparticle systems have appeared upon the introduction of ideas from quantum chaos and quantum gravity that are discussed in Sec. XII.E.

II. TYPOLOGY OF NON-FERMI LIQUIDS

Numerous strongly correlated systems, such as materials with partially filled d- or f-shell orbitals and, more recently, in moiré systems, display a phenomenology that, while metallic, can drastically deviate from the predictions of the standard Fermi-liquid (FL) theory of metals. These *non-Fermi liquids* (NFLs) raise a series of central challenges in condensed matter physics, both experimentally and theoretically. As they are defined by what they are not, they constitute a rich and diverse family of systems. Conceptually, they are not characterized by a few universal experimental traits, unlike Fermi liquids. In practice, they cannot always be clearly identified using simple response functions, unlike other familiar phases of quantum matter with or without spontaneously broken symmetries (such as superconductors, antiferromagnets, and quantum Hall insulators).

The family of SYK models discussed in this review constitute a solvable theoretical route to study a class of

NFL behavior, as they have some of the major characteristics of NFL metals. In particular, we discuss their relation to Planckian metals, characterized by a linear dependence of resistivity with temperature and a characteristic scattering rate $\sim k_B T/\hbar$. To set the stage for this review, we therefore start by discussing a selection of the most important NFL behavior encountered experimentally (Sec. II.A). We then introduce the main theoretical routes that have been proposed to characterize and explain them (Sec. II.B), along with their connections to the aspects of SYK physics discussed in later sections. Finally, in Sec. II.C, we present the general perspective of this review and provide an outline. Readers wanting to go directly to the theoretical models of this paper can skip ahead to Sec. II.C.

A. Experimental signatures of non-Fermi liquids

We start by discussing a few experimental signatures of NFLs, based on a variety of spectroscopic and transport measurements. Since dc transport can be difficult to interpret, it is important not to rely only on it exclusively to characterize NFL behavior. The various signatures include the following.

- "Short" single-particle lifetimes for excitations near the Fermi surface, as deduced from spectroscopic measurements such as angle-resolved photoemission spectroscopy (ARPES) (Damascelli, Hussain, and Shen, 2003). In FL metals, the inverse quasiparticle lifetime (i.e., the scattering rate) scales as $\Gamma_{\mathrm{sp}} \equiv g^2 W (k_B T/E_F^*)^2$, where g is a dimensionless electron-electron interaction strength, W is a bare electronic energy scale (bandwidth or hopping), and E_F^* is a characteristic energy scale below which coherent long-lived quasiparticle excitations emerge. E_F^* can be viewed as a degeneracy scale for the Fermi gas of quasiparticles. In contrast, a strong departure from the previously mentioned form that persists over a large range of energy scales is an indication of breakdown of FL behavior. In a number of experimental systems that display NFL behavior, $\Gamma_{\mathrm{sp}}(\omega, T) \sim \max(\omega, k_B T/\hbar)$ (Valla *et al.*, 1999; Wang *et al.*, 2004).

- A power-law temperature dependence of the dc resistivity deviating from the expected FL form $\sim T^2$ (due to umklapp scattering) over a broad range of temperatures, without any signs of crossovers or saturation. One of the most commonly reported behaviors is $\rho = \rho_0 + AT$, over an extended range $T_{\mathrm{coh}} < T < T_{\mathrm{uv}}$ (Hartnoll and Mac-Kenzie, 2021); see Sec. III.B. However, other power laws $\Delta\rho (\equiv \rho - \rho_0) \sim T^\alpha$ have also been observed (Allen *et al.*, 1996; Lee *et al.*, 2002). Identifying a material as a NFL on the basis of an observation of T-linear resistivity above T_{coh} requires special care since electron-phonon scattering in conventional metals leads to a trivial example of the same (Ziman, 1960). However, T-linear resistivity presents an indication of behavior at odds with the Boltzmann theory of FL transport in examples where T_{coh} is significantly low compared to the Debye (or Bloch-Grüneissen) scale, the linearity persists without any crossovers across multiple phonon energy scales, and there are no obvious collective modes to which a similar phonon-type argument can be directly applied. We return to a discussion of the physical significance of

T_{coh} in subsequent sections. Note that in some materials, such as optimally doped cuprates (Giraldo-Gallo *et al.*, 2018), certain heavy-fermion materials (Stewart, 2001) and twisted bilayer graphene (Jaoui *et al.*, 2022), this behavior persists down to a low $T_{\mathrm{coh}} \to 0$.

- Bad-metallic behavior (Emery and Kivelson, 1995; Gunnarsson, Calandra, and Han, 2003; Hussey, Takenaka, and Takagi, 2004) with a resistivity that is an increasing function of temperature with $\rho \gtrsim \rho_Q$ ($\rho_Q = h/e^2[a]^{d-2}$, where a is a microscopic length scale and $h/e^2 \simeq 25.8 \ \mathrm{k}\Omega$ is the quantum of resistance) is also indicative of NFL behavior. A majority of the systems of interest to us are quasi two dimensional (with appreciable transport anisotropy in the a-b plane versus along the c axis), and it is thus useful to quote the results for the sheet resistivities in units of h/e^2. While bad metals can arise at high temperatures for simple reasons, the key puzzle is often related to their smooth evolution into a low-temperature regime without any characteristic crossovers, which defies Fermi-liquid behavior. In the literature, the expression *bad*, or *strange*, is often used to refer to certain NFL metals. In this review, we reserve the term bad metals to designate systems in which the resistivity is larger than the Mott-Ioffe-Regel value and strange metals to indicate materials with a resistivity smaller than this value but displaying a set of behavior incompatible with the quasiparticle-based framework of Fermi-liquid theory. We discuss bad-metallic transport in the high-temperature regime in more detail in Sec. III.A.

- An anomalous power-law dependence of the optical conductivity $\sigma(\omega) \sim 1/\omega^{\gamma}$ over an extended range of frequencies, thus differing from conventional Drude behavior. This is observed in cuprates (Schlesinger *et al.*, 1990; El Azrak *et al.*, 1994; Baraduc, Azrak, and Bontemps, 1996; van der Marel *et al.*, 2003; Hwang, Timusk, and Gu, 2007) and has also been reported in other materials (Kostic *et al.*, 1998; Schwartz *et al.*, 1998; Dodge *et al.*, 2000; Mena *et al.*, 2003; Limelette *et al.*, 2013; Phanindra, Agarwal, and Rana, 2018). This is also often accompanied by ω/T scaling as a function of temperature, i.e., $\sigma(\omega, T) \sim 1/\omega^{\gamma} F(\omega/T)$ (Lee *et al.*, 2002; van der Marel *et al.*, 2003, 2006; Limelette *et al.*, 2013; Michon *et al.*, 2022; van Heumen *et al.*, 2022). At higher energy or temperature, a transfer of spectral weight over energy scales larger (sometimes much larger) than $k_B T$ are also typically observed as temperature is varied (Georges *et al.*, 1996; Rozenberg, Kotliar, and Kajueter, 1996; Basov *et al.*, 2011). A simultaneous analysis of both dc transport and optical conductivity (or other frequency-dependent response functions) is often crucial to reaching an understanding of the NFL phenomenology in a specific material.

- An unconventional charge-density response exemplified by a featureless continuum extending over a broad range of energy scales, as measured in Raman scattering experiments (Bozovic *et al.*, 1987; Slakey *et al.*, 1991). Recent measurements using momentum-resolved electron energy-loss spectroscopy have further revealed a featureless two-particle continuum and an overdamped

plasmon excitation (Mitrano *et al.*, 2018; Husain *et al.*, 2019, 2020), which is at odds with the expectations for a Fermi-liquid metal.

B. Theoretical models of non-Fermi liquids

Classifying insulating *gapped* phases of matter in terms of their symmetry and topological properties using the lens of many-body entanglement has been a highly successful venture (Wen, 2017). On the other hand, classifying *gapless* phases of matter, and non-Fermi liquids, in particular, remains an outstanding challenge. We do not attempt to embark on such an endeavor here. This review focuses on a few distinct classes of NFLs without quasiparticles that can be described using various generalizations of the solvable SYK model. We find it useful nevertheless to first provide a broader overview of some of the theoretical frameworks and routes that lead to examples of non-Fermi liquids in clean crystalline systems without disorder.

- A class of models involves the quantum-critical fluctuations of a bosonic degree of freedom coupled to an electronic Fermi surface (Löhneysen *et al.*, 2007). These fluctuations are associated with the order parameter corresponding to the spontaneous breaking of a point-group ("nematic"), translational (spin-density- or charge-density-wave), or spin-rotation (ferromagnetism) symmetry. In the absence of any other instability, such as pairing, the resulting ground state is a NFL that controls the properties of the system in a range of temperatures above the critical point. The nature of the low-energy excitations near the Fermi surface differs depending on whether the order parameter carries zero or a finite center-of-mass momentum $\boldsymbol{Q}$. This framework of an electronic Fermi surface coupled to the low-energy fluctuations of a Landau order parameter often goes under the name of Hertz-Millis-Moriya criticality (Moriya, 1985; Millis, 1993; Sachdev, 1999). A critical boson with $\boldsymbol{Q} = 0$ (nematic order) can destroy electronic quasiparticles around the entire Fermi surface [Fig. 1(a)]. At the critical point, the resulting state realizes a classic example of a critical Fermi surface (Metlitski and Sachdev, 2010; Mross *et al.*, 2010) and provides an ideal setting for studying the interplay of NFL physics and superconductivity (Metlitski *et al.*, 2015; Wang *et al.*, 2016; Berg *et al.*, 2019). The low-energy field theory for such metallic criticality in $2 + 1$ dimensions presents a significant theoretical challenge (Lee, 2009). The insights provided by the solvable SYK model into such systems are reviewed in Sec. XI. A critical boson with $\boldsymbol{Q} \neq 0$ (density-wave order) destroys electronic quasiparticles near only certain special points on the Fermi surface ("hot spots") as it gets reconstructed into pockets, while much of the Fermi surface continues to host long-lived quasiparticles. See Lee (2018) and Berg *et al.* (2019) for some recent complementary theoretical progress in both classes of such order-parameter-based metallic criticality.

- A different form of quantum criticality leading to NFL behavior is associated with the disappearance of entire electronic Fermi surfaces (Coleman *et al.*, 2001). Prominent examples of such criticality include continuous metal-insulator transitions between a FL metal and a paramagnetic Mott insulator at fixed density [Fig. 1(b)] (Florens and Georges, 2004; Senthil, 2008a, 2008b); see also Kotliar (1995) and a Kondo-breakdown transition in a heavy Fermi liquid to a fractionalized FL [Fig. 1(c)] (Schröder *et al.*, 2000; Coleman *et al.*, 2001; Si *et al.*, 2001, 2003; Burdin, Grempel, and Georges, 2002; Senthil, Sachdev, and Vojta, 2003; Senthil, Vojta, and Sachdev, 2004; Paul, Pépin, and Norman, 2007, 2008, 2013). The critical point across both of these transitions also hosts an electronic critical Fermi surface without low-energy
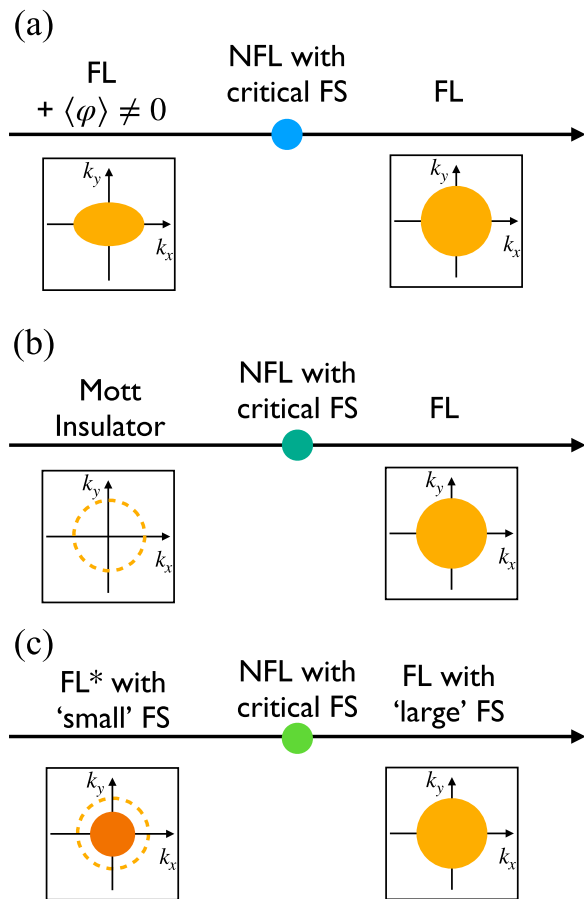

(a) FL + $\langle \varphi \rangle \neq 0$ — NFL with critical FS — FL

(b) Mott Insulator — NFL with critical FS — FL

(c) FL* with 'small' FS — NFL with critical FS — FL with 'large' FS

FIG. 1. (a) NFL obtained by coupling a critical boson (nematic order with $Q = 0$) to an electronic Fermi surface. (b) Bandwidth-tuned metal to paramagnetic Mott insulator transition. The Mott insulator hosts a neutral Fermi surface (dashed circle) of fractionalized degrees of freedom coupled to an emergent gauge field. (c) A Fermi volume changing transition between two distinct metals across a "Kondo breakdown" quantum-critical point. The quantum-critical point hosts a critical Fermi surface of electrons in all the examples. The Mott insulator and the FL* phases host a critical Fermi surface of "spinons" in (b) and (c), respectively.

Landau quasiparticles (Senthil, Vojta, and Sachdev, 2004; Senthil, 2008a). All currently known low-energy theories for describing such continuous transitions involve fractionalized degrees of freedom coupled to emergent dynamical gauge fields. Most theoretical descriptions of these continuous transitions have a remnant Fermi surface of the fractionalized degrees of freedom (and not of electrons) coupled to dynamical gauge fields on one side of the critical point; we continue to refer to these as critical Fermi surfaces in this review. Continuous metal-insulator transitions without any remnant Fermi surface of even fractionalized degrees of freedom provide examples of a new form of "deconfined" metallic quantum criticality; see Zhang and Sachdev (2020) and Zou and Chowdhury (2020) for recent progress in describing such transitions. In particular, all of these transitions fall beyond the previously described order-parameter-based Hertz-Millis-Moriya framework. Insights from a SY model with random-exchange interactions in the presence of a uniform Kondo exchange for two-orbital models are applied to the study of a special case of such abrupt Fermi volume changing transitions in Sec. VIII.

- In contrast to the previous examples that arise at certain $T = 0$ quantum-critical points, a NFL can arise as a stable phase at zero temperature. One of the most well-known examples of such NFL behavior is found in a two-dimensional electron gas at a high magnetic field at a filling factor $\nu = 1/2$. The metallic NFL state is compressible and otherwise known as the composite Fermi liquid (CFL); it hosts a sharp Fermi surface on which the low-energy excitations are not electrons but instead composite fermions (CF) (Jain, 2007). The low-energy theory for the CFL is described in terms of a CF Fermi sea coupled to a dynamical gauge field (Halperin, Lee, and Read, 1993; Son, 2015). Other examples of NFL phases at $T = 0$ have also been observed in numerical studies of lattice models (Jiang *et al.*, 2013).

  We note that there are *insulating* (and *incompressible*) phases of matter that are expected to arise in a class of paramagnetic Mott insulators, where fractionalized degrees of freedom (such as spinons) form a Fermi surface and are coupled minimally to an emergent gauge field (Lee, 1989; Altshuler, Ioffe, and Millis, 1994). The low-energy field theory for such phases shares similarities with the theory for the CFLs, but there are important conceptual differences. A theoretical description of the low-energy field theory for the Fermi surface of spinons coupled to a dynamical gauge field suffers from the same problem as was noted earlier (Lee, 2009); the solvable SYK model of Sec. XI offers a controlled complementary understanding of this problem.

- For sufficiently strong interactions and over a range of intermediate temperatures, it is possible that NFL behavior emerges generically and is not controlled

by the proximity to a quantum-critical point (or phase). Moreover, the NFL regime appears only as a crossover regime at intermediate temperatures, while the ground state is a conventional phase (a FL, a superconductor, etc.). These NFL regimes can be described as "infrared (IR) incomplete," unlike the examples described earlier, which are, in principle, controlled by $T = 0$ fixed points. Some prominent and well understood examples of such IR-incomplete behavior include the classic electron-phonon system above the Debye temperature (Ziman, 1960), spin-incoherent Luttinger liquids (Fiete, 2007), generic lattice models with a finite bandwidth at high temperatures (Mukerjee, Oganesyan, and Huse, 2006) [see also Lindner and Auerbach (2010)], and certain holographic non-Fermi liquids (Faulkner, Liu *et al.*, 2011; Liu, McGreevy, and Vegh, 2011). A number of theoretical examples of such IR-incomplete behavior are accompanied by an extensive residual entropy that is obtained from an extrapolation to the limit of $T \to 0$; the excess entropy is then relieved below the crossover to the conventional phase. Our treatment of such systems appears in the discussion on lattice models of one- and two-band models of SYK atoms in Sec. X.

C. Perspective of this review

An important idea in our approach is that it is possible to make progress on many intractable problems in the theory of non-Fermi liquids by considering models with random interactions. At first sight, this appears to be counterintuitive because spatial randomness introduces new phenomena associated with localization that are not of interest to us here. However, most of the models considered here live on fully connected lattices on which disorder-induced localization cannot take place. Indeed, the local electronic properties are strongly self-averaging, and the observable properties of a single sample with disorder are indistinguishable from the average of an ensemble of samples in the infinite-volume limit. Furthermore, one could argue that the strong incoherence associated with the absence of quasiparticles also removes localization effects that require quantum coherence and interference processes (Lee and Ramakrishnan, 1985). A non-Fermi-liquid system without disorder thermalizes in the shortest possible time, and this implies chaotic behavior in which the memory of the initial conditions is rapidly lost. Consequently, it is possible to view averaging over disorder as a technical tool that allows access to the collective properties of a system with strong many-body quantum chaos.

We can also restrict the disorder exclusively to a flavor space, and thus study non-Fermi liquids with full translational symmetry, as we do in Secs. X and XI. Here the idea is that, after some renormalization group flow, a large set of theories flow to the same universal low-energy behavior. And we find that it is easier to access the universal theory by averaging over a suitable set of microscopic couplings.

Indeed, the idea of using an average over random systems to understand quantum chaos has long been present in the theory

of single-particle quantum chaos. We discuss this in Sec. IV, where we review the random-matrix theory of noninteracting fermions: this has been a successful model of the quantum theory of particles whose classical dynamics is chaotic.

Section V introduces the SYK model of fermions with random two-body interactions with N single-particle states. We present the exact solution of the many-body system without quasiparticle excitations obtained in the $N \to \infty$ limit. Much is also understood about the finite N fluctuations, including some results with a noteworthy accuracy of $\exp(-N)$. This fluctuation theory relies on a mapping to a low-energy effective theory of time reparametrization fluctuations (which is also the theory of a "boundary graviton" in the quantum theory of certain black holes of Einstein-Maxwell theory of gravity and electromagnetism, as discussed in Sec. XII).

Section VI turns to a quantum generalization of the thoroughly studied Sherrington-Kirkpatrick model of a classical spin glass with Ising spins $\sigma_i = \pm 1$ ($i = 1, \ldots, N \to \infty$) with random and all-to-all interactions J_{ij} with zero mean. The quantum model replaces σ_i with quantum $S = 1/2$ SU(2) spins S_i, which have random Heisenberg interactions J_{ij}. We review a variety of studies of this model here involving numerical exact diagonalization, renormalization group, and large-M expansions of models with SU(M) spin symmetry. These results show that the $S = 1/2$ SU(2) model has spin-glass order similar to that of the classical Sherrington-Kirkpatrick model. However, the spin-glass order parameter is small, and for a wide range of intermediate frequencies the dynamical spectrum of the SU(2) model matches that of the SYK model (obtained here in the large-M limit).

Sections VII and VIII discuss the familiar and intensively studied single-band Hubbard and two-band Kondo-Heisenberg models, respectively, of strong electronic correlations. We consider models with an additional random exchange interaction J_{ij} that can be used to justify an extended dynamic mean-field theory with self-consistency conditions on both the single-electron and spin correlators. Such theories also apply to models with nonrandom single-particle dispersion, but it is useful to focus on a simplified limit with a random and all-to-all single-electron hopping t_{ij}. We use methods similar to those in Sec. VI to show that these models exhibit quantum phase transitions between two metals: a metallic spin glass and a Fermi liquid. In the quantum-critical region, we find a non-Fermi liquid with SYK-like correlations. Section IX presents an overview of recent advances in the numerical methods employed for the analyses in Secs. VII and VIII.

Section X presents a different approach toward generalizing SYK models to lattice systems. We consider a lattice of "SYK atoms," where each lattice site has N orbitals and the intra-atomic electronic interactions are assumed to have the random SYK form. We consider the case where all SYK atoms are identical (so that there is lattice translational symmetry) versus the case where the interactions are different random instances on each site, and then comment on their similarities and differences. These models can be used to realize non-Fermi liquids with a SYK character and no singular spatial correlations, but with a bad-metallic resistivity. Generalizations of these models to include additional orbitals, in the spirit of

two-band models of heavy-fermion materials, lead to strange metals with T-linear resistivity, critical Fermi surfaces, and a marginal Fermi-liquid behavior (Varma *et al.*, 1989).

Section XI returns to models of Fermi surfaces coupled to critical bosons, which we introduced in Sec. II.B. We describe how a systematic large-N theory of a class of non-Fermi liquids can be obtained by applying SYK-like approaches to these well-studied models. We generalize the models to $\sim N$ flavors of fermions and bosons, with a random Yukawa coupling between the fermions and bosons. The randomness can be independent of space so that the models have translational symmetry.

Section XII explores the connections between the SYK model and the quantum theory of black holes. We highlight some recent developments, particularly those that we think are of interest to condensed matter physicists. We conclude with an outlook on open questions in Sec. XIII.

III. BAD METALS AND PLANCKIAN METALS

As previously emphasized, a prime signature of NFL behavior is unconventional transport. In this section, we provide a qualitative discussion contrasting high-temperature bad-metallic behavior with "Planckian transport" persisting down to low-T. This review focuses mostly on solvable models aiming at providing insight into the latter.

A. Bad metals: Mott-Ioffe-Regel criterion and a high-temperature perspective

In considering transport in semiconductors, Ioffe and Regel (1960) and Mott (1974) argued that metallic transport in the conventional sense requires that the mean free path ℓ of quasiparticles should be longer than the typical lattice spacing a. For a quasi-two-dimensional conductor with a single parabolic band and a simple cylindrical Fermi surface of radius k_F, the Drude expression for conductivity $\sigma = ne^2\tau/m$ can be rewritten as

$$\sigma = \frac{e^2}{h}\frac{1}{c}k_F\ell, \qquad (3.1)$$

where c is the interlayer distance. Hence, when the sheet conductance becomes smaller than the conductance quantum e^2/h, the Mott-Ioffe-Regel (MIR) criterion is violated, which suggests that a Drude-Boltzmann description of transport is no longer valid. The criterion itself is not a quantitatively precise one, depending on whether ℓ is compared to a or the Fermi wavelength $\lambda_F = 2\pi/k_F$.

"Good" metals typically have resistivities that are much smaller than ρ_Q and, correspondingly, $\ell \gg a$. In the context of unconventional metallic transport, the physical significance of the MIR criterion has been a confusing issue for quite a while, as reviewed by Gunnarsson, Calandra, and Han (2003) and Hussey, Takenaka, and Takagi (2004). Some materials, such as A15 compounds (Fisk and Webb, 1976), display a resistivity saturation as the MIR value is approached, leading to the speculation that resistivity saturation should perhaps be a general fact. Note that there is no fundamental theoretical understanding for resistivity

saturation in metals.[1] Moreover, a wealth of experimental data collected on materials with strong electronic correlations, most notably transition-metal oxides, came in to contradict the notion of resistivity saturation. Indeed, resistivity in many such materials can increase significantly above the MIR value without any trend toward saturation or even any characteristic feature signaling this crossover in the temperature dependence of ρ. The term bad metal was coined to highlight this behavior (Emery and Kivelson, 1995). A material displaying bad-metallic behavior at a high temperature can become a good Fermi liquid at a low temperature with long-lived coherent quasiparticles, with a good example being Sr_2RuO_4 (Tyler *et al.*, 1998). Low-carrier density materials such as doped $SrTiO_3$ also have bad-metallic behavior at high T (Collignon *et al.*, 2020) while displaying quantum oscillations and coherent transport at low T (Collignon *et al.*, 2019).

Recent studies (Deng *et al.*, 2013, 2014) have considerably clarified the physical significance of the MIR criterion. It is now understood that the temperature T_{MIR} at which the resistivity becomes of the order of the MIR value corresponds to the complete disappearance of quasiparticles. Typically, in systems which become FL at low T, the scale T_F^* below which long-lived coherent Landau quasiparticles with $\Gamma_{sp} \sim T^2$ are observed is significantly smaller than T_{MIR}. In Sr_2RuO_4, $T_F^* \simeq 30$ K, while T_{MIR} is several hundred kelvins. Studies of the doped Hubbard model in the dynamical mean-field theory (DMFT) framework documented this interpretation in a precise manner. There T_{MIR} was found to be of the order of the Brinkman-Rice scale $\sim pt$ (with p the doping level and t the typical hopping or bare Fermi energy), while a much lower scale is associated with T_F^*. For a renormalization group interpretation of that scale, see Held, Peters, and Toschi (2013). It was shown that "resilient quasiparticles" exist in the intermediate regime $T_F^* < T < T_{MIR}$: the spectral function displays a broadened but well-defined peak and transport can still be described in terms of these excitations, which is reminiscent of the notions introduced (Prange and Kadanoff, 1964) for electron-phonon scattering. It was also shown (Deng *et al.*, 2014) that the quasiparticle lifetime follows a $1/T^2$ law up to a higher temperature than the transport lifetime itself, and hence than the temperature at which the resistivity deviates from T^2.

Considerable insight in interpreting transport results can be gained by simultaneously considering spectroscopy experiments, most notably optical conductivity, and the corresponding transfers of spectral weight upon changing the temperature. In studies of the doped Hubbard model (Deng *et al.*, 2013), it was shown that these transfers are limited to the low-energy region between the Drude peak and the midinfrared range for $T_F^* < T < T_{MIR}$, while the MIR crossover is signaled by spectral weight transfers over a much larger energy range, leading to a broad featureless optical conductivity for $T > T_{MIR}$.

---

[1]Recent work has analyzed resistivity saturation, and a lack thereof, in solvable models of electrons coupled to a large number of phonon modes (Werman and Berg, 2016; Werman, Kivelson, and Berg, 2017).

At temperatures exceeding the finite bandwidth for lattice fermions, it is natural to find bad-metallic transport with a resistivity scaling linearly with temperature. We review here the physical nature of this high-T regime, which is now well understood. One approach to this regime is to start with the following Kubo formula for the optical conductivity:

$$\sigma(\omega, T) = \pi \frac{1 - e^{-\beta \hbar \omega}}{\omega Z} \sum_{n,m} e^{-\beta E_n} |J_{nm}|^2 \delta(E_n - E_m - \hbar \omega), \quad (3.2)$$

where n and m label the eigenstates of the generic many-body Hamiltonian with energies E_n and E_m, respectively. The matrix elements of the total current operator between the two states are denoted as J_{nm} and $Z = \sum_n e^{-\beta E_n}$ is the partition function. When T is the largest energy scale in the problem, this expression reduces to

$$\sigma(\omega, T) = \frac{\pi}{k_B T} \frac{1}{Z} \sum_{n,m} |J_{nm}|^2 \delta(E_n - E_m - \hbar \omega). \quad (3.3)$$

For generic lattice models, and more generally any system for which the sum is finite in the thermodynamic limit, Eq. (3.3) implies that T-linear resistivity is expected in the high-T regime; for generic nonintegrable models the matrix elements J_{nm} are expected to have a "random-matrix" form even in the absence of any randomness (Mukerjee, Oganesyan, and Huse, 2006). This analysis was recently extended to study several interacting models over a wider range of temperatures (Patel and Changlani, 2022). The expression for the conductivity in Eq. (3.2) looks deceptively simple but usually presents a significant computational challenge when evaluated for the entire many-body spectrum.

The origin of T-linear resistivity (and deviations thereof at lower T) can also be approached from a systematic high-T expansion of the optical conductivity (Lindner and Auerbach, 2010; Perepelitsky *et al.*, 2016). Computational investigations of transport in two-dimensional Hubbard models in the high-T regime have appeared recently, using quantum Monte Carlo simulations (Huang *et al.*, 2019) and the finite-temperature Lanczos method (Vučičević *et al.*, 2019; Vranić *et al.*, 2020).

Complementary and model-independent insights into this high-T regime can be obtained by considering the Einstein-Sutherland relation relating the dc conductivity σ_{dc}, the charge diffusion coefficient D_c, and the charge compressibility χ_c (Gunnarsson, Calandra, and Han, 2003); see also Hartnoll (2015) and Perepelitsky *et al.* (2016).

When thermoelectric effects can be neglected, this relation reads

$$\sigma_{\mathrm{dc}} = \chi_c D_c, \qquad \chi_c = \frac{\partial n}{\partial \mu}, \quad (3.4)$$

with n the average density and μ the chemical potential. In the high-temperature limit, where the gas of Fermi particles is nondegenerate, the origin of $\sigma_c \sim 1/T$ is tied simply to the thermodynamic property $\chi_c \sim 1/T$ rather than the T dependence of D_c (or, equivalently, of the scattering rate). Hence, in that regime bad-metallic transport does correspond to a saturation phenomenon, although not of the resistivity itself but rather of the diffusion constant or scattering rate. Indeed, in a lattice model it is natural that the minimum possible value

of the diffusion constant should be of the order of $D_c \sim a^2/\tau_0$, with a the lattice spacing, and the microscopic timescale $\tau_0 \sim \hbar/t$, with t the bare hopping.

In the solid-state context, probing experimentally the regime where T is comparable to the hopping amplitude is challenging, except in flat-band materials, but is usually complicated by the intervening role of phonons and other remote dispersive bands. From that perspective, cold atomic gases in optical lattices offer an ideal platform for studying transport in "hot" or intermediate temperature regimes, as documented by recent experimental investigations (Anderson *et al.*, 2019; Brown *et al.*, 2019; Xu *et al.*, 2019). Figures 2(a) and 2(b) display the measured diffusion constant and compressibility, and the "resistivity" calculated using the Einstein-Sutherland relation for two-component fermions in an optical lattice realizing a two-dimensional Hubbard model, measured as a function of temperature in the range $T/t = 0.3$–8 (Brown *et al.*, 2019). It is seen that the regime dominated by thermodynamics $\chi_c \sim 1/T$, $D_c \sim$ const is indeed observed at the highest temperatures, crossing over into a regime at lower T in which both the diffusion constant and the compressibility exhibit T-dependent crossovers. Correspondingly, the resistivity as given by Eq. (3.4) becomes smaller than the MIR value at the lowest temperature while exhibiting a T-linear behavior without any noticeable feature or change of slope across the crossover.

The high-T mechanism for T-linear bad-metallic transport should be contrasted with the "Planckian regime" (Zaanen, 2004), discussed later in more detail, in which the diffusion constant (or scattering time) is temperature dependent ($D_c \sim a^2 \hbar/k_B T$), while the compressibility is temperature independent (Hartnoll, 2015). In most of the low-temperature NFLs exhibiting T-linear resistivity, it is widely believed that it is the scattering rate that is temperature dependent and not the compressibility. However, establishing this is in general difficult in the solid-state setting. Recent experimental progress has allowed for direct measurements of the electronic compressibility in two-dimensional gate-tunable materials (Zondiner *et al.*, 2020), indeed demonstrating that the Planckian regime of low-temperature transport in magic-angle twisted bilayer graphene (Polshyn *et al.*, 2019; Cao *et al.*, 2020; Jaoui *et al.*, 2022) corresponds to $D_c \sim 1/T$ (Park *et al.*, 2021). It should be noted that Planckian behavior and bad-metallic behavior are not mutually exclusive: indeed, we discuss in Secs. VII.D.1 and X models in which $D_c \sim 1/T$, while the resistivity is larger than the MIR value.

In the remainder of this review, we continue to refer to bad metals as systems with a resistivity larger than the MIR value. We reserve the term strange metal for systems or regimes with a resistivity smaller than the MIR value but having an unconventional power-law behavior at odds with expectations in a Fermi liquid. This review devotes special attention to the latter, only occasionally discussing bad metals when relevant.

B. Planckian relaxation: Unity in diversity?

Carrier numbers and effective masses may differ significantly from one material to another, and thus it is often not a meaningful exercise to compare the actual values of the resistivity across different materials. Instead, comparing the
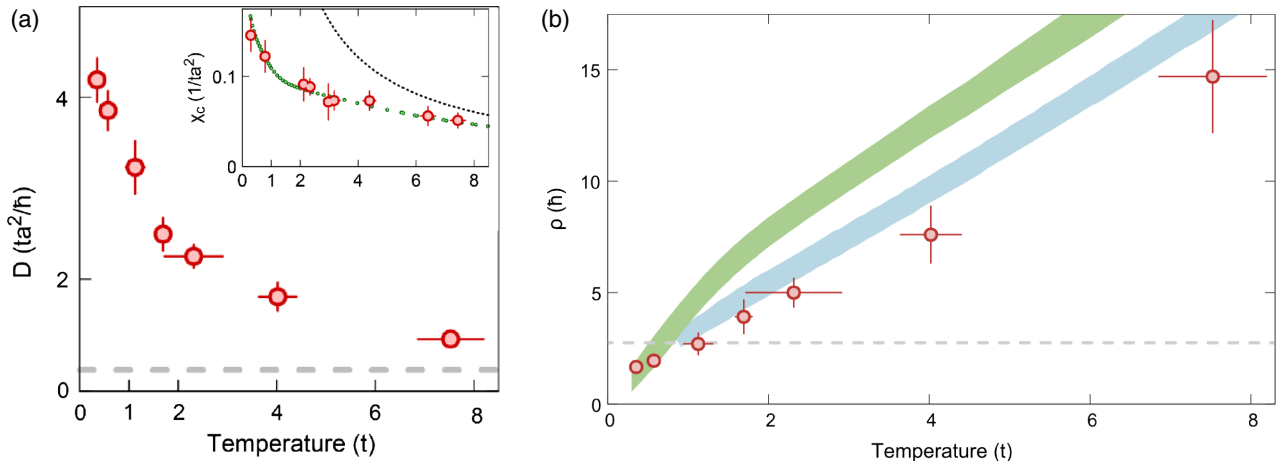
FIG. 2. Measurement of (a) the diffusion constant and (inset) compressibility for a gas of ultracold ^{6}Li atoms in an optical lattice, with a two-dimensional Fermi-Hubbard model realized with $U/t \simeq 7.5$ at a density $n \simeq 0.825$. (b) Reconstructed resistivity using Einstein-Sutherland relation. The gray horizontal dashed line represents the estimated MIR value. Theoretical calculations using DMFT (in green) and the finite-T Lanczos method (in blue) are shown; the band representation indicates the estimated error bars. Adapted from Brown *et al.*, 2019.

relaxation timescales associated with transport can shed light on the universal mechanisms that govern NFL properties. Obtaining a transport lifetime from measurements of a dc resistivity is not a straightforward exercise.

We focus here on instances in which a resistivity depending linearly on temperature $\rho = \rho_0 + AT$ is observed; see Fig. 3 for some examples and Hussey (2008), Proust and Taillefer (2019), Varma (2020), and Hartnoll and MacKenzie (2021) for reviews. A particular procedure that has been adopted to extract a temperature-dependent transport scattering rate Γ_{dc} in such materials (Bruin *et al.*, 2013) relies on a Drude fit,[2] where one expresses $\rho = m^* \Gamma_{dc}/n_c e^2$. Assuming that the effective mass m^* and carrier concentration n_c are temperature independent, one writes

$$\Gamma_{dc} \equiv \alpha \frac{k_B T}{\hbar}, \qquad \alpha = \frac{\hbar}{k_B} \frac{e^2 n_c}{m^*} A. \qquad (3.5)$$

In the experimental analysis, m^* and n_c are typically extracted from low-temperature measurements [i.e., $n_c \equiv n_c(T \to 0)$ and $m^* \equiv m^*(T \to 0)$], which does not always coincide with the regime in which the clearest signature of an extended T-linear resistivity is observed. The previous analysis becomes especially difficult in multiorbital systems and the effective masses are often extracted from quantum oscillations or specific heat; it is far from clear why this is a relevant quantity that should determine the momentum relaxation rate even within Drude theory.

Nevertheless, it is noteworthy that for a number of metals exhibiting a broad regime of T-linear resistivity including the cuprates, pnictides, ruthenates, organics, and rare-earth element materials, the previously mentioned "operational" definition of a scattering rate leads to $\alpha \approx 1$ (Bruin *et al.*, 2013). A similar analysis in magic-angle twisted bilayer

graphene near half filling of the electron and holelike flat bands (Cao *et al.*, 2020; Jaoui *et al.*, 2022), in twisted transition-metal dichalcogenides (Ghiotto *et al.*, 2021), several cuprates over an extended range of doping levels (Legros *et al.*, 2019) and a nonsuperconducting iron pnictide (Nakajima *et al.*, 2020) have also found indications of a Planckian scattering rate with $\alpha \approx 1$. Recent measurements of angle-dependent magnetoresistance (ADMR) near the pseudogap critical point in Nd-LSCO also reveal a Fermi surface with an isotropic Planckian scattering set at $\alpha \approx 1$ (Grissonnanche *et al.*, 2021). Note that this conclusion holds in the latter case provided that a T-independent effective mass associated with intermediate energy scales (and consistent with ARPES and ADMR) is used, rather than the thermodynamic effective mass associated with specific heat, which displays a logarithmic T dependence.

Note that a T-linear resistivity with a Planckian scattering rate [Eq. (3.5)] is observed in conventional metals like copper and gold. This is not a surprise and, as noted earlier, the behavior is associated with electron-phonon scattering where the phonons are in a classical equipartition regime. There have been discussions (Sadovskii, 2020, 2021) of a possible rationale for $\alpha \simeq 1$ in regimes where electron-phonon and electron-electron interactions contribute to T linearity on a similar footing. However, Planckian scattering that persists down to extremely low temperatures (Giraldo-Gallo *et al.*, 2018; Cao *et al.*, 2020; Jaoui *et al.*, 2022) in NFLs that are not low-density materials, and where the behavior persists across multiple phonon frequencies without any crossovers, presents a challenge to theory. A more in-depth discussion of Planckian timescales across solid-state materials appeared in a recent review (Hartnoll and MacKenzie, 2021).

We end this section by noting that there is not a universal definition of a "transport scattering rate," making it difficult to formulate a precise theoretical Planckian bound. Even experimentally, as previously seen, the procedure used most often to extract a scattering rate relies on a number of approximations. In that sense, the use of the Einstein-Sutherland relation to
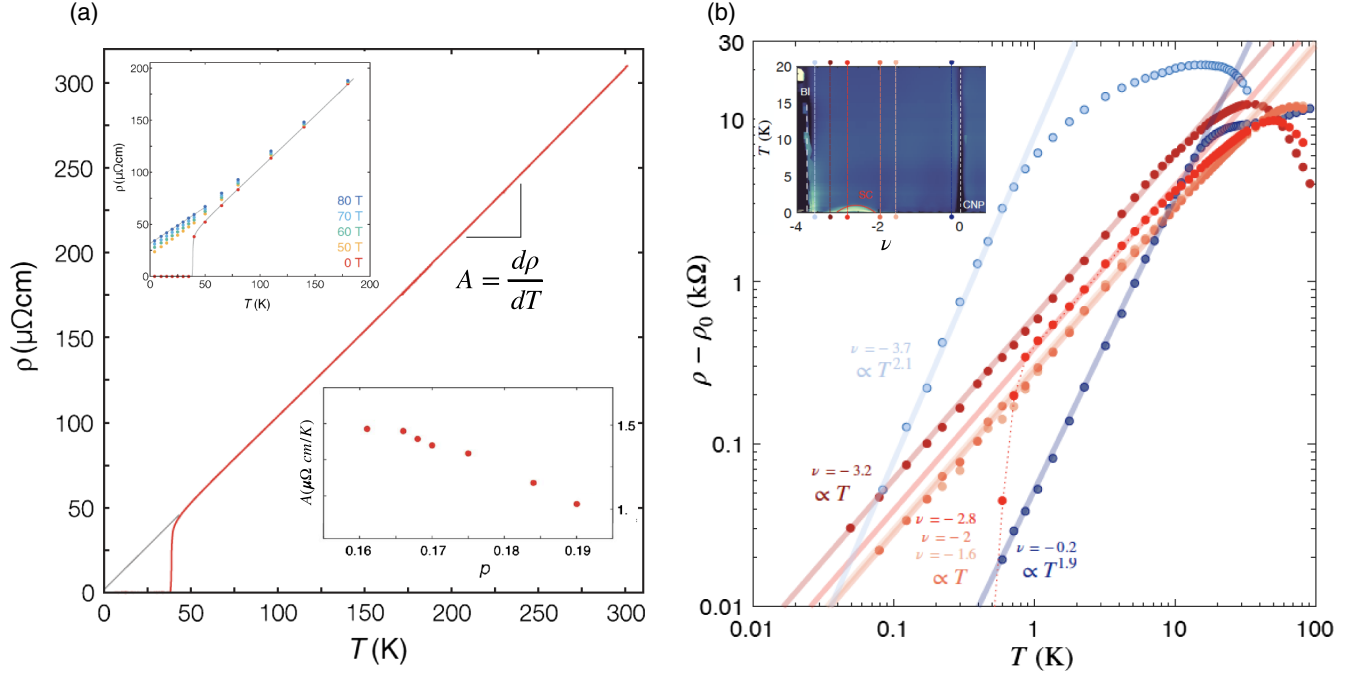
---

[2]The dc transport need not have a Drude-like form in generic NFL metals.

(a)

$$A = \frac{d\rho}{dT}$$

(b)

FIG. 3. Examples of T-linear resistivity extending over a wide range of temperature scales in (a) hole-doped $La_{2-x}Sr_xCuO_4$ (LSCO) near optimal doping and (b) magic-angle twisted bilayer graphene (MATBG) near $\nu \approx -2$ relative to the charge neutrality $\nu = 0$. In LSCO, T_{coh} can be inferred to be much lower than any characteristic energy scales by turning on a magnetic field and accounting for the finite magnetoresistance [(a)-top inset]; the variation of the slope (A) on hole-doping is shown in the bottom inset of (a). In MATBG, the linearity for a range of dopings near $\nu \approx -2$ [inset of (b)] persists down to $\sim$40 mK. Both families of materials also display a Planckian form of Γ_{dc} [Eq. (3.5)]. (a) Adapted from Giraldo-Gallo *et al.*, 2018. (b) Adapted from Jaoui *et al.*, 2022.

extract a diffusion constant, combined with the recent progress in measuring the previously discussed electronic compressibility, may be a safer route to follow whenever possible.

Optical spectroscopy measurements of the complex conductivity are often parametrized in terms of a frequency and temperature-dependent optical timescale and effective mass enhancements as (Basov *et al.*, 2011) $4\pi\sigma(\omega)/\omega_p^2 = [1/\tau_{opt}(\omega) - i\omega m_{opt}^*(\omega)/m)]^{-1}$, which can be directly determined from experimental data as $1/\tau_{opt} = \omega_p^2/4\pi\text{Re}[1/\sigma]$, $m_{opt}^*/m = \omega_p^2/4\pi\text{Im}[1/\sigma]$ once a normalization of the spectral weight $\omega_p^2/4\pi$ has been chosen.

In a subset of the previously highlighted NFL metals, including optimally doped cuprates (van der Marel *et al.*, 2003), the low-frequency limit of $1/\tau_{opt}$ was also shown to have a Planckian form and ω/T scaling was observed.

In later sections of this review, we will discuss a number of recent studies that have demonstrated the existence of a Planckian time-scale for transport in solvable models of correlated electrons.

IV. RANDOM-MATRIX MODEL: FREE FERMIONS

In a study of charge transport in mesoscopic structures, much experimental effort has focused on electrons moving through "quantum dots" (Alhassid, 2000). We can idealize a quantum dot as a "billiard," a cavity with irregular walls. The electrons scatter off the walls before eventually escaping through the leads. If we treat the electron motion classically, we can follow a chaotic trajectory of particles bouncing off the

walls of the billiard. Much mathematical effort has been devoted to the semiclassical quantization of such noninteracting particles: the "quantum billiard" problem. The Bohigas-Giannoni-Schmit conjecture (Bohigas, Giannoni, and Schmit, 1984) states that many statistical properties of this quantum billiard can be described using a model in which the electrons hop on a random matrix; there has been recent progress toward establishing this conjecture (Müller *et al.*, 2009; Anantharaman and Macia, 2011). We describe this random-matrix problem in this section.

Many properties of the random-matrix model are similar to a model of a disordered metal in which the electrons occupy plane wave eigenstates that scatter off randomly placed impurities with a short-range potential. However, unlike the random impurity case, there is no regime in which the eigenstates of a random matrix can be localized. As every site is coupled to every other site, there is no sense of space or distance along which the eigenstate can decay exponentially. The absence of localization also extends to nonfully connected lattices with infinite connectivity, such as a regular hybercubic lattice in d dimensions in the $d \to \infty$ limit. Indeed, it can be shown that in this limit the local density of states self-averages (see later discussion), which implies the absence of Anderson localization (Dobrosavljević and Kotliar, 1997).

A. Green's function

We consider electrons c_i (assumed spinless for simplicity) hopping between sites labeled $i = 1, \ldots, N$, with a hopping matrix element $t_{ij}/\sqrt{N}$:

$$H_2 = \frac{1}{(N)^{1/2}} \sum_{i,j=1}^{N} t_{ij} c_i^\dagger c_j - \mu \sum_i c_i^\dagger c_i, \qquad (4.1a)$$

$$c_i c_j + c_j c_i = 0, \qquad c_i c_j^\dagger + c_j^\dagger c_i = \delta_{ij}, \qquad (4.1b)$$

$$\frac{1}{N} \left\langle \sum_i c_i^\dagger c_i \right\rangle = \mathcal{Q}. \qquad (4.1c)$$

The t_{ij} are chosen to be independent random complex numbers with $t_{ij} = t_{ji}^*$, $\overline{t_{ij}} = 0$, and $\overline{|t_{ij}|^2} = t^2$. The $1/\sqrt{N}$ scaling of the hopping was chosen so that the bandwidth of the single-electron eigenstates will be of the order of unity in the $N \to \infty$ limit, and therefore (as there are N eigenstates) the spacing between the successive eigenvalues will be of the order of $1/N$. We also included a chemical potential so that the average density of electrons on each site would be $\mathcal{Q}$. The subscript 2 in the Hamiltonian H_2 denotes that it includes only two electron operators.

For a given set of t_{ij}, one can numerically diagonalize the $N \times N$ matrix t_{ij} to solve this problem. We denote by $\{|\lambda\rangle, \epsilon_\lambda\}$ the spectrum of eigenstates of the matrix t_{ij} for a given realization.

However, in the limit of large N it turns out that certain quantities are self-averaging. This means that, for a given sample t_{ij}, their value converges with probability 1 in the $N \to \infty$ limit to their averaged value over all samples. We are interested only in such observables here.

We define the single-particle Green's function as usual as

$$G_{ij}(\tau) = -\langle T_\tau c_i(\tau) c_j^\dagger(0) \rangle, \qquad (4.2)$$

with τ the imaginary time and $G_{ij}(\tau + \beta) = -G_{ij}(\tau)$. For a given sample, we can expand this function in terms of the one-particle eigenstates as

$$G_{ij}(z) = \frac{1}{N} \sum_\lambda \langle i|\lambda \rangle \frac{1}{z + \mu - \epsilon_\lambda} \langle \lambda|j \rangle, \qquad (4.3)$$

where z denotes a complex frequency such as the Matsubara frequencies $\omega_n = (2n+1)\pi/\beta$.

In the limit of large N for a given site i, the local Green's function self-averages as follows:

$$G_{ii}(\tau) \to G(\tau), \qquad (4.4)$$

with $G = (1/N)\sum_i G_{ii}$, which is also identical to the average over all samples $\overline{G_{ii}}$. In contrast, $G_{i \neq j}$ is of the order of $1/\sqrt{N}$ for a given pair of sites i and j and depends on the specific sample.

The simplest way to establish this result consists of evaluating averages of G_{ij} order by order in a perturbation theory in t_{ij}. At zeroth order, the Green's function is simply

$$G_{ij}^0(i\omega_n) = \frac{\delta_{ij}}{i\omega_n + \mu}. \qquad (4.5)$$

The Feynman graph expansion consists of a single-particle line, with an infinite set of possible products of G_{ij}^0 and t_{ij}.
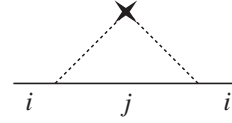

FIG. 4. Graph of the electron self-energy $\Delta(\tau)$ in Eq. (4.6b). Solid lines denote fully dressed electron Green's functions. The dashed line represents the disorder averaging associated with $|t_{ij}|^2$.

We then average each graph over the distribution of t_{ij}. In the $N \to \infty$ limit, only a simple set of graphs survive (Fig. 4), and the average Green's function is a solution of the following set of equations:

$$G(i\omega_n) = \frac{1}{i\omega_n + \mu - \Delta(i\omega_n)}, \qquad (4.6a)$$

$$\Delta(\tau) = t^2 G(\tau), \qquad (4.6b)$$

$$G(\tau = 0^-) = \mathcal{Q}. \qquad (4.6c)$$

The solution of Eq. (4.6b) reduces to solving a quadratic equation for $G(z)$, and we thus obtain the following for a complex frequency z:

$$G(z) = \frac{1}{2t^2} \left(z + \mu \pm \sqrt{(z+\mu)^2 - 4t^2} \right). \qquad (4.7)$$

The sign in front of the square root $(\text{sgn}[\text{Im}(z+\mu)])$ is chosen such that $G(z)$ has the following correct analytic properties.
- $G(|z| \to \infty) = 1/z$.
- $\text{Im}\, G(\omega + i0^+) < 0$ for real ω.
- $\text{Im}\, G(\omega + i0^-) > 0$ for real ω.

All of these constraints can be obtained from the spectral representation of the Green's function. We can also define the density of single-particle states as

$$\rho(\omega) = -\frac{1}{\pi} \text{Im}\, G(\omega - \mu + i0^+) = \frac{1}{2\pi t^2} \sqrt{4t^2 - \omega^2} \qquad (4.8)$$

for $\omega \in [-2t, 2t]$, and as $\rho(\omega) = 0$ otherwise. This is the Wigner semicircle density of states for the random matrix (Mehta, 2004).

The chemical potential is fixed by requiring that Eq. (4.6c) is satisfied and can be written as

$$\int_{-2t}^{2t} d\omega\, \rho(\omega) f(\omega - \mu) = \mathcal{Q}, \qquad (4.9)$$

where $f(\varepsilon) = 1/(e^{\varepsilon/T} + 1)$ is the Fermi function. Performing a Sommerfeld expansion of the left-hand side for $T \ll t$, we obtain

$$\int_{-2t}^{\mu} d\omega\, \rho(\omega) + \frac{\pi^2 T^2}{6} \rho'(\mu) = \mathcal{Q}, \qquad (4.10)$$

where $\rho'(\omega) = d\rho/d\omega$. To satisfy this equation for all T in the low-T regime, μ or, alternatively, $\mathcal{Q}$ must depend on T (depending upon the particular ensemble). In particular, if we keep $\mathcal{Q}$ fixed and vary T, then

$$\mu(T) = \mu_0 - \frac{\rho'(\mu_0)}{\rho(\mu_0)} \frac{\pi^2 T^2}{6}, \qquad (4.11)$$

where $\mu_0 = \mu(T = 0)$.

An alternative way to prove the self-averaging properties is to use the "cavity" construction, which is also a useful method to establish the local effective action associated with interacting models considered later in this review. In a nutshell [see Georges *et al.* (1996) for details], this consists of integrating over all sites $i = 2, \ldots, N$ except site $i = 1$ and noting that the term $\sum_{i>1} c_i^\dagger (t_{i1} c_1)$ can be viewed as a source term coupling to $c_i^\dagger$. Performing the integration over sites is a Gaussian problem in this noninteracting case and leads to the following effective action for site 1:

$$\int d\tau \int d\tau' c_1^\dagger(\tau)[\delta(\tau-\tau')(\partial_\tau - \mu) + \Delta_1(\tau-\tau')]c_1(\tau'), \quad (4.12)$$

with

$$\Delta_1(z) = \frac{1}{N} \sum_{i \neq 1} t_{1i}^2 G_{ii}^{[1]}(z) + \frac{1}{N} \sum_{i \neq j, i, j > 1} t_{1i} t_{1j} G_{ij}^{[1]}(z). \quad (4.13)$$

In Eq. (4.13), $G_{ij}^{[1]}(z)$ denotes the Green's function of the lattice with one fewer site (site 1 removed, $N-1$ sites) and also removing all connections to that site. We see that the sum over i in the first term amounts to a statistical average as $N \to \infty$, and we note that $G_{ii}^{[1]}(z)$ does not depend on t_{1i}. Hence, the two terms under the sum can be averaged independently, yielding $t^2 G$. Similar reasoning shows that the second term vanishes since the average of the t_{ij}'s is zero. This proves the self-averaging of the local Green's function G_{11}. Inverting the quadratic kernel leads us to Eq. (4.6b), $G^{-1}(z) = z + \mu - t^2 G(z)$. This also proves that the local one-particle density of states for a given sample $(1/N) \sum_\lambda |\langle i|\lambda\rangle|^2 \delta(\epsilon - \epsilon_\lambda)$ converges with probability 1 to the Wigner semicircular law in the thermodynamic limit $N \to \infty$. For a given single-particle energy ϵ within this distribution, one can consider the following energy-resolved Green's function:

$$G(\epsilon, i\omega_n) = \frac{1}{i\omega_n + \mu - \epsilon}, \qquad (4.14)$$

which allows one to locate the position $\epsilon = \mu$ of the Fermi energy of this random but self-averaging model and the corresponding energy distribution of particles $\theta(\mu - \epsilon)$ at $T = 0$.

B. Many-body density of states

A quantity that plays an important role in our subsequent discussion of the SYK model is the many-body density of states $\mathcal{N}(E)$. Unlike the single-particle density of states $\rho(\omega)$, this is not an intensive quantity. However, it is typically exponentially large in N because there is an exponentially large number of ways of making states within a small window of an energy $E \sim N$. In the grand canonical ensemble, we can relate the grand potential $\Omega(T)$ to $\mathcal{N}(E)$ via the following expression for the grand partition function:

$$Z = \exp\left(-\frac{\Omega(T)}{T}\right) = \int_{-\infty}^{\infty} dE\, \mathcal{N}(E) e^{-E/T}. \qquad (4.15)$$

Note that we have absorbed a contribution $-\mu N \mathcal{Q}$ into the definition of the grand energy E, as is frequently done in Fermi-liquid theory. Thus, we can obtain $\mathcal{N}(E)$ by an inverse Laplace transform of $\Omega(T)$.

We first evaluate $\Omega(T)$. Using the standard Sommerfeld expansion for free fermions, we have

$$\Omega(T) = -NT \int_{-2t}^{2t} d\omega\, \rho(\omega) \ln\left(1 + e^{-(\omega-\mu)/T}\right)$$

$$= N \int_{-2t}^{\mu} d\omega(\omega - \mu)\rho(\omega) - \frac{N\pi^2 T^2}{6} \rho(\mu)$$

$$\equiv E_0 - \frac{N\pi^2 T^2}{6} \rho(\mu). \qquad (4.16)$$

We now have to insert Eq. (4.16) into Eq. (4.15) and determine $\mathcal{N}(E)$. Rather than perform the inverse Laplace transform, we guess the form of $\mathcal{N}(E)$. First, it is not difficult to see that $\mathcal{N}(E < E_0) = 0$. Second, we expect $\mathcal{N}(E)$ to be exponentially large in N when $E - E_0 \sim N$. Therefore, we make the guess

$$\mathcal{N}(E) \sim \exp\left\{aN[(E - E_0)/N]^b\right\}, \qquad E > E_0, \qquad (4.17)$$

for the constants a and b. We then insert Eq. (4.17) into Eq. (4.15) and perform the integral over E using the steepest descent method in the large-N limit. Matching the result to the left-hand side of Eq. (4.15), we obtain the following main result of this section:

$$\mathcal{N}(E) \sim \exp[S(E)],$$

$$S(E) = \begin{cases} \pi\sqrt{2N\rho(\mu)(E - E_0)/3}, & E > E_0 \\ 0, & E < E_0 \end{cases}, \qquad (4.18)$$

where $S(E)$ is the entropy as a function of the energy. Consideration of the derivation shows that this result is valid for

$$1 \ll \rho(\mu)(E - E_0) \ll N \qquad (4.19)$$

in the limit of large N. Note that the entropy vanishes as $E \searrow E_0$ in Eq. (4.18). We show numerical results for $\mathcal{N}(E)$ for a closely related random Majorana fermion model in Fig. 5. When $E - E_0 \sim N$, the entropy $S(E)$ is extensive, the energy level spacing is exponentially small ($\sim e^{-aN}$, with $a > 0$), and $\mathcal{N}(E) \sim e^{aN}$ is exponentially large. However, when $E - E_0 \sim 1/N$, we expect the energy levels to be few particle excitations with energies $\sim 1/N\rho(\mu)$, and therefore
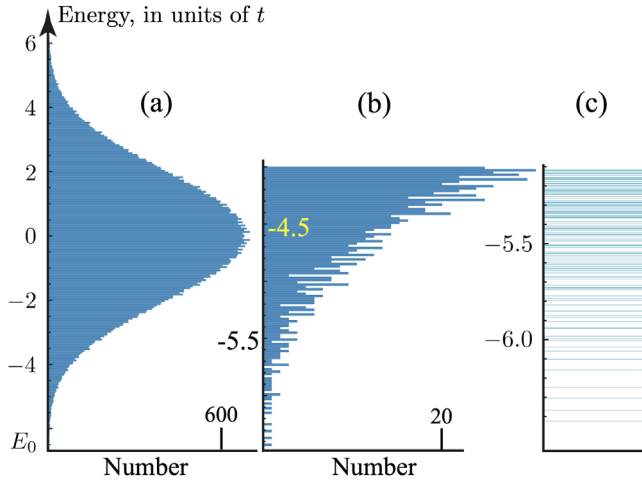
FIG. 5. Display of 65 536 many-body eigenvalues of an $N = 32$ Majorana matrix model with random $q = 2$ fermion terms. $\mathcal{N}(E)$ is plotted in (a) and (b) in 200 and 100 bins, while (b) and (c) are enlargements of the bottom of the band. Individual energy levels are shown in (c) and are expected to have the spacing $1/N\rho(\mu)$ at the bottom of the band as $N \to \infty$.

$\mathcal{N}(E) \sim N$. This rapid decrease of $\mathcal{N}(E)$ near the bottom of the band is evident in Fig. 5(a) from the "tails" in the density of states. A more complete analysis of the finite-N corrections is needed to understand the behavior of the $\mathcal{N}(E)$ at low energy, along the lines of recent analyses (Liao, Vikram, and Galitski, 2020; Liao and Galitski, 2021).

We also show in Fig. 6 the corresponding results for the Majorana SYK model. These results are discussed further in Sec. V.F.2, but for now note the absence of the tails in $\mathcal{N}(E)$ in Fig. 6(a) relative to Fig. 5(a).
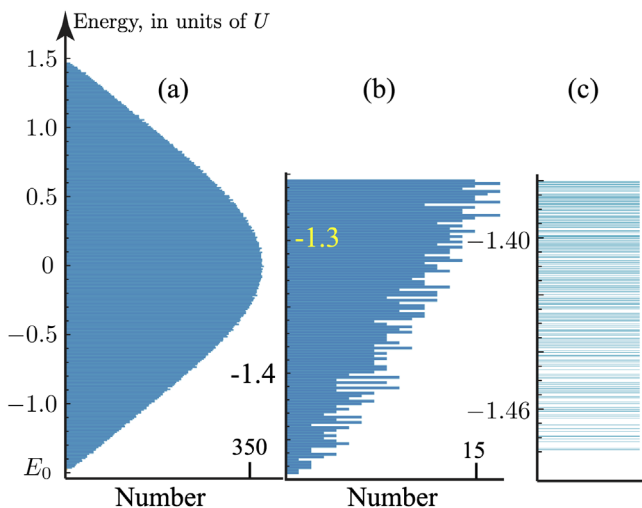

FIG. 6. Display of 65 536 many-body eigenvalues of an $N = 32$ Majorana SYK Hamiltonian with random $q = 4$ fermion terms. $\mathcal{N}(E)$ is plotted in (a) and (b) in 200 and 100 bins, while (b) and (c) are enlargements of the bottom of the band. Individual energy levels are shown in (c) and are expected to have the spacing e^{-NS} at the bottom of the band as $N \to \infty$. Compare this to Fig. 5 for the random-matrix model, which has a much sparser spacing $\sim 1/N$ at the bottom of the band.

There is an interpretation of Eq. (4.18) that gives us some insight into the structure of the random-matrix eigenenergies and also highlights a key characteristic of many-body systems with quasiparticle excitations. It is known that the eigenvalues of a random matrix undergo level repulsion and that their spacings obey Wigner-Dyson statistics (Mehta, 2004). For a zeroth-order picture, we assume that the random-matrix eigenvalues are rigidly equally spaced, with energy level spacing (near the chemical potential) of $1/N\rho(\mu)$. Now we ask for the number of ways to create a many-body excitation with energy $E - E_0$. With the simplifying assumption that we made on the one-particle spectrum, each many-body eigenstate can be described using a unique set of particle-hole excitations, each of which has an excitation energy that is an integer n_i times the level spacing $1/N\rho(\mu)$. This mapping is the essence of bosonization in one dimension; see Sachdev (1999) and Giamarchi (2003). Hence, the excitation energy reads

$$N\rho(\mu)(E - E_0) = n_1 + n_2 + n_3 + n_4 + \cdots, \qquad (4.20)$$

where n_i are the excitation numbers of the particle-hole excitations. Thus, we estimate the number of such excitations to be equal to the number of partitions of the integer $N\rho(\mu)(E - E_0)$. Now we use the Hardy-Ramanujan result that the number of partitions of an integer n is $p(n) \sim \exp(\pi\sqrt{2n/3})$ at large n. This immediately yields Eq. (4.18). Note that the special case with exactly equally spaced quasiparticle levels (which is the case for the linearly dispersing free Fermi gas in one dimension) has many-body levels with a spacing $\sim 1/N$ but an exponentially large degeneracy; in contrast, the generic random-matrix case has no degeneracy but an exponentially small many-body level spacing.

This argument highlights a key feature of the many-body spectrum: it is just the sum of single-particle excitation energies. We expect that if we add four-fermion interactions to the random-matrix model, we will obtain quasiparticle excitations in a Fermi-liquid state whose energies add to give many-particle excitations. This can be checked for weak interactions using a perturbative calculation in SYK models with random hopping (Parcollet and Georges, 1999; Song, Jian, and Balents, 2017), and also holds nonperturbatively, as shown by dynamical mean-field theory (Georges *et al.*, 1996), which is exact for the random-matrix Hubbard model with a local interaction. Therefore, we expect the general form of Eq. (4.18) to continue to hold even with interactions. However, we see at the end of Sec. V.F.2 that such a decomposition into quasiparticle excitations does not hold for the SYK model.

We can also estimate the lifetime of the quasiparticles at weak coupling using a perturbative computation based on Fermi's golden rule: we obtain $1/\tau \sim U^2 T^2/t^3$ at low T, with U the strength of the local interaction. As this is parametrically smaller than a thermal excitation energy $\sim T$, quasiparticles remain well-defined excitations. The existence of such quasiparticles can be diagnosed from the poles of the energy-resolved Green's function to be presented in Eq. (7.8), supplemented by the self-energy as defined in Sec. VII.A to account for interactions, while the energy integrated local

Green's function equation (4.7) yields the disorder-averaged total density of states.

V. THE SYK MODEL

As in the random-matrix model, we consider electrons (assumed to be spinless for simplicity) that occupy sites labeled $i = 1, 2, …, N$. However, instead of a random one-particle hopping t_{ij}, we now have only the following random two-particle interaction $U_{ij;k\ell}$:

$$H_4 = \frac{1}{(2N)^{3/2}} \sum_{ijk\ell=1}^{N} U_{ij;k\ell} c_i^\dagger c_j^\dagger c_k c_\ell - \mu \sum_i c_i^\dagger c_i, \quad (5.1a)$$

$$c_i c_j + c_j c_i = 0, \qquad c_i c_j^\dagger + c_j^\dagger c_i = \delta_{ij}, \quad (5.1b)$$

$$Q = \frac{1}{N} \sum_i \langle c_i^\dagger c_i \rangle. \quad (5.1c)$$

We choose the couplings $U_{ij;k\ell}$ to be independent random variables with zero mean $\overline{U_{ij;k\ell}} = 0$, while satisfying $U_{ij;k\ell} = -U_{ji;k\ell} = -U_{ij;\ell k} = U_{k\ell;ij}^*$. All the random variables have the same variance $\overline{|U_{ij;k\ell}|^2} = U^2$.

A model similar to H_4 appeared in nuclear physics, where it was called the two-body random ensemble (Bohigas and Flores, 1971; Brody *et al.*, 1981) and studied numerically. The existence and structure of the large-N limit was understood (Sachdev and Ye, 1993; Parcollet and Georges, 1999; Georges, Parcollet, and Sachdev, 2000, 2001) in the context of a closely related model that we examine in Sec. VI. More recently a Majorana version was introduced (Kitaev, 2015), and the large-N limit of H_4 was obtained (Sachdev, 2015).

The useful self-averaging properties of the random-matrix model as $N \to \infty$ also apply to the SYK model [Eq. (5.1a)]. Indeed, the self-averaging properties are much stronger, as the average takes place over the many-body Hilbert space of size $e^{\alpha N}$ rather than the single-particle Hilbert space of size N. Proceeding just as in the random-matrix model, we perform a Feynman graph expansion in $U_{ij;k\ell}$ and then average graph by graph. In the large-N limit, only the so-called melon graphs survive (Fig. 7), and the determination of the on-site Green's function reduces to the solution of the following equations:
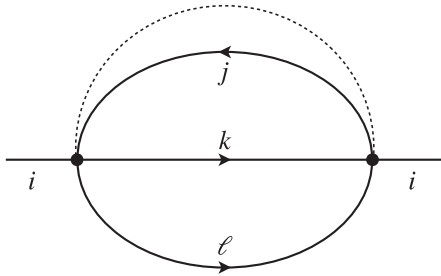

FIG. 7. The "melon graph" for the electron self-energy $\Sigma(\tau)$ in Eq. (5.2b). Solid lines denote fully dressed electron Green's functions. The dashed line represents the disorder averaging associated with the interaction vertices (denoted as solid circles) $|U_{ij;k\ell}|^2$.

$$G(i\omega_n) = \frac{1}{i\omega_n + \mu - \Sigma(i\omega_n)}, \quad (5.2a)$$

$$\Sigma(\tau) = -U^2 G^2(\tau) G(-\tau), \quad (5.2b)$$

$$G(\tau = 0^-) = Q. \quad (5.2c)$$

Unlike the random-matrix equations, Eqs. (5.2a)–(5.2c) cannot be solved analytically as a result of their nonlinearity, and a full solution can be obtained only numerically. However, it is possible to make significant analytic progress at frequencies and temperatures much smaller than U, as we describe in Secs. V.A–V.F.

Before embarking on a general low-energy solution of Eqs. (5.2a)–(5.2c), we note a noteworthy feature that can be deduced on general grounds (Sachdev and Ye, 1993): any nontrivial solution (i.e., with $Q \neq 0, 1$) must be gapless. Suppose otherwise and assume that there is a gapped solution with $\mathrm{Im}\, G(\omega) = 0$ for $|\omega| < E_G$. By examining the spectral decomposition of the equation for the self-energy in Eq. (5.2b), we can then establish that $\mathrm{Im}\, \Sigma(\omega) = 0$ for $|\omega| < 3E_G$. Inserting this back into Dyson's equation (5.2a), we obtain the contradictory result that $\mathrm{Im}\, G(\omega) = 0$ for $|\omega| < 3E_G$. Therefore, the only possible value is $E_G = 0$.

A. Low-energy solution at $T = 0$

Knowing that the solution must be gapless, we assume that we have a power-law singularity at zero frequency. Thus, we assume (Sachdev and Ye, 1993)

$$G(z) = C \frac{e^{-i(\pi\Delta+\theta)}}{z^{1-2\Delta}}, \quad \mathrm{Im}(z) > 0, \quad |z| \ll U. \quad (5.3)$$

We have a prefactor $C > 0$, a power-law singularity determined by the exponent $\Delta > 0$, and a spectral asymmetry angle θ that yields distinct density of states for particle and hole excitations. We now have to insert the *Ansatz* (5.3) into Eqs. (5.2a) and (5.2b) and find the values of C, Δ, and θ for which there is a self-consistent solution. The solution also has to satisfy the constraint arising from the spectral representation $\mathrm{Im}\, G(\omega + i0^+) < 0$; for Eq. (5.3) this translates to

$$-\pi\Delta < \theta < \pi\Delta. \quad (5.4)$$

We now want to obtain the Green's function as a function of imaginary time τ. For this purpose, we write the spectral representation using the density of states $\rho(\Omega) = -(1/\pi)\mathrm{Im}\, G(\omega + i0^+) > 0$ so that

$$G(z) = \int_{-\infty}^{\infty} d\Omega \frac{\rho(\Omega)}{z - \Omega}. \quad (5.5)$$

We can take a Fourier transform and obtain

$$G(\tau) = \begin{cases} -\int_0^\infty d\Omega\, \rho(\Omega) e^{-\Omega\tau} & \text{for } \tau > 0, \\ \int_0^\infty d\Omega\, \rho(-\Omega) e^{\Omega\tau} & \text{for } \tau < 0. \end{cases} \quad (5.6)$$

Using Eq. (5.6) we obtain in τ space

$$G(\tau) = \begin{cases} -[C\Gamma(2\Delta)\sin(\pi\Delta+\theta)]/\pi|\tau|^{2\Delta} & \text{for } \tau \gg 1/U, \\ [C\Gamma(2\Delta)\sin(\pi\Delta-\theta)]/\pi|\tau|^{2\Delta} & \text{for } \tau \ll -1/U, \end{cases}$$

$$(5.7)$$

corresponding to the following low-frequency behavior of the spectral function:

$$\rho(\Omega) = \begin{cases} \sin(\pi\Delta+\theta)(C/\pi|\Omega|^{1-2\Delta}) & \text{for } 0 < \Omega \ll U, \\ \sin(\pi\Delta-\theta)(C/\pi|\Omega|^{1-2\Delta}) & \text{for } -U \ll \Omega < 0. \end{cases}$$

$$(5.8)$$

Equation (5.8) makes it clear that θ determines the particle-hole asymmetry associated with the fermion propagation forward and backward in time (positive and negative frequencies). For our later purposes, it is also useful to parametrize the asymmetry in terms of a real number $-\infty < \mathcal{E} < \infty$ so that

$$G(\tau) \sim \begin{cases} -e^{\pi\mathcal{E}}/|\tau|^{2\Delta} & \text{for } \tau \gg 1/U, \\ e^{-\pi\mathcal{E}}/|\tau|^{2\Delta} & \text{for } \tau \ll -1/U, \end{cases}$$

$$(5.9)$$

and we then have

$$e^{2\pi\mathcal{E}} = \frac{\sin(\pi\Delta+\theta)}{\sin(\pi\Delta-\theta)}, \qquad (5.10)$$

and $\mathcal{E} = \theta = 0$ is the particle-hole symmetric case. This spectral asymmetry plays a key role in the physics of the complex SYK model, as well as in the large-M solution of multichannel Kondo models (Parcollet *et al.*, 1998), where the notation $\alpha = 2\pi\mathcal{E}$ was used.

We also use the following spectral representation for the self-energy:

$$\Sigma(z) = \int_{-\infty}^{\infty} d\Omega \frac{\sigma(\Omega)}{z - \Omega}. \qquad (5.11)$$

Using Eqs. (5.2b) and (5.7) to obtain $\Sigma(\tau)$ and performing the inverse Laplace transform as with $G(\tau)$, we obtain

$$\sigma(\Omega) = \begin{cases} \Upsilon(\Delta)[\sin(\pi\Delta+\theta)]^2[\sin(\pi\Delta-\theta)]|\Omega|^{6\Delta-1} \\ \quad \text{for } \Omega > 0, \\ \Upsilon(\Delta)[\sin(\pi\Delta+\theta)][\sin(\pi\Delta-\theta)]^2|\Omega|^{6\Delta-1} \\ \quad \text{for } \Omega < 0, \end{cases}$$

$$(5.12)$$

where $\Upsilon(\Delta) = [U^2/\Gamma(6\Delta)][C\Gamma(2\Delta)/\pi]^3$. Finally, we insert the $\Sigma(i\omega_n)$ obtained from Eqs. (5.11) and (5.12) back into Eq. (5.2a). To understand the structure of the solution, we first assume that $0 < 6\Delta - 1 < 1$; we soon find that this is indeed the case and that no other solution is possible. As $|\omega_n| \to 0$, the frequency dependence in $\Sigma(i\omega_n)$ is much larger than that from the $i\omega_n$ term in Eq. (5.2a). In addition, we have $1 - 2\Delta > 0$, so $G(z)$ in Eq. (5.3) diverges as $|z| \to 0$. Thus, we find that a solution of Eq. (5.2a) is possible only under the following two conditions:

$$\mu - \Sigma(0) = 0,$$
$$1 - 2\Delta = 6\Delta - 1 \Rightarrow \Delta = \tfrac{1}{4}. \qquad (5.13)$$

Matching the divergence in the coefficient of $G(z)$ as $z \to 0$, we also obtain the following value of C:

$$C = \left(\frac{\pi}{U^2 \cos(2\theta)}\right)^{1/4}. \qquad (5.14)$$

The value of the asymmetry angle θ remains undetermined by the solutions of Eqs. (5.2a) and (5.2b). As we see in Sec. V.B, the value of θ is fixed by a generalized Luttinger's theorem, which relates it to the value of the fermion density $\mathcal{Q}$ (Georges, Parcollet, and Sachdev, 2001). But without further computation we can conclude that at the particle-hole symmetric point, with $\mathcal{Q} = 1/2$, we have $\mathcal{E} = \theta = 0$.

The main result of this section is therefore summarized in Eq. (5.9). The fermion has "dimension" $\Delta = 1/4$, and its two-point correlator decays as $1/\sqrt{\tau}$; there is a particle-hole asymmetry determined by $\mathcal{E}$ (which is unknown at this stage but determined in Sec. V.B). Contrast this with the corresponding features of the random-matrix model with a Fermi-liquid ground state: the two-point fermion correlator decays as $1/\tau$, and the leading decay is particle hole symmetric.

B. Luttinger's theorem

In Fermi-liquid theory, Luttinger's theorem relates an equal time property (the total electron density) to a low-energy property, the Fermi wave vector that is the location of the zero energy excitations. There turns out to be a similar low- to high-energy mapping that can be made in a "generalized" Luttinger theorem for the SYK model, relating the angle θ characterizing the particle-hole asymmetry at long times in Eq. (5.3) to the fermion density $\mathcal{Q}$ (Georges, Parcollet, and Sachdev, 2001). As in the conventional Luttinger analysis, we start by manipulating the expression for $\mathcal{Q}$ into two terms

$$\mathcal{Q} - 1 = \int_{-\infty}^{\infty} \frac{d\omega}{2\pi} G(i\omega) e^{-i\omega 0^+} = I_1 + I_2,$$
$$I_1 = i \int_{-\infty}^{\infty} \frac{d\omega}{2\pi} \frac{d}{d\omega} \ln[G(i\omega)] e^{-i\omega 0^+},$$
$$I_2 = -i \int_{-\infty}^{\infty} \frac{d\omega}{2\pi} G(i\omega) \frac{d}{d\omega} \Sigma(i\omega) e^{-i\omega 0^+}. \qquad (5.15)$$

In Fermi-liquid theory, I_2 vanishes because of the existence of the Luttinger-Ward functional (Luttinger and Ward, 1960; Abrikosov, Gorkov, and Dzyaloshinskii, 1963), while I_1 is easily evaluated because it is a total derivative, and this yields the Luttinger theorem. The situation is more complicated for the SYK model because of the singular nature of $G(\omega)$ as $|\omega| \to 0$. Indeed, both I_1 and I_2 are logarithmically divergent at small $|\omega|$, although their sum is well defined. Nevertheless, the separation of $\mathcal{Q}$ into I_1 and I_2 is useful because it allows us to use the special properties of the Luttinger-Ward functional to account for the unknown high-frequency behavior of the Green's function. We define $I_{1,2}$ using a regularization procedure, and it is important that the same regularization be

used for both I_1 and I_2. We employ the symmetric principal value, with

$$\int_{-\infty}^{\infty} d\omega \Rightarrow \lim_{\eta \to 0} \left[\int_{-\infty}^{-\eta} d\omega + \int_{\eta}^{\infty} d\omega \right]. \qquad (5.16)$$

We now evaluate I_1 using the usual procedure: we distort the contour of integration to the real-frequency axis and have to evaluate

$$i \lim_{\eta \to 0} \int_0^{\infty} \frac{d\omega}{2\pi} \frac{d}{d\omega} \ln \left[\frac{G(\omega + i\eta)}{G(\omega - i\eta)} \right]$$

$$= -\frac{1}{\pi} \lim_{\eta \to 0} [\arg G(\infty + i\eta) - \arg G(i\eta)]. \qquad (5.17)$$

In a Fermi liquid, this is the only contribution to I_1 that evaluates to unity outside the Fermi surface and vanishes inside the Fermi surface. In this case, however, the imaginary frequency integral (5.16) differs from the real-frequency integral (5.17) because of the singularity at $\omega = 0$, for which a small contour encircling the origin must be introduced, finally leading via Eq. (5.3) to

$$I_1 = -\frac{1}{2} - \frac{\theta}{\pi}. \qquad (5.18)$$

Note that this yields a contribution $1/2 - \theta/\pi$ to $\mathcal{Q}$, which obeys $\mathcal{Q} \to 1 - \mathcal{Q}$ under $\theta \to -\theta$ as dictated by particle-hole symmetry but does not have the expected limits $\mathcal{Q} \to 0, 1$ as $\theta \to \pm\pi/4$. This is already a hint that I_2 must yield a nonzero contribution.

In the evaluation of I_2 we must substitute Eq. (5.2b) for Σ into I_2 because then we ensure cancellations at high frequencies arising from the existence of the Luttinger-Ward functional as follows:

$$\Phi_{\mathrm{LW}}[G] = -\frac{U^2}{4} \int d\tau \, G^2(\tau) G^2(-\tau). \qquad (5.19)$$

Using $\Sigma = \delta\Phi_{\mathrm{LW}}/\delta G$ and ignoring the singularity at $\omega = 0$, we obtain, as in Fermi-liquid theory, $I_2 = -i \int_{-\infty}^{\infty} d\omega (d/d\omega)\Phi_{\mathrm{LW}} = 0$. Thus, the entire contribution to I_2 arises from the regularization of singularity near $\omega = 0$. We can therefore evaluate I_2 using Eq. (5.2b) for Σ, the regularization in Eq. (5.16), and the low-frequency spectral density in Eq. (5.12). We ignore the high-frequency contribution to I_2. The explicit evaluation of the integral is somewhat involved (Georges, Parcollet, and Sachdev, 2001; Gu *et al.*, 2020). The result can be guessed, however, from a heuristic argument (Georges, Parcollet, and Sachdev, 2001), which can also be generalized to the SYK model with q-fermion interactions (Davison *et al.*, 2017). The low-energy contribution to I_2 involves a product of G and Σ and must be a homogeneous polynomial of degree 4 in the two coefficients that enter the low-energy behavior of G [Eq. (5.8)]. Using particle-hole symmetry and imposing the absence of singularity as $\theta \to \pm\pi/4$, one sees that only the combination $C^4[\sin^3(\pi/4+\theta)\times \sin(\pi/4-\theta) - \sin^3(\pi/4-\theta)\sin(\pi/4+\theta)] \propto \sin 2\theta$ is allowed. The proportionality coefficient is fixed by imposing the

condition that $\mathcal{Q} = +1$ for $\theta = -\pi/4$ in Eq. (5.15). Indeed, the explicit evaluation yields

$$I_2 = -\frac{\sin(2\theta)}{4}. \qquad (5.20)$$

Combining Eqs. (5.15), (5.18), and (5.20), we obtain our generalized Luttinger theorem (Georges, Parcollet, and Sachdev, 2001; Davison *et al.*, 2017; Gu *et al.*, 2020),

$$\mathcal{Q} = \frac{1}{2} - \frac{\theta}{\pi} - \frac{\sin(2\theta)}{4}. \qquad (5.21)$$

Equation (5.21) evaluates to the limiting values $\mathcal{Q} = 1, 0$ for the limiting values of $\theta = -\pi/4, \pi/4$ in Eq. (5.4) and decreases monotonically in between. $\mathcal{Q}$ is also a monotonically decreasing function between the limits of $-\infty < \mathcal{E} < \infty$ via Eq. (5.10).

All our results thus far have been obtained by an analytic analysis of the low-energy behavior. A numerical analysis is needed to ensure that such low-energy solutions have high-energy continuations that also obey Eqs. (5.2a) and (5.2b). Such analyses show that complete solutions exist only for a range of values around $\mathcal{Q} = 1/2$ (Azeyanagi, Ferrari, and Massolo, 2018); for values of $\mathcal{Q}$ close to $0, 1$, there is phase separation into the trivial $\mathcal{Q} = 0, 1$ state and densities closer to half filling. However, this conclusion is only for the specific microscopic Hamiltonian in Eq. (5.1): other Hamiltonians, with additional q-fermion terms (see Appendix E) with $q > 4$, could have solutions with the same low-energy behavior as previously described for a wider range of $\mathcal{Q}$ because these higher q terms are irrelevant at low energy.

C. Nonzero temperatures

It turns out to be possible to extend the solutions for the $T = 0$ Green's functions obtained thus far to nonzero $T \ll U$ by employing a subtle argument involving conformal invariance. However, we first take a simple approach to look for a solution directly from Eqs. (5.2a) and (5.2b) and show that we can guess a solution.

We initially limit consideration to the particle-hole symmetric case with $\mathcal{Q} = 1/2$ and $\theta = 0$. We use the similarity to multichannel Kondo problems (Parcollet *et al.*, 1998) to generalize the τ dependence of the Green's function in Eq. (5.7) to (Parcollet and Georges, 1999)

$$G(\tau) = B \, \mathrm{sgn}(\tau) \left| \frac{\pi T}{\sin(\pi T \tau)} \right|^{1/2}, \qquad T, |\tau|^{-1} \ll U, \qquad (5.22)$$

where B is a T-independent constant. Making contact with the notations of Sec. V.A, we have $-B = C\Gamma(1/2)\sin(\pi/4)/\pi = C/\sqrt{2\pi}$, with $C^4 = \pi/U^2$ for this case with $\theta = 0$. Note that Eq. (5.22) reduces to Eq. (5.7) for $1/U \ll |\tau| \ll 1/T$. The self-energy is then

$$\Sigma(\tau) = U^2 B^3 \mathrm{sgn}(\tau) \left| \frac{\pi T}{\sin(\pi T \tau)} \right|^{3/2}, \qquad T, |\tau|^{-1} \ll U.$$

Taking Fourier transforms, we have the following as a function of the Matsubara frequency ω_n:

$$G(i\omega_n) = [iB]\frac{T^{-1/2}\Gamma(1/4 + \omega_n/2\pi T)}{\Gamma(3/4 + \omega_n/2\pi T)}, \qquad (5.23a)$$

$$\Sigma_{\text{sing}}(i\omega_n) = [i4\pi U^2 B^3]\frac{T^{1/2}\Gamma(3/4 + \omega_n/2\pi T)}{\Gamma(1/4 + \omega_n/2\pi T)}, \qquad (5.23b)$$

where we have subtracted $\Sigma(\omega = 0, T = 0)$ in $\Sigma_{\text{sing}}(i\omega_n)$. Now the singular part of Dyson's equation is

$$G(i\omega_n)\Sigma_{\text{sing}}(i\omega_n) = -1. \qquad (5.24)$$

The Γ functions in Eqs. (5.23a) and (5.23b) appear with just the right arguments so that they can obey Eq. (5.24) for all ω_n, and the amplitude indeed obeys $4\pi U^2 B^4 = 1$.

A deeper understanding of the origin of Eq. (5.22) and its generalization to the particle-hole asymmetric case can be obtained by analyzing the low-energy limit of the original saddle-point equations (5.2a) and (5.2b). These equations are characterized by a large set of emergent symmetries, which we describe in Appendix A. The final result for the Green's function in imaginary time away from the particle-hole symmetric point is

$$G(\tau) = -C\frac{e^{-2\pi\mathcal{E}T\tau}}{\sqrt{1 + e^{-4\pi\mathcal{E}}}}\left(\frac{T}{\sin(\pi T\tau)}\right)^{1/2} \qquad (5.25)$$

for $0 < \tau < 1/T$. Equation (5.25) can be extended to all real τ using the Kubo-Martin-Schwinger (KMS) condition [Eq. (A5)]. Performing a Fourier transform and analytically continuing to real frequencies leads one as follows to the Green's function (Parcollet and Georges, 1999; Sachdev, 2015):

$$G(\omega + i0^+) = \frac{-iCe^{-i\theta}}{(2\pi T)^{1/2}}\frac{\Gamma(1/4 + i\mathcal{E} - i\omega/2\pi T)}{\Gamma(3/4 + i\mathcal{E} - i\omega/2\pi T)}. \qquad (5.26)$$

We show a plot of the imaginary part of the Green's function in Fig. 8.

For later comparison with other models, we note that these results imply that the singular part of the electron self-energy in Eq. (5.23b) obeys the scaling form

$$\Sigma(\omega, T) = U^{1/2}T^{1/2}\Phi\left(\frac{\hbar\omega}{k_B T}\right), \qquad (5.27)$$

where Φ is a universal scaling function with a known dependence on the particle-hole asymmetry parameter $\mathcal{E}$.

The universal dependence of the self-energy on the Planckian ratio ($\hbar\omega/k_B T$) implies the absence of electronic quasiparticles (Sachdev, 1999): the characteristic lifetime of the excitations $\sim\hbar/k_B T$ is of the same order as their energy $\sim\hbar\omega$, so quasiparticles are not well defined. This behavior is different from the random-matrix model studied in Sec. IV.B, where the self-energy was negligible at low T.

A Planckian lifetime has also been obtained by nonequilibrium studies of SYK models, which display a recovery of
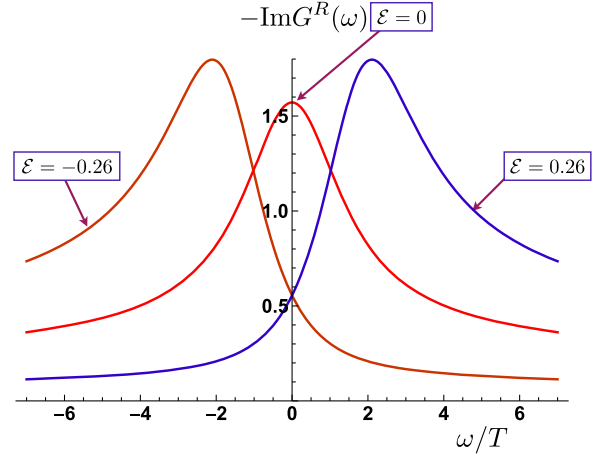

FIG. 8.   Electron spectral density in the SYK model, obtained from imaginary part of Eq. (5.26).

thermal Green's functions in a time that is independent of U and proportional to the inverse final temperature (Eberlein *et al.*, 2017; Kourkoulou and Maldacena, 2017; Almheiri, Milekhin, and Swingle, 2019; Bhattacharya, Jatkar, and Sorokhaibam, 2019; Dhar *et al.*, 2019; Zhang, 2019; Rossini *et al.*, 2020; Lensky and Qi, 2021; Samui and Sorokhaibam, 2021). For closely related and complementary insights, see Sonner and Vielma (2017), Haque and McClarty (2019), Haldar *et al.* (2020), Kuhlenkamp and Knap (2020), Bandyopadhyay *et al.* (2021), Cheipesh *et al.* (2021), and Larzul and Schiró (2021).

D. Computation of the $T \to 0$ entropy

We have now presented detailed information on the nature of the Green's function of the SYK model at low T. We proceed to use this information to compute some key features of the low-T thermodynamics.

We first establish some properties of the behavior of the chemical potential, μ as $T \to 0$ at a fixed $\mathcal{Q}$. Recall that for the random-matrix model, and more generally for any Fermi liquid, there was a $\sim T^2$ correction to the chemical potential that depended upon the derivative of the density of single-particle states. For the SYK model, the leading correction is much stronger: the correction $\sim T$, which is universally related to parameters in the Green's function (Georges, Parcollet, and Sachdev, 2001).

A simple way to determine the linear-T dependence of μ is to examine the particle-hole asymmetry of the Green's function at $T > 0$. From Eqs. (5.9) and (5.25) we determine that this is given by the ratio

$$\lim_{T \to 0}\frac{G(\tau)}{G(1/T - \tau)} = e^{2\pi\mathcal{E}}, \qquad (5.28)$$

where the limit is taken at a fixed $\tau \gg 1/U$. We now use a crude picture of the low-energy physics and imagine that all the low-energy degrees of freedom are essentially at zero energy compared to U. Thus, we compare Eq. (5.28) to the following corresponding ratio for a zero energy fermion whose chemical potential has been shifted by $\delta\mu$:

$$\frac{G_0(\tau)}{G_0(1/T - \tau)} = e^{-(\delta\mu)(1/T - 2\tau)}. \qquad (5.29)$$

From this comparison, we conclude that there is a linear-in-T dependence of the chemical potential that keeps the particle-hole asymmetry fixed as $T \to 0$:

$$\mu - \mu_0 = \delta\mu = -2\pi\mathcal{E}T + \text{terms vanishing as } T^p \text{ with } p > 1, \qquad (5.30)$$

with μ_0 a nonuniversal constant. Note that the density of the zero energy fermion $= 1/(e^{-\delta\mu/T} + 1)$ remains fixed as $T \to 0$, so Eq. (5.30) applies at fixed $\mathcal{Q}$.

A more formal analysis (Parcollet *et al.*, 1998; Georges, Parcollet, and Sachdev, 2001; Sachdev, 2015) leading to the same result for the T dependence of μ relates the long-time conformal Green's function (valid for $\tau \gg 1/U$) to its short-time behavior. In particular, at $|\omega_n| \gg U$ we have

$$G(i\omega_n) = \frac{1}{i\omega_n} - \frac{\mu}{(i\omega_n)^2} + \cdots , \qquad (5.31)$$

which implies the following for the spectral density of the Green's function $\rho(\Omega)$:

$$\mu = -\int_{-\infty}^{\infty} d\Omega\, \Omega\rho(\Omega), \qquad (5.32)$$

which makes it evident that μ depends only upon the particle-hole asymmetric part of the spectral density. Next, using the spectral relations, we can relate the Ω integrals to the derivative of the imaginary-time correlator

$$\mu = -\partial_\tau G(\tau = 0^+) - \partial_\tau G(\tau = (1/T)^-). \qquad (5.33)$$

We pull out an explicitly particle-hole asymmetric part of $G(\tau)$ by defining

$$G(\tau) \equiv e^{-2\pi\mathcal{E}T\tau} G_c(\tau), \qquad 0 < \tau < \frac{1}{T}, \qquad (5.34)$$

where G_c is given by a particle-hole symmetric conformal form at low T and low ω. We then obtain

$$\mu = 2\pi\mathcal{E}T\{G(\tau = 0^+) + G[\tau = (1/T)^-]\}$$
$$+ \text{terms dependent on } G_c$$
$$= -2\pi\mathcal{E}T + \text{terms dependent on } G_c.$$

It can be shown that all the terms dependent upon G_c have a T dependence that is weaker than linear in T provided that $\mathcal{Q}$ is held fixed. Hence, we obtain Eq. (5.30).

Now we can deduce the T dependence of the entropy using the Maxwell relation

$$\left(\frac{\partial\mu}{\partial T}\right)_\mathcal{Q} = -\frac{1}{N}\left(\frac{\partial S}{\partial\mathcal{Q}}\right)_T, \qquad (5.35)$$

where the $1/N$ term is needed because we define S to be the total extensive entropy, so we must use the total number $N\mathcal{Q}$ in the Maxwell relation. Applying this to Eq. (5.30), we obtain

$$\frac{1}{N}\left(\frac{\partial S}{\partial\mathcal{Q}}\right)_T = 2\pi\mathcal{E} \neq 0 \quad \text{as } T \to 0. \qquad (5.36)$$

In Sec. V.B, we obtained an "extended" Luttinger relationship between the density $\mathcal{Q}$ and the particle-hole asymmetry parameter $\mathcal{E}$. Assuming that $S = 0$ at $\mathcal{Q} = 0$, we can now integrate Eq. (5.36) to obtain for the entropy S as (Georges, Parcollet, and Sachdev, 2001)

$$S(T \to 0) = N\mathcal{S}, \qquad \mathcal{S} = 2\pi\int_0^\mathcal{Q} d\tilde{\mathcal{Q}}\mathcal{E}(\tilde{\mathcal{Q}}). \qquad (5.37)$$

Equation (5.37) can be rewritten using Eqs. (5.10) and (5.21) in the following parametric form:

$$\mathcal{S}(\Theta) = \int_{-\pi/4}^\Theta d\theta \ln\frac{\sin(\pi/4 + \theta)}{\sin(\pi/4 - \theta)}\frac{\partial\mathcal{Q}}{\partial\theta}, \qquad (5.38)$$

$$\mathcal{Q}(\Theta) = \frac{1}{2} - \frac{\Theta}{\pi} - \frac{\sin 2\Theta}{4}. \qquad (5.39)$$

Figure 9 displays the entropy density versus $\mathcal{Q}$ obtained from Eq. (5.39).

The noteworthy feature of this result is that the entropy S is extensive, i.e., proportional to N, as $T \to 0$. Specifically, we have

$$\lim_{T \to 0}\lim_{N \to \infty}\frac{S}{N} \neq 0. \qquad (5.40)$$

The order of limits is crucial here; the order of limits defines the zero-temperature entropy density, in which the thermodynamic limit is taken before the zero-temperature limit. If we had taken the other order of limits, we would have obtained the ground state entropy density, which does indeed vanish.

E. Corrections to scaling

All of our low-energy results for the SYK model thus far have been obtained in a scaling limit in which the $i\omega_n$ term in the Green's function in Eq. (5.2a) was neglected, as discussed
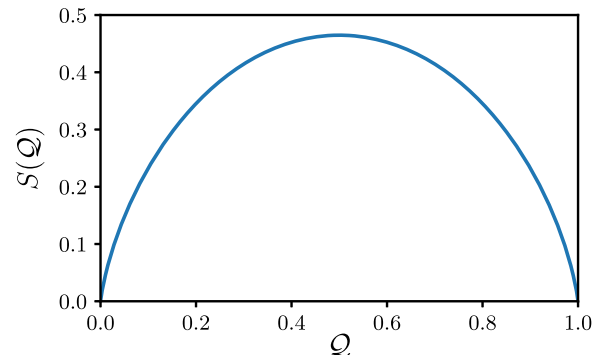

FIG. 9. $T = 0$ entropy density $\mathcal{S}$ vs $\mathcal{Q}$. From Georges, Parcollet, and Sachdev, 2001.

prior to Eq. (5.13). This section considers the structure of the corrections that arise when this $i\omega_n$ term is included. We emphasize that all of the computations here are in the $N = \infty$ limit, and we are computing corrections to the low-energy approximation to the saddle-point equations. A significant result of our computations will be T-dependent corrections to the entropy in Eq. (5.37); these will continue to be proportional to N. We consider finite-N corrections to such saddle-point results in Sec. V.F.

To understand the structure of the possible corrections, we postulate that the low-energy corrections can be computed from an effective action of the following form:

$$I = I_* + \sum_h g_h \int_0^\beta d\tau \, O_h(\tau), \qquad (5.41)$$

where O_h are a set of scaling operators with scaling dimension h. One of our tasks in this section is to determine the possible values of h, and we accomplish this shortly. The term I_* is the leading critical theory that leads to the results described thus far, in particular, to the Green's function in Eqs. (5.3) and (5.26) and the entropy in Eq. (5.37). We normalize the perturbing operators using the two-point correlator

$$\langle O_h(\tau)O_h(0)\rangle = \frac{1}{|\tau|^{2h}}. \qquad (5.42)$$

The coefficient g_h is then fully specified. In general, g_h are a set of nonuniversal numbers of the order of U^{1-h} whose precise values depend upon the details of the underlying theory on possible higher-order fermion interaction terms that we can add to the SYK Hamiltonian.

Given Eq. (5.41), we can easily estimate the form of the corrections to the grand potential $\Omega(T)$. We expect that

$$\langle O_h\rangle_{T*} = \Omega_h T^h, \qquad (5.43)$$

where the expectation value is evaluated at a temperature T in I_* and the T dependence follows from the scaling dimension of O_h. Taking the expectation value of the action, we obtain

$$\Omega(T) = E_0 - N\mathcal{S}T + \sum_h g_h\Omega_h T^h, \qquad (5.44)$$

where E_0 is the ground state energy, $\mathcal{S}$ is the entropy in Eq. (5.37), and the set of coefficients Ω_h were specified in Eq. (5.43). Similarly, we can write the corrections to the Green's function in Eq. (5.7) from the O_h perturbations as

$$G(\tau) = G_*(\tau)\left(1 + \sum_h \frac{g_h\alpha_h}{|\tau|^{h-1}}\right), \qquad (5.45)$$

where we now use G_* to denote the leading-order result in Eq. (5.22) and we have used $\dim[g_h] = 1 - h$ from Eq. (5.41). Here we limit ourselves to the particle-hole symmetric case with $\theta = 0$, $\mu = 0$, and $\mathcal{E} = 0$; see Tikhanovskaya *et al.* (2021a) for the general case. The coefficients Ω_h and α_h are universal dimensionless numbers.

Our remaining task is to determine the allowed values of h. We consider only (Gross and Rosenhaus, 2017; Klebanov and Tarnopolsky, 2017; Klebanov, Popov, and Tarnopolsky, 2018) the "antisymmetric" operators O_h that are represented at short times by $O_{h_n} = c_i^\dagger \partial_\tau^{2n+1} c_i$, with $n = 0, 1, 2, \ldots$. The needed information is contained in the three-point functions

$$v_h(\tau_1, \tau_2, \tau_0) = \langle c(\tau_1)c^\dagger(\tau_2)O_h(\tau_0)\rangle. \qquad (5.46)$$

In the large-N limit, this three-point function obeys the integral equation shown in Fig. 10. In the long-time scaling limit, we can drop the bare first term on the right-hand side, and Fig. 10 then reduces to the eigenvalue equation (Gross and Rosenhaus, 2017)

$$k(h)v(\tau_1, \tau_2, \tau_0) = \int d\tau_3 d\tau_4 K(\tau_1, \tau_2; \tau_3, \tau_4)v_h(\tau_3, \tau_4, \tau_0), \qquad (5.47)$$

where the kernel K is

$$K(\tau_1, \tau_2; \tau_3, \tau_4) = -3U^2 G_*(\tau_{13})G_*(\tau_{24})G_*(\tau_{34})^2, \qquad (5.48)$$

with $\tau_{ij} \equiv \tau_i - \tau_j$, and we have introduced an eigenvalue $k(h)$ by hand that must obey

$$k(h) = 1. \qquad (5.49)$$

For our purposes, it is sufficient to solve Eq. (5.47) in the limit $\tau_0 \to \infty$. We can then use the operator product expansion to write

$$c(\tau_1)c^\dagger(\tau_2) \sim \text{sgn}(\tau_{12})\sum_h \frac{c_h}{|\tau_{12}|^{1/2-h}}O_h(\tau_1) + \cdots \qquad (5.50)$$

for some constants c_h, where the sum over h now includes the identity operator with $h = 0$. Inserting Eq. (5.50) into Eq. (5.46), we conclude that $v \sim \text{sgn}(\tau_{12})/|\tau_{12}|^{1/2-h}$ as $\tau_0 \to \infty$. Equation (5.47) then yields the following eigenvalue:

$$k(h) = -\frac{3\tan(\pi h/2 - \pi/4)}{2h - 1}. \qquad (5.51)$$

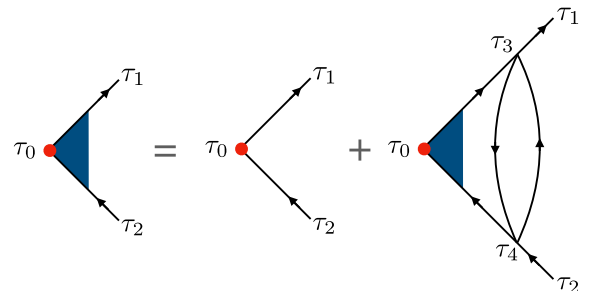FIG. 10. Large-N equation satisfied by the three-point correlator in Eq. (5.46). The red circles represent the operator O_h.

The solution of Eqs. (5.49) and (5.51) finally yields the needed values of h. There are an infinite number of solutions, and the lowest values are

$$h = 2, \quad 3.773\,54\ldots, \quad 5.567\,946\ldots, \quad 7.631\,97\ldots. \quad (5.52)$$

Only the lowest value $h = 2$ is an integer, and all higher values are irrational numbers.

We have a particular interest here in the $h = 2$ operator. This plays a special role in the finite-N fluctuations and eventually leads to a violation of scaling, as discussed in Sec. V.F. At $N = \infty$, it is also the lowest dimension operator, and thus yields the most important corrections to Eqs. (5.44) and (5.45). For the entropy at a fixed $\mathcal{Q}$, we can take a derivative of Eq. (5.44) and write the correction to Eq. (5.37) as (Maldacena and Stanford, 2016; Kitaev and Suh, 2018; Gu *et al.*, 2020)

$$S(T \to 0, \mathcal{Q}) = N[\mathcal{S} + \gamma T], \quad (5.53)$$

where $\gamma \sim 1/U$ is the nonuniversal coefficient of the linear-in-T specific heat at a fixed $\mathcal{Q}$, a quantity familiar from Fermi-liquid theory. The SYK non-Fermi liquid has a similar specific heat, but note the presence of the residual entropy $\mathcal{S}$ that vanishes in a Fermi liquid. We see in Sec. V.F that γ also appears to be the coefficient of the Schwarzian effective action for finite-N fluctuations.

F. Finite-N fluctuations

This section turns to a theory of the fluctuations about the previously examined large-N saddle point. We focus on the corrections to the result for the entropy in Eqs. (5.37) and (5.53). The dominant finite-N corrections arise from a universal, exactly soluble theory for the low-energy fluctuations about the large-N saddle point. Along the way, we also obtain an example of the corrections discussed in Sec. V.E associated with irrelevant operators in the $N = \infty$ saddle-point theory. This will lead to the T-dependent correction in Eq. (5.53) and allow us to identify γ with a coupling in the effective action.

We begin with a path-integral representation of the underlying SYK Hamiltonian (5.1a). To treat the random couplings, we need to perform a quenched average using the replica method. However, the strongly self-averaging properties that we later compute do not depend upon the replica structure, so we will simply ignore these technicalities and work directly with the averaged theory. Thus, after averaging over the $U_{ijk\ell}$ the path integral becomes

$$\bar{\mathcal{Z}} = \int \mathcal{D}c_i(\tau) \exp\left[-\sum_i \int_0^\beta d\tau\, c_i^\dagger \left(\frac{\partial}{\partial \tau} - \mu\right) c_i \right.$$
$$\left. + \frac{U^2}{4N^3} \int_0^\beta d\tau\, d\tau' \left|\sum_i c_i^\dagger(\tau) c_i(\tau')\right|^4\right], \quad (5.54)$$

where $\beta = 1/T$. We now introduce the following "trivial" identity in the path integral,

$$1 = \int \mathcal{D}G(\tau_1, \tau_2) \mathcal{D}\Sigma(\tau_1, \tau_2)$$
$$\times \exp\left[-N \int_0^\beta d\tau_1 d\tau_2 \Sigma(\tau_1, \tau_2) \Big(G(\tau_2, \tau_1)\right.$$
$$\left. + \frac{1}{N}\sum_i c_i(\tau_2) c_i^\dagger(\tau_1)\Big)\right] \quad (5.55)$$

and interchange the orders of integration. The partition function can then be written as follows as a $G - \Sigma$ theory, a path integral with an action $I[G, \Sigma]$ for the Green's function, and a self-energy analogous to a Luttinger-Ward functional (Georges, Parcollet, and Sachdev, 2001; Maldacena and Stanford, 2016; Kitaev and Suh, 2018):

$$\bar{\mathcal{Z}} = \int \mathcal{D}G(\tau_1, \tau_2) \mathcal{D}\Sigma(\tau_1, \tau_2) \exp(-NI[G, \Sigma])$$

$$I[G, \Sigma] = -\ln \det\left[(\partial_{\tau_1} - \mu)\delta(\tau_1 - \tau_2) + \Sigma(\tau_1, \tau_2)\right]$$
$$- \text{Tr}(\Sigma \cdot G) - \frac{U^2}{4}\text{Tr}(G^2 \cdot G^2). \quad (5.56)$$

We have integrated over the fermions to obtain the ln det term. This is an exact representation of the averaged partition function. Notice that it involves G and Σ as bilocal fields that depend upon two times, and we have introduced the following compact notation for such fields:

$$\text{Tr}(f \cdot g) \equiv \int d\tau_1 d\tau_2 f(\tau_2, \tau_1) g(\tau_1, \tau_2). \quad (5.57)$$

See Appendix A for a discussion of the symmetries of the bilocal fields, where we also show that after ignoring the explicit time derivative in Eq. (5.56) the action is invariant under time reparametrization and gauge symmetries [Eq. (A2c)].

The path integral in Eq. (5.56) is complicated to evaluate in general. We now make a low-energy approximation by integrating only along directions in the vast (G, Σ) space where the variation $S[G, \Sigma]$ is small at low energies (Maldacena and Stanford, 2016; Kitaev and Suh, 2018). Given the unimportance of ∂_τ in Eq. (5.56) and the resulting symmetries of the action, a solid conclusion is that we need only perform the path integral along trajectories where the Green's function obeys Eq. (B2) (and a similar approach for the self-energy). In this manner, we formally convert the $G - \Sigma$ path integral into a path integral over the time reparametrization $f(\tau)$ and the gauge transformation $\phi(\tau)$ as follows (Maldacena and Stanford, 2016; Davison *et al.*, 2017; Kitaev and Suh, 2018; Gu *et al.*, 2020):

$$\bar{\mathcal{Z}} \approx e^{-E_0/T + N\mathcal{S}} \int \mathcal{D}f(\tau)\mathcal{D}\phi(\tau) \exp\left(-I_{\text{eff}}[f, \phi]\right), \quad (5.58)$$

where $E_0 \propto N$ is the ground state energy (including the $-\mu\mathcal{Q}N$ contribution). We soon deduce the form of $I_{\text{eff}}[f, \phi]$ from symmetry arguments. But before we turn to that, we note that the combination of Eqs. (B2) and (5.58) also yield the most important contributions to the fluctuation corrections to the following Green's function:

$$G(\tau_1 - \tau_2) = \frac{e^{-E_0/T + N\mathcal{S}}}{\bar{\mathcal{Z}}} \int \mathcal{D}f(\tau)\mathcal{D}\phi(\tau)$$

$$\times \exp\left(-I_{\text{eff}}[f, \phi]\right)[f'(\tau_1)f'(\tau_2)]^{1/4}$$

$$\times G_c(f(\tau_1) - f(\tau_2))e^{i\phi(\tau_1) - i\phi(\tau_2)}, \tag{5.59}$$

where the conformal saddle-point Green's function $G_c(\tau)$ is given by Eq. (5.25).

Now our task is to determine the action $I_{\text{eff}}[f, \phi]$ and then evaluate the path integrals in Eqs. (5.58) and (5.59). It turns out that the partition function for the free energy in Eq. (5.58) can be evaluated exactly. The consequences of the path integral in Eq. (5.59) for the long-time behavior of $G(\tau)$ have also been investigated (Kitaev, 2015; Bagrets, Altland, and Kamenev, 2016, 2017; Kitaev and Suh, 2018; Altland, Bagrets, and Kamenev, 2019b; Kruchkov *et al.*, 2020; Kobrin *et al.*, 2021): they lead to a violation of scaling at times of the order of N/U, but we do not describe this further here.

The form of $I_{\text{eff}}[f, \phi]$ is strongly constrained by the requirement that I vanish for the case where $f(\tau)$ and $\phi(\tau)$ are given by Eq. (B3). This follows immediately from the fact that Eq. (B3) leads to no changes in the form of the saddle-point Green's function when it is inserted into Eq. (B2). As the action was originally a functional of the Green's function, it can also not change. The action $I_{\text{eff}}[f, \phi]$ with the smallest number of derivatives that satisfies this requirement is (Maldacena and Stanford, 2016; Davison *et al.*, 2017; Kitaev and Suh, 2018; Gu *et al.*, 2020)

$$I_{\text{eff}}[f, \phi] = \frac{NK}{2}\int_0^\beta d\tau\left(\frac{\partial\phi}{\partial\tau} + i(2\pi\mathcal{E}T)\frac{\partial f}{\partial\tau}\right)^2$$

$$- \frac{N\gamma}{4\pi^2}\int_0^\beta d\tau\{\tan[\pi Tf(\tau)], \tau\}. \tag{5.60}$$

The curly brackets in Eq. (5.60) represent the following Schwarzian derivative:

$$\{g, \tau\} \equiv \frac{g'''}{g'} - \frac{3}{2}\left(\frac{g''}{g'}\right)^2. \tag{5.61}$$

Equation (5.61) has the defining property that

$$\left\{\frac{a\tau + b}{c\tau + d}, \tau\right\} = 0, \tag{5.62}$$

which ensures that $I_{\text{eff}}[f, \phi]$ vanishes for Eq. (B3). [We note that there are coupled SYK models that are not described by a Schwarzian effective action (Maldacena, Stanford, and Yang, 2016; Milekhin, 2021).]

For the origin of $f(\tau)$ and $\phi(\tau)$ as time reparametrization and gauge transformations of the Green's function, we must also place some constraints on the nature of the path integral over them. The function $f(\tau)$ must be monotonic and must obey

$$f(\tau + \beta) = f(\tau) + \beta. \tag{5.63}$$

Moreover, we should sum over all possible phase windings with

$$\phi(\tau + \beta) = \phi(\tau) + 2\pi n, \tag{5.64}$$

where n is an integer.

The action in Eq. (5.60) has two dimensionful coupling constants K and γ. By dimensional analysis, we can see that $K \sim \gamma \sim 1/U$, the only energy scale at $T = 0$. Determining the precise values of K and γ is not simple and requires a numerical study of the higher energy properties of the SYK model. We now relate the values of K and γ to thermodynamic observables of the $N = \infty$ theory, and a numerical computation of these observables is usually the simplest way to determine K and γ.

At $T = 0$, the action for ϕ represents the path integral of a particle of mass NK moving on a ring of circumference 2π. Thus, the energy levels are $\ell^2/2NK$, where the integer ℓ measures the total fermion number. With a chemical potential shift $\delta\mu$, the energy levels will shift as $\ell^2/2NK - \delta\mu\ell$. From the optimum value of this function for different ℓ, we conclude that K is simply the compressibility

$$K = \frac{d\mathcal{Q}}{d\mu}, \qquad T = 0. \tag{5.65}$$

Turning to the value of γ, note that the action $I_{\text{eff}}[f, \phi]$ does not vanish at the $N = \infty$ saddle point $f(\tau) = \tau$. Evaluating Eq. (5.60) for this value of $f(\tau)$ and setting $\phi = 0$, we obtain the following grand potential at $N = \infty$ for small $T > 0$:

$$\Omega(T) = E_0 - N\mathcal{S}T - \tfrac{1}{2}N(\gamma + 4\pi^2\mathcal{E}^2K)T^2. \tag{5.66}$$

Taking the T derivative, we obtain the following leading low-temperature correction to the entropy in Eq. (5.37):

$$S(T \to 0, \mu) = N[\mathcal{S} + (\gamma + 4\pi^2\mathcal{E}^2K)T]. \tag{5.67}$$

As previously denoted, Eq. (5.67) is the entropy at a fixed chemical potential. We can use standard thermodynamic relations to compute the entropy at fixed $\mathcal{Q}$ using the thermodynamic relations (5.36) and (5.65) and obtain Eq. (5.53). Indeed, the coefficient of the Schwarzian was chosen so that the entropy would obey the form in Eq. (5.53). The T-dependent corrections in Eqs. (5.67) and (5.53) are proportional to N, and thus constitute corrections from irrelevant operators that were studied in Sec. V.E, and identify the Schwarzian as representing the corrections arising from the $h = 2$ operator.

In the remainder of our discussion of the SYK model, we evaluate the path integral in Eq. (5.58), and thus obtain the finite-N corrections to the free energy and entropy in Eqs. (5.66) and (5.67). These results also allow us to compute the many-particle density of states $D(E)$.

A key observation in the evaluation of Eq. (5.58) is that the path integrals factorize. To establish this, we use the boundary conditions in Eqs. (5.63) and (5.64) to parametrize

$$f(\tau) = \tau + \epsilon(\tau),$$
$$\phi(\tau) = 2\pi n T\tau + \bar{\phi}(\tau), \tag{5.68}$$

where the "winding number" n is an integer and ϵ and $\bar{\phi}$ are periodic functions of τ with period β. In the first term in Eq. (5.60), we can absorb ϵ with a shift in $\bar{\phi}$; the remaining dependence on ϵ is then only in the Schwarzian. In this manner, we can write Eq. (5.58) as (Gu *et al.*, 2020)

$$\bar{\mathcal{Z}} = e^{-E_0/T} \mathcal{Z}_\mathcal{Q} \mathcal{Z}_{\text{Sch}}. \tag{5.69}$$

We evaluate $\mathcal{Z}_\mathcal{Q}$ and $\mathcal{Z}_{\text{Sch}}$ in Secs. V.F.1 and V.F.2.

1. Rotor path integral

The partition function $\mathcal{Z}_\mathcal{Q}$ represents fluctuations in the total charge on the SYK dot. It is expressed as follows as a path integral over the coordinates of a particle moving on a unit circle (a "rotor"):

$$\mathcal{Z}_\mathcal{Q} = \left(\sum_{n=-\infty}^{\infty} \exp\left[-2\pi^2 NKT(n+i\mathcal{E})^2 \right] \right)$$
$$\times \int \frac{\mathcal{D}\bar{\phi}}{\text{U}(1)} \exp\left[-\frac{NK}{2} \int_0^\beta d\tau [\bar{\phi}'(\tau)]^2 \right]. \tag{5.70}$$

The second term is simply the imaginary-time amplitude for a "free particle" of mass NK to return to its starting point in a time β divided by the volume (2π) of the U(1) group [because a τ-independent ϕ does not make any changes to the Green's function in Eq. (B2)]. Thus, we obtain the following expression for $\mathcal{Z}_\mathcal{Q}$ that is useful at temperatures $T \gg 1/NK$:

$$\mathcal{Z}_\mathcal{Q} = \left(\sum_{n=-\infty}^{\infty} \exp\left[-2\pi^2 NKT(n+i\mathcal{E})^2 \right] \right) \sqrt{\frac{NKT}{2\pi}}. \tag{5.71}$$

For lower temperatures ($T \ll 1/NK$), we can apply the Poisson summation formula to Eq. (5.71) and obtain

$$\mathcal{Z}_\mathcal{Q} = \frac{1}{2\pi} \sum_{p=-\infty}^{\infty} \exp\left[-\frac{p^2}{2NKT} - 2\pi\mathcal{E}p \right]. \tag{5.72}$$

We note, however, that both Eqs. (5.71) and (5.72) are convergent and exact at all T (Gu *et al.*, 2020).

The physical interpretation of Eq. (5.72) is especially transparent. It describes a quantum dot with equilibrium charge $N\mathcal{Q}$, which has fluctuations to states with charge $N\mathcal{Q} + p$. The energy of a charge p fluctuation is determined by a "capacitance" NK, and a temperature-dependent chemical potential $-2\pi\mathcal{E}T$. Note that the chemical potential shift is exactly what appears in Eq. (5.30), and indeed the present analysis can be viewed as another derivation of Eq. (5.30). Recall that the key relation for the entropy in Eq. (5.59) followed after the application of a Maxwell thermodynamic relation to Eq. (5.30).

The previous physical interpretation also indicates that in a fixed $\mathcal{Q}$ ensemble we should take $\mathcal{Z}_\mathcal{Q} = 1$. That turns out to be not quite correct, and a more careful analysis of finite-N corrections shows that $\mathcal{Z}_\mathcal{Q} \sim 1/N^2$.

2. Schwarzian path integral

The other component of Eq. (5.69) is the Schwarzian path integral

$$\mathcal{Z}_{\text{Sch}} = e^{NS} \int \frac{\mathcal{D}f(\tau)}{\text{SL}(2,\text{R})} \exp\left[\frac{N\gamma}{4\pi^2} \int_0^\beta d\tau \{\tan[\pi T f(\tau)], \tau\} \right]. \tag{5.73}$$

We have normalized the path integral by the infinite volume of the noncompact group $\text{SL}(2,\text{R})$ because, as we argued earlier, the action must vanish under $\text{SL}(2,\text{R})$ transformations. This quotient will be crucial in obtaining a well-defined answer.

Stanford and Witten (2017) showed that the path integral in Eq. (5.73) can be evaluated exactly. The key to their result is the fact that a Gaussian approximation to the path integral is in fact exact. We exploit this by simply evaluating Eq. (5.73) in the Gaussian approximation.

To this end, we expand the Schwarzian action in dimensional Fourier coefficients of $\epsilon(\tau)$ in Eq. (5.68) as

$$\epsilon(\tau) = \frac{1}{T} \sum_{n=-\infty}^{\infty} \epsilon_n e^{-2\pi i n T \tau} \tag{5.74}$$

and obtain

$$I_{\text{eff}}[\epsilon] = -\frac{N\gamma T}{2} + 2\pi^2 N\gamma T \sum_n n^2(n^2-1)|\epsilon_n|^2. \tag{5.75}$$

Now notice that $I_{\text{eff}}[\epsilon]$ vanishes for the three smallest Matsubara frequencies $\omega_n = 0, \pm 2\pi T$. Indeed, the action was designed to vanish for any time reparametrization that belongs to $\text{SL}(2,\text{R})$, a three-dimensional noncompact space. And here we have discovered three Fourier components that cause no variation in the action to second order: we can identify the frequency components at $n = 0, \pm 1$ as the infinitesimal limit of the $\text{SL}(2,\text{R})$ transformations. At Gaussian order, the path integral over these action-free normal modes therefore cancels against the volume of $\text{SL}(2,\text{R})$ in Eq. (5.73). Actually, this cancellation also happens for large $\text{SL}(2,\text{R})$ transformations, but we do not prove that here.

Performing the Gaussian integral over the remaining modes, we obtain the following for the logarithm of the partition function:

$$\ln \mathcal{Z}_{\text{Sch}} = NS + \frac{N\gamma T}{2} - \frac{1}{2} \sum_{n\neq 0,\pm 1} \ln\left[2\pi^2 N\gamma T n^2(n^2-1) \right]. \tag{5.76}$$

The sum over the Matsubara frequency ω_n is divergent, and should be cut off at a frequency $|\omega_n| \sim U$, above which our low-energy Schwarzian theory does not apply. We describe the regulation of the divergence in Appendix D. There is a contribution $\sim U/T$, but this can be absorbed into a redefinition of E_0 in Eq. (5.69). The needed subleading term is $\sim \ln(U/T)$, and an important result is that the coefficient of the $\ln(T)$ term is universal; we find, for $T \ll U$ (Maldacena and Stanford, 2016; Stanford and Witten, 2017; Kitaev and Suh, 2018),

$$\ln \mathcal{Z}_{\text{Sch}} = N\mathcal{S} + \frac{N\gamma T}{2} - \frac{3}{2}\ln\left(\frac{U}{T}\right). \qquad (5.77)$$

Apart from the finite-N corrections in the rotor components (which had a simple physical interpretation), we have now obtained our first nontrivial finite-N correction to the SYK model: the $-(3/2)\ln(1/T)$ correction to the logarithm of the partition function. Note that the logarithm in Eq. (5.77) becomes as large as the leading term only at an exponentially low $T \sim Ue^{-N}$, below which the large-N theory does not apply.

It is also useful to compare Eq. (5.77) to our earlier large-N result for $-T\ln Z$ in the random-matrix model in Eq. (4.16). That had a leading $N\gamma T/2$ term, but there was no T-independent term proportional to N, as the random-matrix model does not have an extensive entropy in the zero-temperature limit.

The $-(3/2)\ln(1/T)$ correction to Eq. (5.77) has important consequences for the many-body density of states $\mathcal{N}_{\text{Sch}}(E)$. We define this as

$$\mathcal{Z}_{\text{Sch}}(T) = \int_0^\infty dE\, \mathcal{N}_{\text{Sch}}(E) e^{-E/T}. \qquad (5.78)$$

As we have absorbed the $\sim 1/T$ term in Eq. (5.77) into a redefinition of E_0 in Eq. (5.69), we can assume in Eq. (5.78) that $\mathcal{N}_{\text{Sch}}(E)$ vanishes for $E < 0$. It turns out to be possible to determine $\mathcal{N}_{\text{Sch}}(E)$ by performing the inverse Laplace transform exactly using the value in Eq. (5.77). This yields (Bagrets, Altland, and Kamenev, 2017; Cotler *et al.*, 2017; García-García and Verbaarschot, 2017; Stanford and Witten, 2017; Kitaev and Suh, 2018)

$$\mathcal{N}_{\text{Sch}}(E) \propto e^{N\mathcal{S}} \sinh\left(\sqrt{2N\gamma E}\right). \qquad (5.79)$$

It is easier to insert the resulting equation (5.79) into Eq. (5.78), perform the E integral, and verify that we obtain Eq. (5.77).

The resulting equation (5.79) is accurate for $E \ll NU$, and even down to $E \sim U/N$. Near the lower bound it predicts a many-body density of states $\sim e^{N\mathcal{S}}$, in sharp contrast to the random-matrix model of Sec. IV, which did not have an exponentially large density of states at such low energies. We showed numerical plots of the many-body density of states (Fu and Sachdev, 2016; Cotler *et al.*, 2017; Gharibyan *et al.*, 2018) for the closely related Majorana fermion model in Fig. 6. Notice the much larger density of states and much smaller level spacing near the bottom of the band relative to the free fermion random-matrix model in Fig. 5 of the same size. This is also evident from a comparison of the Schwarzian result in Eq. (5.79) to the free fermion result in Eq. (4.18): the most important difference is the presence of the prefactor of $e^{N\mathcal{S}}$ in Eq. (5.79).

We now recall our discussion at the end of Sec. IV.B, where we argued that the low-lying many-body eigenstates at excitation energies of order $1/N$ could be interpreted as the sums of quasiparticle energies. In the SYK model we have order $\sim e^{N\mathcal{S}}$ energy levels even within energy $\sim 1/N$ above the many-body ground states. It is impossible to construct these

many-body eigenstates from order $\sim N$ quasiparticle states. This is therefore strong evidence that there is no quasiparticle decomposition of the many-body eigenstates of the SYK model. Note that the presence of an extensive entropy as $T \to 0$ (the nonzero value of $\mathcal{S}$) is a sufficient but not necessary condition for the absence of quasiparticles: the models that we study in Sec. XI do not have quasiparticles but also do not have an extensive entropy as $T \to 0$, as described in more detail in Sec. XI.A.3.

Finally, we combine the results for the rotor and Schwarzian partition functions, and obtain corresponding results for the SYK model (Gu *et al.*, 2020). Using the $n = 0$ term in Eqs. (5.71) and (5.77) in Eq. (5.69), we obtain the following for $U/N \ll T \ll U$:

$$\Omega = E_0 - N\mathcal{S}T - \frac{N(\gamma + 4\pi^2 \mathcal{E}^2 K)T^2}{2} + 2T\ln\left(\frac{U}{T}\right) + \cdots. \qquad (5.80)$$

Equation (5.80) contains the $1/N$ correction to the result Eq. (5.66) for the grand partition function: the $2T\ln(1/T)$ term. As for the random-matrix model, we can invert Eq. (5.80) as follows to obtain the many-body density of states in the grand canonical ensemble for grand energies $U/N \ll E \ll NU$:

$$\mathcal{N}(E) \sim \exp\left[S(E)\right],$$
$$S(E) = N\mathcal{S} + \sqrt{2N(\gamma + 4\pi^2 \mathcal{E}^2 K)(E - E_0)} \qquad (5.81)$$

for $E > E_0$, and $S(E) = 0$ for $E < E_0$. Comparing this to the random-matrix model, we find that $S(E)$ has a similar functional form of E but without the leading $N\mathcal{S}$ term.

VI. RANDOM-EXCHANGE QUANTUM MAGNETS

The SYK model discussed thus far provides valuable insight into quantum systems without quasiparticle excitations. However, the microscopic Hamiltonian in Eq. (5.1a) has a shortcoming, namely, that strong local (i.e., on-site) interactions are absent. As a result, there are no Mott insulating phases at any commensurate density in the large-N limit. Such local correlations are important to understanding the interplay of electron itinerancy and the tendency for interaction-induced localization in numerous correlated electron materials.

We now turn to a number of random and fully connected models that restore "Mottness." We use Mottness here as a generic term to qualitatively indicate the tendency of electrons to localize due to strong repulsive interactions in the vicinity of a Mott transition. In this section we discuss the original SY model (Sachdev and Ye, 1993), a pure spin model in which explicit on-site charge fluctuations are absent. In Sec. VII, we introduce charge fluctuations and consider itinerant electron models with a strong, on-site repulsive interaction U. We find substantial evidence that near critical points and/or over significant intermediate energy scales, these correlated models exhibit singular behavior that is connected to the critical properties of the SYK model. Section VIII extends the present

random quantum magnet in a different manner by adding a second band of free electrons (similar to that in Sec. IV), and thus describe a random-exchange Kondo-Heisenberg model.

Unlike the SYK model, the models introduced in this section are not analytically solvable in the limit of a large number of sites N. We follow two routes toward understanding their phase diagram. First, analytical results can be obtained by extending the spin symmetry from SU(2) to SU(M) and taking the large-M limit or, in the SU(2) case, using renormalization group methods in the vicinity of specific fixed points. Second, modern computational algorithms now provide a controlled numerical solution of such models in the SU(2) case directly, even close to quantum-critical points. Some algorithms are reviewed in Sec. IX.

This section applies the previously mentioned approaches to random-exchange quantum magnets. We consider insulating quantum magnets with a Hamiltonian of the form

$$H_J = \frac{1}{\sqrt{N}} \sum_{1 \le i < j \le N} J_{ij} \mathbf{S}_i \cdot \mathbf{S}_j, \tag{6.1}$$

where $\mathbf{S}_i$ are quantum spin operators on site i and J_{ij} are independent random variables with vanishing mean and variance J. In the most important case, the spins belong to the SU(2) algebra and we have $S = 1/2$ states on each site. As previously noted, we also consider generalizations to SU(M) spins here.

Models like Eq. (6.1) with classical spins have served as the foundations of spin-glass theory, and more generally of optimization problems and also neural networks (Mézard, Parisi, and Virasoro, 1987). Here we see that such models are also a valuable starting point for understanding correlated electron systems without quasiparticle excitations.

A. SU(M) symmetry with M large

As previously stated, Eq. (6.1) is not analytically solvable in the SU(2) case, even in the limit of $N \to \infty$. We return to the SU(2) case in Sec. VI.C, but here we consider the extension to SU(M) spin symmetry, with M large, that was originally examined by Sachdev and Ye (1993). We later see that the limit $N \to \infty$ followed by the limit $M \to \infty$ leads to the same saddle-point equations and $G - \Sigma$ action as the SYK model of Sec. V.

For the SU(M) case, we employ the representation of spin using fermionic spinons $f_{i,\alpha}$, $\alpha = 1, \ldots, M$. These fermions obey the constraint

$$\sum_{\alpha=1}^{M} f_{i\alpha}^{\dagger} f_{i\alpha} = \kappa M \tag{6.2}$$

on each site i, where $0 < \kappa < 1$. The SU(2) case corresponds to $M = 2$ and $\kappa = 1/2$. We can then write the spin operators as $S_{i,\alpha\beta} = f_{i\alpha}^{\dagger} f_{i\beta}$ and generalize Eq. (6.1) as

$$H_J = \frac{1}{\sqrt{NM}} \sum_{\alpha,\beta=1}^{M} \sum_{1 \le i < j \le N} J_{ij} f_{i\alpha}^{\dagger} f_{i\beta} f_{j\beta}^{\dagger} f_{j\alpha}. \tag{6.3}$$

This fermionic spinon representation has *fractionalized* the spin operator, where the U(1) gauge transformation $f_{i\alpha} \to e^{i\phi_i} f_{i\alpha}$ leaves the spin operator invariant. We later see that in the large-M limit f_{α} form a SYK state: in the context of the random quantum magnet, this state is a critical, gapless, *spin liquid*. In the present large-N, large-M expansion, the Lagrange multiplier λ_i (introduced later) plays the role of an emergent gauge field in this spin liquid.

We proceed (Sachdev and Ye, 1993) with an analysis of Eq. (6.3) similar to that presented for Eq. (5.1a). We average over J_{ij}, and obtain the following averaged partition function analogous to Eq. (5.54):

$$\bar{Z} = \int \mathcal{D} f_{i\alpha}(\tau) \mathcal{D} \lambda_i(\tau) e^{-\mathcal{S}_B - \mathcal{S}_J},$$

$$\mathcal{S}_B = \sum_i \int_0^{\beta} d\tau \left\{ f_{i\alpha}^{\dagger} \left(\frac{\partial}{\partial \tau} + i\lambda \right) f_{i\alpha} - i\lambda\kappa M \right\},$$

$$\mathcal{S}_J = -\frac{J^2}{4NM} \int_0^{\beta} d\tau d\tau' \left| \sum_i f_{i\alpha}^{\dagger}(\tau) f_{i\beta}(\tau) f_{i\gamma}^{\dagger}(\tau') f_{i\delta}(\tau') \right|^2. \tag{6.4}$$

In the large-N limit we assume self-averaging among the sites, and in the large-M limit we can replace the quartic operator of fermions with the product of the Green's functions of the f fermions as follows:

$$f_{\alpha}^{\dagger}(\tau) f_{\beta}(\tau) f_{\gamma}^{\dagger}(\tau') f_{\delta}(\tau') = \delta_{\alpha\delta} \delta_{\beta\gamma} G(\tau, \tau') G(\tau', \tau). \tag{6.5}$$

The analysis then proceeds just as in the SYK model, and we obtain an expression for the $G - \Sigma$ action that is nearly identical to that in Eq. (5.56), but with a prefactor of N replaced by NM as follows:

$$I[G, \Sigma, \lambda] = -\ln \det\{[\partial_{\tau_1} + i\lambda(\tau_1)]\delta(\tau_1 - \tau_2) + \Sigma(\tau_1, \tau_2)\}$$
$$- \text{Tr}(\Sigma \cdot G) - \frac{J^2}{4} \text{Tr}(G^2 \cdot G^2) - i\kappa \int_0^{\beta} d\tau \lambda(\tau). \tag{6.6}$$

Consequently, the subsequent results for the fermion Green's function and the large-NM thermodynamics are identical to those in Sec. V after the replacements $U \to J$ and $\mathcal{Q} \to \kappa$.

The local spin-spin correlation can also be obtained as

$$Q(\tau) = \frac{1}{M^2} \langle f_{\alpha}^{\dagger}(\tau) f_{\beta}(\tau) f_{\beta}^{\dagger}(\tau') f_{\alpha}(\tau') \rangle$$
$$= \frac{C^2 e^{-2\pi\mathcal{E}}}{1 + e^{-4\pi\mathcal{E}}} \frac{T}{\sin(\pi T \tau)}, \qquad 0 < \tau < \frac{1}{T}, \tag{6.7}$$

which has been obtained from Eq. (5.25). We can obtain the spin spectral density ρ_Q using a Fourier transform that yields (Parcollet and Georges, 1999)

$$\rho_Q(\omega) \sim \tanh\left(\frac{\omega}{2T}\right). \tag{6.8}$$

At $T = 0$, this corresponds to a spin density of states $\sim \mathrm{sgn}(\omega)$, which is a starting assumption in the original theory of the marginal Fermi liquid (Varma *et al.*, 1989).

Recent work (Tikhanovskaya *et al.*, 2021a) obtained corrections to the correlators of the quantum magnet H_J from perturbations of the critical theory by leading irrelevant operators described in Sec. V.E. The most important corrections arise from an operator with a scaling dimension $h = 2$, and as in Eqs. (5.44) and (5.45) we obtain

$$\rho_Q(\omega) \sim \tanh\left(\frac{\omega}{2T}\right)\left[1 - \mathcal{C}\gamma\omega\tanh\left(\frac{\omega}{2T}\right)\right], \quad (6.9)$$

where $\gamma \sim 1/J$ is the coefficient of the Schwarzian in Eq. (5.60), and also the linear-in-T coefficient of the specific heat in Eq. (5.53). The dimensionless number $\mathcal{C}$ is universal,

$$\mathcal{C} = \frac{24}{\pi[2\cos(2\theta) + 3\pi\cos^2(2\theta)]}. \quad (6.10)$$

In Eq. (6.10) θ is the spectral asymmetry angle that appeared in Eq. (5.3) and that is related by the Luttinger theorem in Eq. (5.21) to κ in Eq. (6.2). We compare Eq. (6.9) to numerical studies of the SU(2) magnet in Sec. VI.B.

B. SU(2) model

We now return to the original model in Eq. (6.1) and examine it for the physically important case with SU(2) symmetry. We proceed as in the analyses of classical spin-glass problems by introducing replicas and then averaging over the replicated partition function. This yields a self-consistent problem of a single quantum spin with replica indices (Bray and Moore, 1980). The replica structure is important for the spin-glass phase (Georges, Parcollet, and Sachdev, 2000, 2001; Biroli and Parcollet, 2002), but in this review we focus mostly on the disordered paramagnetic phase above the spin-glass ordering temperature or on quantum-critical points corresponding to the destruction of spin-glass order at $T = 0$ (Secs. VII.B and VII.C) In these cases, it is permissible at large N to ignore the replica indices and consider the following path integral for a single quantum spin $S = 1/2$:

$$\mathcal{Z}_J = \int \mathcal{D}\mathbf{S}(\tau)\delta(\mathbf{S}^2 - 1)e^{-\mathcal{S}_B - \mathcal{S}_J},$$

$$\mathcal{S}_B = \frac{i}{2}\int_0^1 du \int d\tau\, \mathbf{S} \cdot \left(\frac{\partial \mathbf{S}}{\partial \tau} \times \frac{\partial \mathbf{S}}{\partial u}\right),$$

$$\mathcal{S}_J = -\frac{J^2}{2}\int d\tau d\tau' Q(\tau - \tau')\mathbf{S}(\tau) \cdot \mathbf{S}(\tau'). \quad (6.11)$$

Equation (6.11) is a coherent state path integral and $\mathcal{S}_B$ is the geometric Berry phase, closely connected to the spin commutation relations. The spin has a temporal self-interaction with itself represented by the function $Q(\tau)$. The value of $Q(\tau)$ is to be determined self-consistently by computing the correlator

$$\bar{Q}(\tau - \tau') \equiv \frac{1}{3}\langle \mathbf{S}(\tau) \cdot \mathbf{S}(\tau')\rangle_{\mathcal{Z}_J} \quad (6.12)$$

and then imposing the self-consistency condition

$$Q(\tau) = \bar{Q}(\tau). \quad (6.13)$$

A major difference with the SU(M) model in the fermionic large-M limit is that the SU(2) model has a spin-glass phase at low temperatures. A semiclassical picture of this phase is that of local moments pointing randomly in all directions so that the global magnetization vanishes but the variance of the distribution of local magnetizations $(1/N)\sum_i m_i^2 = q_{\mathrm{EA}}$ is nonzero. The latter is the Edwards-Anderson order parameter of the spin-glass phase (Mézard, Parisi, and Virasoro, 1987). A hallmark of the spin-glass phase is also that local quantities (starting with the local magnetization itself) are no-longer self-averaging.

The existence of a spin-glass phase in the SU(2) case can be established in two ways. First, the replica diagonal effective action [Eq. (6.11)] for the disorder-averaged Green's functions can be solved numerically exactly using quantum Monte Carlo methods in the paramagnetic phase (Grempel and Rozenberg, 1998). At low temperatures, the spin-glass susceptibility diverges at $T = T_{\mathrm{SG}} \approx 0.14J$ at the boundary of the spin-glass phase.

Second, exact diagonalization of finite size systems have been performed directly in the spin-glass phase for many realizations (10^3 to 10^5) of the quenched disorder (Arrachea and Rozenberg, 2002; Shackleton *et al.*, 2021). The local dynamical spin susceptibility $\chi''_{\mathrm{loc}}(\omega)$ was computed from both a full diagonalization of small systems at finite T and the Lanczos method at $T = 0$. From a finite size scaling analysis, the $T = 0$ disorder-averaged susceptibility in the thermodynamic limit is of the form

$$\chi''_{\mathrm{loc}}(\omega) = q_{\mathrm{EA}}\pi\beta\omega\delta(\omega) + \chi''_{\mathrm{reg}}(\omega), \quad (6.14)$$

where $q_{\mathrm{EA}} \approx 0.02$ is the Edwards-Anderson parameter (Shackleton *et al.*, 2021) and χ''_{reg} is the regular part. Figure 11 presents numerical results for $\chi''_{\mathrm{loc}}(\omega)$ for the t-J model for various dopings p; this discussion is for $p = 0$, and the doped cases are discussed in Sec. VI.B. Apart from the delta function spin-glass contribution at low frequencies, the structure of $\chi''_{\mathrm{reg}}(\omega)$ is notable. Specifically, the theory of the gapless spin fluid phase studied in Sec. VI.A generally predicts that

$$\chi''_{\mathrm{reg}}(\omega) = C_1\mathrm{sgn}(\omega)[1 - C_2|\omega| + \cdots], \quad T = 0. \quad (6.15)$$

Formally, this result follows from taking the $T \to 0$ limit of the large-M result in Eq. (6.9). However, the structure of Eq. (6.15) is much more general: $\mathrm{sgn}(\omega)$ is linked to the exact SU(2) exponent that we obtain in Eq. (6.23). The $|\omega|$ correction term is similarly robust and is related to the Schwarzian operator with $h = 2$, as in Eq. (5.45) (in Sec. XII.B, we relate this $h = 2$ mode to the boundary graviton in the holographic dual). As shown in Fig. 11, the form in Eq. (6.15) provides a good fit to the numerical susceptibility of the $p = 0$ SU(2) model, apart from the low-frequency peak associated with spin-glass order. We can
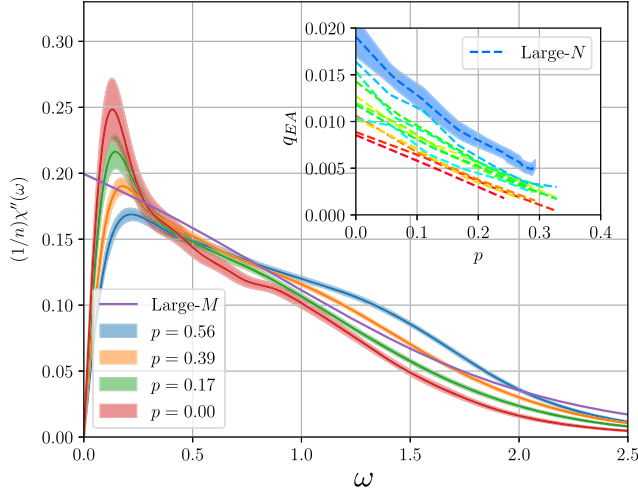
FIG. 11. Local spin response function for the spin-1/2 doped random-exchange t-J model, as obtained by exact diagonalization of an $N = 18$ site cluster averaged over 100 disorder realizations, for $t = J = 1$. $n = 1 - p$ is the particle density. From Shackleton *et al.*, 2021.

therefore conclude that the spin-glass order $q \approx 0.02$ is weak, and there is evidence of the SY spin-liquid behavior at intermediate energy scales in the SU(2) random-exchange quantum magnet.

A theory for the quantum spin-glass state can be obtained using bosonic spinons, and the spin-glass order appears when the bosonic spinons condense (Georges, Parcollet, and Sachdev, 2000, 2001). Such a theory is applicable when q_{EA} is large, and it yields $\chi''_{\text{reg}}(\omega) \sim \omega$ in Eq. (6.14) at small $|\omega|$ after an assumption of marginal stability in the replica symmetry-breaking structure. More recently, the onset of spin-glass order has been studied (Christos, Haehl, and Sachdev, 2022) using the fermionic spinon large-M theory of Sec. VI.A. Such a theory yields an estimate of the critical temperature to spin-glass order

$$T_{\text{SG}} \sim J \exp\left(-\sqrt{M\pi}\right) \qquad (6.16)$$

and also has $\chi''_{\text{reg}}(\omega) \sim \omega$ for $|\omega| < \omega_*$. The fermionic spinon theory describes the crossover above the frequency $\omega_* = Jq_{\text{EA}}$ to the spin-liquid spectrum in Eq. (6.15) or (6.9). The exponential factor in Eq. (6.16) is small even for $M = 2$, $e^{-\sqrt{2\pi}} = 0.0815\ldots$, and this could be the justification for the applicability of the large-M theory to the SU(2) case.

C. Renormalization group (RG) analysis of the SU(2) model

We now turn to an analytical study of the SU(2) model, as this will help us understand the structure of nonzero frequency spin susceptibility observed in the numerics, as described in Eq. (6.15).

We present here a systematic RG procedure to analyze the problem defined in Eqs. (6.11)–(6.13). We begin by assuming that there is a critical solution in which $Q(\tau)$ has a power-law decay in time. Notice that this is similar to the assumption

made for the SYK model in Eq. (5.3): in that case we were able to solve the self-consistency problem exactly at low energies. That is not possible here, and we therefore have to introduce the ϵ expansion defined later. We assume the power-law decay

$$Q(\tau) \sim \frac{\gamma^2}{|\tau|^\alpha} \qquad (6.17)$$

and postpone consideration of the self-consistency condition. We then have to solve the well-defined problem of computing $\bar{Q}(\tau)$ from Eq. (6.12) given $Q(\tau)$ in Eq. (6.17).

This problem can be reduced to the solution of a quantum impurity problem, sometimes called the Bose-Kondo problem (Sengupta, 2000; Beccaria, Giombi, and Tseytlin, 2022; Cuomo *et al.*, 2022; Nahum, 2022; Weber and Vojta, 2022). We begin by decoupling the $\mathbf{S}(\tau) \cdot \mathbf{S}(0)$ interaction in Eq. (6.11) with a bosonic field ϕ_a, $a = 1, \ldots, 3$. We assume that there is a bosonic "bath" field that lives in d spatial dimensions $\phi_a(x, \tau)$, and the decoupling field is $\phi_a(x = 0, \tau)$. The path integral for $\mathcal{Z}_J$ in Eq. (6.11) then reduces to the solution of the following Bose-Kondo Hamiltonian of an $S = 1/2$ spin S_a coupled to a bosonic scalar field $\phi_a(x, \tau)$:

$$H_{\text{imp}} = \gamma S_a \phi_a(0) + \frac{1}{2} \int d^d x [\pi_a^2 + (\partial_x \phi_a)^2]. \qquad (6.18)$$

In Eq. (6.18) π_a is canonically conjugate to the field ϕ_a, and $\phi_a(0) \equiv \phi_a(x = 0)$. We identify $Q(\tau)$ with the temporal correlator of $\phi_a(0)$, and from Eq. (6.17) we then conclude that we need $\alpha = d - 1$.

We now determine the properties of the theory H_{imp} in a renormalized perturbation expansion in the coupling γ. A simple determination of scaling dimensions at tree level shows that γ has the scaling dimension $(3 - d)/2$, so an expansion in powers of γ is equivalent to a RG expansion in

$$\epsilon = 3 - d = 2 - \alpha. \qquad (6.19)$$

Such a computation can be performed (Sachdev, Buragohain, and Vojta, 1999; Smith and Si, 1999; Sengupta, 2000; Sachdev, 2001; Beccaria, Giombi, and Tseytlin, 2022; Cuomo *et al.*, 2022; Nahum, 2022) while one imposes the fermion constraint in Eq. (6.2) for SU(2) exactly, and it yields the following two-loop β function:

$$\beta(\gamma) = -\frac{\epsilon}{2}\gamma + \gamma^3 - \gamma^5 + \cdots. \qquad (6.20)$$

Equation (6.20) has a stable fixed point at $\gamma^{*2} = \epsilon/2 + \epsilon^2/4 + \cdots$ that provides the needed critical theory of $\mathcal{Z}_J$ with the interaction in Eq. (6.17).

To solve the self-consistent theory, we need to compute $\bar{Q}(\tau)$ in Eq. (6.12) at this fixed point. The scaling dimension of the spin operator dim[S] can be computed using standard RG methods order by order in ϵ, but we encounter an unexpected simplification. Because of the quantized Berry phase (Wess-Zumino-Witten) term, the renormalization of the coupling γ is given only by the wave function renormalization, and this fixes the scaling dimension of the spin operator at the

nontrivial fixed point of the β function: we find that (Vojta, Buragohain, and Sachdev, 2000; Sachdev, 2001)

$$\dim[\mathbf{S}] = \epsilon/2, \tag{6.21}$$

exact to all orders in ϵ. This implies the correlator

$$\bar{Q}(\tau) = \frac{1}{3}\langle \mathbf{S}(\tau) \cdot \mathbf{S}(0) \rangle \sim \frac{1}{|\tau|^{2-\alpha}}. \tag{6.22}$$

Finally, we impose the self-consistency condition in Eq. (6.13) at least at the level of the exponent. Comparing Eqs. (6.17) and (6.22), we conclude that the self-consistent value is $\alpha = 1$. Note that this value is well outside the domain of applicability of the ϵ expansion given Eq. (6.19). Nevertheless, given that Eq. (6.21) has been obtained to all orders in ϵ, the only requirement for the validity of Eq. (6.22) is the continued existence of the nontrivial fixed point of the β function at ϵ of the order of unity. The self-consistent spin correlator is therefore

$$\langle \mathbf{S}(\tau) \cdot \mathbf{S}(0) \rangle \sim \frac{1}{|\tau|}. \tag{6.23}$$

Comparing Eq. (6.23) with the large-M result in Eq. (6.7), we find perfect agreement between the large-M and RG exponents.

As discussed in Sec. VI.B, the ground state of Eq. (6.1) is actually a spin glass for SU(2) spins. The analysis obtaining the result in Eq. (6.22) is certainly correct for SU(2) and applies exactly to the Bose-Kondo impurity model defined in Eq. (6.18) for small ϵ. Recent studies showed (Beccaria, Giombi, and Tseytlin, 2022; Cuomo *et al.*, 2022; Nahum, 2022; Weber and Vojta, 2022) that the fixed point is not present at large ϵ, and this is consistent with the appearance of spin-glass order.

Despite the direct inapplicability of the RG to the SU(2) model in Eq. (6.1), the analysis presented here turns out to be useful. A closely related RG applies to the SU(M) generalization considered in Sec. VI.A (Joshi *et al.*, 2020), and from this we can conclude that there are no corrections to the exponent in Eq. (6.21) [which is related to the exponent in Eq. (6.7)] at all orders in $1/M$. Moreover, extensions of the RG of the Bose-Kondo model obtained here apply to the correlated electrons models considered in the following sections: i.e., the superspin Bose-Fermi-Kondo model in Sec. VII.D.3 and the Bose-Fermi-Kondo model in Sec. VIII.D.

VII. RANDOM-EXCHANGE *t-U-J* HUBBARD MODELS

In the following, we consider models of itinerant electrons on a fully connected lattice with a strong local interaction and random-exchange constants. One such example is the "*t-U-J*" model, in which random J_{ij}'s are added to the Hubbard model with random hoppings as follows:

$$
\begin{aligned}
H_{tUJ} = &-\frac{1}{\sqrt{N}}\sum_{i,j=1}^{N}\sum_{\alpha=1}^{M} t_{ij}c_{i\alpha}^{\dagger}c_{j\alpha} - \mu\sum_{i\alpha}c_{i\alpha}^{\dagger}c_{i\alpha} \\
&+\frac{U}{2}\sum_{i}\left(\sum_{\alpha}c_{i\alpha}^{\dagger}c_{i\alpha} - M/2\right)^{2} + \frac{1}{\sqrt{N}}\sum_{1\le i<j\le N} J_{ij}\mathbf{S}_{i}\cdot\mathbf{S}_{j}.
\end{aligned}
\tag{7.1}
$$

In Eq. (7.1), we introduce M "colors" of fermions so that the model has U(M) = U(1) × SU(M) symmetry corresponding to an extension of the spin symmetry to SU(M). The usual SU(2), $S = 1/2$ Hubbard model corresponds to $M = 2$ ($\alpha = \uparrow, \downarrow$). The electron spin operators $\mathbf{S}_{i} = \sum_{\alpha\beta}c_{\alpha}^{\dagger}(\boldsymbol{\sigma}_{\alpha\beta}/2)c_{\beta}$, with $\boldsymbol{\sigma}/2$ the $M^{2}-1$ generators of SU(M) ($\boldsymbol{\sigma}$ are the Pauli matrices for $M = 2$). As before, the t_{ij}'s and J_{ij}'s are drawn from distributions with zero mean and variances $\overline{t_{ij}^{2}} = t^{2}$ and $\overline{J_{ij}^{2}} = J^{2}$; however, as we later note, closely related results also apply to the case where the t_{ij} are nonrandom and lead to an electronic dispersion $\epsilon_{\mathbf{k}}$. Note a change in notation from the previously mentioned SYK model: U designates here the on-site repulsion, while the variance J of the random bonds is more directly analogous to the variance of the random SYK interactions. Note also that the chemical potential μ is defined with reference to the half-filled case ($M/2$ electrons per site).

We can also consider the *t-J* limit of this model (Parcollet and Georges, 1999), which reads

$$
\begin{aligned}
H_{tJ} = &-\frac{1}{\sqrt{N}}\sum_{i,j=1}^{N}\sum_{\alpha} t_{ij}\mathcal{P}c_{i\alpha}^{\dagger}c_{j\alpha}\mathcal{P} - \mu\sum_{i\alpha}c_{i\alpha}^{\dagger}c_{i\alpha} \\
&+\frac{1}{\sqrt{N}}\sum_{1\le i<j\le N} J_{ij}\mathbf{S}_{i}\cdot\mathbf{S}_{j},
\end{aligned}
\tag{7.2}
$$

in which the operator $\mathcal{P}$ enforces the following Gutzwiller-type projection such that the total number of fermions on each site is at most $M/2$:

$$\sum_{\alpha}c_{i\alpha}^{\dagger}c_{i\alpha} \le \frac{M}{2} \quad \forall\ i. \tag{7.3}$$

At half filling ($\mu = 0$) this reduces to the random-bond Heisenberg (SY) model of Sec. VI.

A. Effective local action

In the thermodynamic limit $N \to \infty$, the calculation of the single-particle Green's function and self-energy of this model, as well as that of the local spin-spin correlator, reduces to a local effective action subject to a self-consistency condition. This corresponds to the extended dynamical mean-field theory construction (EDMFT) (Sengupta and Georges, 1995; Georges *et al.*, 1996; Si and Lleweilun Smith, 1996; Chitra and Kotliar, 2000; Smith and Si, 2000), which is exact for these random fully connected models. The term "extended" is commonly used to indicate that the mapping involves a self-consistency over both single-particle and two-particle correlation functions. When one considers the system

outside the spin-glass phase, all local correlators are self-averaging and this mapping is most easily derived following the cavity construction, as in Sec. IV. We skip the details here since the reasoning is completely analogous to that in Sec. IV. One obtains the single-site effective action

$$
\mathcal{S}_{tUJ} = \int d\tau \sum_\alpha c_\alpha^\dagger(\tau) \left(\frac{\partial}{\partial\tau} - \mu \right) c_\alpha(\tau)
$$
$$
+ \frac{U}{2} \int d\tau \left(\sum_\alpha c_\alpha^\dagger c_\alpha - M/2 \right)^2
$$
$$
+ \int d\tau d\tau' \Delta(\tau - \tau') \sum_\alpha c_\alpha^\dagger(\tau) c_\alpha(\tau')
$$
$$
- \frac{1}{2} \int d\tau d\tau' \mathcal{J}(\tau - \tau') \boldsymbol{S}(\tau) \cdot \boldsymbol{S}(\tau'). \tag{7.4}
$$

From Eq. (7.4) we have to determine the Green's function and spin correlator as follows:

$$
G(\tau - \tau') \equiv -\frac{1}{M} \sum_\alpha \langle c_\alpha(\tau) c_\alpha^\dagger(\tau') \rangle_{\mathcal{S}_{tUJ}},
$$
$$
\chi(\tau - \tau') \equiv \frac{1}{M^2 - 1} \langle \boldsymbol{S}(\tau) \cdot \boldsymbol{S}(\tau') \rangle_{\mathcal{S}_{tUJ}}, \tag{7.5}
$$

and impose the following self-consistency condition that results from the cavity construction:

$$
\Delta(\tau) = t^2 G(\tau), \qquad \mathcal{J}(\tau) = J^2 \chi(\tau). \tag{7.6}
$$

The electronic self-energy can be defined by referring to the noninteracting system $U = J = 0$ (the random-matrix model of Sec. IV) as $G_{ij}^{-1}(i\omega_n) = i\omega_n + \mu - t_{ij} - \Sigma_{ij}$ for a given sample $\{t_{ij}\}$. In the infinite-volume limit $N \to \infty$, the self-energy becomes local ($\Sigma_{ij} = \Sigma_{ii}\delta_{ij}$) and self-averaging when not in the spin-glass phase. The local Green's function G_{ii} is also self-averaging and is related to Σ by

$$
G_{ii}(i\omega_n) = \sum_\lambda |\langle i|\lambda\rangle|^2 G(i\omega_n, \varepsilon_\lambda)
$$
$$
\to \int \rho_0(\varepsilon) G(i\omega_n, \varepsilon) = G(i\omega_n), \tag{7.7}
$$

with ρ_0 the semicircular density of states defined in Sec. IV and where

$$
G(i\omega_n, \varepsilon) = \frac{1}{i\omega_n + \mu - \varepsilon - \Sigma(i\omega_n)} \tag{7.8}
$$

is the Green's function in the basis of the single-particle states of the free system at an energy ε. The self-energy Σ coincides with that of the effective action [Eq. (7.4)] and hence reads

$$
\Sigma(i\omega_n) = i\omega_n + \mu - t^2 \Delta(i\omega_n) - G^{-1}(i\omega_n). \tag{7.9}
$$

Substituting Eq. (7.9) into Eq. (7.8) and performing the Hilbert transform of ρ_0, one recovers the self-consistency condition $\Delta = t^2 G$ (Georges *et al.*, 1996).

When a spin-glass phase exists, self-averaging of the local observables does not hold inside the ordered phase. A mapping onto a local effective action still applies, however, after one introduces n replicas and performs the average of $(Z^n - 1)/n$ over the t_{ij} and J_{ij} random variables. The $n \to 0$ limit must then also be taken, allowing for the possibility of replica symmetry breaking. We do not write these equations in detail here, and instead refer the interested reader to Georges, Parcollet, and Sachdev (2000, 2001).

To make contact with the (E)DMFT literature, we use in this section notations that are rather standard in the field. In particular, $\Delta(\tau)$ is the dynamical mean field (quantum generalization of the Weiss field) describing the hybridization between a local site and its self-consistent bath. In the following, we often use a somewhat different notation that is more commonly used in the SY and SYK literature, such as $\Delta \to t^2\bar{R}$, $G \to \bar{R}$, $\mathcal{J} \to J^2 Q$, and $\chi \to \bar{Q}$.

We also note that the single-site effective action permits a spin-glass phase after we include replica off-diagonal components of the correlators (Georges, Parcollet, and Sachdev, 2000, 2001). In the replica diagonal components $\mathcal{J}(\tau \to \infty) \neq 0$ at zero temperature. Naively, such a nonzero limit signals a problem in the replica diagonal action in Eq. (7.4), as the expectation value of the last term in the action diverges as $\sim\beta^2$ as $\beta \to \infty$, implying a divergent ground state energy. However, this problem is cured upon including the replica off-diagonal components and taking the replica $n \to 0$ limit (Read, Sachdev, and Ye, 1995). This issue highlights the difficulty in interpreting the EDMFT framework in the magnetically ordered phase for nonrandom systems (Si *et al.*, 2001, 2003; Pankov, Kotliar, and Motome, 2002; Kirchner *et al.*, 2020).

B. SU(2) Hubbard model at half filling

The SU(2) *t*-*U*-*J* model in Eq. (7.1) was previously studied at half filling in the EDMFT framework (Cha, Wentzell *et al.*, 2020). Earlier work studied this in the large-*M* limit (Florens *et al.*, 2013). The phase diagram is reproduced in Fig. 12 as a function of t/U and temperature, as obtained by a quantum Monte Carlo solution of the EDMFT equations; see Sec. IX. A quantum-critical point (QCP) at $U = U_c$ separates a Fermi-liquid phase at small U from an insulator at large U that orders into a spin-glass phase at low temperatures. At the quantum-critical point, the spin correlation decays as $\chi(\tau) \sim 1/\tau$, as in the large-*M* limit of the SY model, while it is the expected $\chi(\tau) \sim 1/\tau^2$ in the Fermi-liquid phase.

The electronic self-energy Σ is strongly affected by the QCP. While it takes its regular form in the Fermi liquid, the coherence temperature vanishes at the QCP, where a linear temperature behavior $\mathrm{Im}\,\Sigma(\omega = 0, T) \propto T$ is found numerically. As detailed in Sec. VII.E, this behavior leads at the QCP to a T-linear dependence of the resistivity that is smaller than the MIR value. Furthermore, in the accessible range of temperatures, the frequency dependence of the self-energy is compatible with a marginal Fermi-liquid form. Finally, we note a theoretical study (Tarnopolsky *et al.*, 2020) analyzing the metal-insulator transition at half filling, related to the finite doping theoretical models that are described in Sec. VII.D.
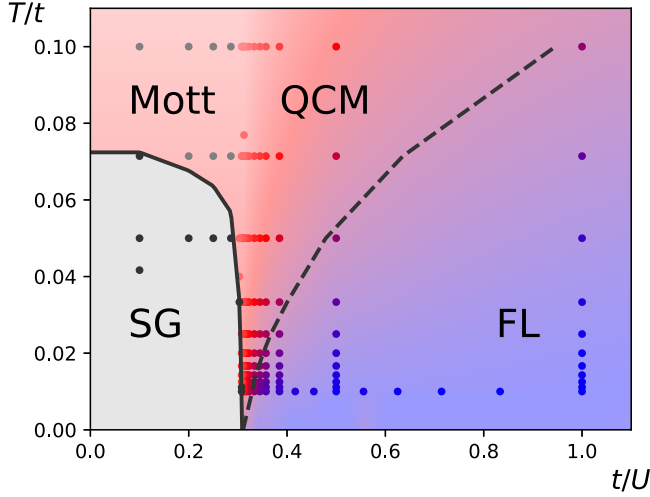
FIG. 12. Phase diagram of the spin-1/2, half-filled, random-exchange t-J-U model. At low temperatures, a quantum-critical point separates the spin-glass (SG) phase from a Fermi-liquid (FL) phase. The background color corresponds to the fitted power-law exponent of the local spin correlation function $\chi(\tau) \sim 1/\tau^{2\Delta}$, with $2\Delta \simeq 1$ in the quantum-critical metal (QCM) (red) and $\Delta = 1$ in the Fermi liquid (blue). At high temperatures and U, one obtains a Mott insulator. From Cha, Wentzell *et al.*, 2020.

C. SU(2) Hubbard model away from half filling

Section VII.B showed that the Hubbard model exhibits a novel phase transition at half filling: between a Fermi liquid at small U/t and a metallic spin glass at large U/t. Next we turn to the case with hole doping p away from half filling. Here we assume throughout that U/t is large so that at $p = 0$ we obtain the insulating spin-glass phase described in Sec. VI.B. We review numerical studies (Otsuki and Vollhardt, 2013; Shackleton *et al.*, 2021; Dumitrescu *et al.*, 2022) showing that the spin-glass order survives in a metallic state up to a critical doping $p = p_c$, and that there is a Fermi liquid for $p > p_c$. [We note an exact diagonalization study (Kumar, Sachdev, and Tripathi, 2021) that presents evidence for the spin-glass transition from quasiparticle spectra.] The critical point at $p = p_c$ displays a SYK-like criticality, with some similarities to the $U = U_c$ critical point at $p = 0$ described in Sec. VII.B. Analytical analyses of the $p > 0$ Hubbard model appear afterward in Sec. VII.D.

A recent study (Shackleton *et al.*, 2021) approached the large-U and $p \geq 0$ Hubbard model in the t-J model framework by performing exact diagonalizations of fully connected clusters of N sites, up to $N = 18$, for a fixed sample of random hopping amplitudes and exchange constants, then taking averages or histograms over the samples. Shackleton *et al.* confirmed the existence of a spin-glass phase at low doping, which survives up to $p_c \simeq 0.3$ [in agreement with earlier analytic arguments (Joshi *et al.*, 2020) presented in Secs. VII.D.2 and VII.D.3]. Their result for the local spin response function $\chi''(\omega)$ is displayed in Fig. 11. The spin-glass phase is signaled by a sharp low-frequency peak in $\chi''(\omega)$ that is absent for $p > p_c$, and the spin-fluctuation

spectrum close to the critical point is seen to be well approximated by the large-M SYK theory of Sec. VI.A. They also computed thermodynamic properties (entropy, specific heat, and entanglement entropy) as a function of temperature and found that the specific-heat coefficient $\gamma = C/T$ displays a maximum as a function of doping for $p \simeq p_c$.

A different and complementary approach (Otsuki and Vollhardt, 2013) was used recently (Dumitrescu *et al.*, 2022). The EDMFT equations of Sec. VII.D were solved using the quantum Monte Carlo algorithms reviewed in Sec. IX and correspond to a direct solution in the thermodynamic limit $N = \infty$ for disorder-averaged observables. The model considered (Dumitrescu *et al.*, 2022) is actually a finite-U random-exchange model, with U/t large enough that the physics of a doped Mott insulating spin glass is captured. The phase diagram obtained in that study is displayed in Fig. 13. The spin-glass phase itself (requiring replica off-diagonal terms) was not studied in that work, but the location of the critical boundary in the T-U plane was identified from the criterion $J\chi_{\mathrm{loc}} = 1$. The $T = 0$ critical doping was found to be at $p_c \simeq 0.17$ for the finite value of U/t studied, in contrast to the higher value $p_c \simeq 0.3$ for the $U = \infty$ model. Accordant with the exact diagonalization study (Shackleton *et al.*, 2021), the local spin dynamics at the critical point is of the SYK type with $\chi(\tau) \propto 1/\tau$. The self-energy obeys interesting scaling properties near the critical point: the imaginary-time data for different temperatures can be collapsed onto

$$\frac{\Sigma(\tau)}{\Sigma(\beta/2)} = \frac{e^{2\pi\mathcal{E}(\tau/\beta - 1/2)}}{(\sin \pi\tau/\beta)^{\nu}}, \qquad (7.10)$$

which corresponds to the following conformally invariant scaling form for the real-frequency scattering rate:
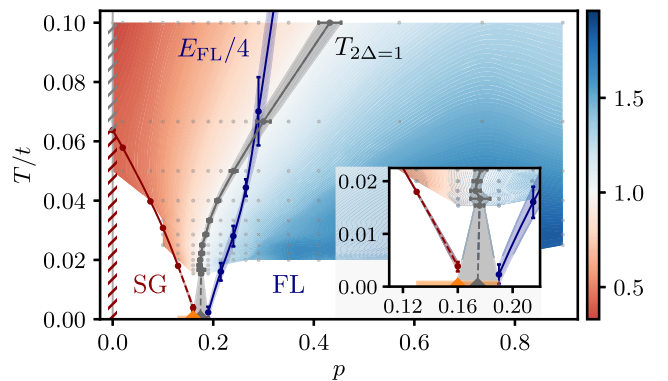
FIG. 13. Phase diagram (Dumitrescu *et al.*, 2022) of the spin-1/2 doped random-exchange t-U-J model as obtained using a quantum Monte Carlo solution of the EDMFT equations. FL, Fermi liquid; SG, metallic spin glass for $p \neq 0$. The background color corresponds to the fitted power-law exponent of the local spin correlation function $\chi(\tau) \sim 1/\tau^{2\Delta}$ (color scale on the right). Along the dashed gray line, SYK behavior $2\Delta \simeq 1$ is found. A linear-in-T resistivity is obtained in the quantum-critical region with a resistivity that becomes lower than the MIR resistivity. Inset: Enlargement close to the quantum-critical point.

$$-\frac{1}{\pi}\operatorname{Im}\Sigma(\omega + i0^+) = \lambda T^\nu \Phi_{\nu,\mathcal{E}}\left(\frac{\omega}{T}\right),$$

$$\Phi_{\nu,\mathcal{E}}(x) = \cosh\frac{x}{2}\left|\Gamma\left[\frac{1+\nu}{2} + i\frac{x}{2\pi} + i\mathcal{E}\right]\right|^2. \quad (7.11)$$

The exponent ν at criticality was estimated to be in the range $\nu \simeq 0.6$–0.8. Note that a value of ν smaller than unity implies that the lifetime of single-electron excitations (inverse width of the spectral function) satisfies Planckian T-linear behavior as follows:

$$\frac{1}{\tau^*} \equiv -Z\operatorname{Im}\Sigma(i0^+) = c\frac{\hbar}{k_B T}. \quad (7.12)$$

This is the case since, as detailed in Sec. VII.E, $Z = [1 - \partial\operatorname{Re}\Sigma(\omega)/\partial\omega|_{\omega=0}]^{-1}$ vanishes as $Z \propto \lambda T^{1-\nu}$ at low T. The overall coupling constant λ cancels in the expression of τ^* to dominant order; hence, the prefactor c is generically of the order of unity. This quantity is displayed in Fig. 14. The spectral asymmetry $\mathcal{E}$ was found to be nonzero but temperature dependent over some extended range of T. Whether there is an intrinsic particle-hole asymmetry of the scaling function at criticality down to $T = 0$ is an open question.

The metallic state is a Fermi liquid for $p > p_c$, which satisfies the Luttinger theorem with a large Fermi energy associated with a fermion density of $1 - p$; see Sec. VIII.C for a discussion of the Luttinger theorem in disordered systems. For the present system, it is expressed using the relation $\mu - \operatorname{Re}\Sigma(0) = \varepsilon_F$ at $T = 0$, with ε_F the Fermi energy of the noninteracting system (random-matrix model) for a density $n = 1 - p$. When one solves the EDMFT equations without allowing for spin-glass ordering, a sudden breakdown of this relation is found for $p < p_c$ (Otsuki and Vollhardt, 2013; Dumitrescu *et al.*, 2022), thereby signaling a breakdown of the Luttinger theorem. These solutions correspond to a metastable state with unquenched local magnetic moments. These local moments order into a spin glass that is the actual stable phase. The finite size exact diagonalization results (Shackleton *et al.*, 2021) suggest that the Fermi energy may collapse to a small one of volume p in this metallic spin-glass
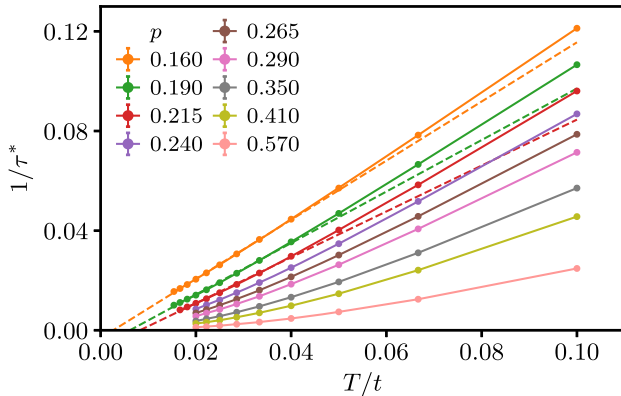

FIG. 14. Inverse single-electron excitations lifetime $1/\tau^*$ as a function of temperature T in the spin-$1/2$ doped random-exchange t-U-J model for different doping p. A Planckian behavior [Eq. (7.12)] is observed close to the quantum-critical point.

phase. This interesting possibility awaits confirmation from an infinite-volume solution of the EDMFT equations inside the spin-glass phase.

D. Doped $t - J$ model: Analytical insights

We now extend the analytic considerations of Secs. VI.A and VI.C from the undoped quantum magnet at $p = 0$ to the nonzero doping t-J model with $p \neq 0$. This provides insight into the numerical results presented in Sec. VII.C for the doped Hubbard model. This analysis is carried out in the $U \to \infty$ limit, employing the t-J model in Eq. (7.2).

In the SU(2) ($M = 2$) case, the Hilbert space of the t-J model on each site consists of the following three states:

$$|0\rangle, \quad c_\uparrow^\dagger|0\rangle, \quad c_\downarrow^\dagger|0\rangle. \quad (7.13)$$

We treat these three states in close analogy to the two spin states of the random magnet in Eq. (6.1) (Fritz and Vojta, 2004; Vojta and Fritz, 2004). Apart from the increase in the number of states, a crucial difference is the Fermi statistics of the electron operator, which requires the three states to be components of a *superspin*. However, there remains a choice on whether the spinful or spinless component of the superspin is fermionic. In an exact treatment of the problem, either choice is permitted and should lead to equivalent results. However, in approximate treatments one choice or the other may be superior, and it is often useful to exploit this freedom. For now, we present our discussion by representing the superspin as follows as a spinless boson b (the holon) and a spinful fermion f_α (the spinon):

$$|0\rangle \Rightarrow b^\dagger|v\rangle, \qquad c_\alpha^\dagger|0\rangle \Rightarrow f_\alpha^\dagger|v\rangle. \quad (7.14)$$

The physical states are obtained when the constraint

$$f_\alpha^\dagger f_\alpha + b^\dagger b = 1 \quad (7.15)$$

is obeyed [we implicitly sum over SU(2) indices in this discussion for $M = 2$]. Hence, the physical states are invariant under the U(1) gauge transformation that generalizes the one in Sec. VI.A ($f_\alpha \to f_\alpha e^{i\phi}$, $b \to b e^{i\phi}$), while individual spinon and holon excitations carry U(1) gauge charges. At the moment, the fractionalized representation (and the associated emergent gauge symmetry) is simply a convenient exact description of the Hilbert space. But we see later in Secs. VII.D.2 and VII.D.3 that the fractionalized operators yield a simple way to understand the exponents at a non-Fermi-liquid critical point as a realization of a critical doped spin liquid.

The following physical electron (c_α) and spin (S) operators can be viewed as rotation operators of the superspin:

$$c_\alpha = b^\dagger f_\alpha, \qquad S = \tfrac{1}{2}f_\alpha^\dagger \boldsymbol{\sigma}_{\alpha\beta} f_\beta. \quad (7.16)$$

If we combine these operators with an operator V that measures the electron density

$$V = b^\dagger b + \tfrac{1}{2} f_\alpha^\dagger f_\alpha$$
$$= 1 - \tfrac{1}{2} c_\alpha^\dagger c_\alpha, \tag{7.17}$$

we obtain all the generators of the supergroup SU(1|2). The notation indicates that this group acts on a superspin with one bosonic component $b^\dagger |v\rangle$ and two fermionic components $f_\alpha^\dagger |v\rangle$. These generators realize the superalgebra SU(1|2), which is

$$[S^a, S^b] = i\epsilon_{abc} S^c, \tag{7.18a}$$

$$\{c_\alpha, c_\beta\} = 0, \tag{7.18b}$$

$$\{c_\alpha, c_\beta^\dagger\} = \delta_{\alpha\beta} V + \sigma_{\alpha\beta}^a S^a, \tag{7.18c}$$

$$[S^a, c_\alpha] = -\tfrac{1}{2}\sigma_{\alpha\beta}^a c_\beta, \tag{7.18d}$$

$$[S^a, V] = 0, \tag{7.18e}$$

$$[V, c_\alpha] = \tfrac{1}{2} c_\alpha. \tag{7.18f}$$

If we had made the opposite choice and used spinful bosonic spinons and spinless fermionic holons, we would have obtained the superalgebra SU(2|1), which is isomorphic to SU(1|2).

The effective local action associated with this model along the lines of Sec. VII.A can be viewed as that of a single SU(1|2) superspin, which is in complete analogy with Eqs. (6.11)–(6.13) for the self-consistent dynamics of a single SU(2) spin. The local effective action can be written in terms of the spinon and holon fields as

$$\mathcal{Z}_{tJ} = \int \mathcal{D}f_\alpha(\tau)\mathcal{D}b(\tau)\mathcal{D}\lambda(\tau) e^{-\mathcal{S}_B - \mathcal{S}_{tJ}},$$

$$\mathcal{S}_B = \int d\tau \left[f_\alpha^\dagger(\tau)\left(\frac{\partial}{\partial\tau} + i\lambda\right) f_\alpha(\tau) \right.$$
$$\left. + b^\dagger(\tau)\left(\frac{\partial}{\partial\tau} + i\lambda\right) b(\tau) - i\lambda \right],$$

$$\mathcal{S}_{tJ} = s_0 \int d\tau f_\alpha^\dagger f_\alpha - \frac{J^2}{2} \int d\tau d\tau' Q(\tau - \tau') \mathbf{S}(\tau) \cdot \mathbf{S}(\tau')$$
$$- t^2 \int d\tau d\tau' R(\tau - \tau') f_\alpha^\dagger(\tau) b(\tau) b^\dagger(\tau') f_\alpha(\tau') + \text{H.c.}$$
$$\tag{7.19}$$

The action $\mathcal{S}_B$ is the Berry phase of an SU(1|2) superspin, which we have expressed as the path integral over canonical bosonic and fermionic fields while imposing the constraint Eq. (7.15) with the field $\lambda(\tau)$. The chemical potential μ of the *t-J* Hamiltonian is now represented by the coupling s_0. From this action we have to determine the correlators

$$\bar{R}(\tau - \tau') = -\tfrac{1}{2}\langle c_\alpha(\tau) c_\alpha^\dagger(\tau')\rangle_{\mathcal{Z}_{tJ}},$$
$$\bar{Q}(\tau - \tau') = \tfrac{1}{3}\langle \mathbf{S}(\tau) \cdot \mathbf{S}(\tau')\rangle_{\mathcal{Z}_{tJ}}, \tag{7.20}$$

in a manner analogous to Eq. (6.12). And then we impose the self-consistency conditions in Eqs. (7.5) and (7.6), which take the form

$$R(\tau) = \bar{R}(\tau), \qquad Q(\tau) = \bar{Q}(\tau), \tag{7.21}$$

in a manner analogous to Eq. (6.13).

It is not possible to solve exactly the quantum problem defined by Eqs. (7.19)–(7.21). Sections VII.D.1–VII.D.3 describe various theoretical expansions and numerical results, in a matter analogous to the discussion in Sec. VI for the random quantum magnet.

1. SU(M) symmetry: The Fermi-liquid large-M limit

A first approach (Parcollet and Georges, 1999) is to extend the SU(M) large-M model of Sec. VI.A using fermionic spinons f_α with an index $\alpha = 1, \ldots, M$, while the bosonic holons b have no index. In this case, the constraints [Eqs. (6.2) and (7.15)] become

$$\sum_{\alpha=1}^{M} f_{i\alpha}^\dagger f_{i\alpha} + b_i^\dagger b_i = \frac{M}{2} \tag{7.22}$$

on each site i; we are restricting to the case with self-conjugate representations of SU(M) at half filling, with $\kappa = 1/2$. We also fix the doping density p by

$$\frac{1}{N}\sum_i b_i^\dagger b_i = \frac{Mp}{2}. \tag{7.23}$$

This large-M limit is similar to that employed for non-random *t-J* models (Kotliar, 1995; Lee, Nagaosa, and Wen, 2006) and has the crucial feature that the bosonic holons are strongly condensed at $T = 0$. Indeed, in the large-M limit, we may replace the boson with a number $b_i = \sqrt{Mp}$ obtained from the constraint in Eq. (7.23). The fermions f_α then have the same quantum numbers as an electron, with spin $S = 1/2$ and charge -1. The effective theory of these electrons is a sum of the random-matrix Hamiltonian H_2 in Eq. (4.1a), and the SYK Hamiltonian H_4 in Eq. (5.1a). We discuss similar Hamiltonians in a different context in Sec. X and defer a complete discussion until then.

For now, we note a few important features of this large-M limit. The phase diagram (Parcollet and Georges, 1999) is displayed in Fig. 15. At $p = 0$, we have the SYK spin-liquid state described in Sec. VI. At any nonzero p, because of the condensation of the holons b we obtain a disordered Fermi-liquid ground state, with quasiparticles moving with an effective hopping tp. These quasiparticles are present at a large Fermi energy below which there are states of $(1 - p)/2$ electrons per spin. There is a characteristic doping $p^* \sim J/t$ that separates two different regimes with a distinct doping dependence of the effective mass enhancement and spectral weight Z of these quasiparticles. For $p > p^*$, the usual Brinkman-Rice (Brinkman and Rice, 1970) behavior $m^*/m = 1/Z \propto 1/p$ is recovered, as in the absence of random-exchange couplings. In contrast, for $p < p^*$ much heavier quasiparticles are found with $m^*/m = 1/Z \propto (p^*/p)^2$. Correspondingly, the Fermi-liquid coherence scale is $T_{\text{coh}} \sim (pt)^2/J$ in this regime. Hence, the random exchanges strongly modify the usual Brinkman-Rice behavior of the doped Mott insulator at low doping. For $p < p^*$, there is an interesting
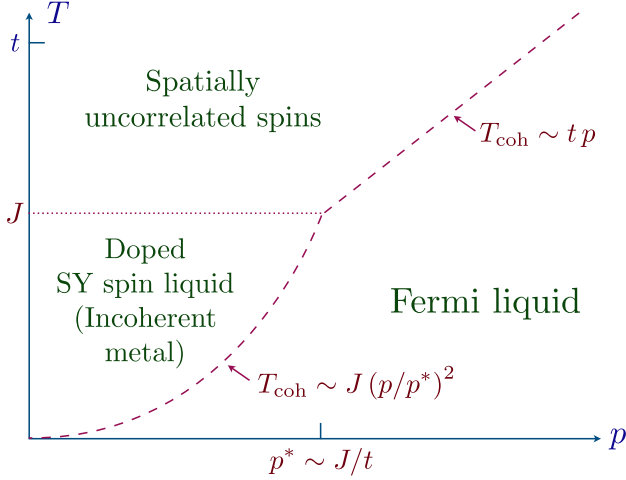
FIG. 15. Phase diagram (Parcollet and Georges, 1999) of the doped *t-J* model in the large-*M* limit with a condensed bosonic holon *b*. The SY spin liquid (incoherent metal) displays linear-in-*T* resistivity with a large bad metal resistivity.

crossover at $T \gtrsim T_{\text{coh}}$, above which non-Fermi-liquid behavior with spin-liquid local correlations of the SYK type are recovered (Fig. 15). This regime corresponds to a bad metal with a resistivity larger than the MIR limit and depending linearly on temperature; see Sec. VII.E for a discussion of related models for which we define a proper notion of transport. The mechanism for this *T*-linear dependence is unusual. Indeed, in this regime the single-particle scattering rate has the $\text{Im}\,\Sigma \propto \sqrt{\omega}, \sqrt{T}$ dependence of the spinon self-energy characteristic of the SYK regime. Despite this, the resistivity is found to be linear in *T* because the dispersion of the quasiparticles is negligible compared to this large scattering rate, so the conductivity as obtained from the Kubo formula is proportional to $1/(\text{Im}\,\Sigma)^2 \propto 1/T$.

These conclusions can be drawn by examining the large-*M* equation for the spinon Green's function G_f, which reads (Parcollet and Georges, 1999)

$$G_f^{-1} = i\omega_n + \mu - \bar{\lambda} - (pt)^2 G_f - \Sigma_f(i\omega_n), \quad (7.24)$$

where $i\lambda = \bar{\lambda}$ at the saddle point and $\Sigma_f(\tau) = -J^2 G_f^2(\tau) G_f(-\tau)$ as in the large-*M* SY model. The doping-induced term $(pt)^2 G_f$ is a singular perturbation that cuts off the SYK behavior. Indeed, substituting $\Sigma_f \propto \sqrt{J\omega}$ into Eq. (7.24), which corresponds to $G_f \propto 1/\sqrt{J\omega}$, we see that a stable solution of this type can exist only for $(pt)^2/\sqrt{J\omega} \lesssim \sqrt{J\omega}$, which yields $\omega \gtrsim (pt)^2/J \sim T_{\text{coh}}$, which corresponds to the previously described crossover regime. For $T, \omega \lesssim T_{\text{coh}}$, the consistent solution of Eq. (7.24) is a Fermi liquid.

2. SU(*M*) symmetry: Non-Fermi-liquid large-*M* limit

We know from the numerical studies of the random quantum magnet discussed in Sec. VI.B that the actual ground state of the undoped model ($p = 0$) is a spin glass, in contrast to the spin liquid appearing in Sec. VII.D.1. It is reasonable to expect that this spin-glass state survives for a range of nonzero

p, and this has been confirmed by the numerical studies discussed in Sec. VII.C. In the large-*M* method of Sec. VII.D.1 the boson *b* condenses at any nonzero doping, so the correlated spin liquid (or its associated spin-glass state) is absent at $T = 0$ away from the insulator. In this section, we discuss an alternative large-*M* approach in which the boson need not condense at nonzero doping and can instead form a SYK-like critical state.

We consider a large-*M* theory of an SU(*M'*|*M*) supersin in which large-*M* and large-*M'* limits are taken with $k = M'/M$ fixed (Joshi *et al.*, 2020; Tikhanovskaya *et al.*, 2021b). This requires a theory of fermionic spinons $f_\alpha, \alpha = 1, \ldots, M$, just as in Sec. VII.D.1. However, the bosonic holons b_ℓ now have an additional "orbital" index $\ell = 1, \ldots, M'$. The electrons $c_{\ell\alpha}$ have an additional orbital index ℓ and are related to the spinons f_α and holons b_ℓ by

$$c_{\ell\alpha} = f_\alpha b_\ell^\dagger,$$

$$\sum_{\alpha=1}^{M} f_\alpha^\dagger f_\alpha + \sum_{\ell=1}^{M'} b_\ell^\dagger b_\ell = \frac{M}{2}. \quad (7.25)$$

The doping density *p* is given by

$$\frac{1}{N}\sum_{i\ell} b_{i\ell}^\dagger b_{i\ell} = M'p. \quad (7.26)$$

The physical case corresponds to $M = 2$, $M' = 1$, and $k = 1/2$.

We can now take the large-*M* limit in a manner that closely parallels Sec. VI. We then obtain the following SYK-like equations for the boson and fermion Green's functions, now describing a critical doped spin liquid:

$$G_b(i\omega_n) = \frac{1}{i\omega_n + \mu_b - \Sigma_b(i\omega_n)},$$

$$\Sigma_b(\tau) = -t^2 G_f(\tau) G_f(-\tau) G_b(\tau),$$

$$G_f(i\omega_n) = \frac{1}{i\omega_n + \mu_f - \Sigma_f(i\omega_n)},$$

$$\Sigma_f(\tau) = -J^2 G_f^2(\tau) G_f(-\tau) + kt^2 G_f(\tau) G_b(\tau) G_b(-\tau). \quad (7.27)$$

Equations (7.27) share some similarities with those introduced in a study (Haule *et al.*, 2002) of the nonrandom *t-J* model using the noncrossing approximation in the EDMFT framework. They can be obtained from a $G - \Sigma$ action that generalizes those in Eqs. (5.56), (6.6), and (8.8) as follows:

$$\begin{aligned} I[G, \Sigma] = &-\ln\,\det\left[(\partial_\tau - \mu_f)\delta(\tau_1 - \tau_2) + \Sigma_f(\tau_1, \tau_2)\right] \\ &+ k\ln\,\det\left[(\partial_\tau - \mu_b)\delta(\tau_1 - \tau_2) + \Sigma_b(\tau_1, \tau_2)\right] \\ &+ k\text{Tr}(\Sigma_b \cdot G_b) + \frac{kt^2}{2}\text{Tr}([G_f G_b] \cdot [G_f G_b]) \\ &- \text{Tr}(\Sigma_f \cdot G_f) - \frac{J^2}{4}\text{Tr}(G_f^2 \cdot G_f^2). \end{aligned} \quad (7.28)$$

In Eq. (7.28) μ_f and μ_b are chemical potentials chosen to satisfy

$$\langle f^\dagger f \rangle = \tfrac{1}{2} - kp, \qquad \langle b^\dagger b \rangle = p. \qquad (7.29)$$

As for the SYK model, we search for solutions of Eq. (7.27) with the following low-energy critical behavior:

$$G_f(z) = C_f \frac{e^{-i(\pi\Delta_f + \theta_f)}}{z^{1-2\Delta_f}}, \qquad \text{Im}(z) > 0,$$

$$G_b(z) = C_b \frac{e^{-i(\pi\Delta_b + \theta_b)}}{z^{1-2\Delta_b}}, \qquad \text{Im}(z) > 0,$$

$$\frac{\theta_f}{\pi} + \left(\frac{1}{2} - \Delta_f\right) \frac{\sin(2\theta_f)}{\sin(2\pi\Delta_f)} = kp,$$

$$\frac{\theta_b}{\pi} + \left(\frac{1}{2} - \Delta_b\right) \frac{\sin(2\theta_b)}{\sin(2\pi\Delta_b)} = \frac{1}{2} + p. \qquad (7.30)$$

The last two equations of Eqs. (7.30) follow from Luttinger theorems similar to those discussed in Sec. V.B (Georges, Parcollet, and Sachdev, 2001; Gu *et al.*, 2020). Inserting this *Ansatz* into Eq. (7.27), we find that self-consistency of the terms involving the hopping t leads to the following constraint on the scaling dimensions of the fermion (Δ_f) and boson (Δ_b):

$$\Delta_f + \Delta_b = \tfrac{1}{2}. \qquad (7.31)$$

Inserting the *Ansätze* for G_b and G_f into the correlation functions for the electron and spin operators [as in Eq. (6.7)], we obtain for the gauge-invariant observables

$$\langle c_\alpha(\tau) c_\alpha^\dagger(0) \rangle \sim \begin{cases} A_+/|\tau|, & \tau > 0, \\ -(A_-/|\tau|), & \tau < 0, \end{cases}$$

$$\langle \boldsymbol{S}(\tau) \cdot \boldsymbol{S}(0) \rangle \sim \frac{1}{|\tau|^{4\Delta_f}}. \qquad (7.32)$$

The electron Green's function is similar to that of a Fermi liquid, with the difference that the present large-M limit allows for solutions with a particle-hole asymmetry with $A_+ \neq A_-$, whereas a Fermi liquid always has $A_+ = A_-$. We note that this is an unusual situation in which the $T = 0$ spectral function is discontinuous at $\omega = 0$; the electron Green's function obtained from the RG analysis presented in Sec. VII.D.3 does not share this feature. A Fermi liquid would also have a spin correlation function with a $1/\tau^2$ decay, which is potentially different from the previously discussed $1/|\tau|^{4\Delta_f}$ decay.

Our discussion thus far has been general, but the nature of the state obtained strongly depends on the values of the exponents Δ_f and Δ_b. Determining their values requires further analysis of Eq. (7.27), and we now describe the three distinct possibilities.

a. $\Delta_b = \Delta_f = 1/4$: Doped SY spin liquid

In such a solution, the J terms in Eq. (7.27) also contribute to determining the parameters in the scaling *Ansatz* in Eq. (7.30). The scaling dimension of the spinons and the spin operator are the same as those in the insulating SY spin liquid described in Sec. VI.A. Numerical analyses of Eq. (7.27) at all energies (Tikhanovskaya *et al.*, 2021b) show that such solutions do indeed exist, but only at small values of the doping p.

b. $\Delta_b = 0$, $\Delta_f = 1/2$: Disordered Fermi liquid

This state is the same as that obtained in the large-M limit of Sec. VII.D.1, but it turns out not to be a valid solution of the saddle-point equations in Eq. (7.27) of the present large-M limit (Christos *et al.*, 2022). If $\Delta_b = 0$, we have a b condensate with $\langle b(\tau \to \infty) b^\dagger(0) \rangle \neq 0$ at $T = 0$. Inserting this condensate into the equation for Σ_b in Eq. (7.27), we find a contribution $\Sigma_b(\omega) \sim |\omega|$ from the fermion polarizability, which leads to a $\ln(1/\tau)$ contribution to $G_b(\tau)$, which is inconsistent with the presence of a b condensate.

c. $0 < \Delta_b < 1/4$, $\Delta_f = 1/2 - \Delta_b$: Critical metal

Numerical analysis (Christos *et al.*, 2022) of Eq. (7.27) shows that this is indeed a valid solution for a wide range of doping p. The J terms in Eq. (7.27) are subdominant to the critical *Ansatz* at low energies, but they do contribute at higher energies. The exponents in this critical metal vary continuously as a function of the doping and J/t and can be determined by demanding numerically that Eq. (7.27) apply at all energies. For finite M, the critical metal can be stable to spin-glass order at $T = 0$ for $\Delta_f < 1/4$, unlike the finite-T instability in Eq. (6.16) for the SY spin liquid. There can be an instability to a metallic spin glass below a critical doping p_c (Christos *et al.*, 2022), and this is indicated in the schematic phase diagram in Fig. 16. This spin-glass phase can be described (Christos *et al.*, 2022) using a theory of bosonic spinons $\mathfrak{b}_\alpha$ similar to that used for the insulating spin glass (Georges, Parcollet, and Sachdev, 2000, 2001) in a related large-M limit of an $SU(M|M')$ superspin (Tikhanovskaya *et al.*, 2021b), as indicated in Fig. 16.

3. RG analysis for SU(2) symmetry

This section returns to the original *t-J* model with SU(2) spin symmetry, as defined by Eqs. (7.19)–(7.21). We describe here a RG treatment similar to that for the insulating quantum magnet presented in Sec. VI.C. The RG finds a critical point with one relevant direction, which is naturally identified with the deviation of the doping density p from the critical
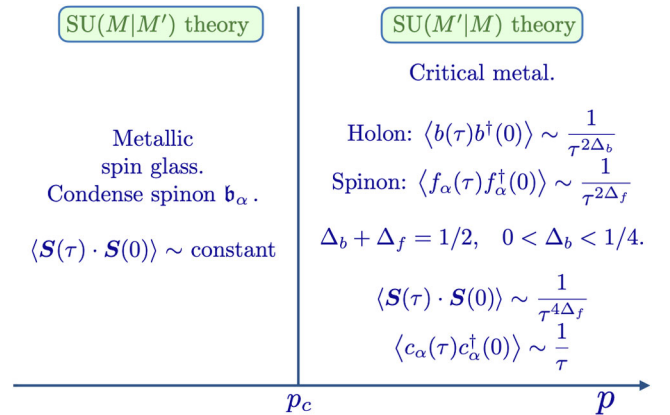

FIG. 16. Schematic phase diagram of the *t-J* model in the non-Fermi-liquid M limit of Sec. VII.D.2 (Christos *et al.*, 2022). In the critical metal phase, the exponents obey $0 < \Delta_b < 1/4$ and $\Delta_f = 1/2 - \Delta_b$, and Δ_b decreases monotonically toward 0 (the Fermi-liquid value) with increasing p.

density p_c. Moreover, the theory of this critical point turns out to be similar to the large-M theory described in Sec. VII.D.2.

We proceed (Joshi *et al.*, 2020) in a manner that parallels Sec. VI.C. We first assume power-law decays for the correlators in the action in Eq. (7.19),

$$Q(\tau) \sim \frac{1}{|\tau|^{d-1}}, \qquad R(\tau) \sim \frac{\mathrm{sgn}(\tau)}{|\tau|^{r+1}}, \qquad (7.33)$$

and ignore the self-consistency condition [Eq. (7.21)] to begin with. We decouple the J^2 and t^2 terms in the action by introducing bosonic $(\phi_a, a = 1, \dots, 3)$ and fermionic (ψ_α) baths. The problem then reduces to the following solution of the impurity Hamiltonian:

$$H_{\mathrm{imp}} = (s_0 + \lambda)f_\alpha^\dagger f_\alpha + \lambda b^\dagger b + g_0[f_\alpha^\dagger b \psi_\alpha(0) + \mathrm{H.c.}]$$
$$+ \gamma_0 f_\alpha^\dagger \frac{\sigma_{\alpha\beta}^a}{2} f_\beta \phi_a(0) + \int |k|^r dk\, k\psi_{k\alpha}^\dagger \psi_{k\alpha}$$
$$+ \frac{1}{2}\int d^d x\,[\pi_a^2 + (\partial_x \phi_a)^2], \qquad (7.34)$$

where the constraint in Eq. (7.15) is imposed exactly by taking $\lambda \to \infty$ (Fritz and Vojta, 2004), $a = (x, y, z)$, σ^a are Pauli matrices, π_a is canonically conjugate to the field ϕ_a, $\phi_a(0) \equiv \phi_a(x = 0)$, and $\psi_\alpha(0) \equiv \int |k|^r dk\, \psi_{k\alpha}$. We identify $Q(\tau)$ with the temporal correlator of $\phi_a(0)$ and identify $R(\tau)$ with the temporal correlator of $\psi_\alpha(0)$, and it can be verified that these correlators decay as in Eq. (7.33).

Therefore, we have reduced the problem to an impurity Hamiltonian of a SU(1|2) superspin interacting with separate bosonic and fermionic baths. By analogy with the Bose-Kondo model in Eq. (6.18), we can identify it as a superspin Bose-Fermi-Kondo model where both the fermionic and bosonic baths have to be determined self-consistently. Such a model can be analyzed using a RG computation that performs the exact path integral over the superspin space, i.e., imposes the constraint in Eq. (7.15) exactly. The methods are similar to those used for the insulating spin problem that was employed to obtain Eq. (6.20), which ultimately depended only upon the spin commutation relations. In a similar manner, the RG results follow from the SU(1|2) commutation relations in Eq. (7.18a). We also note that the same RG equations would have been obtained from the commutation relations of the isomorphic SU(2|1) algebra; i.e., we get the same results from the formulation in terms of either the bosonic spinons or the fermionic spinons.

The impurity has three coupling constants, and we represent their renormalized values by γ, g, and s. The coupling γ measures the coupling to the bosonic bath, just as in Eq. (6.18). Similarly, g is the coupling to the fermionic bath. We see shortly that g and γ can be chosen to be nearly marginal with appropriate choices of the exponents in Eq. (7.33). The coupling s tunes the relative energies of the spin and holon states, as is clear in Eq. (7.34). This is the relevant perturbation mentioned at the start of this section, and its flow leads to the phase diagram in Fig. 17. For $s \to +\infty$, the energy of the holon is much lower and we expect the holon b to condense, leading to a disordered Fermi liquid.
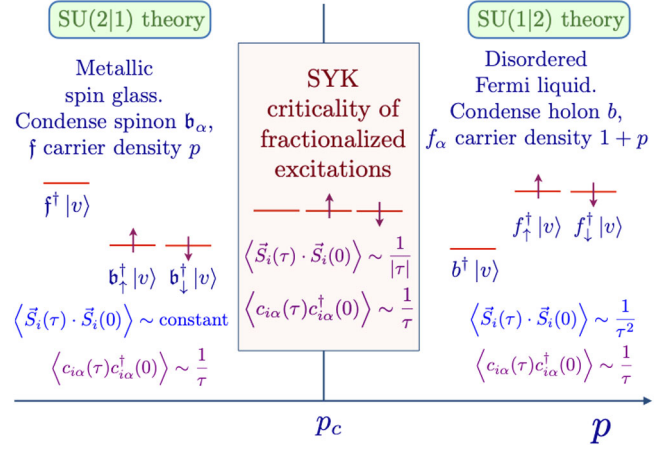

FIG. 17. Schematic phase diagram of the RG analysis of the random, fully connected $t - J$ model. The spinon and holon states are nearly degenerate in the critical spin-liquid theory, while the holon (spinon) states have lower energy for $p > p_c$ $(p < p_c)$. From Joshi *et al.*, 2020.

Conversely, for $s \to -\infty$ the spinons will condense [in the SU(2|1) formulation, as in Fig. 17], leading to a spin glass. And in between, at some $s = s_c$ we will have the fixed point that describes the critical theory we are interested in. To zeroth order in g and γ, the critical point is at $s_c = 0$: this corresponds a threefold degeneracy in the three states of the superspin (see Fig. 17) and a doping density $p_c = 1/3$. Therefore, we have the prediction that the critical doping density of the fully connected random t-J model is close to $p = 1/3$, a result that is indeed supported by the numerical results (Shackleton *et al.*, 2021) reviewed in Sec. VII.C.

The one-loop RG equations are (Joshi *et al.*, 2020)

$$\beta(g) = -\bar{r}g + \tfrac{3}{2}g^3 + \tfrac{3}{8}g\gamma^2,$$
$$\beta(\gamma) = -\frac{\epsilon}{2}\gamma + \gamma^3 + g^2\gamma,$$
$$\beta(s) = -s + 3g^2 s - g^2 + \tfrac{3}{4}\gamma^2. \qquad (7.35)$$

We have introduced the variables

$$\epsilon = 3 - d, \qquad \bar{r} = (1 - r)/2, \qquad (7.36)$$

and it is clear from Eq. (7.35) that the fixed points at small ϵ and $\bar{r}$ are under perturbative control in powers of ϵ and $\bar{r}$. The RG flows in the g-γ plane are shown in Fig. 18: there is a fixed point in this plane at g^{*2}, γ^{*2} of the order of $\epsilon, \bar{r}$. The relevant perturbation s induces flows away from this fixed point in a direction that is predominantly transverse to the g-γ plane. There are also fixed points in Fig. 18 along the $g = 0$ line, corresponding to the fixed point of the insulating magnet in Eq. (6.20), and along the $\gamma = 0$ line, corresponding to the fixed point of the asymmetric pseudogap Anderson impurity (Fritz and Vojta, 2004; Vojta and Fritz, 2004), and has properties similar to the large-M critical metal solution of Sec. VII.D.2 in Fig. 16.

Finally, we can compute the scaling dimensions of the electron and spin operators at the red fixed point in Fig. 18. As in Sec. VI.C, these scaling dimensions are protected by the
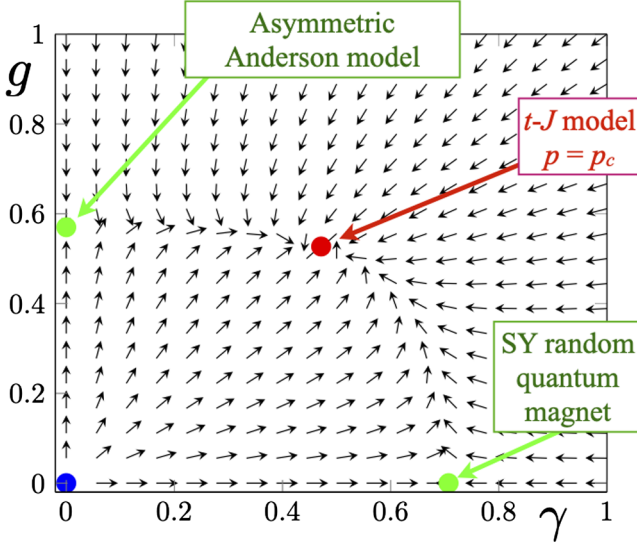
FIG. 18. RG flow of Eq. (7.35) in the γ-g plane plotted for $\epsilon = 1$ and $\bar{r} = 0.5$. The red circle is the stable fixed point in this plane, which is unstable only to flows predominantly in the s direction out of the plane; this fixed point describes the $p = p_c$ critical state in Fig. 17, and $p - p_c$ tunes the coefficient of the relevant perturbation (not shown), which presumably drives the system into the $p > p_c$ and $p < p_c$ phases shown in Fig. 17. From Joshi *et al.*, 2020.

Berry phase term in Eq. (7.19) that imposes the SU(1|2) commutation relations at any fixed point at nonzero g^* and γ^*. Therefore, we are able to compute the exponents in Eq. (7.20) to all loop order; we find that

$$\langle c_\alpha(\tau) c_\alpha^\dagger(0)\rangle \sim \frac{\text{sgn}(\tau)}{|\tau|^{1-r}},$$
$$\langle \boldsymbol{S}(\tau) \cdot \boldsymbol{S}(0)\rangle \sim \frac{1}{|\tau|^{3-d}}. \tag{7.37}$$

We now restore the self-consistency condition in Eq. (7.21) and find the self-consistent values $r = 0$ and $d = 2$. These self-consistent exponents are the same as those obtained for the doped SY spin-liquid case in the large-M computation of Eq. (7.32). There is, however, an interesting difference that merits further study: the electron correlator in Eq. (7.32) is allowed to have particle-hole asymmetry with $A_+ \neq A_-$, but that is not the case for the present RG analysis.

E. Transport in random-exchange *t-U-J* models

Discussing conductivity requires a slightly different setup than a fully connected lattice in order to properly define transport and the current operator. One possibility is to consider the model on the Bethe lattice with nonrandom hopping amplitudes $t_{ij} = t/\sqrt{z}$, with z the connectivity of the lattice. In the limit $z \to \infty$, the self-energy and the local Green's function obey the same equations as the model with random t_{ij} (Georges *et al.*, 1996). Another possibility is to consider a translationally invariant lattice of fully connected dots, as in Sec. X.

The conductivity is given as follows by the Kubo formula:

$$\sigma_{\text{dc}} = \frac{2\pi e^2}{\hbar} \int d\omega \frac{\beta}{4\cosh^2(\beta\omega/2)} \int d\epsilon \, \phi(\epsilon) A(\epsilon, \omega)^2. \tag{7.38}$$

In Eq. (7.38), ϵ is the energy of a bare single-particle state within the band and $A(\epsilon, \omega) = -(1/\pi)\text{Im}\, G^R(\epsilon, \omega)$ is the energy- (momentum-) resolved spectral function. The transport function $\phi(\epsilon)$ is defined on a Bravais lattice by

$$\phi(\epsilon) = \int \frac{d^d k}{(2\pi)^d} v_{kx}^2 \delta(\epsilon - \epsilon_{\boldsymbol{k}}), \tag{7.39}$$

in which $v_{kx} = (\nabla_{\boldsymbol{k}} \epsilon_{\boldsymbol{k}})_x / \hbar$ is the velocity in the considered direction. On the infinite-connectivity Bethe lattice $\phi(\epsilon) = \phi(0)[1 - (\epsilon/2t)^2]^{3/2}$ (Georges *et al.*, 1996). Here we have assumed that the self-energy as well as the two-particle vertex function depends only on frequency. As a result, because the current vertex is odd in momentum, vertex corrections to the conductivity vanish and the full Kubo formula reduces to the fermionic bubble in Eq. (7.38) (Khurana, 1990). Note that this is not the case for other correlation functions that are even parity (such as charge or spin) (Georges *et al.*, 1996).

We now discuss the behavior of the resistivity following from Eq. (7.38) in two different situations. We first consider a case in which $\text{Im}\,\Sigma$ is much larger than the dispersion of the band itself (i.e., the range over which ϵ varies in the integral). The dispersion can then be entirely neglected and we obtain $\sigma_{\text{dc}} \propto \int d\omega \{\beta/[4\cosh^2(\beta\omega/2)]\}(\text{Im}\, 1/\Sigma)^2$. This applies to the large-M limit of the random-exchange *t-J* model discussed in Sec. VII.D.1 in the SYK regime where $T > T_{\text{coh}}$. In that case, $\text{Im}\,\Sigma \propto \sqrt{JT} f(\omega/T)$, where $f(\cdots)$ is a scaling function. Inserting this into the previous expression leads one to $\rho(T)/\rho_Q \propto T/T_{\text{coh}}$, i.e., a resistivity that is T linear but larger than the MIR value (introduced in Sec. III). This bad-metallic behavior corresponds, however, to a Planckian regime with a diffusion constant $\propto 1/T$ since the compressibility is temperature independent. The conductivity is proportional to the square of the transport scattering rate in this regime; the latter is T linear while the single-particle scattering rate is $\propto \sqrt{JT}$. This mechanism for a Planckian bad metal with T-linear resistivity was first discussed by Parcollet and Georges (1999).

In the second case $\text{Im}\,\Sigma$ is, in contrast, smaller than the band dispersion. This applies in the low-T limit of most of the models discussed in this review. The integral in Eq. (7.38) can then be approximated as $\int d\epsilon \, \phi(\epsilon) A(\epsilon, \omega)^2 \sim \phi[\omega + \mu - \text{Re}\,\Sigma(\omega)]/[2\pi|\text{Im}\,\Sigma(\omega)|]$. Owing to the derivative of the Fermi function in the numerator, one can set $\omega = 0$ in the numerator. Defining the renormalized Fermi level as $\epsilon_F = \mu - \text{Re}\,\Sigma(0,0)$ (which coincides with the bare Fermi energy when Luttinger's theorem is satisfied), one obtains

$$\sigma_{\text{dc}} \simeq \frac{e^2 \phi(\epsilon_F)}{\hbar} \int d\omega \frac{\beta}{4\cosh^2(\beta\omega/2)} \frac{1}{|\text{Im}\,\Sigma(\omega, T)|}. \tag{7.40}$$

Equation (7.40) is similar to Drude-Boltzmann theory, but we emphasize that it is valid even when the scattering rate has a

non-Fermi-liquid form. For example, when $\mathrm{Im}\,\Sigma = T^\nu f(\omega/T)$, we obtain $\rho \propto T^\nu$; $\nu = 1$ corresponds to a Planckian metal. Evidence for such NFL behavior of the scattering rate was previously discussed for the quantum-critical regime of the random bond t-J and Hubbard models (Cha, Wentzell *et al.*, 2020; Dumitrescu *et al.*, 2022). We emphasize that, as is well known from transport theory, the wave function normalization $Z(T) \propto [1 - \partial \mathrm{Re}\,\Sigma(\omega, T)/\partial\omega|_{\omega=0}]^{-1}$ does not enter the expression of the conductivity, in contrast to the width of the one-electron spectral function, which is $\propto Z|\mathrm{Im}\,\Sigma|$ (and can be interpreted as the inverse of the quasiparticle lifetime in a Fermi liquid). Note that, for a NFL with $\mathrm{Im}\,\Sigma \propto T^\nu$ and $\nu < 1$, the latter always displays Planckian behavior $\propto T$, regardless of the value of the exponent ν, since $Z(T, \omega = 0)$ vanishes as $Z(T) \propto T^{1-\nu}$. Indeed, the real part of the self-energy is related to the imaginary part by $\mathrm{Re}\,\Sigma(\omega) = -\int d\omega' [\mathrm{Im}\,\Sigma(\omega')/\pi]/(\omega - \omega')$, from which it follows for $\nu < 1$ that $\mathrm{Re}\,\Sigma(\omega) = T^\nu \tilde{f}(\omega/T)$, and hence $1/Z = 1 - \partial_\omega \mathrm{Re}\,\Sigma = 1 - T^{\nu-1} \tilde{f}'(\omega/T)$; see Georges and Mravlje (2021) for details.

We note that Eq. (7.38) also applies to nonrandom models in the DMFT limit of infinite connectivity. An interesting connection was recently noted (Cha, Patel *et al.*, 2020) between the T-linear behavior of the resistivity in such models in the high-T bad metal regime (Pálsson and Kotliar, 1998; Perepelitsky *et al.*, 2016) discussed in Sec. III.A and the SYK equations for the self-energy. Whether such a connection also exists in the lower temperature regime is an interesting open question; for a recent study of T-linear resistivity in the nonrandom Hubbard model using cluster extensions of DMFT, see Wu, Wang, and Tremblay (2021). Possible connections between the SYK model and NFL regimes of nonrandom multiorbital models have also been pointed out (Werner, Kim, and Hoshino, 2018; Tsuji and Werner, 2019). Relevance of SYK criticality to possible instabilities of "Luttinger surfaces" has also been discussed (Setty, 2020, 2021).

Thermoelectric transport has also been analyzed in random-exchange and SYK models. It was pointed out (Davison *et al.*, 2017; Kruchkov *et al.*, 2020) that the thermopower of a lattice of SYK islands is directly related to the spectral asymmetry parameter $\mathcal{E}$ introduced in Eq. (5.25), and hence offers a possible probe of the residual $T = 0$ entropy. That relation may be more involved in general, however (Kruchkov *et al.*, 2020; Pavlov and Kiselev, 2021). Recently Georges and Mravlje (2021) emphasized that the intrinsic particle-hole asymmetry of the ω/T scaling function in Eq. (7.11), which is characteristic of "skewed" Planckian (or sub-Planckian) metals, has noteworthy consequences for the sign and T dependence of the thermopower down to low T, even in the presence of additional elastic scattering. The possible relevance to Seebeck measurements on cuprate superconductors has been explored (Gourgout *et al.*, 2021).

F. General mechanism for T-linear resistivity as $T \to 0$ from time reparametrization

The quantum-critical T-linear resistivity computed numerically in Sec. VII.C (and also in Sec. VII.B) is somewhat mysterious when compared with the analytical results. Recall

that we found a leading Fermi-liquid-like behavior in the electron Green's function at the quantum-critical point in the non-Fermi-liquid large-M limit in Eq. (7.32), and also in the RG analysis for $M = 2$ in Eq. (7.37). The RG analysis also makes clear that this Fermi-liquid exponent for the electron operator is likely to be exact to all orders in $1/M$. Inserting such an electron spectral density into Eq. (7.38), we obtain temperature-independent residual resistivity as $T \to 0, \rho(0)$. We note that this large residual resistivity, present even for a large dimension lattice without hopping disorder, appears to be an artifact of the non-Fermi-liquid large-M limit of Sec. VII.D.2 (Guo, Gu, and Sachdev, 2020). The Fermi-liquid large-M limit of Sec. VII.D.1 has vanishing residual resistivity (Parcollet and Georges, 1999), and this also appears to be the case in the numerical study in the SU(2) limit (Dumitrescu *et al.*, 2022). It is possible that the non-Fermi-liquid large-M limit of Sec. VII.D.2 has a crossover in the residual resistivity at a frequency that vanishes as M becomes large.

We obtain a T dependence to the resistivity as $T \to 0$ by considering corrections to scaling for the electron operator in the $N = \infty$ theory. The structure of these corrections can be easily deduced from the theory described in Sec. V.E, which generalizes directly to the t-J model (Tikhanovskaya *et al.*, 2021b). As for the entropy in Eq. (5.53) and the spin spectral density in Eq. (6.9), we consider the corrections due to the $h = 2$ operator. The scaling dimension of this operator is also "protected" at $h = 2$, given its connection to the Schwarzian theory in Sec. V.F; i.e., it is the "time reparametrization" operator, and the "boundary graviton" in the holographic theory to be discussed in Sec. XII.B. Therefore, we do not expect the $h = 2$ scaling dimensions to acquire any $1/M$ corrections. By the same arguments that lead to Eq. (6.9) for the spin spectral density, we now obtain for the temperature dependence for the resistivity (Guo, Gu, and Sachdev, 2020)

$$\rho(T) = \rho(0)[1 + \mathcal{C}_\rho \gamma T + \cdots].   (7.41)$$

The linear-T dependence is the power T^{h-1}, which is related to that in Eq. (5.45), for the time reparametrization mode with $h = 2$. The parameter γ is the same as that in the entropy in Eq. (5.53), and $\mathcal{C}_\rho$ is a dimensionless universal number similar to $\mathcal{C}$ in Eq. (6.9). The value of $\mathcal{C}_\rho$ can be computed in the large-M limit of the t-J model (Guo, Gu, and Sachdev, 2020). While the coefficient of linear-T resistivity is controlled by the residual resistivity in this large-M computation, that is not the case for the numerical SU(2) computation in Fig. 14, with the corresponding phase diagram given in Fig. 13 (Dumitrescu *et al.*, 2022). We also note that the large-M theory of the doped t-J model has operators with $h < 2$. However, the scaling dimension of these operators is not protected, and their contribution to the resistivity is numerically small in the large-M theory (Tikhanovskaya *et al.*, 2021b).

G. Experimental relevance

The models described in this section are not meant to be microscopically realistic models of materials displaying NFL behavior, such as the cuprate strange metal. Nonetheless, as we now discuss, the physics of the doped Hubbard and t-J models with the previously addressed random-exchange

couplings present rather striking similarities to some of the salient phenomenology of the cuprates and can serve as a building block for capturing certain universal aspects of NFL behavior in general. We recall two of the most fundamentally interesting phenomena observed in these materials.

- The appearance of a pseudogap regime below a critical doping ($p < p^*$). At low T and high fields, quantum oscillations have revealed the existence of pocket Fermi surfaces (Doiron-Leyraud *et al.*, 2007; Proust and Taillefer, 2019). These oscillations appear in a regime with long-range charge-density-wave order, but a simple model of reconstruction of the large Fermi surface by the charge-density-wave order cannot explain the details of the quantum oscillations. At higher T or at dopings $p_{CDW} < p < p^*$ (where p_{CDW} is the doping below which there is charge-density-wave order), there is no known long-range order, and there is clear experimental evidence that the electronic spectrum cannot be explained by the large Fermi surface. The observations include angle-dependent magnetoresistance (Fang *et al.*, 2022) and the "Fermi arcs" in ARPES (Damascelli, Hussain, and Shen, 2003).

- Near p^*, several properties are evocative of quantum criticality, most notably (i) T-linear resistivity with a transport scattering time obeying Planckian behavior $\tau \simeq \alpha \hbar / k_B T$ down to low temperatures (Homes *et al.*, 2004; Zaanen, 2004; Hussey, 2008; Bruin *et al.*, 2013; Legros *et al.*, 2019; Varma, 2020; Grissonnanche *et al.*, 2021); (ii) ω/T scaling observed in several spectroscopies, such as optical conductivity (van der Marel *et al.*, 2003; Michon *et al.*, 2022; van Heumen *et al.*, 2022) and ARPES (Reber *et al.*, 2019); and (iii) a diverging specific-heat coefficient near p^*, with logarithmic dependence of C/T upon T at $p = p^*$ (Michon *et al.*, 2019).

Seen in this perspective, the previously described doped random-exchange models offer a simple platform in which to study some of these phenomena. We have reviewed the findings that they display a critical point upon doping at which quantum-critical scaling is observed, and that the Luttinger theorem breaks down at this critical doping. We find clear evidence of the Luttinger breakdown in the value of the chemical potential at temperatures above the spin-glass transition for $p < p_c$ in the Monte Carlo study (Dumitrescu *et al.*, 2022) and at zero temperature within the metallic spin glass in the exact diagonalization study (Shackleton *et al.*, 2021). The precise nature of the Fermi surface reconstruction, and possible volume collapse, is still to be investigated in the low-T metallic spin-glass phase for $p < p_c$ and is one of the interesting open questions in the field.

Most notably, these doped random-exchange and SYK models are among the few theoretical models in which Planckian behavior of transport (Zaanen, 2004) in the absence of coherent quasiparticles can be studied in a controlled manner [we note that this issue has been investigated in the marginal Fermi-liquid context (Varma *et al.*, 1989; Varma, 2016, 2020)]. The randomness of the exchange constants helps introduce "frustration" and is, at the theoretical level, a simple way to account for the fact that the physics of short-range spin correlations is important in the pseudogap phase,

but without true long-range order. One can also argue, as emphasized early on (Parcollet and Georges, 1999), that randomness of the exchange constants can be motivated at a more microscopic level. In this respect, recent nuclear magnetic resonance and ultrasound measurements have revealed that the spin-glass phase extends up to $p = p^*$ for $La_{2-x}Sr_xCuO_4$ subject to a high magnetic field (Frachet *et al.*, 2020). The critical theory of the random-exchange models is not particle hole symmetric, and the possible relevance of the intrinsic particle-hole asymmetry of the ω/T scaling function associated with the scattering rate has recently been emphasized for the interpretation of Seebeck measurements on the cuprates (Georges and Mravlje, 2021; Gourgout *et al.*, 2021).

Another indication of Planckian behavior is the anomalous continuum observed in dynamic charge response measurements (Mitrano *et al.*, 2018; Husain *et al.*, 2019) on optimally doped $Bi_{2.1}Sr_{1.9}Ca_{1.0}Cu_{2.0}O_{8+x}$ using momentum-resolved electron energy-loss spectroscopy. This has been studied in a model with additional random density-density interactions (Joshi and Sachdev, 2020).

VIII. RANDOM-EXCHANGE KONDO-HEISENBERG MODEL

This section will combine the random-matrix model of mobile electrons of Sec. IV with the random quantum magnet of Sec. VI and couple them with a nonrandom, antiferromagnetic Kondo exchange coupling J_K. Thus, we have the Kondo-Heisenberg Hamiltonian

$$H_{KH} = \frac{1}{(N)^{1/2}} \sum_{i,j=1}^{N} t_{ij} c_{i\alpha}^\dagger c_{j\alpha} - \mu \sum_i c_{i\alpha}^\dagger c_{i\alpha}$$
$$+ \frac{1}{\sqrt{N}} \sum_{1 \le i < j \le N} J_{ij} S_i \cdot S_j + \frac{J_K}{2} \sum_i S_i \cdot (c_{i\alpha}^\dagger \sigma_{\alpha\beta} c_{i\beta}), \quad (8.1)$$

which has been used extensively as a theory of numerous rare-earth intermetallics (usually in the absence of random exchange), the so-called heavy-fermion compounds. This model exhibits a "heavy Fermi-liquid" (HFL) ground state, which is a Fermi liquid with electronlike quasiparticle excitations with a large effective mass for models with nonrandom t_{ij}. Moreover, the Fermi energy is large because the occupied states count both the conduction electrons $c_{i\alpha}$ and the spins S_i. The fully connected random model also has such a heavy Fermi-liquid phase that obeys a Luttinger theorem with this large Fermi energy (Burdin, Grempel, and Georges, 2002; Nikolaenko *et al.*, 2021), as we discuss further in Sec. VIII.C.

Our interest here is in other possible phases of the Kondo-Heisenberg lattice model, and on the quantum-critical points to these phases starting from the HFL. A possibility of particular interest is the fractionalized Fermi liquid (FL*) (Burdin, Grempel, and Georges, 2002; Senthil, Sachdev, and Vojta, 2003; Paramekanti and Vishwanath, 2004; Senthil, Vojta, and Sachdev, 2004), in which the Fermi surface is "small" and includes only the volume of the conduction electrons. The spins S_i form a spin-liquid state with fractionalized excitations, and the fractionalized excitations are required to exist to allow deviation of the Fermi surface

volume from the Luttinger value (Paramekanti and Vishwanath, 2004; Senthil, Vojta, and Sachdev, 2004; Bonderson *et al.*, 2016; Else, Thorngren, and Senthil, 2021); we also make note of other discussions of FL* and related states (Andrei and Coleman, 1989; Coleman, Marston, and Schofield, 2005; Paul, Pépin, and Norman, 2007, 2008, 2013; Pixley, Yu, and Si, 2014; Chowdhury, Sodemann, and Senthil, 2018; Si, 2010; Paschen and Si, 2021). In the random fully connected model, the S_i spins form the SYK spin liquid of Sec. VI in the large-M limit, as we describe in Sec. VIII.B. A number of recent experiments have reported the existence of a paramagnetic metallic phase with a Fermi surface volume that does not appear to include the local moment electrons in $YbRh_2(Si_{0.95}Ge_{0.05})_2$ (Custers *et al.*, 2003, 2010), CePdAl (Zhao *et al.*, 2019), and $CeCoIn_5$ (Maksimovic *et al.*, 2022), which resembles some aspects of the FL* phase.

A third possible phase of the Kondo-Heisenberg lattice model has broken spin rotation symmetry and associated magnetic order. For the random fully connected model in Eq. (8.1) with SU(2) spin symmetry, this is likely realized as a spin-glass phase. We discuss a RG analysis of the SU(2) model in Sec. VIII.D, and this has a fixed point that is expected to describe the transition from the spin glass to the HFL. There have been a number of experimental studies of such a transition (Seaman *et al.*, 1991; Aronson *et al.*, 1995; Schröder *et al.*, 1998; Soldevilla *et al.*, 2000; Vollmer *et al.*, 2000; Theumann and Coqblin, 2004; Shimizu *et al.*, 2012; Gannon *et al.*, 2018; Zapf *et al.*, 2001) in the heavy-fermion compounds. Other reviews (Stewart, 2001; Kirchner *et al.*, 2020) further discuss the connections between the Kondo-Heisenberg model and experiments on the heavy-fermion compounds.

A. Effective local action

We begin our analysis, as in Sec. VII.A, by averaging over disorder and formulating the problem in terms of a self-consistent single-site problem. We average over t_{ij} and J_{ij} in Eq. (8.1), and in the large-N limit we obtain the following single-site averaged partition function:

$$
\bar{\mathcal{Z}}_{KH} = \int \mathcal{D}c_\alpha(\tau)\mathcal{D}\mathbf{S}(\tau)\delta(\mathbf{S}^2 - 1)e^{-\mathcal{S}_B - \mathcal{S}_{KH}},
$$

$$
\mathcal{S}_B = \frac{i}{2}\int_0^1 du \int d\tau \mathbf{S} \cdot \left(\frac{\partial \mathbf{S}}{\partial \tau} \times \frac{\partial \mathbf{S}}{\partial u}\right) + \int d\tau \left[c_\alpha^\dagger \frac{\partial c_\alpha}{\partial \tau}\right],
$$

$$
\mathcal{S}_{KH} = \int d\tau \left[-\mu c_\alpha^\dagger c_\alpha + \frac{J_K}{2}\mathbf{S} \cdot (c_\alpha^\dagger \boldsymbol{\sigma}_{\alpha\beta} c_\beta)\right]
$$

$$
- \frac{J^2}{2}\int d\tau d\tau' Q(\tau - \tau')\mathbf{S}(\tau) \cdot \mathbf{S}(\tau')
$$

$$
- t^2 \int d\tau d\tau' R(\tau - \tau')c_\alpha^\dagger(\tau) c_\alpha(\tau') + \text{H.c.} \quad (8.2)
$$

From this action we determine the correlators

$$
\bar{R}(\tau - \tau') = -\frac{1}{2}\langle c_\alpha(\tau) c_\alpha^\dagger(\tau')\rangle_{\mathcal{Z}_{KH}},
$$

$$
\bar{Q}(\tau - \tau') = \frac{1}{3}\langle \mathbf{S}(\tau) \cdot \mathbf{S}(\tau')\rangle_{\mathcal{Z}_{KH}}, \quad (8.3)
$$

and finally impose the self-consistency conditions

$$
R(\tau) = \bar{R}(\tau), \qquad Q(\tau) = \bar{Q}(\tau). \quad (8.4)
$$

As was the case in the *t-J* model in Sec. VII.D, closely related equations can also be obtained in the case of nonrandom t_{ij} involving an electron dispersion ϵ_k.

Note the difference between the single-site self-consistency problem for the *t-J* model of Sec. VII.D and the present Kondo-Heisenberg model. The Berry phase term $\mathcal{S}_B$ reflects the different quantum degrees of freedom on the site: (i) For the *t-J* model we have the three states of the previously described SU(1|2) superspin. (ii) For the Kondo-Heisenberg model we have the two states of the SU(2) spin-1/2 $\mathbf{S}$ and the four states of the electron c_α, for a total of eight states. The two models have similar bosonic and fermionic baths but differ in the on-site Hamiltonian: the present model has a Kondo coupling J_K.

The self-consistent single-site quantum problem defined by Eqs. (8.2)–(8.4) cannot be solved exactly, and we address it in the remainder of Sec. VIII with the same methods as used earlier for the random quantum magnet problem defined in Eqs. (6.11)–(6.13) and the Hubbard model problem defined in Eqs. (7.4)–(7.6).

B. SU(*M*) symmetry with *M* large

The large-M analysis of the fully connected Kondo-Heisenberg model (Burdin, Grempel, and Georges, 2002) proceeds by generalizing the model in Eqs. (8.2)–(8.4) to SU(*M*) symmetry just as in Sec. VI.A for the random quantum magnet. We introduce fermionic spinons $f_\alpha, \alpha = 1, ..., M$, treat the random J_{ij} exchange as in Sec. VI.A, and decouple the J_K exchange by a bosonic field $P(\tau) \sim c_\alpha^\dagger(\tau) f_\alpha(\tau)$. Note that because the J_K exchange is nonrandom, this decoupling variable is not bilocal in time.

In this manner, Eqs. (8.2)–(8.4) reduce to the following equations for the fermion Green's functions, self-energies, and time-independent saddle-point values $i\lambda(\tau) = \bar{\lambda}$ and $P(\tau) = \bar{P}$. The Green's function acquires "band" indices associated with the f and c fermions, so Dyson's equation has a matrix form

$$
\begin{pmatrix} G_f(i\omega_n) & G_{fc}(i\omega_n) \\ G_{cf}(i\omega_n) & G_c(i\omega_n) \end{pmatrix}^{-1}
$$

$$
= \begin{pmatrix} i\omega_n - \bar{\lambda} - \Sigma_f(i\omega_n) & -\bar{P} \\ -\bar{P} & i\omega_n + \mu - \Delta(i\omega_n) \end{pmatrix}. \quad (8.5)
$$

The f fermion self-energy Σ_f is the same as that used for the random magnet in Sec. VI.A, and the dynamical mean-field Δ is the same as that of the random-matrix model in Eq. (4.6b):

$$
\Sigma_f(\tau) = -J^2 G_f^2(\tau)G_f(-\tau),
$$

$$
\Delta(\tau) = t^2 G_c(\tau). \quad (8.6)
$$

Finally, the hybridization parameter $\bar{P}$ is determined by the self-consistency equation

$$\bar{P} = J_K G_{fc}(\tau = 0^-). \qquad (8.7)$$

Equations (8.5)–(8.7) can be obtained as follows from a G-Σ action analogous to Eqs. (5.56) and (6.6):

$$I[G, \Sigma, \Delta, \lambda, P] = \int_0^\beta d\tau \left[\frac{|P(\tau)|^2}{J_K} - \frac{i\lambda(\tau)}{2} \right]$$
$$- \ln \det \begin{bmatrix} [\partial_{\tau_1} + i\lambda(\tau_1)]\delta(\tau_1 - \tau_2) + \Sigma_f(\tau_1, \tau_2) \\ -P^*(\tau_1)\delta(\tau_1 - \tau_2) \\ \qquad -P(\tau_1)\delta(\tau_1 - \tau_2) \\ (\partial_{\tau_1} - \mu)\delta(\tau_1 - \tau_2) + \Delta(\tau_1, \tau_2) \end{bmatrix}$$
$$- \text{Tr}(\Delta \cdot G_c) + \frac{t^2}{2}\text{Tr}(G_f \cdot G_f)$$
$$- \text{Tr}(\Sigma_f \cdot G_f) - \frac{J^2}{4}\text{Tr}(G_f^2 \cdot G_f^2). \qquad (8.8)$$

A complete solution of Eqs. (8.5)–(8.7) requires a numerical analysis, but much can be understood from a low-frequency analysis similar to that in Sec. VII.D.2 (Burdin, Grempel, and Georges, 2002). The phase diagram as a function of T and J is shown in Fig. 19. A key determinant of the phase structure is the value of $\bar{P}$. We have $\bar{P} \neq 0$ below the line labeled T_K in Fig. 19: this line approaches the single-site Kondo temperature in the limit $J \to 0$. In this regime we have the HFL phase, in which both the spins and the electrons are part of the Fermi volume, as described in more detail in Sec. VIII.C. The transition across the line where $\bar{P}$ vanishes is expected to turn into a smooth crossover once $1/M$ corrections have been included, as there is no underlying order in the HFL phase at $T > 0$. However, the situation is different at $T = 0$: $\bar{P}$ vanishes at the red circle in Fig. 19, which denotes a
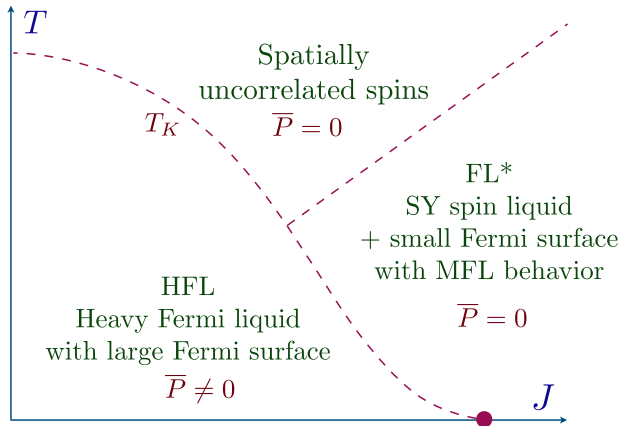

FIG. 19. Phase diagram of the large-M Kondo lattice with random exchange. The dashed lines are crossovers, but the $T = 0$ filled circle marks a quantum phase transition. The FL* phase and the quantum-critical point exhibit linear-in-T resistivity with the small carrier density of the conduction electrons. The HFL exhibits Fermi-liquid T^2 resistivity with a large carrier density of both the conduction electrons and the local moments. The critical theory of the HFL-FL* transition at $T = 0$ has also been discussed for models with full translational symmetry (Senthil, Sachdev, and Vojta, 2003; Senthil, Vojta, and Sachdev, 2004). From Burdin, Grempel, and Georges, 2002.

quantum-critical point between the HFL and FL* phases: this point is expected to survive $1/M$ corrections because of the discontinuous change in the Fermi volume described in Sec. VIII.C. Moreover, the critical theory has $\bar{P} = 0$, so the critical point has a small Fermi energy, in contrast to that for the t-J model, as we discuss at the end of Sec. VIII.D.

Despite the absence of a sharp phase transition between them, there is a qualitative difference between the observable properties of the HFL and FL* phases at $T > 0$. In the HFL phase, the nonzero $\bar{P}$ quenches the singular SYK behavior of the spins at low frequency, just as in Sec. VII.D.1; consequently, we expect Fermi-liquid-like behavior of the quasiparticles at nonzero T around a large Fermi energy. In particular, the resistivity $\sim T^2$ and the associated carrier density will include both the conduction electrons and the spins. In contrast, while the FL* is also a metal, the carrier density is small and includes only the conduction electrons. Moreover, in the present fully connected model, the singular SYK behavior of the spins survives. In the large-M limit, the spins are decoupled from the conduction electrons when $\bar{P} = 0$, but there will be a coupling at higher orders in $1/M$. Therefore, although $\Sigma_c = 0$ at $M = \infty$, the leading correction to the imaginary part of the self-energy is (Burdin, Grempel, and Georges, 2002)

$$\text{Im} \Sigma_c(\omega = 0) \sim \left(\frac{J_K}{M} \right)^2 \int_0^\infty \frac{d\Omega}{\sinh(\beta\Omega)} \frac{\rho_Q(\Omega)}{t}, \qquad (8.9)$$

where $\rho_Q(\Omega)$ is the SYK spin spectral density obtained in Eq. (6.8). This leads to marginal Fermi-liquid behavior (Varma *et al.*, 1989) for the small density of conduction electrons, with $\text{Im} \Sigma_c(\omega = 0) \sim T$ and a linear-in-T resistivity, using transport computations as defined in Sec. VII.E.

This mechanism for the linear-in-T resistivity in the Kondo lattice model is distinct from that for the t-J model in Sec. VII.F. Here the carrier density at the critical point is small, i.e., it does not involve the spins due to the breakdown of the Kondo effect. In contrast, the carrier density in Sec. VII.F was large and involved all the electrons. Moreover, here the linear-in-T resistivity already arose in the leading scaling results for the SYK model, while those in Sec. VII.F required corrections to scaling.

C. Luttinger theorem

The Luttinger theorem is normally applied to metallic phases of electrons, and we obtained an instance of this in Sec. VII.D.1 for the Fermi-liquid phase of the t-J model. But we also saw a modified Luttinger theorem in Sec. VI.A for spins in an insulating Kondo magnet. The Kondo Hamiltonian (8.1) has both spins and mobile electrons, and there now are distinct realizations of the Luttinger theorem in the HFL and FL* phases (Senthil, Sachdev, and Vojta, 2003; Senthil, Vojta, and Sachdev, 2004).

It is convenient to present the discussion in the large-M formulation of the theory in Sec. VIII.B, although all statements in Sec. VIII.C hold to all orders in $1/M$. When expressed in terms of the spinons f_α, the theory in Eq. (8.2) has a U(1) gauge symmetry along with global

U(1) symmetries associated with the total charge of the c_α electrons, $(M/2)p$, and the total spin $\mathcal{S}_z$. In principle, all three U(1) symmetries will lead to their own and distinct Luttinger constraints, unless there are condensates of bosons carrying U(1) charges (Coleman, Paul, and Rech, 2005; Powell, Sachdev, and Büchler, 2005) [we review this connection between U(1) symmetries and the Luttinger constraints at the end of Sec. XI.A.2]. In our discussion, the relevant boson is the hybridization $P \sim c_\alpha^\dagger f_\alpha$, and this is a Higgs boson because it carries a U(1) gauge charge.

1. FL* phase

In the FL* phase, there is no Higgs condensate $\langle P \rangle = 0$, so all three Luttinger constraints apply. An important property of this phase is that the off-diagonal Green's function vanishes at all frequencies $G_{fc} = 0$. Consequently, the constraints arising from the gauge U(1) and $\mathcal{S}_z$ symmetries are essentially identical to those considered for insulating quantum magnets in Sec. VI.A, which are in turn related to the discussion in Sec. V.B. Thus, we need only consider the constraint associated with the c_α fermion charge, which is

$$G_c(\tau = 0^-) = \frac{p}{2}. \qquad (8.10)$$

We can write G_c in the FL* phase in the general form

$$G_c(i\omega_n) = \frac{1}{i\omega_n + \mu - t^2 G_c(i\omega_n) - \Sigma_c(i\omega_n)}. \qquad (8.11)$$

We have now included a self-energy $\Sigma_c(i\omega_n)$ that arises from the $1/M$ corrections. This obeys $\mathrm{Im}\,\Sigma_c(i0^+) = 0$ at $T = 0$, and that is not the case for $\Delta(\omega)$ in Eq. (8.6). Another important point is that the $1/M$ contributions to $\Sigma_c(i\omega_n)$ can be obtained from a Luttinger-Ward functional, and the Luttinger constraint will then follow straightforwardly. We first solve Eq. (8.11) to write

$$G_c(i\omega_n) = \int_{-\infty}^{\infty} d\Omega \frac{\rho(\Omega)}{i\omega_n + \mu - \Sigma_c(i\omega_n) - \Omega}, \qquad (8.12)$$

where $\rho(\Omega)$ is the single-particle density of states of the random-matrix model in Eq. (4.8). We now proceed with an analysis of the Luttinger constraint as in Sec. V.B: we expect the contribution from the frequency derivative of the self-energy to vanish ($I_2 = 0$), and such an analysis then shows that Eq. (8.10) implies

$$\int_{-2t}^{E_F} d\Omega\, \rho(\Omega) = \frac{p}{2}, \qquad (8.13)$$

where the Fermi energy is

$$E_F = \mu - \Sigma_c(0). \qquad (8.14)$$

We note that the analog of the previous analysis also applies to the disordered Fermi-liquid phase of Sec. VII.D.1 (Parcollet and Georges, 1999).

2. HFL phase

In the HFL phase of the Kondo-Heisenberg lattice, we do have a Higgs condensate $\langle P \rangle \neq 0$, so there is no separate Luttinger constraint from the U(1) gauge symmetry. The analysis of the Luttinger constraint (Burdin, Georges, and Grempel, 2000) with the conservation of the electron charge then leads to a large Fermi energy of size $(1 + p)/2$ per spin [for the particle-hole symmetric value $\kappa = 1/2$ in Eq. (6.2) for the SU(M) spins].

We begin by writing Dyson's equation in Eq. (8.5) in a general form valid beyond the large-M limit. We define an auxiliary matrix Green's function as

$$[\mathcal{G}(i\omega_n, \Omega)]^{-1} = \begin{pmatrix} i\omega_n - \bar{\lambda} & 0 \\ 0 & i\omega_n + \mu - \Omega \end{pmatrix} - \Sigma(i\omega_n), \qquad (8.15)$$

where $\Sigma(i\omega_n)$ is the matrix self-energy that obeys $\mathrm{Im}\,\Sigma(i0^+) = 0$ at $T = 0$. As in Eq. (8.12), we have replaced the $t^2 G_c(i\omega_n)$ in Eqs. (8.5) and (8.6) with Ω. The presence of the Higgs condensate in the HFL phase requires that the off-diagonal matrix elements of $\Sigma(i\omega_n)$ are nonzero, and this is crucial for the Luttinger constraint here.

We now state a useful identity, which can be verified by explicit computation, for the following trace of the matrix Green's function $G(i\omega)$ (which counts both the f_α and c_α fermions):

$$\mathrm{Tr}\, G(i\omega) = \int_{-\infty}^{\infty} d\Omega \rho(\Omega) \left[i\frac{d}{d\omega} \ln\, \det[\mathcal{G}(i\omega, \Omega)] \right.$$
$$\left. - i\mathrm{Tr}\left(\mathcal{G}(i\omega, \Omega) \frac{d}{d\omega} \Sigma(i\omega) \right) \right]. \qquad (8.16)$$

Notice the similarity of Eq. (8.16) to the identity used for the SYK model in Eq. (5.15). The subsequent analysis proceeds as it does there. In this situation, the I_2 contribution of the second term in Eq. (8.16) vanishes from the usual Luttinger-Ward functional argument because we are in a Fermi-liquid phase and there is no anomaly at $\omega = 0$. For $p < 1$, the first term in Eq. (8.16) yields the Luttinger constraint (Burdin, Georges, and Grempel, 2000; Nikolaenko *et al.*, 2021)

$$\int_{-2t}^{E_F} d\Omega \rho(\Omega) = \frac{1 + p}{2}, \qquad (8.17)$$

which, unlike Eq. (8.13), counts both the c_α electrons and the spins. The expression for the Fermi energy in Eq. (8.14) is now replaced by

$$\det\, [\mathcal{G}(0, E_F)]^{-1} = 0. \qquad (8.18)$$

D. RG analysis for SU(2) symmetry

We now analyze $\bar{\mathcal{Z}}_{\mathrm{KH}}$ in Eq. (8.2) by combining the RG analysis of Sec. VI.C with the "poor-man's scaling" RG of the Kondo problem.

This analysis will be carried out perturbatively in J_K, as in the poor-man's scaling (Hewson, 1997). At leading order, with $J_K = 0$ but the mean-square hopping t arbitrary, the equations for the c_α Green's function reduce precisely to those solved

earlier in Sec. IV for the random-matrix problem. These yield a fermion Green's function with a constant density of states at the Fermi level $\sim 1/t$, as in Eq. (4.8). Note that this is a Fermi level only of the c electrons, and thus is a small Fermi surface: therefore, the present RG analysis is an expansion about the small Fermi surface. After a Fourier transform, the constant density of states implies that $G(\tau) \sim 1/t\tau$ at large $|\tau|$. We therefore replace the fermion c_α with a bath fermion ψ_α, which is the analog of the bosonic field ϕ_a that we introduced in Sec. VI.C for the random quantum magnet. Similarly, we endow ψ_α with a momentum and a dispersion, with the dispersion chosen such that $\psi_\alpha(x = 0)$ has the same temporal correlator as c_α. In this manner, we can express the problem as follows in terms of an impurity Hamiltonian of a single $S = 1/2$ spin coupled to fermionic and bosonic baths (Sengupta, 2000):

$$H_{\text{imp}} = \gamma \mathbf{S} \cdot \boldsymbol{\phi}(0) + \frac{J_K}{2} \mathbf{S} \cdot [\psi_\alpha^\dagger(0)\boldsymbol{\sigma}_{\alpha\beta}\psi_\beta(0)]$$
$$+ \int dk\, k\psi_{k\alpha}^\dagger \psi_{k\alpha} + \frac{1}{2}\int d^d x[\pi_a^2 + (\partial_x \phi_a)^2]. \quad (8.19)$$

The bath correlators are

$$Q(\tau) \sim \frac{1}{|\tau|^{d-1}}, \qquad R(\tau) \sim \frac{\text{sgn}(\tau)}{|\tau|}, \qquad (8.20)$$

and the value of d is to be determined by solving the self-consistency condition for Q in Eq. (8.4). We have argued that the self-consistency condition for R is satisfied by a Fermi-liquid constant density of states (of the small Fermi surface) at the Fermi level, and that dictated the $R(\tau)$ in Eq. (8.20).

The impurity Hamiltonian in Eq. (8.19) has two couplings J_K and γ, and their RG flow equations can be computed by combining the analyses of the usual Kondo model (Hewson, 1997) and those for the random quantum magnet in Eq. (6.20). This analysis is perturbative in J_K and $\epsilon = 3 - d$, and the one-loop RG equations are (Smith and Si, 1999; Sengupta, 2000; Zhu and Si, 2002)

$$\beta(\gamma) = -\frac{\epsilon}{2}\gamma + \gamma^3,$$
$$\beta(J_K) = \gamma^2 J_K - J_K^2. \quad (8.21)$$

The resulting RG flow is plotted in Fig. 20. The random quantum magnet fixed point of Sec. VI.C is stable to turning on a small J_K, implying the stability of a small Fermi surface phase. For SU(2), this small Fermi surface phase has spin-glass order; but more generally, in models which are not fully connected, it could be a spin liquid, leading to a FL* state as in Sec. VIII.B. For larger J_K, there is an unstable fixed point beyond which the flow is toward $J_K \to \infty$, presumably to a large Fermi surface HFL. We label this fixed point as the "Kondo breakdown" (Sengupta, 2000; Si *et al.*, 2001; Burdin, Grempel, and Georges, 2002; Senthil, Sachdev, and Vojta, 2003; Si *et al.*, 2003; Senthil, Vojta, and Sachdev, 2004) because it separates the HFL phase with Kondo screening from the small Fermi surface without Kondo screening.
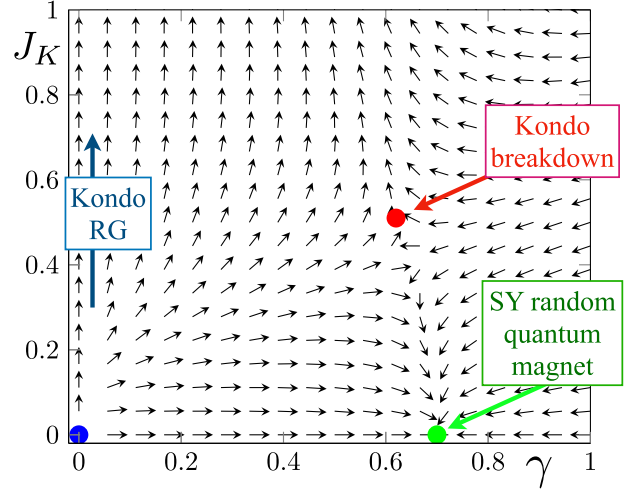

FIG. 20. RG flow of Eq. (8.21) for $\epsilon = 1$. The $\gamma = 0$ axis corresponds to the usual Kondo RG flow (Hewson, 1997). The Kondo-breakdown fixed point has one relevant direction and describes a phase transition between a small Fermi surface phase [likely with magnetic order for SU(2)] associated with the random quantum magnet fixed point of Sec. VI.C, and a large Fermi surface HFL at large J_K. Compare this to Fig. 18 for the random *t*-*J* model. From Sengupta, 2000.

It remains to solve the self-consistency equation in Eq. (8.4) to determine the value of ϵ. As in Secs. VI.C and VII.D.3, the scaling dimension of the spin operator can be determined (Zhu and Si, 2002) to all orders at a fixed point $\gamma^* \neq 0$, and we find the same result as in Eq. (7.37). The self-consistent value is again $\epsilon = 1$, $d = 2$, as in the *t*-*J* model.

Compare the RG flow diagram for the Kondo-Heisenberg model in Fig. 20 to that for the *t*-*J* model in Fig. 18. In both cases, we have a critical fixed point with one relevant direction, and similar critical correlators for the electron and spin operators: a Fermi-liquid-like critical electron correlator, and a SYK-like critical spin correlator, as in Eq. (7.37) for $d = 2$ and $r = 0$. However, the density of electrons participating in the electron correlator in Eq. (7.37) is different in the two cases: at the Kondo-breakdown fixed point the density of electrons is small and does not count the spins (as is clear in Sec. VIII.C for $\bar{P} = 0$, and in the large-*M* analysis in Sec. VIII.B), while in the *t*-*J* model fixed point the density of electrons is large and counts all electrons.

E. Numerical analysis

A complete numerical analysis of the single-site, self-consistent quantum problem defined by Eqs. (8.2)–(8.4) with SU(2) symmetry has not yet been carried out. However, there have been a number of studies of related models, motivated by an uncontrolled EDMFT analysis of low-dimensional models with nonrandom exchange (Si *et al.*, 2001, 2003; Kirchner *et al.*, 2020), and a self-consistency condition of the spin correlator that differs from that in Eq. (8.4). The self-consistency in spin correlators has been systematically justified only in models with random exchange, like those considered earlier, as we noted at the end of Sec. VII.A. The numerical analyses were carried out for Ising spin symmetry (Grempel and Si,

2003; Zhu, Grempel, and Si, 2003; Glossop and Ingersent, 2007; Zhu *et al.*, 2007), although recent works have also examined SU(2) spin symmetry (Cai *et al.*, 2020; Hu, Cai, and Si, 2020). Aspects of these studies are similar to the RG results described in Sec. VIII.D, with a SYK-like spin spectral density [i.e., spin correlations similar to Eq. (6.23)] at a critical point between a Fermi-liquid phase and another phase that is presumed to break spin symmetry.

IX. OVERVIEW OF NUMERICAL ALGORITHMS FOR FULLY CONNECTED SU(2) MODELS

In the large-M limit, the action in Eq. (7.4) is solved using a saddle-point technique that reduces to nonlinear integral equations for the Green's function G as in Eq. (5.2) and a simple expression of higher correlators in terms of G using Wick's theorem. The SU(2) case is more complex. The action in Eq. (7.4) is still a local quantum many-body problem (at $\mathcal{J} = 0$, it is the Anderson quantum impurity model), and more advanced algorithms are required to solve it.

In this section, we provide an introduction for nonexperts to the algorithms used to solve the previously addressed SU(2) models and discuss their strengths and limitations. The goal is to solve the local action in Eq. (7.4) for fixed bath Δ and retarded spin-spin interaction $\mathcal{J}$. The self-consistency condition on Δ and $\mathcal{J}$ is then solved with an iterative technique (Georges *et al.*, 1996). Note, however, that the self-consistency can generate a nontrivial frequency dependence for the bath Δ and the interaction $\mathcal{J}$, respectively, which complicates the solution. For example, any technique based on a flat bath spectral function with a large high energy cut-off, such as integrability, is inoperable in this context.

Significant progress has been made in the last two decades on numerical algorithms to solve such quantum impurity models with complex baths and interactions in the context of DMFT and its extensions (Gull *et al.*, 2011). Several classes of algorithms are available, in particular, action-based quantum Monte Carlo– (QMC-) or Hamiltonian-based methods (exact diagonalization, numerical renormalization group, density matrix renormalization group, and tensor network methods). The QMC ones are the methods of choice here due to the retarded spin-spin interaction term in Eq. (7.4).

The SU(2) insulating case was first studied in the paramagnetic phase using an auxiliary field QMC technique (Grempel and Rozenberg, 1998) with a sampling method of the auxiliary field in the Matsubara frequency space. Local moment solutions were obtained at low temperatures as discussed in Sec. VI.B (Grempel and Rozenberg, 1998; Dumitrescu *et al.*, 2022).

Recent works, however, have used the continuous time QMC (CTQMC) family of algorithms for quantum impurity models. The central idea is to perform an expansion of the partition function Z either in powers of the interaction U and $\mathcal{J}$ around the noninteracting limit [CT-INT (Rubtsov, Savkin, and Lichtenstein, 2005) or CT-AUX (Gull *et al.*, 2008) algorithms] or in powers of the bath hybridization Δ around the atomic limit [CT-HYB algorithm (Werner *et al.*, 2006)].

We first consider the CT-INT algorithm used in Secs. VII.B and VII.C (Cha, Wentzell *et al.*, 2020; Dumitrescu *et al.*, 2022). The partition function Z,

$$Z \equiv \int \mathcal{D}c_\sigma^\dagger(\tau)\mathcal{D}c_\sigma(\tau)e^{-S_{UJ}(c_\sigma^\dagger(\tau),c_\sigma(\tau))}, \quad (9.1)$$

is expanded in both U and $\mathcal{J}$ to any order as

$$Z = \sum_{n\geq 0}\sum_{p\geq 0}\frac{(-U)^n}{n!p!2^p}\int_0^\beta \prod_{i=1}^n d\tau_i \prod_{j=1}^p d\tau_j' d\tau_j'' \mathcal{J}(\tau_j' - \tau_j'')$$

$$\times \sum_{a_j=x,y,z}\left\langle \mathcal{T}_\tau \prod_{i=1}^n n_\uparrow(\tau_i)n_\downarrow(\tau_i)S^{a_j}(\tau_j')S^{a_j}(\tau_j'')\right\rangle_0. \quad (9.2)$$

The average is taken in the noninteracting model and, via Wick's theorem, can be expressed as a determinant in terms of the noninteracting impurity Green's function.

The principle of the CTQMC is to sample Z stochastically with a Metropolis Monte Carlo algorithm, computing integrals of various dimensions simultaneously. A Monte Carlo algorithm is defined by its configuration space and the elementary steps constituting the Markov chain in this space. When the integrals with a Riemann sum on a regular grid of step $\delta\tau$ are discretized, the configurations $\mathcal{C}$ are simply given by the orders n and p and the set of τ_i, τ_i', and τ_j''. Formally, Z can then be written as

$$Z = \sum_{n\geq 0}\sum_{p\geq 0}\sum_{\mathcal{C}_{np}}(\delta\tau)^{n+2p}f_{\mathcal{C}_{np}}(\tau_i, \tau_i', \tau_j''), \quad (9.3)$$

where $f_{\mathcal{C}_{np}}$ is given by the time-ordered correlator in Eq. (9.2). The weight of a configuration $\mathcal{C}_{np}$ is $w_{\mathcal{C}_{np}} = (\delta\tau)^{n+2p}|f_{\mathcal{C}_{np}}|$. The MC Markov chain consists of elementary steps in adding or removing one (or two) vertices at some randomly chosen times, sampling all the integrals simultaneously. The various correlation functions are then computed from this Markov chain, as their expansions are similar (Gull *et al.*, 2011). The typical order of the expansion explored by the algorithm can be shown to be proportional to β, and in practice can go up to several hundred. In this model, CT-INT can develop a sign problem at low temperatures in some parameter regimes due to the $\mathcal{J}$ term. In practice, however, it can often be strongly reduced using Gaussian counterterms added to both the bare action and the U interaction term (Rubtsov, Savkin, and Lichtenstein, 2005; Dumitrescu *et al.*, 2022).

The CT-HYB algorithm is similar to CT-INT but is based on a double expansion around the atomic limit, i.e., in powers of $\Delta(\tau)$, and $\mathcal{J}_\perp$, where the retarded spin-spin interaction is rewritten as $\mathcal{J}S(\tau)\cdot S(\tau') = \mathcal{J}_\parallel S^z(\tau)S^z(\tau') + \mathcal{J}_\perp\sum_{a=\pm}S^a(\tau)S^{-a}(\tau')$. Expanding Eq. (9.1) in Δ and $\mathcal{J}_\perp$ and using the antisymmetric property of time-ordered fermionic correlators, the partition function Z reads

$$Z = \sum_{n\geq 0}\sum_{p\geq 0}\frac{1}{2^p p!n!^2}\int_0^\beta \prod_{i=1}^n d\tau_i d\tau_i' \prod_{j=1}^p d\bar{\tau}_j d\bar{\tau}_j'$$

$$\times \prod_{j=1}^p \mathcal{J}_\perp(\bar{\tau}_j - \bar{\tau}_j')\sum_{\sigma_i=\uparrow,\downarrow}\sum_{a_j=\pm}\det_{1\leq i,j\leq n}[\Delta_{\sigma_i}(\tau_i - \tau_j')]$$

$$\times \left\langle \mathcal{T}_\tau \prod_{i=1}^n c_{\sigma_i}^\dagger(\tau_i)c_{\sigma_i}(\tau_i')\prod_{j=1}^p S^{a_j}(\bar{\tau}_j)S^{-a_j}(\bar{\tau}_j')\right\rangle_{\text{atomic}},$$

$$(9.4)$$

where the atomic correlators are taken in the isolated atom, i.e., $\Delta = 0$ and $\mathcal{J}_\perp = 0$. The CT-HYB algorithm was introduced in the DMFT case $\mathcal{J} = 0$ (Werner *et al.*, 2006) and later extended to the EDMFT case $\mathcal{J} \neq 0$ (Otsuki, 2013; Otsuki and Vollhardt, 2013). The $\mathcal{J}_\parallel$ component of the retarded spin-spin interaction can be taken into account exactly in the atomic correlator. The second expansion in $\mathcal{J}_\perp$, however, is necessary since no efficient algorithm is known to compute the atomic correlators in the presence of a retarded non-Abelian spin-spin interaction term.

The CTQMC algorithms provide an exact solution in Matsubara time. The main advantages over the previous generation of QMC impurity solvers (Hirsch and Fye, 1986) are the ability to treat general atomic interactions (including retarded interactions) and the absence of time discretization, as the algorithm can be performed directly in the continuous time limit $\delta\tau \to 0$ (hence its name). The last point can be illustrated easily on a CT-INT. We consider a Monte Carlo step from a configuration $\mathcal{C}$ of the order of (n, p) to a configuration $\mathcal{C}'$ of the order of $(n + 1, p)$. Their weights $w_\mathcal{C}$ and $w_{\mathcal{C}'}$ are proportional to $(\delta\tau)^{n+2p}$ and $(\delta\tau)^{n+1+2p}$, respectively, as seen in Eq. (9.3). However, the Markov chain steps can be chosen such that the Metropolis ratio

$$R_{\mathcal{C} \to \mathcal{C}'} = \frac{T_{\mathcal{C}' \to \mathcal{C}} w_{\mathcal{C}'}}{T_{\mathcal{C} \to \mathcal{C}'} w_\mathcal{C}} \tag{9.5}$$

(where $T_{\mathcal{C} \to \mathcal{C}'}$ is the proposition probability of the step) is finite for $\delta\tau \to 0$. Indeed, $T_{\mathcal{C} \to \mathcal{C}'} = \delta\tau/\beta$ (the probability to randomly pick up one new time on the imaginary axis) and $T_{\mathcal{C}' \to \mathcal{C}} = 1/(n + 1)$ (the probability to randomly select one time to remove from the configuration $\mathcal{C}'$). As R controls the Metropolis algorithm, its finite limit ensures the continuous time limit of the algorithm even though the weights themselves vanish at $\delta\tau \to 0$. The absence of time grid extrapolation is a great advantage in practice at low temperatures (Gull *et al.*, 2011).

The main limitations of the CTQMC algorithms include some sign problem (depending on the exact algorithm and the parameter regime), a poor scaling with temperature (like β^3), and most importantly their restriction to imaginary time. Some delicate analytical continuation are required to access real-frequency correlations. Note that a third generation of QMC methods for impurity problems that work directly in real time has recently appeared (Cohen *et al.*, 2015; Profumo *et al.*, 2015; Maček *et al.*, 2020). They are based on diagrammatic computations of physical quantities rather than the partition function. It is an open question whether these new approaches, when properly generalized to handle the retarded spin-spin interaction, will allow us to solve some of the remaining challenges presented by these systems, including the low-temperature behavior.

X. LATTICE MODELS OF SYK ATOMS

This section returns to the SYK model of Sec. V and follows a different strategy toward connecting it to the physics of quantum matter. In Secs. VI–VIII we imposed Mottness on the SYK model by adding an on-site repulsion on each site i; this approach then connected naturally to dynamical mean-field theories of correlated materials. This section examines an alternative approach in which the SYK model is viewed as a multiorbital atom, and i labels the orbitals on such an atom. We then examine a lattice of such "SYK atoms" and find that such models can also exhibit regimes of non-Fermi-liquid behavior with linear-in-T resistivity. For models with a single band of SYK atoms, these non-Fermi liquids are invariably bad metals at temperatures higher than the renormalized bandwidth, in that the resistivity exceeds the MIR resistivity, where the quantum of resistance is redefined as h/Ne^2 for the N-orbital atom. This is in contrast to the non-Fermi liquids obtained using a two-band generalization of these models in Sec. X.B and those introduced in Sec. VII, which display resistivities smaller than the MIR resistivity.

The models described in this section characterize the anomalous transport properties of non-Fermi-liquid metals with short-range interactions in crystalline settings. We address the fate of the electronic Fermi surface in the regime of strong interactions when there are no long-lived low-energy quasiparticles. Therefore, it is natural to address the extent to which the models introduced thus far can serve as elementary building blocks for addressing these fundamental questions in a controlled setting. In Secs. X.A–X.D, we discuss properties of a number of different variants of the SYK models.

A. Breakdown of a heavy Fermi liquid

We begin by writing a model for electrons with orbital labels $i = 1, 2, \ldots, N$ and hopping on the sites $\boldsymbol{r}$ of a d-dimensional hypercubic lattice (Fig. 21). The Hamiltonian $H_c = H_{\mathrm{kin}} + H_{\mathrm{int}}$ is given by

$$H_{\mathrm{kin}} = -\sum_{\boldsymbol{r},\boldsymbol{r}'} t_{\boldsymbol{r}\boldsymbol{r}'} c_{\boldsymbol{r}i}^\dagger c_{\boldsymbol{r}'i} - \mu \sum_i c_{\boldsymbol{r}i}^\dagger c_{\boldsymbol{r}i}, \tag{10.1a}$$

$$H_{\mathrm{int}} = \frac{1}{(2N)^{3/2}} \sum_{\boldsymbol{r}} \sum_{ijk\ell=1}^{N} U_{ij;k\ell} c_{\boldsymbol{r}i}^\dagger c_{\boldsymbol{r}j}^\dagger c_{\boldsymbol{r}k} c_{\boldsymbol{r}\ell}. \tag{10.1b}$$

Equations (10.1a) and (10.1b) are thus a generalization of a completely $(0 + 1)$-dimensional model $H_2 + H_4$, as
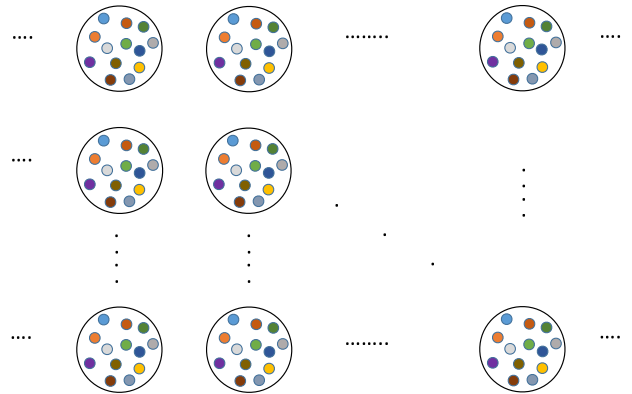

FIG. 21. Basic building block for studying translationally invariant lattice models constructed out of SYK atoms with N orbitals per site. The different sites are coupled together by single-electron hopping terms.

introduced in Eqs. (4.1a) and (5.1a), respectively. The simplest choice for the hopping and interaction parameters is to make them both random variables (Song, Jian, and Balents, 2017). Alternatively, the hopping parameters can be made translationally invariant such that they depend only on the spatial separation $|\boldsymbol{r} - \boldsymbol{r}'|$ (Zhang, 2017; Haldar, Banerjee, and Shenoy, 2018). Of special interest is the situation where additionally the interaction terms $U_{ij;k\ell}$ are also assumed to be independent of the site label $\boldsymbol{r}$ (Chowdhury *et al.*, 2018). H_{int} is then constructed as a repeated array of the H_4 term in Eq. (5.1) for every site $\boldsymbol{r}$ and $U_{ij;k\ell}$ are identical at every site, thereby preserving an exact (instead of statistical) translational invariance. The couplings are still chosen from a Gaussian random distribution with zero mean $\overline{U_{ij;k\ell}} = 0$ and variance $\overline{|U_{ij;k\ell}|^2} = U^2$. Appealing to the self-averaging properties of the SYK model in the large-N limit, we can compute correlation functions of a typical translationally invariant realization (where crystalline momentum is a good quantum number) by averaging over the disorder realizations. The chemical potential μ allows us to tune the electron density $\mathcal{Q}$. Variants of the one-band lattice model without any hopping terms (i.e., $t_{\boldsymbol{rr}'} = 0$) and with only four-fermion interactions that couple together different sites have also been studied (Davison *et al.*, 2017; Gu, Qi, and Stanford, 2017), with properties that are vastly different from what we discuss later. A different family of lattice SYK models defined in terms of Majorana fermions has been used to study insulating transitions out of a diffusive metal (Jian, Bi, and Xu, 2017; Jian and Yao, 2017) and the effects of longer-range correlated couplings on diffusive transport (Khveshchenko, 2018b).

In the large-N limit, once again only the melon graphs survive (Fig. 7), but the Green's function now includes an additional contribution due to H_{kin} and takes a more nontrivial form than Eqs. (5.2a) and (5.2b):

$$G(i\omega_n, \boldsymbol{k}) = \frac{1}{i\omega_n - \varepsilon_{\boldsymbol{k}} - \Sigma(i\omega_n, \boldsymbol{k})},$$
$$\Sigma(i\omega_n, \boldsymbol{k}) = -U^2 T \sum_{i\Omega_n} \int_{\boldsymbol{k}_1} G(i\Omega_n, \boldsymbol{k}_1) \Pi(i\omega_n + i\Omega_n, \boldsymbol{k} + \boldsymbol{k}_1),$$

$$(10.2a)$$

$$\Pi(i\Omega_n, \boldsymbol{q}) = T \sum_{i\omega_n'} \int_{\boldsymbol{k}'} G(i\omega_n', \boldsymbol{k}') G(i\omega_n' + i\Omega_n, \boldsymbol{k}' + \boldsymbol{q}),$$

$$(10.2b)$$

where $\int_{\boldsymbol{k}} \equiv \int d^d\boldsymbol{k}/(2\pi)^d$ and $\varepsilon_{\boldsymbol{k}}$ is the electron dispersion. Equations (10.2a) and (10.2b) are reminiscent of the usual DMFT equations, but where the electron self-energy is allowed to be momentum dependent. As we later discuss, in the strong-coupling limit, the momentum dependence becomes parametrically weaker than the frequency-dependent renormalization, stemming from the local SYK physics (Chowdhury *et al.*, 2018).

Equations (10.2a) and (10.2b) are in general difficult to solve analytically as a function of frequency and momenta; the full solution can be obtained numerically across the entire Brillouin zone. However, significant insights can be gained analytically by starting with a low-energy guess for a self-consistent solution. Recall that in the limit where the sites are all decoupled, at energies $\omega \ll U$ for H_4 in Eq. (5.1), the electron scaling dimension $\Delta = 1/4$. By simple power counting arguments, H_{kin} is a relevant perturbation; as a result, the power-law solution for the Green's function obtained earlier cannot survive down to the lowest energies and there will be a crossover to a regime dominated by H_{kin} that can nevertheless be strongly renormalized due to interactions (Parcollet and Georges, 1999; Song, Jian, and Balents, 2017).

At the lowest energies, we assume the self-energy to take the following Fermi-liquid form:

$$\Sigma(i\omega_n, \boldsymbol{k}) = -i(Z^{-1} - 1)\omega_n + \Delta\varepsilon_{\boldsymbol{k}}, \qquad (10.3)$$

where Z is the quasiparticle residue and $\Delta\varepsilon_{\boldsymbol{k}}$ is the renormalization associated with the dispersion, which is to be determined self-consistently. As a further simplification, zooming in on the near vicinity of the Fermi surface, we can parametrize $\Delta\varepsilon_{\boldsymbol{k}} = (\Delta v_F)k$, where Δv_F is the Fermi velocity renormalization and k is measured relative to the Fermi surface. The self-consistency condition then reduces to

$$Z^{-1} - 1 = \nu_0^2 U^2 Z, \qquad (10.4a)$$

$$\frac{\Delta v_F}{v_F} \sim \nu_0^2 U^2 Z^2, \qquad (10.4b)$$

where ν_0 is the bare density of states at the Fermi energy. In the strong-coupling limit $U \gg W$, where W is the unrenormalized single-particle bandwidth, we immediately obtain $Z \sim 1/\nu_0 U$ and $\Delta v_F/v_F \sim \mathrm{O}(1)$. Thus, the dominant self-energy renormalization in Eq. (10.3) is frequency dependent, with a much weaker momentum dependence. As a result, we also immediately infer the effective mass renormalization $(m^*/m = 1/Z)$. The ground state is thus a heavy Fermi liquid with a sharp Fermi surface at any strength of interaction.

This picture of a Fermi liquid breaks down as a function of increasing energy. Naively, one would expect this to occur for energies comparable to W; this is incorrect, and the crossover instead occurs at a much reduced scale of $W^* \sim W^2/U$, which also serves as the renormalized bandwidth of the heavy Fermi liquid. Consider the following coherent part of the Green's function:

$$G(i\omega, \boldsymbol{k}) = \frac{Z}{i\omega - Z\bar{\varepsilon}_{\boldsymbol{k}} + i\alpha\nu_0^2 U|\omega|^2 \ln(W^*/|\omega|)\mathrm{sgn}(\omega)}, \quad (10.5)$$

where $\bar{\varepsilon}_{\boldsymbol{k}} = \varepsilon_{\boldsymbol{k}} + \Delta\varepsilon_{\boldsymbol{k}}$ and $\alpha \sim \mathrm{O}(1)$ is constant; the $\ln(\cdots)$ term is specific to $d = 2$. After analytically continuing to real frequencies, the imaginary part of the self-energy in Eq. (10.5) becomes $\Sigma''(\omega) \sim \omega^2/W^*$, such that $\Sigma''(W^*) \sim W^*$. Thus, at energies approaching W^* the scattering rate of the quasiparticles becomes comparable to the renormalized bandwidth. This is a sign that the quasiparticle picture and the sharp Fermi surface associated with the low-energy Fermi liquid are breaking down.

We can instead approach the problem from higher energy scales. For $\omega \gg W^*$, it is appropriate to start with the solutions to Eqs. (10.2a) and (10.2b) in the decoupled limit and treat the hopping perturbatively (i.e., in powers of $\varepsilon_{\boldsymbol{k}}$). In this limit, we

reproduce the completely local form of the electron Green's function obtained earlier in Eq. (5.3). The leading momentum dependence can be obtained in the strong-coupling regime as follows by expanding in powers of ϵ_k:

$$G(i\omega, \mathbf{k}) = \frac{i\,\mathrm{sgn}(\omega)}{\sqrt{U|\omega|}} - B(\omega)\frac{\epsilon_k}{U|\omega|} \quad (W^* \ll |\omega| \ll U), \quad (10.6)$$

where $B(\omega)$ is a frequency-independent constant whose value depends on the sign of ω and descends from the spectral asymmetry discussed in Sec. V. This is an incoherent regime where the electronic quasiparticles are not well defined. Note that the momentum-dependent correction becomes comparable to the local term at $\omega \sim W^*$.

The previous description leads to a simple picture for the properties of the model in Eqs. (10.1a) and (10.1b). At the lowest energy scales, the system is a heavy Fermi liquid with a sharp Fermi surface satisfying Luttinger's theorem. All interaction-induced corrections are predominantly frequency dependent, with a weak residual momentum dependence. The DMFT-like behavior is linked to the properties of the single SYK cluster. As a function of increasing energy, the quasiparticle scattering rate increases until they are no longer well defined; at scales approaching the renormalized bandwidth W^*, the Fermi surface and the quasiparticles are completely destroyed. Starting at higher energies, W^* also marks the crossover where the completely local picture of the decoupled SYK dots with perturbative spatial corrections breaks down and is accompanied by the incipient formation of a Fermi surface. Going beyond the large-N results discussed here, the fate of the low-temperature phase can be vastly different (Altland, Bagrets, and Kamenev, 2019a).

We note that if the model in Eqs. (10.1a) and (10.1b) is defined with a random $t_{\mathbf{r}\mathbf{r}'}$ and an uncorrelated $U_{ij;k\ell}$ at different sites (Song, Jian, and Balents, 2017), the properties of the previously discussed incoherent regime remain unchanged since the spatial correlations are completely local. The low-energy disordered FL regime is similar in many aspects to the previously discussed FL but is notably different in the presence of the sharp Fermi surface. We return to some of the consequences of this subtle difference when we discuss transport in Sec. X.C.

Finally, we note a model (Patel and Sachdev, 2019) in which the random interactions are restricted to be "resonant": this has $W^* \to 0$, and the Planckian behavior holds down to zero temperature. The rationale for such a model is that the nonresonant interactions have already been absorbed in effective $t_{\mathbf{r}\mathbf{r}'}$ for the quasiparticles. The resonance condition can be interpreted in terms of a scalar field needed to impose the constraints, and this indicates that Planckian behavior should appear more readily and naturally in Yukawa-SYK models of fermions and bosons with random Yukawa couplings: we consider such models in Sec. XI.

B. Marginal Fermi liquid and critical Fermi surface from incoherent "flavor" fluctuations

Our theoretical discussion of the metallic non-Fermi liquids discussed in this review thus far has lacked any interesting spatial structure. Even for the lattice model considered in Sec. X.A, the incoherent regime had no singular momentum-dependent features. However, it is possible to add additional electronic degrees of freedom to the model introduced in Eqs. (10.1a) and (10.1b) and engineer a critical Fermi surface (a sharp electronic Fermi surface without any low-energy electronic quasiparticles) over a wide range of energy scales. These additional electronic degrees of freedom realize a "marginal" Fermi liquid where the single-particle lifetime $\Gamma_{\mathrm{sp}} \sim \max(\omega, T)$ (Chowdhury *et al.*, 2018; Patel *et al.*, 2018).

Consider an additional band of electrons $d_{\mathbf{r}i}$ defined on the sites of the same hypercubic lattice with orbital labels $i = 1, \ldots, N$, with a separately conserved density $\mathcal{Q}_d$. We are interested in Hamiltonians of the form

$$H = H_c + H_d, \tag{10.7a}$$

$$H_d = \sum_{\mathbf{k},i} \epsilon_{\mathbf{k}} d_{\mathbf{k}i}^\dagger d_{\mathbf{k}i} + \frac{1}{N^{3/2}} \sum_{\mathbf{r}} \sum_{ijk\ell=1}^{N} V_{ij;k\ell} c_{\mathbf{r}i}^\dagger d_{\mathbf{r}j}^\dagger d_{\mathbf{r}k} c_{\mathbf{r}\ell}, \tag{10.7b}$$

where $\epsilon_{\mathbf{k}}$ is the dispersion for d electrons (including the respective chemical potential) and H_c continues to be defined by Eqs. (10.1a) and (10.1b). The $V_{ij;k\ell}$ are assumed to be identical at every site, thereby preserving translational symmetry, and chosen from a Gaussian random distribution with $\overline{V_{ij;k\ell}} = 0$ and variance $\overline{|V_{ij;k\ell}|^2} = V^2$. We are particularly interested in the regime where the bandwidth for d electrons W_d far exceeds the c-electron bandwidth W. The setup here is reminiscent of the periodic Anderson model for an itinerant "conduction" electron band coupled to a strongly interacting, narrow band (Hewson, 1997), except that the interaction terms now are chosen to have a purely SYK form. A different variant of the two-band model involving an interband hybridization that conserves only the total density has also been analyzed (Ben-Zion and McGreevy, 2018).

In the large-N limit, only the following set of coupled melon graphs survive for the Green's function corresponding to both c and d electrons (Fig. 22):
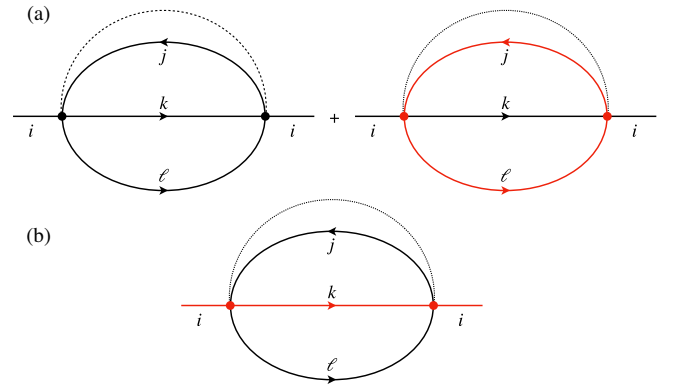

FIG. 22.   Melon graphs for the model in Eq. (10.7) for the electron self-energies for (a) c and (b) d electrons, respectively. Solid black (red) lines denote fully dressed c (d) Green's functions. The dashed (dotted) line represents the disorder averaging associated with the interaction vertex $|U_{ij;k\ell}|^2$ ($|V_{ij;k\ell}|^2$).

$$G(i\omega_n, \boldsymbol{k}) = \frac{1}{i\omega_n - \varepsilon_{\boldsymbol{k}} - \Sigma(i\omega_n, \boldsymbol{k}) - \Sigma'_d(i\omega_n, \boldsymbol{k})}, \quad (10.8a)$$

$$G_d(i\omega_n, \boldsymbol{k}) = \frac{1}{i\omega_n - \epsilon_{\boldsymbol{k}} - \Sigma_d(i\omega_n, \boldsymbol{k})}, \quad (10.8b)$$

$$\Sigma'_d(i\omega_n, \boldsymbol{k}) = -V^2 T \sum_{i\Omega_n} \int_{\boldsymbol{k}_1} G(i\Omega_n, \boldsymbol{k}_1) \Pi_d(i\omega_n + i\Omega_n, \boldsymbol{k} + \boldsymbol{k}_1),$$
$$(10.8c)$$

$$\Sigma_d(i\omega_n, \boldsymbol{k}) = -V^2 T \sum_{i\Omega_n} \int_{\boldsymbol{k}_1} G_d(i\Omega_n, \boldsymbol{k}_1) \Pi(i\omega_n + i\Omega_n, \boldsymbol{k} + \boldsymbol{k}_1),$$
$$(10.8d)$$

$$\Pi_d(i\Omega_n, \boldsymbol{q}) = T \sum_{i\omega'_n} \int_{\boldsymbol{k}'} G_d(i\omega'_n, \boldsymbol{k}') G_d(i\omega'_n + i\Omega_n, \boldsymbol{k}' + \boldsymbol{q}),$$
$$(10.8e)$$

where $\Sigma(i\omega_n, \boldsymbol{k})$ and $\Pi(i\Omega_n, \boldsymbol{q})$ are as previously defined in Eq. (10.2b).

Over an energy window $W^* \ll \omega$ (or T) $\ll \min(W_d, U)$, when the d electrons scatter off the incoherent fluctuations associated with the c electrons, their self-energy is given by

$$\Sigma_d(i\omega) \sim -i\omega \log\left(\frac{U}{|\omega|}\right), \quad (10.9)$$

which has the marginal Fermi-liquid (MFL) form. We emphasize here that the MFL regime in this setup is generated self-consistently, even after including its feedback on the c electrons, without having to postulate the existence of a featureless bath (Varma *et al.*, 1989).

In the translationally invariant setting discussed here, the d electrons have a sharp Fermi surface. To make this precise, we can take the limit of $W^* \to 0$ at $T = 0$ and identify the location of the Fermi surface from the solution to $G_d^{-1}(0, \boldsymbol{k}) = 0$. The critical Fermi surface satisfies Luttinger's theorem, where its size is now determined solely by $\mathcal{Q}_d$, i.e., the density of c electrons is not included in the size as anticipated and can therefore be characterized as small. The proof of Luttinger's theorem for the critical Fermi surface follows the standard treatment in Fermi liquids (Abrikosov, Gorkov, and Dzyaloshinskii, 1963) and is based on the Luttinger-Ward functional. The two-particle correlators (as in the density response) near the $2k_F$ wave vector have a singular dependence as a function of energy. Note that the singular form of the self-energy in Eq. (10.9) is momentum independent and not tied to the vicinity of the Fermi surface.

This construction leads to a concrete realization of a small critical Fermi surface with marginally defined excitations. However, the critical Fermi surface obtained here is necessarily accompanied by a finite extensive entropy extrapolated to $T \to 0$, which originates from the usual entropy associated with the incoherent regime of the local SYK islands of c electrons. In Sec. XI, we discuss a different class of models where the critical Fermi surface is large (i.e., the size is

determined by the total electronic density) and can arise without an extensive entropy in the $T \to 0$ limit.

C. Thermodynamics and transport

For the single-band model in Eqs. (10.1a) and (10.1b), the Fermi liquid at $T \ll W^*$ has an entropy density $s \sim \gamma_{FL} T$, where $\gamma_{FL} \propto m^* \sim 1/W^*$. In the incoherent regime for $T \gg W^*$, the entropy density is given by that of a single SYK dot [Eq. (5.53)] with weak perturbative corrections of the order of $(W/U)^2$; the extrapolated entropy in the limit of $T \to 0$ from this regime is finite (Georges, Parcollet, and Sachdev, 2001), but the excess entropy is relieved at $T \sim W^*$ across the crossover into the Fermi liquid (Song, Jian, and Balents, 2017). At $T \gg W^*$, electrical transport occurs as a result of the perturbative electron hops between SYK dots. Starting from the Kubo formula for the conductivity and given the completely local form of the single-electron Green's functions, the current-current correlation function reduces simply to a convolution of two spectral functions, much like standard computations of transport within DMFT. This leads to

$$\sigma(\omega, T) = \frac{Ne^2}{h} \frac{W^*}{T} F\left(\frac{\omega}{T}\right), \quad (10.10)$$

where $F(\cdots)$ is a universal scaling function of ω/T. This immediately leads to a bad metal T-linear resistivity (and scattering rate) with values that can far exceed $\rho_Q = h/Ne^2$ over a range of temperatures ($W^* \ll T \ll U$). In the Fermi-liquid regime at $T \ll W^*$, the resistivity crosses over into a conventional regime with $\rho = BT^2$ as long as the Fermi surface is large enough and electron-electron umklapp scattering is allowed. The coefficient (B) of the T^2 term satisfies the Kadowaki-Woods scaling (Kadowaki and Woods, 1986), as can be verified simply by demanding that there is a smooth crossover at $T \sim W^*$ between the two different metallic regimes. We note that the resonant model (Patel and Sachdev, 2019) has $W^* = 0$, and it exhibits strange metal linear T resistivity with values well below ρ_Q.

In the MFL regime of the two-band model introduced in Eq. (10.7), the critical Fermi surface associated with the d electrons gives rise to a singular specific heat $C \sim T \ln(1/T)$ at low temperatures, in addition to the usual contribution from the SYK dot associated with the c electrons. Once again, given the local form of the single-particle self-energy in the MFL regime, transport simplifies considerably, leading to the following T-linear resistivity associated with the d electrons:

$$\rho_d(T) \sim \frac{h}{Ne^2} \left(\frac{V^2}{W_d^2 U}\right) T. \quad (10.11)$$

In the translationally invariant setting of Eq. (10.7a), the finite resistivity arises as a result of momentum relaxation to the bath formed by the local c electrons at every site (Chowdhury *et al.*, 2018).

We end this section by noting that the extrapolated zero-temperature entropy from the strange metal regime of the cuprates vanishes (Loram *et al.*, 1994), unlike the residual

extensive entropy in the limit of $T \to 0$ associated with the models considered here displaying SYK-like critical correlations at large N. There are a number of other materials displaying NFL behavior over intermediate energy scales where the extrapolated entropy is also known to be extensive and finite but relieved below a certain low-temperature coherence scale (Allen *et al.*, 1996; Brühwiler *et al.*, 2006).

D. Superconductivity

Conventional Fermi-liquid metals, even with purely repulsive interactions (i.e., in the absence of phonon-mediated attraction), are unstable to superconductivity at extremely low temperatures. This Kohn-Luttinger mechanism (Kohn and Luttinger, 1965) relies on an effective attraction that is generated in a non-s-wave angular momentum channel at higher orders in the interaction strength. An analogous general statement cannot be made about the non-Fermi-liquid metals introduced in this review and their pairing instabilities, if any, have to be analyzed on an individual basis.

The models introduced thus far in this section do not have any pairing instabilities. By extending these models to include spinful fermions, a number of routes have been used to generate attraction via pair-hopping interactions (Patel, Lawler, and Kim, 2018; Wu *et al.*, 2018), a random Yukawa interaction to a bosonic field (such as a phonon field) (Esterlis and Schmalian, 2019; Wang, 2020; Classen and Chubukov, 2021), and the introduction of additional correlations between the interaction matrix elements $U_{ij;k\ell}$ (Chowdhury and Berg, 2020a). At large N, all of these models have a mean-field-like transition to superconductivity where Eliashberg theory becomes asymptotically exact. However, the instability is not tied to the usual "Cooper logarithm" (Abrikosov, Gorkov, and Dzyaloshinskii, 1963) associated with an underlying Fermi surface and the ratio of gap magnitude to transition temperature is enhanced above the standard mean-field value. When supplemented by an on-site attractive Hubbard interaction, the previously mentioned models display a fluctuation regime resembling a "pseudogap" (Wang *et al.*, 2020) before the superconducting transition. Certain tensor models (Kim *et al.*, 2019) and generalized SYK-type models (Bi *et al.*, 2017; Luo *et al.*, 2019) defined in terms of real fermions have also been studied and were found to exhibit spontaneous symmetry breaking analogous to pairing.

Intrinsic superconducting instabilities of the previously introduced non-Fermi liquids and their analogy with the Kohn-Luttinger mechanism can be seen by introducing a spin label $\sigma = \uparrow, \downarrow$, modifying Eq. (10.1b) to

$$H_{\text{int}} \to \frac{1}{4N^{3/2}} \sum_{\boldsymbol{r}} \sum_{\sigma=\uparrow,\downarrow} \sum_{ijk\ell=1}^{N} U_{ij;k\ell} c_{\boldsymbol{r}i\sigma}^{\dagger} c_{\boldsymbol{r}j\sigma'}^{\dagger} c_{\boldsymbol{r}k\sigma'} c_{\boldsymbol{r}\ell\sigma}, \quad (10.12)$$

and including additional correlations between the interaction matrix elements as $U_{ij;k\ell} = \pm U_{ik;j\ell}$. The physics is qualitatively different depending on the $\pm$ sign here, as can be seen most directly by writing the Bethe-Salpeter equation (Fig. 23) for the intraorbital, spin-singlet vertex in the pairing channel as follows: $\Phi_\ell(\boldsymbol{r} - \boldsymbol{r}') \equiv \epsilon_{\sigma\sigma'} c_{\boldsymbol{r}\ell\sigma} c_{\boldsymbol{r}'\ell\sigma'}$.
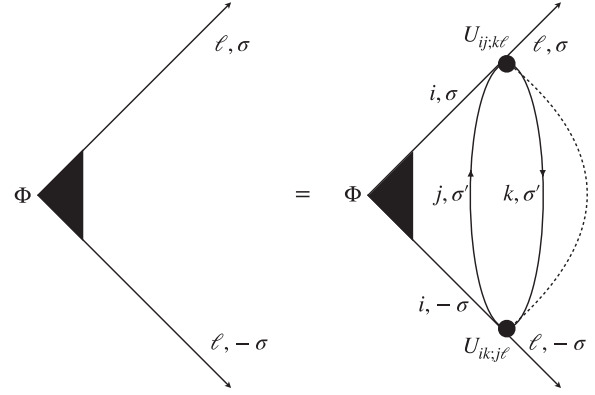

FIG. 23. Bethe-Salpeter equation for the intraorbital pairing vertex Φ in the large-N limit.

At zero external center-of-mass momentum, the linearized equation for Φ_ℓ becomes

$$\Phi_\ell(\omega, \boldsymbol{k}) = \mp U^2 T \sum_{\Omega} \int_{\boldsymbol{q}} \Phi_i(\Omega, \boldsymbol{q}) G(i\omega, \boldsymbol{q}) G(-i\omega, -\boldsymbol{q})$$
$$\times \Pi(i\omega - i\Omega, \boldsymbol{k} - \boldsymbol{q}), \quad (10.13)$$

where $G(i\omega, \boldsymbol{q})$ and $\Pi(i\omega, \boldsymbol{q})$ are as introduced earlier in Eqs. (10.2a) and (10.2b). Introducing the additional spin label and the matrix correlations $U_{ij;k\ell} = \pm U_{ik;j\ell}$ does not change the asymptotic nature of the single-electron Green's functions but can lead to preemptive instabilities to superconductivity depending on the $\pm$ sign (Chowdhury and Berg, 2020a). For the model with $U_{ij;k\ell} = U_{ik;j\ell}$, the eigenvalue problem in Eq. (10.13) has a nontrivial solution with a superconducting $T_c \sim U$. Superconductivity preempts the crossover into the heavy Fermi liquid and arises at the level of a single site due to effectively attractive interactions that are generated at $O(U^2)$; the superfluid stiffness is nevertheless finite and given by $NW^* \gg T_c$. On the other hand, for the model with $U_{ij;k\ell} = -U_{ik;j\ell}$, there is no instability at the level of a single site and, while the pairing susceptibility is enhanced when $T \sim W^*$ is approached from above, the non-Fermi liquid is stable against pairing. However, across the crossover into the heavy Fermi-liquid regime, the momentum dependence in $\Pi(\boldsymbol{q})$ can drive a pairing transition, much like the Kohn-Luttinger mechanism but where T_c is now set by the only relevant scale in the problem W^*. Similar generalizations can also be constructed for the two-band models in Sec. X.B, to analyze the intrinsic pairing instabilities of the marginal Fermi liquid with a critical Fermi surface (Chowdhury and Berg, 2020b). We end by noting that for a variety of non-Fermi liquids involving quantum-critical degrees of freedom, the Eliashberg equations share a similar structure (Abanov and Chubukov, 2020; Wu *et al.*, 2020).

XI. FERMI SURFACES COUPLED TO GAPLESS BOSONS

This section will turn to a different, and extensively studied, approach to non-Fermi liquids in clean metals. We begin with a Fermi liquid with a well-defined Fermi surface and long-lived quasiparticles and examine the breakdown of

quasiparticles due to scattering from a gapless boson: this gapless boson can be associated with either an order parameter near a symmetry-breaking transition or an emergent excitation associated with fractionalization. Note, however, that the Fermi surface remains sharp in momentum space even though the quasiparticles are not well defined and the spectra are broad in energy space: a "critical Fermi surface" is realized, as discussed in Sec. II.B.

As we later describe, there are difficulties (Lee, 2009) in applying conventional large-N methods to the critical Fermi surface problem. However, progress has recently become possible (Esterlis *et al.*, 2021) with the incorporation of insights from a class of Yukawa-SYK models describing fermions and bosons with a three-body Yukawa coupling (Fu *et al.*, 2017; Murugan, Stanford, and Witten, 2017; Patel and Sachdev, 2018; Esterlis and Schmalian, 2019; Marcus and Vandoren, 2019; Aldape *et al.*, 2020; Wang, 2020; Wang and Chubukov, 2020; Esterlis *et al.*, 2021; Kim, Altman, and Cao, 2021; Wang *et al.*, 2021). These methods provide a systematic treatment of such critical Fermi surfaces and also expose similarities to SYK non-Fermi liquids. The new approach shows that the required large-N limit can be obtained provided that we allow random coupling constants, as in the Yukawa-SYK models. In this situation, the couplings can be spatially uniform, so translational invariance is maintained (Aldape *et al.*, 2020; Esterlis *et al.*, 2021). Despite the presence of random couplings, many properties self-average in the large-N limit, just as in the Yukawa-SYK models. The central idea is that in a given finite-N system, with a fixed set of coupling constants, there is a RG flow to a common universal low-energy theory. Assuming the existence of such a theory, we attempt to access the universal low-energy physics simply by averaging over couplings. Upon carrying out this procedure, we find that only certain averages over the couplings matter, and the values of these averages cancel out in the low-energy theory, thus supporting the existence of a universal theory. We note that the idea of simplification realized by an average over similar strongly coupled theories has also played an important role in recent investigations in quantum gravity and averages over random matrices or conformal field theories yield systematic large-N holographic realizations of the path integral of simple theories of gravity (Stanford and Witten, 2019; Afkhami-Jeddi *et al.*, 2020; Maloney and Witten, 2020; Pérez and Troncoso, 2020; Chen, Czech, and Wang, 2021; Cotler and Jensen, 2021; Engelhardt, Fischetti, and Maloney, 2021; Datta *et al.*, 2022).

We now consider a specific model of a critical Fermi surface: fermions coupled to an emergent U(1) gauge field. As outlined in Sec. II.B, such a theory arises in a number of different physical contexts, including spin-liquid Mott insulators with a gapless Fermi surface of spinons (Lee, 1989; Altshuler, Ioffe, and Millis, 1994; Polchinski, 1994) and the compressible quantum Hall state in the half-filled Landau level with a gapless Fermi surface of composite fermions (Halperin, Lee, and Read, 1993). The formalism is also easily extended to a number of other examples involving the onset of broken symmetries, identified by order parameters with vanishing lattice momentum, in a metal [such as Ising-nematic order in a Fermi liquid (Metlitski and Sachdev, 2010)].

A. Fermi surface coupled to a dynamical U(1) gauge field

Consider a nonzero density of fermions coupled to an emergent U(1) gauge field A_μ. In the presence of a Fermi surface, the longitudinal components of A_μ are screened just as in an ordinary metal with Coulomb interactions. However, there is no screening in the transverse sector, so we focus only on the transverse spatial components $A_{x,y}$. We can schematically write the theory by generalizing the action for the Fermi liquid to

$$S_{cA} = \int d\tau \left[\int \frac{d^d k}{(2\pi)^d} c_{ka}^\dagger \left(\frac{\partial}{\partial \tau} + \varepsilon(-i\nabla - A) \right) c_{ka} \right.$$
$$\left. + \frac{NK}{2} \int d^2 x (\nabla \times A)^2 \right]. \qquad (11.1)$$

We have not included an explicit time derivative term for A, because it will turn to be subdominant to the frequency dependence induced by the Fermi surface. The coefficient of the Maxwell term $(\nabla \times A)^2$ is determined by short distance physics, and we have included a prefactor of N for future convenience; the gauge-coupling is denoted as K^{-1}. We have restricted our considerations to spatial dimension $d = 2$, where the frequency dependence for the self-energy will be most singular and is also the dimension of most physical applications.

We now proceed with a perturbative but self-consistent analysis of S_{cA} in a "patch" theory: we focus on the vicinity of the point k_0 on the Fermi surface, as in Fig. 24. For the gauge field A, it turns out that we need include only components of their momenta that are tangent to the Fermi surface, closely connected to the following $1/|q_y|$ dependence of the fermion polarizability that is obtained as in Fermi-liquid theory:

$$\Pi(q, i\omega_n) = -\frac{|\omega_n|}{4\pi v_F \kappa |q_y|}. \qquad (11.2)$$

Recalling that we are focusing only on transverse gauge-field fluctuations, we may replace the gauge field with a single scalar field $\phi = A_x$. In this manner, the patch theory limit of Eq. (11.1) is

$$S_{\psi\phi} = \int d\tau dx dy \left[\psi_a^\dagger \left(\frac{\partial}{\partial \tau} - i v_F \frac{\partial}{\partial x} - \frac{\kappa}{2} \frac{\partial^2}{\partial y^2} \right) \psi_a \right.$$
$$\left. + \frac{NK}{2} \left(\frac{\partial \phi}{\partial y} \right)^2 - v_F \phi \psi_a^\dagger \psi_a \right], \qquad (11.3)$$
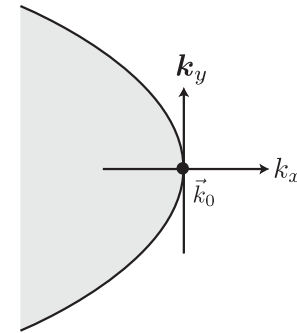

FIG. 24. Extended patch of the Fermi surface with momenta expanded about the point k_0 on the Fermi surface. This yields a theory of two-dimensional fermions ψ in Eq. (11.3).

where, for now, we are considering the case with $a = 1, ..., N$ fermion flavors. This patch theory also applies to the other cases with order parameters, which were identified just before Sec. XI.A.

The fermion polarizability will now appear as a self-energy for the ϕ field, so we can write the ϕ propagator $D(q, i\Omega_n)$ as

$$D(q, i\Omega_n) = \frac{1}{N[Kq_y^2 - v_F^2 \Pi(q, i\Omega_n)]}, \qquad (11.4)$$

where Π is given by Eq. (11.2). The fermion Green's function is expressed as follows in the usual way:

$$G(\boldsymbol{k}, i\omega_n) = \frac{1}{i\omega_n - \varepsilon_k - \Sigma(k, i\omega)}, \qquad (11.5)$$

where now

$$\varepsilon_k = v_F k_x + \kappa \frac{k_y^2}{2}. \qquad (11.6)$$

The self-energy, as a result of scattering off the fluctuations of ϕ, can be evaluated as

$$\begin{aligned}
\Sigma(k, i\omega_n) &= v_F^2 \int \frac{d^2q}{(2\pi)^2} T \sum_{\Omega_n \neq 0} D(q, i\Omega_n) G(k+q, i\Omega_n + i\omega_n) \\
&= -i \frac{v_F^2}{2N} \int \frac{dq_y}{2\pi} T \sum_{\Omega_n \neq 0} \frac{\text{sgn}(\omega_n + \Omega_n)}{Kq_y^2 + |\Omega_n|/4\pi v_F \kappa |q_y|} \\
&= -i \frac{v_F^2}{3\sqrt{3}NK^{2/3}} (4\pi v_F \kappa K)^{1/3} T \sum_{\Omega_n \neq 0} \frac{\text{sgn}(\omega_n + \Omega_n)}{|\Omega_n|^{1/3}}.
\end{aligned}$$
$$(11.7)$$

We dropped the gauge fluctuations at $\Omega_n = 0$ because they require special treatment: this is likely an artifact of the fermion not being gauge invariant. The singularity at $\Omega_n = 0$ in Eq. (11.7) will likely drop out of gauge-invariant observables. In any case, there are no issues at $T = 0$, in which case we find the non-Fermi-liquid self-energy $\Sigma(\omega) \sim \omega^{2/3}$. At $T > 0$, the resulting equation (11.7) obeys the following scaling form, which is similar to that of the SYK model in Eq. (5.27) (Lee, 1989):

$$\Sigma(k, \omega, T) \propto T^{2/3} \Phi\left(\frac{\hbar\omega}{k_B T}\right). \qquad (11.8)$$

This is much larger than the bare ω term in the inverse Green's function and leads to the absence of a quasiparticle pole at the Fermi surface, where the latter is defined as the location where $G^{-1}(k_F, \omega = 0, T = 0) = 0$.

1. Large-*N* limit

As we emphasized earlier, our apparent perturbative computations of the fermion Green's function are actually fully self-consistent in the self-energies of both the gauge field and the fermion. In this sense, the equations have a structure similar to that of the SYK models. Thus, as in the Yukawa-SYK models, we ask whether there is a systemic large-N approach in which these results can be obtained as the saddle point of an action. This will ensure that the solutions are locally stable against all perturbations, determine conditions under which superconducting or other instabilities could exist, and also allow a systematic treatment of corrections.

Despite numerous attempts, a systematic and satisfactory treatment that relies only on a naive large-N expansion has been lacking in the literature. The difficulty is apparent from an examination of Eqs. (11.5) and (11.7). In a model with N fermion flavors, the singular self-energy in Eq. (11.7) has a prefactor of $1/N$, and therefore is formally smaller than the bare dispersion $v_F k_x + \kappa k_y^2/2$. However, the self-energy has to be matched with the bare dispersion to obtain the physical excitations, and thus a power of N is unavoidable in the dispersion of the renormalized excitations. This implies that higher-order Feynman graphs can be enhanced by powers of N not associated with the symmetry factors of the graphs, leading to a breakdown of the $1/N$ expansion; this is indeed what happens (Lee, 2009). Various work-arounds have been attempted (Fitzpatrick *et al.*, 2013, 2014; Damia *et al.*, 2019), but none have been entirely successful because they include N-dependent energy scales.

As noted earlier, recent studies (Aldape *et al.*, 2020; Esterlis *et al.*, 2021) have shown that a systematic large-N theory of the critical Fermi surface can be obtained in a theory with couplings that are random in flavor space but translationally invariant. We now show how such a theory leads to a G-Σ formulation for the critical Fermi surface. We start with the theory Eq. (11.3), promoting the scalar ϕ to now acquire N indices, ϕ_a, and introduce a set of couplings g_{abc} that are random in flavor space but spatially uniform; we also set $v_F = 1$ and $\kappa = 2$. The required theory is then (Esterlis *et al.*, 2021)

$$\begin{aligned}
S_{\psi\phi} = \int d\tau dx dy &\left[\psi_a^\dagger \left(\frac{\partial}{\partial\tau} - i\frac{\partial}{\partial x} - \frac{\partial^2}{\partial y^2} \right) \psi_a \right. \\
&\left. + \frac{K}{2} \left(\frac{\partial\phi_a}{\partial y} \right)^2 - \frac{g_{abc}}{N} \phi_a \psi_b^\dagger \psi_c \right].
\end{aligned} \qquad (11.9)$$

The key new feature is the set of space-independent random complex Yukawa couplings g_{abc} that have zero mean and variance g^2.

We can now proceed just as in the Yukawa-SYK models: we obtain a theory for Green's functions that are bilocal in both space and time. Using the spacetime coordinate $X \equiv (\tau, x, y)$, we can write the averaged partition function

$$\begin{aligned}
\bar{\mathcal{Z}}_{\psi\phi} = \int &\mathcal{D}G(X_1, X_2)\mathcal{D}\Sigma(X_1, X_2)\mathcal{D}D(X_1, X_2) \\
&\times \mathcal{D}\Pi(X_1, X_2) \exp\left[-NI(G, \Sigma, D, \Pi)\right].
\end{aligned} \qquad (11.10)$$

The G-Σ-D-Π action is now

$$I(G, \Sigma, D, \Pi)$$

$$= \frac{g^2}{2} \text{Tr}(G \cdot [GD]) - \text{Tr}(G \cdot \Sigma) + \frac{1}{2} \text{Tr}(D \cdot \Pi)$$

$$- \ln \, \det \left[(\partial_{\tau_1} - i\partial_{x_1} - \partial_{y_1}^2) \delta(X_1 - X_2) + \Sigma(X_1, X_2) \right]$$

$$+ \frac{1}{2} \ln \, \det \left[(-K\partial_{y_1}^2) \delta(X_1 - X_2) - \Pi(X_1, X_2) \right], \quad (11.11)$$

where we introduced notation analogous to that in Eq. (5.57),

$$\text{Tr}(f \cdot g) \equiv \int dX_1 dX_2 f(X_2, X_1) g(X_1, X_2). \quad (11.12)$$

Note the crucial prefactor of N before I in the path integral.

The large-N saddle-point equations of this action are precisely the self-consistent equations that we already solved, apart from differences in factors of N. Assuming that all saddle-point Green's functions depend only upon spacetime differences, we can write them as

$$G(k, i\omega_n) = \frac{1}{i\omega_n - k_x - k_y^2 - \Sigma(k, i\omega_n)},$$

$$D(q, i\Omega_n) = \frac{1}{Kq_y^2 - \Pi(q, \Omega_n)},$$

$$\Sigma(X) = g^2 D(X) G(X),$$

$$\Pi(X) = -g^2 G(X) G(-X). \quad (11.13)$$

From the previous analysis, we can write the solution to these equations as

$$\Pi(q, i\Omega_n) = -\frac{g^2}{8\pi} \frac{|\Omega_n|}{|q_y|},$$

$$\Sigma(k, i\omega_n) = -2i \frac{g^{4/3} \pi^{1/3}}{K^{1/3}} \frac{T}{3\sqrt{3}} \sum_{\Omega_n \neq 0} \frac{\text{sgn}(\omega_n + \Omega_n)}{|\Omega_n|^{1/3}}. \quad (11.14)$$

Note that N does not appear in these saddle-point equations, unlike that in the self-energy in Eq. (11.7).

2. Luttinger's theorem

Despite the absence of a quasiparticle pole, Luttinger's theorem still applies to the critical Fermi surface with essentially no modifications. On general grounds we can expect that, at $T = 0$, $\text{Im} \, G^{-1}(k, i\eta) = 0$ at all k, where η is a positive infinitesimal, and this is obeyed by Eq. (11.7). As in Fermi-liquid theory, the Fermi surface is then defined as $\text{Re} \, G^{-1}(k_F, i\eta) = 0$, with particlelike excitations for $\text{Re} \, G^{-1}(k_F, i\eta) < 0$ and holelike excitations for $\text{Re} \, G^{-1}(k_F, i\eta) > 0$. We proceed as in Sec. V.B and decompose the expression for the charge density per flavor index Q into the following two terms:

$$Q = \int_k \int_{-\infty}^{\infty} \frac{d\omega}{2\pi} G(k, i\omega) e^{-i\omega 0^-} = I_1 + I_2,$$

$$I_1 = i \int_k \int_{-\infty}^{\infty} \frac{d\omega}{2\pi} \frac{d}{d\omega} \ln [G(k, i\omega)] e^{-i\omega 0^-},$$

$$I_2 = -i \int_k \int_{-\infty}^{\infty} \frac{d\omega}{2\pi} G(k, i\omega) \frac{d}{d\omega} \Sigma(k, i\omega) e^{-i\omega 0^-}, \quad (11.15)$$

where $\int_k \equiv \int d^d k / (2\pi)^d$. We evaluate I_1 as in Eq. (5.17) and obtain

$$I_1 = i \lim_{\eta \to 0} \int_k \int_{-\infty}^{0} \frac{d\omega}{2\pi} \frac{d}{d\omega} \ln \left[\frac{G^{-1}(k, \omega + i\eta)}{G^{-1}(k, \omega - i\eta)} \right]$$

$$= -\frac{1}{\pi} \lim_{\eta \to 0} \int_k [\arg \, G^{-1}(k, i\eta) - \arg \, G^{-1}(k, -\infty + i\eta)]. \quad (11.16)$$

The momentum integrand evaluates to $-\pi$ for $\text{Re} \, G^{-1}(k_F, i\eta) > 0$, and 0 otherwise, and hence I_1 evaluates the momentum space volume enclosed by the Fermi surface divided by $(2\pi)^d$.

It now remains to establish that $I_2 = 0$ for the critical Fermi surface case, unlike the SYK model results in Sec. V.B. The self-energy of the critical Fermi surface in Eq. (11.8) is singular at $\omega = 0$, just like the self-energy of the SYK model in Eq. (5.27). Therefore, we might worry that there is an anomalous contribution to I_2 from the singularity at $\omega = 0$, as there was in Sec. V.B. However, that is not the case here because the singularity of the Green's function is much weaker as a result of its momentum dependence; now the low-energy Green's function is

$$G^{-1}(k, \omega) = -v_F k_x - \frac{\kappa}{2} k_y^2 - \Sigma(\omega), \quad (11.17)$$

and this diverges at $\omega = 0$ only on the Fermi surface $v_F k_x + \kappa k_y^2 / 2 = 0$. Indeed, with this form the local density of states is a constant at the Fermi level. Consequently, there is no anomaly at $T = 0$, and $I_2 = 0$ from the Luttinger-Ward functional analysis. Incidentally, we note that the Luttinger-Ward functional in the large-N limit is simply the first term in the action I in Eq. (11.11), which is similar to the SYK model.

To complete this discussion, we add a few remarks on the structure of the Luttinger-Ward functional, and its connection to global U(1) symmetries (Coleman, Paul, and Rech, 2005; Powell, Sachdev, and Büchler, 2005). Consider the general case where were are multiple Green's functions (of bosons or fermions) $G_\alpha(k_\alpha, \omega_\alpha)$. Let the αth particle have a charge q_α under a global U(1) symmetry. For each such U(1) symmetry, the Luttinger-Ward functional will then obey the identity

$$\Phi_{\text{LW}}[G_\alpha(k_\alpha, \omega_\alpha)] = \Phi_{\text{LW}}[G_\alpha(k_\alpha, \omega_\alpha + q_\alpha \Omega)]. \quad (11.18)$$

In Eq. (11.18) we regard Φ_{LW} as a functional of two distinct sets of functions $f_{1,2\alpha}(\omega_\alpha)$, with $f_{1\alpha}(\omega_\alpha) \equiv G_\alpha(k_\alpha, \omega_\alpha + q_\alpha \Omega)$ and $f_{2\alpha}(\omega) \equiv G_\alpha(k_\alpha, \omega_\alpha)$, and Φ_{LW} evaluates to the same value for these two sets of functions. Expanding Eq. (11.18) to first order in Ω and integrating by parts, we establish the corresponding $I_2 = 0$.

3. Thermodynamics

The grand potential can be computed by evaluating Eq. (11.10) for the saddle point in Eq. (11.14). Such a computation (Halperin, Lee, and Read, 1993) shows that the entropy density is given by

$$s \sim T^{2/3}. \qquad (11.19)$$

It is useful to give a scaling interpretation of Eq. (11.19) (Eberlein, Mandal, and Sachdev, 2016). In a critical theory with the dynamic critical exponent z in the spatial dimension d, we expect $s \sim T^{d/z}$. In our case, we have fermionic excitations that disperse as $\omega \sim k_x^{3/2}$, so we identify $z = 3/2$. In this case, Eq. (11.19) matches the scaling expectations in $d = 1$ dimension. Evidently, the free energy is similar to that of chiral fermions dispersing normal to the Fermi surface, and the integral along k_y only determines the prefactor in Eq. (11.19) that is related to the area of the Fermi surface. In scaling terms, it is conventional to denote such a dimensional transmutation in terms of a violation of the hyperscaling exponent θ such that the entropy density scales as $s \sim T^{(d-\theta)/z}$. Equation (11.19) then corresponds to $d = 2$, $\theta = 1$, and $z = 3/2$.

We now extend these scaling arguments to a finite system volume V and compare the behavior to that of the random-matrix model in Sec. IV.B, and that of the SYK model in Sec. V.F.2. Following these earlier treatments, we deal with extensive quantities such as the total entropy $S = sV$. We expect the scaling $V \sim T^{-d/z}$, and thus $S \sim T^{-\theta/z}$. Similarly, we have for the energy density $e \sim Ts \sim T^{(d+z-\theta)/z}$, and the total energy $E = eV \sim T^{(z-\theta)/z}$. Collecting these scaling forms, we express the following total entropy S as a function of the total energy E and the volume V, as in Secs. IV.B and V.F.2:

$$S(E) = V^{\theta/d}\Phi_S(EV^{(z-\theta)/d}), \qquad (11.20)$$

where $\Phi_S(y)$ is a scaling function. As $V \to \infty$, we expect the relationship to involve only intensive quantities, and therefore S/V should be a function only of E/V. This is achieved if

$$\Phi_S(y \to \infty) \sim y^{(d-\theta)/(d-\theta+z)}. \qquad (11.21)$$

The scaling results in Eqs. (11.20) and (11.21) are easily seen to be obeyed by both the random-matrix and SYK models. In these models, we identify the system size N with the volume V, but we cannot accord much meaning to the values of the exponents, because there is no true sense of space. In the random-matrix model, the result in Eq. (4.18) is of the form of Eq. (11.21), with the scaling function $\Phi_S(y) \sim \sqrt{y}$ and $\theta = d - z$. In the SYK model, the result in Eq. (5.81) corresponds to $\Phi_S(y) = c_1 + c_2\sqrt{y}$, for some constants $c_{1,2}$ and the exponents $\theta = d$ and $z = 0$.

For the critical Fermi surface, the important open question is the behavior of $\Phi_S(y \to 0)$. A reasonable conjecture is that $\Phi_S(y \to 0)$ is a nonzero constant. In this case, the total entropy in the $T \to 0$ or $E \to 0$ limit is $S \sim V^{\theta/d} = \sqrt{V}$. Note that this differs from the behavior of the entropy for the critical Fermi surface state obtained in Sec. X.B. In other words, the entropy of the critical Fermi surface here is *subextensive* at low energies, a behavior intermediate between the random-matrix [which has $S(E \to 0) \sim V^0$] and SYK [which has $S(E \to 0) \sim V$] models. The many-body density of states would then behave as $\mathcal{N}(E \to 0) \sim \exp(\sqrt{V})$, although as in all systems $\mathcal{N}(E) \sim \exp(V)$ when E is extensive.

4. Transport

We now couple the fermions on the critical Fermi surface to an external U(1) gauge field [distinct from A in Eq. (11.1)] and discuss the structure of the associated conductivity. The highly singular self-energy in Eq. (11.8) suggests that there will be a strong scattering of charge carriers, and hence a low-T resistivity that is larger than the $\sim T^2$ resistivity of a Fermi liquid. Indeed, it was argued in an early work (Lee, 1989) that the resistivity is $\sim T^{4/3}$; this is weaker than $\Sigma \sim T^{2/3}$ because of the $1 - \cos(\theta)$ factor in the transport scattering time, for scattering by an angle θ, and the dominance of forward scattering.

However, this argument ignores the strong constraints placed by momentum conservation (Hartnoll *et al.*, 2007; Maslov, Yudson, and Chubukov, 2011; Hartnoll *et al.*, 2014; Eberlein, Mandal, and Sachdev, 2016; Hartnoll, Lucas, and Sachdev, 2016) in a theory of critical fluctuations that is described using a translationally invariant continuum field theory such as that given by Eq. (11.3). If we set up an initial state at $t = 0$ with a nonzero current, such a state necessarily has a nonzero momentum, which will remain the same for $t > 0$. The current will decay to a nonzero value that maximizes the entropy subject to the constraint of a nonzero momentum. This nonzero current as $t \to \infty$ implies that the dc conductivity is actually infinite. These considerations are similar to those of "phonon drag" (Peierls, 1930, 1932) leading to the absence of resistivity from electron-phonon scattering. In practice, phonon drag is observed only in clean samples (Hicks *et al.*, 2012) because otherwise the phonons rapidly lose their momentum to impurities. But the electron-phonon coupling is weak, allowing for phonon-impurity interactions before there are multiple electron-phonon interactions. In contrast, for the critical Fermi surface, the fermion-boson coupling is essentially infinite because it leads to the breakdown of electronic quasiparticles. Therefore, the critical Fermi surface must be studied in the limit of strong drag, with vanishing dc resistivity in the critical theory.

Mechanisms extrinsic to the theory in Eq. (11.3) are required to relax the current and obtain a finite dc conductivity. In a system with strong interactions, such processes are most conveniently addressed by a "memory matrix" approach that has been reviewed elsewhere (Hartnoll, Lucas, and Sachdev, 2016); this approach also has close connections to holographic approaches (Lucas, 2015; Lucas and Sachdev, 2015). Various mechanisms have been considered (Maslov, Yudson, and Chubukov, 2011; Hartnoll *et al.*, 2014; Patel and Sachdev, 2014; Wang and Berg, 2019; Else and Senthil, 2021; Lee, 2021) involving spatial disorder or umklapp processes, and these do lead to a singular resistivity at low T.

The behavior of the conductivity σ at a nonzero frequency ω has been argued to be more universal, where the effects of total

momentum conservation are not as singular. In a quantum-critical system, the naive scaling dimension is $d - 2$, and thus we expect $\sigma(\omega) \sim \omega^{(d-2)/z}$, which is frequency independent in $d = 2$. However, we have noted violation of hyperscaling in the free energy in Sec. XI.A.3, and a first guess would be that there is a similar violation of hyperscaling in the conductivity, with $\sigma(\omega) \sim \omega^{(d-2-\theta)/z}$. Using the values of θ and z, we can write the scaling form as (Eberlein, Mandal, and Sachdev, 2016)

$$\mathrm{Re}\,\sigma(\omega \neq 0, T) = \omega^{-2/3}\Phi_\sigma\left(\frac{\omega}{T}\right). \qquad (11.22)$$

This scaling form is consistent with explicit computations of the frequency-dependent conductivity (Kim *et al.*, 1994; Kim, Lee, and Wen, 1995; Eberlein, Mandal, and Sachdev, 2016; Chubukov and Maslov, 2017) but has been questioned in recent analyses working directly with a Fermi surface in $d = 2$ (Darius Shi *et al.*, 2022; Guo *et al.*, 2022).

In a system with momentum conservation, we can define the shear viscosity η in the continuum field theory. This has been computed (Eberlein, Patel, and Sachdev, 2017), and its hyperscaling violation turns out to be different from that of the entropy and the conductivity. The ratio η/s, where s is the entropy density, diverges as $T^{-2/z}$, a result that is consistent with the minimum viscosity conjecture (Kovtun, Son, and Starinets, 2005).

5. Pairing instability

As written in Eq. (11.1), the gauge field mediates a repulsive interaction between antipodal points on the Fermi surface, and thus does not lead to a Cooper pairing instability. However, we can consider closely related problems, either with critical order parameters or with fermions with multiple gauge charges, where the interactions between antipodal fermions is attractive (Metlitski *et al.*, 2015). In the context of the large-N limit of Sec. XI.A.1, the equations determining the pairing instability reduce (Esterlis *et al.*, 2021) to precisely those associated with pairing instabilities of the SYK model (Kim *et al.*, 2019; Klebanov *et al.*, 2020). The pairing vertex $\Phi(i\Omega)$ obeys following the integral equation (Esterlis *et al.*, 2021):

$$E\Phi(i\Omega) = \frac{\mathcal{K}}{3}\int\frac{d\omega}{2\pi}\frac{2\pi\Phi(i\omega)}{|\omega|^{2/3}|\omega - \Omega|^{1/3}}, \qquad (11.23)$$

where ω and Ω are imaginary frequencies and $\mathcal{K}$ is a dimensionless number that can be determined from the structure of the critical Fermi surface problem being considered. Given the scale-invariant structure of Eq. (11.23), we search for solutions with

$$\Phi(i\Omega) = \frac{1}{|\Omega|^\alpha}, \qquad (11.24)$$

and the physical solutions are those values of α for which the eigenvalue $E = 1$. The pairing problem so defined appeared in the context of SYK models (Kim *et al.*, 2019; Klebanov *et al.*, 2020), but also in earlier studies of the quantum-critical

pairing of Fermi surfaces (Moon and Chubukov, 2010; Chubukov and Abanov, 2021). A solution with a real $0 < \alpha < 1/3$ implies that the critical Fermi surface state is stable, and the value of α determines the exponent of critical correlations of the pairing operator (Esterlis *et al.*, 2021). Otherwise, there are solutions with complex α, and these imply a pairing instability. The critical temperature toward pairing is determined by solving a generalization of Eq. (11.23) at nonzero T and examining the T at which the complex solution first appears.

B. Adding spatial disorder

Given the singular transport properties of the critical Fermi surface described in Sec. XI.A.4, it is valuable to have the corresponding large-N analysis of a model that includes the self-consistent influence of weak disorder on the critical Fermi surface, beyond the perturbative analysis provided by the memory function approach (Hartnoll, Lucas, and Sachdev, 2016). The simplest spatial disorder we can add to Eq. (11.9) is potential disorder, which is similar in spirit to that in Sec. IV: this is a term $v_{ab}(x)\psi_a^\dagger(x)\psi_b(x)/\sqrt{N}$, in which v_{ab} is a random matrix uncorrelated at different points in space such that

$$\overline{v_{ab}(x)v_{cd}^*(x')} = v^2\delta_{ac}\delta_{bd}\delta^d(x - x'). \qquad (11.25)$$

Equation (11.25) leads to an additional term in the large-N action in Eq. (11.11). The solution of the saddle-point equations in the theory with both g and v nonzero shows (Guo *et al.*, 2022) that the boson polarizability in Eq. (11.14) is replaced by

$$\Pi(q, i\Omega_n) \sim -\frac{g^2}{v^2}|\Omega_n|, \qquad (11.26)$$

which leads to $z = 2$ behavior in the boson propagator. The corresponding fermion self-energy has a familiar elastic impurity scattering contribution Σ_v, along with an inelastic term Σ_g (Guo *et al.*, 2022) with the following "marginal Fermi-liquid" form (Varma *et al.*, 1989):

$$\Sigma_v(i\omega_n) \sim -iv^2\mathrm{sgn}(\omega_n), \qquad \Sigma_g(i\omega_n) \sim -\frac{g^2}{v^2}\omega_n\ln(1/|\omega_n|). \qquad (11.27)$$

Despite the singularity in Σ_g, Eq. (11.27) does not translate (Guo *et al.*, 2022) into interesting behavior in the transport: the scattering is mostly forward, and the resistivity is Fermi-liquid-like with $\rho(T) = \rho(0) + AT^2$.

While the effect of potential scattering of fermions is weak, a related estimation of the effects of a spatially random ϕ^2 term (i.e., a random scalar mass allowed when ϕ represents a symmetry-breaking order parameter) turns out to be strong (Patel and Sachdev, 2014). It has been argued (Patel *et al.*, 2022) that such disorder should be absorbed by transforming to eigenmodes of the quadratic ϕ action, at the price of introducing spatial randomness into the Yukawa coupling g. A theory with spatial randomness in the boson-fermion Yukawa

coupling included at the outset leads to physical effects that are just right in the large-N limit. We add to the spatially independent Yukawa couplings g_{abc} in Eq. (11.9) a second coupling $g'_{abc}(x)$ that has both spatial and flavor randomness with a vanishing first moment and a second moment

$$\overline{g'_{abc}(x)g'^*_{a'b'c'}(x')} = g'^2\delta^d(x-x')\delta_{aa'}\delta_{bb'}\delta_{cc'}. \qquad (11.28)$$

Along with Eqs. (11.26) and (11.27), we obtain the following additional contributions to the boson and fermion self-energies (Patel *et al.*, 2022):

$$\Pi_{g'}(q, i\Omega_n) \sim -g'^2|\Omega_n|, \qquad \Sigma_{g'}(i\omega_n) \sim -ig'^2\omega_n \ln(1/|\omega_n|). \qquad (11.29)$$

The marginal Fermi-liquid self-energy now contributes significantly to transport (Patel *et al.*, 2022), with a linear-T resistivity $\sim g'^2 T$, while the residual resistivity is determined primarily by v. It is notable that it is the disorder in the interactions that determines the slope of the linear-T resistivity, while it is the potential scattering disorder that determines the residual resistivity.

We also want to examine this theory for Planckian dissipation (Legros *et al.*, 2019; Cao *et al.*, 2020; Nakajima *et al.*, 2020; Grissonnanche *et al.*, 2021; Jaoui *et al.*, 2022; Taupin and Paschen, 2022). This requires one to write the conductivity in the form

$$\sigma = \frac{ne^2\tau^*_{\mathrm{tr}}}{m^*}, \qquad (11.30)$$

where the effective mass m^* is computed from the fermion self-energy in a Fermi-liquid state proximate to the critical theory. For $g' \gg g$, the transport scattering time is found to be (Aldape *et al.*, 2020; Esterlis *et al.*, 2021)

$$\frac{1}{\tau^*_{\mathrm{tr}}} \approx \frac{\pi}{2}\frac{k_B T}{\hbar}, \qquad (11.31)$$

along with factors that are slow logarithmic functions of temperature. However, for smaller values of g'/g there is a significant decrease from the value in Eq. (11.31) (Patel *et al.*, 2022; Taupin and Paschen, 2022).

XII. CONNECTIONS TO QUANTUM GRAVITY

We saw in Sec. V.F that the finite-N fluctuations of the SYK model were described using a path integral over time reparametrizations. This suggests a connection to a theory of quantum gravity. By the holographic principle ('t Hooft, 2001), we expect the gravity theory to acquire an emergent spatial direction. As the SYK path integral is over $0+1$ dimensions, we anticipate a connection to quantum gravity in $1+1$ dimensions. However, Einstein gravity in $1+1$ dimensions has no dynamical modes and thus cannot serve as a holographic partner to the SYK model. As we see in Sec. XII.B, the appropriate theory is a class of $(1+1)$-dimensional theories known as Jackiw-Teitelboim (JT) gravity, which has an additional scalar field Φ. This gravity theory

is most naturally obtained by dimensional reduction from a charged black hole of Einstein gravity in $d+2$ spacetime dimensions ($d \geq 2$). Such a black hole has a $\mathrm{AdS}_2 \times S^d$ near-horizon geometry; the JT-gravity theory resides on AdS_2, and fluctuations of Φ represent the quantum fluctuations in the radius of S^d. The connection between the SYK model and charged black holes was first noted (Sachdev, 2010) by matching characteristics of the $N = \infty$ SYK theory and the classical gravity solution of charged black holes in Einstein gravity. It was later pointed out (Kitaev, 2015) that the connection was stronger and also held for a low-energy sector of the fluctuations.

The AdS_2 near-horizon sector of charged black holes leads to a nonvanishing entropy as $T \to 0$, a key characteristic such black holes share with the SYK model (Sachdev, 2010). Neutral black holes, such as the common Schwarzschild solution of Einstein gravity, do not have AdS_2 horizons and have vanishing entropy as $T \to 0$. Such black holes display a Hawking-Page transition at a nonzero T and have a distinct low-T behavior that we do not further discuss (Schlenker and Witten, 2022).

We proceed by reviewing the quantum theory of charged black holes in $d+2$ spacetime dimensions. We then discuss its low-temperature limit and show, using the previously outlined dimensional reduction, that this yields a version of JT gravity that is in turn equivalent to the Schwarzian theory of the SYK model in Sec. V.F.

There is another, closely related connection between SYK models and black holes that we now mention. Our previous and later discussions focus on the equilibrium thermodynamic properties. In dynamic properties, SYK models are characterized by Planckian time dynamics (Sachdev, 1999), as we discussed in Sec. V.C; other metallic systems have a similar dynamics in theory and experiment, as noted in Secs. XI.B and III.B. Einstein gravity also displays Planckian time dynamics for black holes responding to external perturbations. This is evident in computations of the damping rate of black hole quasinormal modes (Vishveshwara, 1970; Hod, 2007): this purely classical gravity rate is $\sim \hbar/k_B T_H$, where T_H is the Hawking temperature of the black hole (the $\hbar$ in the Planckian time formula cancels with the $\hbar$ in T_H). A recent analysis of LIGO data (Carullo *et al.*, 2021) has confirmed this universality in black hole quasinormal modes.

The quantum fluctuations of gravity and electromagnetism are formally defined by the following path integral:

$$\mathcal{Z}_{\mathrm{EM}} = \int \mathcal{D}g\mathcal{D}A \exp(-I_{\mathrm{EM}}), \qquad (12.1)$$

where I_{EM} is the Einstein-Maxwell action (which we write later) and the path integral is over the metric g of spacetime and the electromagnetic vector potential A. It is almost certainly true that Eq. (12.1) does not make sense as it stands, because of numerous ultraviolet divergencies and gauge-fixing issues. Nevertheless, it turns out to be possible to make sense of Eq. (12.1) in certain limits. For black hole saddle-point solutions of I_{EM}, it was shown (Gibbons and Hawking, 1977) that the evaluation of I_{EM} at the saddle

point in a Euclidean geometry, with a thermal circle of circumference $\hbar/k_B T$ along the temporal direction, gave a consistent description of the quantum thermodynamics of black holes. It is only via the $\hbar$ dependence of this circumference that Planck's constant appears in such computations: there is no $\hbar$ in I_{EM}, the classical Einstein-Maxwell action. We set $\hbar = k_B = 1$ in the remainder of our discussion.

We review the Gibbons-Hawking description of a charged black hole (Chamblin *et al.*, 1999) in Sec. XII.A. There turn out to be precise quantitative connections to the thermodynamics of the SYK model (Sachdev, 2010, 2015).

Fluctuation corrections to the Gibbons-Hawking thermodynamics were computed only recently in the low-T limit for charged holes. In principle, these corrections could have been computed decades ago, but the computations were undertaken only after the connection to the SYK model showed the route that was needed. These computations are reviewed in Sec. XII.B, which shows that the low-energy theory of charged black holes reduces to an effective theory that is identical to the theory in Eqs. (5.58) and (5.60) obtained for the SYK model of complex fermions.

Section XII.C surveys rapid recent developments on coupled SYK models in and out of equilibrium, which are holographically realized by solitons or instantons known as wormholes.

Section XII.D discusses approaches to the theory of strange metals using the AdS/CFT correspondence of supersymmetric Yang-Mills theory (Hartnoll, Lucas, and Sachdev, 2016) and connects these to the SYK model by placing the Yang-Mills theory on a finite sphere.

A. Charged black holes: Einstein-Maxwell theory

We consider the case of spherical black holes in $d + 2$ spacetime dimensions; we assume that $d \geq 2$ in all of the following discussions of quantum gravity. The Einstein-Maxwell theory has the following Euclidean action:

$$I_{\text{EM}} = \int d^{d+2}x \sqrt{g} \left[-\frac{1}{2\kappa^2} \left(\mathcal{R}_{d+2} + \frac{d(d+1)}{L^2} \right) + \frac{1}{4g_F^2} F^2 \right],$$
(12.2)

where $\kappa^2 = 8\pi G_N$ is the gravitational constant, $\mathcal{R}_{d+2}$ is the Ricci scalar, $F = dA$ is the electromagnetic flux, and g_F is a U(1) gauge-coupling constant. We have also included a negative cosmological constant term such that the spacetime at asymptotic infinity is AdS$_{d+2}$ with a radius L; the limit of large L can be taken at the end to obtain the Minkowski spacetime at infinity.

We now describe the spherical charged black hole saddle point of I_{EM}. There is a two parameter family of such solutions, which we specify as the temperature T and the chemical potential μ. All other properties of the black hole saddle point are determined by T, μ, and the constants of nature in I_{EM}: this includes the spacetime metric, the U(1) gauge field, the radius of the horizon r_0, the total charge in the black hole $\mathcal{Q}$, and the black hole entropy S.

The classical Einstein-Maxwell equations yield the following expression for the metric expressed in terms of the

imaginary time τ, the radial coordinate r, and $d\Omega_d^2$, the metric of the d sphere (Chamblin *et al.*, 1999):

$$ds^2 = V(r)d\tau^2 + r^2 d\Omega_d^2 + \frac{dr^2}{V(r)},$$
(12.3)

where

$$V(r) = 1 + \frac{r^2}{L^2} + \frac{\Theta^2}{r^{2d-2}} - \frac{M}{r^{d-1}}.$$
(12.4)

As $r \to \infty$, the metric in Eq. (12.3) is AdS$_{d+2}$. The radius of the horizon is determined by $V(r_0) = 0$, which we write as

$$M = r_0^{d-1} \left(1 + \frac{r_0^2}{L^2} + \frac{\Theta^2}{r_0^{2d-2}} \right).$$
(12.5)

The gauge-field solution has the form

$$A = i\mu \left(1 - \frac{r_0^{d-1}}{r^{d-1}} \right) d\tau.$$
(12.6)

The value of the gauge field at the anti–de Sitter (AdS) boundary defines the chemical potential μ provided that r_0 is the horizon. The Einstein-Maxwell equations applied to Eqs. (12.3) and (12.6) also yield the condition

$$\Theta = \sqrt{\frac{(d-1)}{d}} \frac{\kappa r_0^{d-1}}{g_F} \mu.$$
(12.7)

Thus far, our analysis has been entirely classical. As previously stated, quantum mechanics enters the picture only by the condition that the solution in Eq. (12.3) yields a spacetime that is periodic as a function of τ with the period $1/T$. We can impose periodicity as a function of τ by fiat but have to ensure that there is no singularity at the horizon r_0, where $V(r_0) = 0$. We change radial coordinates to y, where $r = r_0 + y^2$. Near the horizon, the (r, τ) components of Eq. (12.3) then become

$$ds^2 = \frac{4}{V'(r_0)} \left[\frac{[V'(r_0)]^2}{4} y^2 d\tau^2 + dy^2 \right].$$
(12.8)

Notice that the expression in large square brackets in Eq. (12.8) is precisely the metric of the flat plane in polar coordinates, with the radial coordinate y and the angular coordinate $\theta = V'(r_0)\tau/2$. For there to be no real singularity at the origin of polar coordinates, only a coordinate singularity, we must have periodicity in θ with period 2π. Matching this to the period $1/T$ in τ, we determine the Hawking temperature of the black hole as follows:

$$4\pi T = V'(r_0).$$
(12.9)

Equations (12.5), (12.7), and (12.9) determine all the parameters Θ, M, and r_0 in terms of μ and T. Therefore, we have specified a black hole solution in terms of the independent thermodynamic parameters μ and T.

We now quote the free energy and entropy of this black hole, obtained through the evaluation of I_{EM} at the previously mentioned saddle point. The action has to be supplemented by a Gibbons-Hawking boundary term that is required to obtain the classical Einstein-Maxwell equations as saddle-point equations of I_{EM}. Such an evaluation of I_{EM} yields the following grand potential (Chamblin *et al.*, 1999):

$$\Omega(T,\mu) = \frac{s_d[r_0(T,\mu)]^{d-1}}{2\kappa^2}\left(1 - \frac{[r_0(T,\mu)]^2}{L^2}\right) - \frac{s_d(d-1)\mu^2[r_0(T,\mu)]^{d-1}}{2dg_F^2}, \quad (12.10)$$

where $s_d \equiv 2\pi^{(d+1)/2}/\Gamma((d+1)/2)$ is the area of S_d with unit radius. We can evaluate the total charge by taking the μ derivative of Ω as follows:

$$\mathcal{Q}(T,\mu) = \frac{s_d(d-1)\mu[r_0(T,\mu)]^{d-1}}{g_F^2}. \quad (12.11)$$

Equation (12.11) can also be obtained from Gauss's law evaluated as $r \to \infty$. Similarly, the entropy is determined by taking the temperature derivative of Ω to obtain

$$S(T,\mu) = \frac{2\pi s_d}{\kappa^2}[r_0(T,\mu)]^d, \quad (12.12)$$

which is precisely the expression expected from Hawking's result $\mathcal{A}/4G_N$: $\mathcal{A} = s_d r_0^d$ is the area of the horizon. The universality of the Hawking area result can be understood from the fact that the only explicit dependence of the action on T arises from the identification in Eq. (12.9) leading to a circumference $1/T$ on the time circle; the T derivative of Ω can then be shown to arise only from the vicinity of the horizon at $r = r_0$, where the integral over the angular coordinates yields the area (Ross, 2005).

We now take the $T \to 0$ limit of all the previous results while keeping the charge $\mathcal{Q}$ fixed. The horizon radius $r_0 \to R_h$, where

$$\mathcal{Q} = \frac{s_d R_h^{d-1}\sqrt{d[(d+1)R_h^2 + (d-1)L^2]}}{L\kappa g_F}. \quad (12.13)$$

We are interested in the structure of the metric near the horizon at $T = 0$. For this purpose, we transform to near-horizon coordinates, by changing the radial coordinate from r to the coordinate ζ, where

$$r = R_h + \frac{R_2^2}{\zeta}. \quad (12.14)$$

In these coordinates, the $T = 0$ horizon is at $\zeta = \infty$; see Fig. 25. We chose the length scale R_2 to be

$$R_2 = \frac{LR_h}{\sqrt{d(d+1)R_h^2 + (d-1)^2L^2}}. \quad (12.15)$$

As $T \to 0$, the metric in Eq. (12.3) for $\zeta \gg R_h$ [region (A) in Fig. 25] becomes
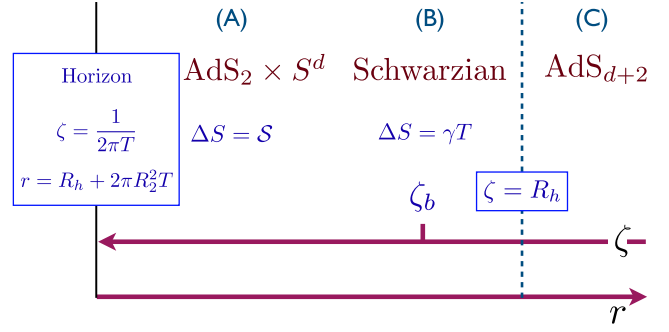

FIG. 25. Spatial crossover boundaries outside a black hole of charge $\mathcal{Q}$. The value of R_h is determined from $\mathcal{Q}$ via Eq. (12.13), and we describe $T \ll 1/R_h$ at a fixed $\mathcal{Q}$ and $R_2 \sim R_h$. We indicate contributions to the entropy ΔS from regions (A) and (B).

$$ds^2 = \frac{R_2^2}{\zeta^2}[d\tau^2 + d\zeta^2] + R_h^2 d\Omega_d^2. \quad (12.16)$$

The metric on the (τ, ζ) spacetime is AdS$_2$, and the complete metric is AdS$_2 \times S^d$. In the same coordinate system, the U(1) gauge field becomes

$$A = i\frac{\mathcal{E}}{\zeta}d\tau, \quad (12.17)$$

where the dimensionless prefactor

$$\mathcal{E} = \frac{g_F R_h L\sqrt{d[(d+1)R_h^2 + (d-1)L^2]}}{\kappa[d(d+1)R_h^2 + (d-1)^2L^2]} \quad (12.18)$$

is a measure of the electric field on the horizon of the black hole. We have chosen the same symbol $\mathcal{E}$ for this prefactor as that appearing in characterizing the particle-hole asymmetry of the SYK model in Eqs. (5.9) and (5.26). This is not arbitrary (Sachdev, 2010, 2015): computations (Faulkner, Liu *et al.*, 2011) of the Green's function of a fermion moving in the background specified by Eqs. (12.16) and (12.17) yield precisely the same result as in Eq. (5.26).

We now turn to a computation of the entropy, where we find noteworthy connections to the SYK model. We write $S(T \to 0) = \mathcal{S}$, and then from Eq. (12.12) get

$$\mathcal{S} = \frac{2\pi s_d}{\kappa^2}R_h^d. \quad (12.19)$$

Thus, we obtain a nonvanishing entropy in the zero-temperature limit similar to that in the SYK model (Sachdev, 2010). Furthermore, by eliminating R_h between Eqs. (12.13) and (12.19) and using Eq. (12.18), we find that

$$\left(\frac{\partial \mathcal{S}}{\partial \mathcal{Q}}\right)_{T\to 0} = 2\pi\mathcal{E}, \quad (12.20)$$

which is exactly the same as the relation in Eq. (5.36) obtained for the SYK model (Sachdev, 2015). We can also compute the low-T dependence of μ and verify that the Maxwell relation (5.35) is satisfied. Furthermore, the T dependence of

entropy computed from Eq. (12.19) is linear in T at low T and fixed $\mathcal{Q}$,

$$S(T \to 0, \mathcal{Q}) = \mathcal{S} + \gamma T, \qquad (12.21)$$

where

$$\gamma = \frac{4\pi^2 d s_d R_2^2 R_h^{d-1}}{\kappa^2}. \qquad (12.22)$$

This is as in the SYK model in Eq. (5.53), where the value of γ was related to the coefficient of a Schwarzian action, and we do the same for the charged black hole in Sec. XII.B.

The appearance of the fundamental relation (12.20) of the SYK model in the theory of a charged black hole may appear to be a coincidence here, but it is not. In fact, Eq. (12.20) is a general property of black holes with AdS$_2$ horizons and follows from careful consideration of their symmetries (Sen, 2005, 2008). These symmetries are similar to those described in Appendix B for the SYK model, which were exploited in Sec. V.D to obtain Eq. (5.36) (Sachdev, 2015; Davison *et al.*, 2017; Gu *et al.*, 2020).

1. Charged black branes

This section notes the limit of the previously mentioned spherical solution when the black hole becomes an infinite, flat charged "black brane," with a near-horizon geometry of AdS$_2 \times R^d$, in contrast to the near-horizon AdS$_2 \times S^d$ considered thus far. These results are helpful in Sec. XII.D, where we discuss the connection to the AdS/CFT correspondence. This limit is obtained by taking $R_h \gg L$ for our results thus far. We introduce the following charge and entropy densities:

$$\mathcal{Q} \equiv \frac{Q}{s_d L^d}, \qquad \mathcal{S} \equiv \frac{S}{s_d L^d}. \qquad (12.23)$$

We then have from Eq. (12.13)

$$\mathcal{Q} = \frac{\sqrt{d(d+1)}}{L \kappa g_F} \left(\frac{R_h}{L}\right)^d. \qquad (12.24)$$

Similarly, the $T \to 0$ entropy in Eq. (12.21) becomes the Hawking entropy density

$$\mathcal{S}(T \to 0, \mathcal{Q}) = \frac{2\pi}{\kappa^2} \left(\frac{R_h}{L}\right)^d \left[1 + \frac{2\pi L^2 T}{(d+1)R_h}\right]. \qquad (12.25)$$

These results for the densities correspond exactly to those obtained earlier (Faulkner, Liu *et al.*, 2011) from a direct solution of the flat black-brane geometry.

B. Charged black holes: Quantum fluctuations

This section examines quantum fluctuations about the saddle-point solution of Einstein-Maxwell theory described in Sec. XII.A. In the "extremal" limit $T \ll 1/R_h$, the theory of these fluctuations coincides with those of the theory described in Eqs. (5.58) and (5.60) obtained from the SYK model (Nayak *et al.*, 2018; Moitra, Trivedi, and Vishal, 2019;

Sachdev, 2019; Gaikwad *et al.*, 2020; Heydeman *et al.*, 2020; Iliesiu and Turiaci, 2020; Boruch *et al.*, 2022). We now outline how this theory may be obtained starting with Eq. (12.1). A more detailed review of these fluctuation computations was presented elsewhere (Sachdev, 2019), but we highlight the key steps here.

(1) Reduce the $d+2$ spacetime dimensional theory in I_{EM} to a $(1+1)$-dimensional theory $I_{EM,2}$ by taking all fields dependent only upon the radial coordinate r and the imaginary time τ.

(2) Take the low-energy limit of $I_{EM,2}$ by mapping it to a near-horizon theory I_{JT} in a $(1+1)$-dimensional spacetime with a boundary. Therefore, we integrate out region (C) in Fig. 25 and obtain an effective theory in regions (A) and (B). In these regions, the near-horizon AdS$_2$ saddle point in Eqs. (12.16) and (12.17) is an exact saddle point of I_{JT}. Outside the boundary, there is a crossover to the full solution of I_{EM} in Eqs. (12.3) and (12.6) to region (C), where the spacetime does not factorize into AdS$_2 \times S_d$.

(3) Compute fluctuations about the AdS$_2$ saddle point of I_{JT}. Einstein gravity in $1+1$ dimensions has no graviton and is "pure gauge." In the JT-gravity theory with boundary, there is a remnant degree of freedom that is a boundary graviton. The action for this boundary graviton is precisely the same as the Schwarzian theory in Eqs. (5.58) and (5.60).

We outline these steps for the gravity sector in Secs. XII.B.1–XII.B.3. The electromagnetic sector produces the action for the phase field ϕ in the Schwarzian theory, as discussed elsewhere (Sachdev, 2019).

1. Dimensional reduction from $d+2$ to $1+1$

We write the $(d+2)$-dimensional metric g of I_{EM} in Eq. (12.2) as follows in terms of a two-dimensional metric h and a scalar field Φ (Davison *et al.*, 2017; Nayak *et al.*, 2018):

$$ds^2 = \frac{ds_2^2}{\Phi^{d-1}} + \Phi^2 d\Omega_d^2. \qquad (12.26)$$

Both h and Φ, as well as the gauge field A, are allowed to be general functions of the two-dimensional coordinates ζ and τ [recall Eq. (12.14) for the definition of the radial coordinate ζ]. Note that the scalar field Φ represents radial fluctuations in the size of the black hole. Equation (12.2) and an associated Gibbons-Hawking boundary term then reduce to [$x \equiv (\tau, \zeta)$]

$$I_{EM,2} = \int d^2x \sqrt{h} \left[-\frac{s_d}{2\kappa^2} \Phi^d \mathcal{R}_2 + U(\Phi) + \frac{Z(\Phi)}{4g_F^2} F^2\right],$$

$$I_{GH} = -\frac{s_d}{\kappa^2} \int_\partial dx \sqrt{h_b} \Phi^d \mathcal{K}_1, \qquad (12.27)$$

along with an additional term not displayed that cancels in $I_{EM,2} + I_{GH}$ (Nayak *et al.*, 2018). The Gibbons-Hawking term is to be evaluated at the boundary at $\zeta \to 0$ or $r \to \infty$. In Eq. (12.27) $\mathcal{R}_2$ is the two-dimensional Ricci scalar and the second integral is over a one-dimensional boundary with

metric h_b and extrinsic curvature $\mathcal{K}_1$. The explicit forms of the potentials $U(\Phi)$ and $Z(\Phi)$ are

$$U(\Phi) = -\frac{s_d}{2\kappa^2}\left(\frac{d(d-1)}{\Phi} + \frac{d(d+1)\Phi}{L^2}\right),$$

$$Z(\Phi) = s_d\Phi^{2d-1}. \tag{12.28}$$

The $(1+1)$-dimensional action in Eqs. (12.27) and (12.28) has exactly the same saddle-point solution as that of the $(d+2)$-dimensional action in Eq. (12.2). The $(1+1)$-dimensional theory $I_{\text{EM},2}$ now involves a metric h and a scalar field Φ, and in terms of the new variables the solution is given by matching Eq. (12.3) with the *Ansatz* in Eq. (12.27). In this manner, it is easy to see that the exact solution for the scalar field is

$$\Phi(\zeta) = R_h + \frac{R_2^2}{\zeta}. \tag{12.29}$$

2. JT gravity in the near-horizon limit

Note that the $T = 0$ horizon is obtained as $\zeta \to \infty$, and the factorization of the metric to $\text{AdS}_2 \times S^d$ fails for $\zeta \lesssim R_h$. Thus, we reduce the theory to the near-horizon spatial region $\zeta > \zeta_b$, with

$$R_h \ll \zeta_b \ll \frac{1}{T}, \tag{12.30}$$

which applies in regions (A) and (B) of Fig. 25. The low-energy limit of the $(1+1)$-dimensional theory of step 1 to $\zeta > \zeta_b$ was argued (Almheiri and Polchinski, 2015; Maldacena, Stanford, and Yang, 2016) to be the JT-gravity theory (Teitelboim, 1983; Jackiw, 1985) of a metric h and a scalar field Φ_1 given by

$$I_{\text{JT}} = -\mathcal{S} + \int d^2x\sqrt{h}\left[-\frac{s_d}{2\kappa^2}\Phi_1\left(\mathcal{R}_2 + \frac{2}{H_b}\right)\right],$$

$$I_{\text{GH}} = -\frac{s_d}{\kappa^2}\int_\partial dx\sqrt{h_b}\Phi_1\mathcal{K}_1, \tag{12.31}$$

where $\mathcal{S}$ is as defined in Eq. (12.19). We also have the boundary conditions

$$h_{\tau\tau}(\zeta \searrow \zeta_b) = \frac{H_b}{\zeta^2},$$

$$\Phi_1(\zeta \searrow \zeta_b) = \frac{\Phi_b}{\zeta}. \tag{12.32}$$

This theory depends upon two constants H_b and Φ_b, and we can obtain their values by matching to the solution for the two-dimensional metric h and scalar field Φ obtained in step 1, which was valid at all ζ. The boundary condition on $h_{\tau\tau}$ is obtained by comparing Eq. (12.26) with Eq. (12.16). Using the leading term in Eq. (12.29) for large ζ we obtain

$$H_b = R_2^2R_h^{d-1}. \tag{12.33}$$

The subleading term in Eq. (12.29) contributes to the coefficient of $\mathcal{R}_2$ in Eqs. (12.27) and (12.31), which from Eq. (12.29) yields

$$\lim_{\zeta\to\infty}[\Phi(\zeta)]^d = R_h^d + \Phi_1(\zeta) + \cdots. \tag{12.34}$$

The boundary value of Φ_1 in Eq. (12.32) then determines

$$\Phi_b = dR_h^{d-1}R_2^2. \tag{12.35}$$

The saddle-point solution of the JT-gravity theory in Eqs. (12.31) and (12.32) coincides with the metric (12.16), which we now generalize to $T > 0$ as follows:

$$ds_2^2 = \frac{R_2^2R_h^{d-1}}{\zeta^2}\left[(1 - 4\pi^2T^2\zeta^2)d\tau^2 + \frac{d\zeta^2}{1 - 4\pi^2T^2\zeta^2}\right],$$

$$\Phi_1(\zeta) = \frac{\Phi_b}{\zeta}. \tag{12.36}$$

Note that the boundary form of Φ_1 in Eq. (12.32) holds for all ζ in the regime of validity of the JT theory, a result that is also evident in Eq. (12.34). The horizon is at $\zeta = 1/2\pi T$, and one can verify that the analog of Eq. (12.9) for the Hawking temperature is satisfied here.

3. From JT gravity to the Schwarzian

We address fluctuations about the saddle-point solution in Eq. (12.36) of the JT-gravity theory defined by Eqs. (12.31) and (12.32). The effective theory now has a simple enough form that these fluctuations can be evaluated reliably (Maldacena, Stanford, and Yang, 2016). The integral over Φ_1 in Eq. (12.31) can be evaluated exactly and yields a constraint on the bulk metric, and the only dynamical degree of freedom in JT gravity is a time reparametrization along the boundary $\tau \to f(\tau)$. To ensure that the bulk metric obeys the boundary condition in Eq. (12.32), we also have to make the spatial coordinate ζ a function of τ, so we map $(\tau, \zeta) \to (f(\tau), \zeta(\tau))$. The boundary metric induced by Eq. (12.36) then equals the value in Eq. (12.32) provided that $\zeta(\tau)$ is related to $f(\tau)$ by

$$\zeta(\tau) = \zeta_bf'(\tau) + \zeta_b^3\left(\frac{[f''(\tau)]^2}{2f'(\tau)} - 2\pi^2T^2[f'(\tau)]^3\right) + \mathcal{O}(\zeta_b^4). \tag{12.37}$$

Finally, we evaluate I_{GH} in Eq. (12.31) along this boundary curve (the bulk contribution I_{JT} vanishes from the equation of motion of Φ_1, which is $\mathcal{R}_2 + 2/H_b = 0$). In this manner we obtain the action (Maldacena, Stanford, and Yang, 2016; Sachdev, 2019) $I_{1,\text{eff}} = -\mathcal{S} + I_{\text{eff}}$ with

$$I_{\text{eff}}[f] = -\frac{s_d\Phi_b}{\kappa^2}\int_0^{1/T} d\tau(\{f(\tau), \tau\} + 2\pi^2T^2[f'(\tau)]^2)$$

$$= -\frac{s_d\Phi_b}{\kappa^2}\int_0^{1/T} d\tau\{\tan[\pi Tf(\tau)], \tau\}. \tag{12.38}$$

Notice that the arbitrary value of ζ_b has been canceled out, and this is an important consistency check on our steps. We have obtained the Schwarzian action, which was found earlier for the SYK model. Here its presence is a consequence of the $SL(2, \mathbb{R})$ symmetry of pure AdS$_2$ discussed in Appendix C, which requires the action to vanish for $f(\tau)$, which are isometries of AdS$_2$. The action for other $f(\tau)$ appears from the "boundary graviton" (Maldacena, Stanford, and Yang, 2016) obtained by embedding AdS$_2$ in the $(d+2)$-dimensional geometry of a charged black hole.

Comparing the action (12.38) to the action for the SYK model in Eq. (5.60), we obtain from the coefficient of the Schwarzian [ignoring the N prefactor in Eq. (5.60)]

$$\gamma = \frac{4\pi^2 s_d \Phi_b}{\kappa^2}. \qquad (12.39)$$

After using the value of Φ_b in Eq. (12.35), we find that this value of γ is in precise agreement with the value in Eq. (12.22), which was computed with the T dependence of the entropy in Eq. (12.12) for the full $(d+2)$-dimensional theory. Thus, the γ coefficients of both charged black holes and the SYK model [in Eq. (5.53)] are given by the coefficient of the Schwarzian effective action.

Finally, we can combine the Schwarzian fluctuation contribution to the entropy in Eq. (5.77) with the leading Bekenstein-Hawking entropy in Eqs. (12.12), (12.15), (12.21), and (12.22) to obtain the universal, leading, low-T form of the entropy of charged black holes when the AdS$_{d+2}$ radius is much larger than the size of the black hole ($L \gg R_h$) (Sachdev, 2019; Iliesiu and Turiaci, 2020),

$$S(T) = \frac{1}{G_N} \left[\frac{\mathcal{A}_0}{4} + \frac{\pi d \mathcal{A}_0^{(d+1)/d}}{2(d-1)^2 s_d^{1/d}} T \right] - \frac{3}{2} \ln\left(\frac{U}{T}\right), \qquad (12.40)$$

where $\mathcal{A}_0 = s_d R_h^d$ is the horizon area at $T = 0$ and the factor in square brackets accounts for the change in the horizon area with increasing T at fixed $\mathcal{Q}$. The nonuniversal energy scale U is now presumably a Planck scale energy, but the $3/2$ coefficient of the logarithm is independent of the nature of the high-energy cutoff. The Schwarzian fluctuation correction to the entropy becomes of the order of the Bekenstein-Hawking term only at an exponentially low temperature $T \sim U \exp(-\mathcal{A}_0/6G_N)$ when the theory breaks down, and the discrete level spacing of the black hole has to be accounted for: the path integral over the Einstein-Maxwell theoretical equation (12.2) has information only on the density of states coarse grained over the exponentially small level spacing. Determining the precise energy levels requires embedding Eq. (12.2) in a higher energy theory like string theory. As in Sec. V.F.2, the logarithmic correction to the entropy in Eq. (12.40) translates to the coarse-grained density of many-body states in Eq. (5.79); for a charged black hole in $(d+2)$-dimensional Minkowski spacetime with $L \gg R_h$, the density of states takes the following form (Sachdev, 2022):

$$D(E) \sim \exp\left(\frac{\mathcal{A}_0 c^3}{4\hbar G_N}\right) \sinh\left(\left[\frac{\pi d \mathcal{A}_0^{(d+1)/d}}{(d-1)^2 s_d^{1/d}} \frac{c^3}{\hbar G} \frac{E}{\hbar c}\right]^{1/2}\right) \qquad (12.41)$$

after restoring factors of $\hbar$ and c. Equation (12.41) is a rare formula that combines Planck's constant $\hbar$ with Newton's gravitational constant G_N: the exponential prefactor was obtained by Hawking, and the sinh term follows from developments ensuing from the solution of the SYK model. Both terms depend only upon the $T = 0$ area of the black hole horizon $\mathcal{A}_0$ and fundamental constants of nature. Note also that there is no dependence upon the electromagnetic coupling g_F.

We note that the previously obtained black hole density of states is significantly different from that obtained in supersymmetric SYK models and black hole solutions of string theory (Fu *et al.*, 2017; Heydeman *et al.*, 2020; Boruch *et al.*, 2022): the latter have an exponentially large exact degeneracy of ground states with multiplicity $\sim \exp(\mathcal{A}_0/4G_N)$ and a gap $\sim 1/\mathcal{A}_0^{1/d}$ to the first excited state. Contrast this with the generic nonsupersymmetric situation with an exponentially small level spacing down to the ground state illustrated in Fig. 6. Indeed, it was the determination of the density of states of the SYK model that led to the understanding that black holes with AdS$_2$ horizons and no low-energy supersymmetry do not have ground states with an exponentially large degeneracy.

C. Wormholes

Thus far we have considered a single SYK model in thermal equilibrium and have argued that it is equivalent to a charged black hole, also in thermal equilibrium. The past few years have seen rapid developments in the theory of more complex configurations of SYK models and black holes, including noteworthy progress in resolving Hawking's quantum information paradox on evaporating black holes. A common thread in these developments have been wormholes, which are the analogs of solitons or instanton tunneling events in quantum gravity.

Consider a pair of identical coupled SYK models, i.e., a homonuclear diatomic SYK molecule, with the Hamiltonian (Sahoo *et al.*, 2020)

$$\begin{aligned} H = \sum_{ij;k\ell} U_{ij;k\ell} \sum_{a=1,2} c_{ia}^\dagger c_{ja}^\dagger c_{ka} c_{\ell a} - \mu \sum_{i,a} c_{ia}^\dagger c_{ia} \\ + \sum_i \kappa(c_{i1}^\dagger c_{i2} + c_{i2}^\dagger c_{i1}). \end{aligned} \qquad (12.42)$$

In Eq. (12.42) $a = 1, 2$ labels the two SYK atoms, and κ is the tunneling amplitude between them. Notice that the random interactions $U_{ij,k\ell}$ are the same on both SYK atoms. This two-atom model is similar to the lattices of SYK atoms considered in Sec. X.A. At half filling, this model can acquire a gapped ground state when the fermions occupy only the lower energy "bonding" orbitals that are eigenstates of the κ term. Holographically, this gapped state corresponds to an eternal wormhole between two black holes with AdS$_2$ horizons, as has been discussed in many recent works (Maldacena and Qi, 2018; García-García *et al.*, 2019; Gao and Jafferis, 2021; Plugge, Lantagne-Hurtubise, and Franz, 2020; Sahoo *et al.*, 2020; Zhou and Zhang, 2020; Nikolaenko *et al.*, 2021; Zhang, 2021, 2022; Zhou *et al.*, 2021).

Next consider a single Majorana $q = 4$ SYK model of N sites (as in Sec. V) coupled to a Majorana $q = 2$ random-matrix model of M sites (as in Sec. IV), with $M \gg N$. This is a heteronuclear diatomic SYK molecule with one atom much larger than the other and is described using the Hamiltonian (Su, Zhang, and Zhai, 2021; Zhang, 2022)

$$H = \sum_{i<j<k<\ell} U^S_{ijkl}\psi_i\psi_j\psi_k\psi_\ell + i\sum_{a<b}U^E_{ab}\chi_a\chi_b + i\sum_{i,a}V_{ia}\psi_i\chi_a.$$
(12.43)

In Eq. (12.43) $i, j, k, \ell = 1, \ldots, N$ and $a, b = 1, \ldots, M$. (The same considerations apply to models of complex fermions, but Majorana fermions were chosen for simplicity.) The SYK atom of ψ fermions models a black hole, and we consider a situation in which it is in some pure excited state with energy E at time $t = 0$. The χ free fermions represent the environment into which the black hole is going to radiate its energy, and thus this setup models an evaporating black hole. At the initial time, the black hole is presumed to be decoupled from the environment, so the entanglement entropy between the black hole and the environment vanishes. In the early stages of the evaporation, the energy E will radiate out into the environment, so the entanglement entropy will increase with time. However, we can also see that as $t \to \infty$ the energy E will all essentially be absorbed by the environment (because $M \gg N$), so the SYK model will be in a low-energy state with small entanglement with the environment. This time evolution of the entanglement is a model of the black hole Page curve (Su, Zhang, and Zhai, 2021; Zhang, 2022). In the holographic representation, the computation of such a Page curve involves spacetime wormholes (Penington *et al.*, 2019; Saad, Shenker, and Stanford, 2019; Almheiri *et al.*, 2020, 2021; Chen, Qi, and Zhang, 2020; Chen, Czech, and Wang, 2021). These works have led to the realization (Bousso *et al.*, 2022) that, upon including wormhole contributions, the path integrals over Einstein-Maxwell theories like Eq. (12.2) are also able to properly compute the time evolution of entanglement entropy in black hole evaporation, along with the density of states noted at the end of Sec. XII.B.3, despite their lack of knowledge of the precise black hole energy levels.

D. AdS/CFT correspondence

An alternative route to a connection between strange metals and quantum gravity uses the AdS/CFT correspondence of string theory. This is a correspondence between a conformal field theory (CFT) in flat d-dimensional space and gravity on a AdS_{d+2} spacetime (Maldacena, 1998; Witten, 1998). The canonical example in spatial dimension $d = 3$ is $SU(N_{YM})$ Yang-Mills gauge theory with $\mathcal{N} = 4$ supersymmetry (Maldacena, 1998) and in spatial dimension $d = 2$ is $SU(N_{YM})$ Yang-Mills gauge theory with $\mathcal{N} = 8$ supersymmetry (Aharony *et al.*, 2008). Both theories are conformally invariant and map to neutral $\mathcal{Q} = 0$ black hole solutions of the action (12.2), with coupling constants

$$\kappa = \bar{\kappa} N_{YM}^{-a} L^{d/2}, \qquad g_F = \bar{g}_F N_{YM}^{-a} L^{(d-2)/2}, \qquad (12.44)$$

where $\bar{\kappa}$ and $\bar{g}_F$ are dimensionless constants of the order of unity, $a = 1$ for $d = 3$, and $a = 3/4$ for $d = 2$.

To obtain a connection to strange metals, we have to dope these CFTs; i.e., we have to place them in a chemical potential coupling to a global U(1) symmetry, which induces a conjugate charge density $N_{YM}^{2a}\mathcal{Q}_{YM}$ (Hartnoll *et al.*, 2007). In the gravity theory, this doped CFT maps to the same charged black hole solutions that we considered for the SYK model, with the important difference that the relevant solutions are the flat black-brane solutions in Sec. XII.A.1, which describe the strange metals produced by doped supersymmetric Yang-Mills theory in infinite d-dimensional space in the limit of large N_{YM}. We note that the doping breaks the supersymmetry, so the low-energy theory has no supersymmetry. The nonzero charge density in the supersymmetric Yang-Mills theory introduces a length scale of the order of $[\mathcal{Q}_{YM}]^{-1/d}$, and we are interested in physics at longer length scales. At these length scales, the black-brane solutions described in Sec. XII.A.1 have a $AdS_2 \times R^d$ geometry (Faulkner, Liu *et al.*, 2011). The doped Yang-Mills theories are described using continuum Lagrangians similar to the disorder-free models of non-Fermi liquids that we considered in Sec. XI (Huijse and Sachdev, 2011; Huijse, Sachdev, and Swingle, 2012). The holographic flow of the doped Yang-Mills theory to a AdS_2 geometry is therefore evidence that models in the class of Sec. XI could have an intermediate energy range over which their physics is described using the SYK-like local criticality. While the SYK-critical state of Sec. VII is unstable to spin-glass order at the lowest temperatures, there could be a crossover from local criticality to the momentum-dependent Fermi surface physics at the lowest energies for the models of Sec. XI. This is in contrast to the supersymmetric doped Yang-Mills theories, for which the AdS_2 geometry is stable down to zero temperature in the large-N_{YM} limit. We note another discussion (Iqbal, Liu, and Mezei, 2011, 2012) with a related point of view.

Some studies of the $AdS_2 \times R^d$ black-brane solutions have focused on their response to additional probe fermions (Cubrovic, Zaanen, and Schalm, 2009, 2011; Faulkner, Iqbal *et al.*, 2011; Faulkner, Liu *et al.*, 2011; Liu, McGreevy, and Vegh, 2011). In particular, it was shown that probe fermions in such a geometry acquired a Fermi surface and a self-energy with some similarities to the critical Fermi surface described in Sec. XI.A, with a self-energy that obeyed a scaling form similar to Eq. (11.8). But there were also significant differences from the microscopic critical Fermi surface theory of Sec. XI.A: (i) the self-energy of the probe fermions had an exponent that varied with momentum across the Fermi surface and (ii) the size of the Fermi surface of the probe fermions was determined by the density of the probe fermions and did not include the large density $N_{YM}^{2a}\mathcal{Q}_{YM}$ of the Yang-Mills theory itself. There is expected to be a separate Fermi surface of the latter background fermions upon including finite-N_{YM} corrections (Sachdev, 2012; Faulkner and Iqbal, 2013). These features imply that the probe fermion black-brane strange metal is really a description of a *spectator* band of fermions (Sachdev, 2010; Huijse and Sachdev, 2011; Huijse, Sachdev, and Swingle, 2012) scattering off a background that has a large density of

low-energy excitations, and the source of the breakdown of the quasiparticles does not arise from interactions between the putative quasiparticles themselves.

1. Connection to the SYK model

The SYK model mapping of Sec. XII.B appeared for a *spherical black hole* horizon of radius R_h, which at temperatures $T \ll 1/R_h$ mapped onto the SYK model at $T \ll U$. We can also place the supersymmetric Yang-Mills theory on a sphere of radius R_{YM}, and this supersymmetric Yang-Mills theories is then connected to the Schwarzian path integral in Eqs. (5.60) and (12.38), as we now discuss.

The Yang-Mills theory is characterized by two length scales (R_{YM} and $[\mathscr{Q}_{\mathrm{YM}}]^{-1/d}$) and the charged black hole solution of Secs. XII.A and XII.B, with a near-horizon $\mathrm{AdS}_2 \times S^d$ geometry, provides a complete holographic description as $1/T$ is varied across these length scales. To make this correspondence precise, we have to relate R_{YM} and $[\mathscr{Q}_{\mathrm{YM}}]^{-1/d}$ to the length scales in the black hole solution, which are R_h, L, and R_2. The connection between the total charge and the charge density in Eq. (12.23) immediately implies

$$L = R_{\mathrm{YM}}, \qquad (12.45)$$

while the total charge of the black hole solution in Eq. (12.13) leads to

$$\mathscr{Q}_{\mathrm{YM}} = \frac{R_h^{d-1}\sqrt{d[(d+1)R_h^2 + (d-1)L^2]}}{L^{2d}\bar{\kappa}\bar{g}_F}. \qquad (12.46)$$

The value of R_2 remains connected to R_h and L as in Eq. (12.15).

Finally, we connect to the low-energy Schwarzian approximation of the charged black hole. The charge density breaks the supersymmetry of the Yang-Mills theory, so we do not need to consider the super-Schwarzian theories that are needed for supersymmetric SYK models and supersymmetric black holes (Fu *et al.*, 2017; Stanford and Witten, 2017; Heydeman *et al.*, 2020; Boruch *et al.*, 2022). If we are at low temperatures such that the thermal length is larger than the charge length $T \ll [\mathscr{Q}_{\mathrm{YM}}]^{1/d}$, and also such that fluctuations of nonconstant horizon modes can be neglected $T \ll 1/R_h$, we can map these values L, R_h, and R_2 to obtain the dimensionless coupling constant g_{Sch} (Stanford and Witten, 2017) of the low-energy Schwarzian theory as follows from Eq. (12.39):

$$\frac{\pi}{g_{\mathrm{Sch}}^2} = \gamma T = \frac{4\pi^2 d s_d N_{\mathrm{YM}}^{2a}}{\bar{\kappa}^2} \frac{R_2^2 R_h^{d-1} T}{L^d}. \qquad (12.47)$$

The ratio of length scales $R_2^2 R_h^{d-1}/L^d$ is to be determined as a function of the length scales R_{YM} and $[\mathscr{Q}_{\mathrm{YM}}]^{-1/d}$ by solving Eqs. (12.45), (12.46), and (12.15). Thus, Eq. (12.47) is the main result of this section, determining the Schwarzian coupling g_{Sch} as a function of the parameters of the Yang-Mills theory, which are the temperature T, the radius of the

sphere R_{YM}, and the charge density $N_{\mathrm{YM}}^{2a}\mathscr{Q}_{\mathrm{YM}}$. Note that the coupling g becomes small in the limit of large N_{YM}.

We now examine the value of g_{Sch} in the limiting regime when the size of the sphere of the Yang-Mills theory is much larger than the size set by the charge density $R_{\mathrm{YM}} \gg [\mathscr{Q}_{\mathrm{YM}}]^{-1/d}$. We then find that $R_h \gg L$, with

$$R_h \sim R_{\mathrm{YM}}[\mathscr{Q}_{\mathrm{YM}}R_{\mathrm{YM}}^d]^{1/d}, \qquad R_2 \sim R_{\mathrm{YM}}, \qquad (12.48)$$

such that

$$\frac{1}{g_{\mathrm{Sch}}^2} \sim N_{\mathrm{YM}}^{2a}[\mathscr{Q}_{\mathrm{YM}}R_{\mathrm{YM}}^d]^{(d-1)/d}R_{\mathrm{YM}}T. \qquad (12.49)$$

We observe that $g_{\mathrm{Sch}}^2 \sim [R_{\mathrm{YM}}]^{-d}$, so the coupling becomes weak in the limit of a large sphere. As always, we have to maintain $T \ll 1/R_h$ to apply the Schwarzian theory, so the minimum possible value of the Schwarzian coupling is

$$g_{\mathrm{Sch,min}}^2 \sim N_{\mathrm{YM}}^{-2a}[\mathscr{Q}_{\mathrm{YM}}R_{\mathrm{YM}}^d]^{(2-d)/d}. \qquad (12.50)$$

E. Out-of-time-order correlations

The connections to quantum gravity have also introduced a new diagnostic, the out-of-time-order correlator, for detecting how quickly local perturbations become entangled with a macroscopic number of degrees of freedom in quantum many-body systems evolving under their own unitary dynamics. Out-of-time-order correlations (OTOCs) were studied a long time ago (Larkin and Ovchinnikov, 1969) as an approach to diagnosing the semiclassical consequences of classical chaos in a quantum system. The modern incarnation of OTOCs appeared (Shenker and Stanford, 2014) in the study of shock waves in black holes (Dray and 't Hooft, 1985), where they were proposed as a signature of intrinsically quantum chaos in a strongly interacting many-body system. Shenker and Stanford argued that any strongly interacting quantum system, which is holographically dual to a black hole described using a theory containing Einstein gravity, has an OTOC of local operators V and W that has an exponential growth at early times,

$$\langle W(t)V(0)W(t)V(0)\rangle \sim \exp(\lambda_L t), \qquad (12.51)$$

and the Lyapunov growth rate exponent is given by

$$\lambda_L = 2\pi T. \qquad (12.52)$$

This value of λ_L is a direct consequence of Einstein gravity and the circumference of the Euclidean temporal circle being equal to $\hbar/k_B T$. This exponential growth was argued to be related to a rapid loss of memory of the initial perturbations with time, a characteristic also expected from the absence of quasiparticle excitations. It was subsequently argued (Maldacena, Shenker, and Stanford, 2016), without the use of a holographic connection, that the inequality $\lambda_L \leq 2\pi T$ must apply to all strongly interacting quantum systems. The bound has also been shown to follow directly from the structure of generic operators that satisfy the eigenstate

thermalization hypothesis (Murthy and Srednicki, 2019). A complementary bound has also been proposed on a closely related quantity that diagnoses operator growth (Parker *et al.*, 2019). However, none of these statements suggest that generic quantum many-body systems necessarily display an exponential growth of the OTOC.

The OTOC ideas have found a precise realization in the SYK model. For the model of Sec. V, we define the OTOC as

$$
\begin{aligned}
&\text{OTOC}(t_1, t_3, ; t_2, t_4) \\
&= \frac{1}{N^2} \sum_{i,j} \langle c_i^\dagger(t_1) c_j(t_3) c_i(t_2) c_j^\dagger(t_4) \rangle_{\text{conn}}.
\end{aligned}
\tag{12.53}
$$

We examine the real time regime with $t_1 \approx t_2 \gg 1/T$ and $t_3 \approx t_4$ and define the "center-of-mass" time separation as

$$
t = \tfrac{1}{2}(t_1 + t_2 - t_3 - t_4).
\tag{12.54}
$$

The OTOC of the SYK model can be computed by generalizing the expression Eq. (5.59) for Schwarzian fluctuations corrections from two-point to four-point correlators. In imaginary time, we have the four-point correlator

$$
\begin{aligned}
\mathcal{F}(\tau_1, \tau_3; \tau_2, \tau_4) = \langle [f'(\tau_1) f'(\tau_2) f'(\tau_3) f'(\tau_4)]^{1/4} \\
\times G_c[f(\tau_1) - f(\tau_2)] G_c[f(\tau_3) - f(\tau_4)] \rangle_{\bar{Z}},
\end{aligned}
\tag{12.55}
$$

where the average is over the Schwarzian path integral in Eq. (5.58) (we have omitted the unimportant fluctuations of ϕ) and the conformal saddle-point Green's function $G_c(\tau)$ is given by Eq. (5.25). After the careful analytic continuation of this correlator to real times, it was found that in the time range $1 \lesssim Tt \ll \ln N$ there is the following exponential growth of the OTOC (Kitaev, 2015; Maldacena and Stanford, 2016; Kitaev and Suh, 2018):

$$
\text{OTOC}(t_1, t_3, ; t_2, t_4) \propto \frac{1}{N} \exp(2\pi Tt).
\tag{12.56}
$$

Therefore, the chaos inequality (Maldacena, Shenker, and Stanford, 2016) is saturated by the SYK model, which has the same chaos growth rate as systems that are holographically dual to Einstein gravity.

The spatial structure associated with the OTOC is equally interesting and directly diagnoses operator growth. In Eq. (12.51), if the operators are spatially separated $[W(t, \boldsymbol{r}), V(0,0)]$, the OTOC exhibits a ballistic wave front associated with the growing operators as a function of $(t - |\boldsymbol{r}|/v_B)$. The "butterfly velocity" v_B is an intrinsic speed associated with the quantum many-body state and can, in principle, be parametrically smaller than the microscopic scales associated with the Hamiltonian (Swingle and Chowdhury, 2017).

OTOCs have been studied in a variety of models, including the critical Fermi surface model of Sec. XI.A (Patel and Sachdev, 2017; Tikhanovskaya, Sachdev, and Patel, 2022), the lattice models related to those of Sec. X (Gu, Lucas, and Qi, 2017; Gu and Kitaev, 2019; Guo, Gu, and Sachdev, 2019),

disordered metals (Patel *et al.*, 2017), and conformal field theories (Stanford, 2016; Chowdhury and Swingle, 2017; Grozdanov, Schalm, and Scopelliti, 2019; Steinberg and Swingle, 2019; Kim, Altman, and Cao, 2021), and all find a regime of exponential growth with a λ_L that obeys the chaos bound, accompanied by a sharp ballistic wave front. All of these settings involve a large-N or a weak-coupling semiclassical limit. Direct numerical studies of realistic lattice models in one dimension (Bohrdt *et al.*, 2017; Luitz and Lev, 2017; Xu and Swingle, 2020) have revealed a ballistic growth of operators but no indication of a well-defined (i.e., position- and velocity-independent) Lyapunov exponent and a sharp front.

There have also been studies involving random unitary circuits with a finite-dimensional local Hilbert space and no semiclassical limit that observed a behavior of the OTOC that is qualitatively distinct from the previously mentioned models (Khemani, Huse, and Nahum, 2018; Nahum, Vijay, and Haah, 2018; von Keyserlingk *et al.*, 2018; Xu and Swingle, 2019); the growth is not identified by a well-defined λ_L, and the ballistic wave front is not sharp. However, these models do not have a conserved energy and an associated notion of temperature, thereby making a direct comparison to the chaos bound far from clear. A recent study (Keselman, Nie, and Berg, 2021) demonstrated a way to access a regime of exponential growth of the OTOC even in random unitary circuits by effectively tuning $v_B \gg \lambda_L \times$ (microscopic length scale), thereby presenting evidence that a finite Hilbert space can have an exponential growth of the OTOC.

The relevance of λ_L and v_B for measurable transport quantities has been scrutinized in a number of works. Bounds on transport quantities, such as the viscosity (Kovtun, Son, and Starinets, 2005) and charge diffusion coefficient (Hartnoll, 2015), have been suggested to hold for strongly interacting phases without quasiparticle excitations. Both of these bounds can be interpreted in terms of a bound on the diffusion coefficient $D \sim \hbar v^2/k_B T$, where v is a characteristic (but unknown) velocity scale in the problem. The statement of the bound was sharpened with the proposition (Blake, 2016) that the relevant velocity scale is set by $v = v_B$. While there are a number of holographic examples where these bounds have been shown to apply and even be saturated (Gu, Qi, and Stanford, 2017), there are explicit counterexamples where the proposed bounds are violated (Lucas and Steinberg, 2016; Gu, Lucas, and Qi, 2017). Stepping away from concrete models, a hydrodynamic understanding of some aspects of operator growth and chaos has also been developed in situations where the exponential regime exists (Blake, Lee, and Liu, 2018).

In general, the relation between diffusive spreading of conserved charges and ballistic growth of nonconserved operators is complicated. For a class of generic random unitary circuits with conserved charges, it was shown that a spreading operator consists of a conserved part spreading diffusively, which acts as a source of nonconserved operators and leads to dissipation at a rate set by the local diffusion current (Khemani, Vishwanath, and Huse, 2018). The nonconserved operators spread ballistically at a butterfly speed, becoming increasingly entangled with a macroscopic number

of degrees of freedom in the system and acting as a dissipative bath. Therefore, in this random unitary circuit approach, the diffusion coefficient need not be related to any of the metrics associated with the OTOCs.

However, a close relationship has been found between the OTOC λ_L and the thermal diffusivity in computations for the critical Fermi surface (Patel and Sachdev, 2017), and in a wide class of holographic models (Blake, Davison, and Sachdev, 2017). The relationship between the thermal diffusivity and v_B^2/λ_L has also been analyzed in a family of strongly interacting bosonic variants of the SYK model (Tulipman and Berg, 2021), which are more closely related to the quantum spherical p-spin-glass model (Cugliandolo, Grempel, and Santos, 2001), which was inspired by the observation of Planckian diffusivities in a class of complex insulators (Zhang *et al.*, 2019; Mousatov and Hartnoll, 2020). A simplified interpretation is that both quantum chaos and thermal diffusivity are related to a loss of phase coherence. The time derivative of a local phase is the local energy density, and the fluctuation-dissipation theorem relates energy fluctuations to thermal transport.

The exact relation between OTOCs and universal aspects of transport remains unclear. Inspired by the universality of scattering rates across distinct materials displaying non-Fermi-liquid properties, it has been conjectured (Chowdhury *et al.*, 2018) that there is an emergent length scale $\ell \gg a$ ($\equiv$ lattice spacing) that is characterized by maximal chaos with a Lyapunov exponent $\lambda_L = 2\pi T$ at low temperatures (i.e., as either $T \to 0$ or $T > W^*$ but still small compared to microscopic energy scales) and effectively reaches local thermal equilibrium in a time of the order of $1/T$ (Sachdev, 1999). The universal coarse-grained description for the non-Fermi liquids can then possibly be built by coupling the islands of typical size ℓ. This does not imply that the system is necessarily maximally chaotic at the scale of the system size. In contrast, in a system with quasiparticles that does not display any non-Fermi-liquid behavior, we expect $\lambda_L \ll T$ as $T \to 0$.

We end by noting that a different diagnostic of quantum chaos that measures the correlations between energy levels and diagnoses the spectral "rigidity" is the spectral form factor (SFF). The SFF has been analyzed in the past in the context of mesoscopic physics and random-matrix theory (Altshuler and Shklovskii, 1986). The ramp-plateau form of the SFF beyond the Thouless time signifies the onset of chaotic random-matrix-like behavior and has been analyzed for the SYK model using a variety of different methods (Cotler *et al.*, 2017; García-García and Verbaarschot, 2017; Altland and Bagrets, 2018; Gharibyan *et al.*, 2018; Saad, Shenker, and Stanford, 2018; Liao, Vikram, and Galitski, 2020; Winer, Jian, and Swingle, 2020; Altland *et al.*, 2021).

XIII. OUTLOOK

Finding models of interacting electrons that can be solved reliably in the regime of strong interactions and at finite temperatures, without making uncontrolled approximations, remains a key challenge in quantum many-body physics. The family of models studied in this review offer a useful starting point for describing compressible metallic phases without any

Landau quasiparticles at strong interactions. Furthermore, they naturally lead to NFL regimes exhibiting electronic interaction-induced T-linear resistivity and Planckian behavior over a wide range of energy scales and are accompanied by ω/T scaling. The theoretical results reviewed here are consistent with much of the universal experimental NFL phenomenology across numerous distinct microscopic materials. Therefore, it is natural to consider the possibility that a large class of strongly interacting microscopic models describing real materials flow (in a RG sense) to the different families of models considered in this review over a significant intermediate energy range. Proving this remains a challenge.

A notable recent result in the study of non-Fermi liquids is the phase diagram of Fig. 13 (Shackleton *et al.*, 2021; Dumitrescu *et al.*, 2022). This presents the results of a numerical study of the doped random-exchange t-U-J Hubbard model. Many features of the phase diagram are reminiscent of the observations in the hole-doped cuprates, as discussed in Sec. VII.G. These include a doping-induced transition from a disordered Fermi liquid satisfying Luttinger's theorem for $p > p_c$ to a low-temperature metallic spin glass for $p < p_c$. At higher temperatures, the latter has a small carrier density and violates Luttinger's theorem. The quantum-critical metal near $p = p_c$ exhibits a single-particle lifetime that has a Planckian form (see Fig. 14) with an O(1) coefficient; in the low-temperature limit the inferred resistivity is significantly below the MIR value. The quantum-critical spin correlations are given by those of the SY spin liquid.

At first sight, this concordance is noteworthy and puzzling: the theory relies on a random-exchange coupling with zero mean, which is far from the physical situation in the cuprates. We can take the concordance as an indication that AdS_2/SYK local criticality has a robustness and can be present in models over a significant intermediate energy range. We make note of the renormalization group arguments (Patel and Sachdev, 2019) that enhancement of resonant scattering can lead to the emergence of local SYK criticality. We also discussed holographic evidence of such a crossover (Iqbal, Liu, and Mezei, 2011, 2012; Liu and Sonner, 2020) in disorder-free non-Fermi liquids of Fermi surfaces coupled to gauge fields in Sec. XII.D. See also Khveshchenko (2018a, 2022) for other thoughts on the emergence of SYK local criticality.

The universality of the models studied is also encoded in their notable maximal many-body chaos, as diagnosed using the OTOC. Whether this aspect also indirectly controls the universality of Planckian transport scattering rates across distinct NFL materials is an important and nontrivial theoretical question. A recent work has highlighted some of the fundamental differences between the growth of operators in maximally chaotic versus nonmaximally chaotic quantum systems (Blake and Liu, 2021), which could be of some relevance to understanding transport in NFL without quasiparticles.

For the disordered models considered in Sec. VII, the SY spin-liquid behavior (Joshi *et al.*, 2020) cannot extend down to $T = 0$, because of the divergence of the spin-glass susceptibility (Georges, Parcollet, and Sachdev, 2000, 2001) (although this instability is not visible over the accessible temperature range in the Planckian behavior in Fig. 14). Thus, we expect the eventual appearance of a metallic spin glass or a disordered Fermi liquid in which the zero-temperature entropy

is quenched, with the SY spin liquid surviving at $T = 0$ only at the "spinoidal" critical point where the Fermi-liquid solution disappears. In more realistic models with weak disorder, we can expect the pseudogap to acquire the topological order of a fractionalized Fermi liquid or have spin or charge-density wave order. The critical theory asymptotically close to the pseudogap critical point will also be different: for the models of Sec. VII, we can expect a transition from a disordered Fermi liquid to a metallic spin glass, as described in theories without fractionalization (Sachdev, Read, and Oppermann, 1995; Sengupta and Georges, 1995). Another possibility, present in the non-Fermi-liquid large-M limit of Sec. VII.D.2, is that the entire overdoped regime is a critical metal with linear-T resistivity (Christos *et al.*, 2022), and the critical point is then also a deconfined theory. The connections between the previously outlined transition and "deconfined" metallic criticality (Zhang and Sachdev, 2020; Zou and Chowdhury, 2020) associated with abrupt Fermi surface changing transitions in clean systems, and in the absence of fractionalization in the adjacent phase, remain an interesting open problem.

A consequence of models with J_{ij} having zero mean is that there is no superconductivity. Adding a nonzero mean J_{ij} or another attractive interaction should lead to superconductivity (Patel, Lawler, and Kim, 2018; Esterlis and Schmalian, 2019; Chowdhury and Berg, 2020a; Hauck *et al.*, 2020; Wang, 2020; Wang *et al.*, 2020), and a theory is needed for the onset of superconductivity from the Planckian metal phase of Figs. 13 and 14.

We discussed theories of non-Fermi liquids with critical Fermi surfaces in Sec. XI. Without disorder, such theories have zero resistivity in the absence of exponentially weak umklapp scattering, and thus cannot produce linear-in-T resistivity at low T. Adding potential scattering disorder to such a critical Fermi surface does produce a nonzero residual resistivity, but the temperature dependence of the resistivity is Fermi-liquid-like, even though there is marginal Fermi-liquid behavior in the fermion self-energy (Patel *et al.*, 2022). An interesting recent observation (Patel *et al.*, 2022) is that spatial disorder in the interaction strength does indeed produce a linear-T resistivity [along with a $T \ln(1/T)$ specific heat]. Two different types of disorder are therefore responsible for the residual resistivity and the slope of the linear-T resistivity: the former arises from potential disorder and the latter results from interaction disorder. This feature has promise in explaining observations, and a better understanding is needed of the strengths of these disorders in the context of microscopic models.

An emerging application of the SYK model is to mesoscopic systems, and this was not covered in our review. In this context, the behavior of the SYK model at finite N is important, and we have to reverse the orders of limit of $N \to \infty$ (which we generally have taken first) and a long-time $t \to \infty$. The SYK model has a new emergent criticality for $t > N/U$, some aspects of which were covered in Sec. V.F. Note that even for finite but large N we do not immediately have a crossover to a regime where the discreteness of the energy spectrum is important; in a many-body system, the energy level spacing $\sim \exp(-\alpha N)$, and therefore even for $t > N/U$ we deal with an effectively continuous spectrum. See the literature (Franz and Rozali, 2018) for studies of applications to quantum dots and graphene flakes (Pikulin and Franz, 2017; Gnezdilov, Hutasoit, and Beenakker, 2018; Altland, Bagrets, and Kamenev, 2019a, 2019b; Micklitz, Monteiro, and Altland, 2019; Khveshchenko, 2020a; Kruchkov *et al.*, 2020; Kobrin *et al.*, 2021), lattices of quantum dots (Altland, Bagrets, and Kamenev, 2019a; Khveshchenko, 2020b), Majorana fermions (Chew, Essin, and Alicea, 2017; Chen *et al.*, 2018), ultracold atoms (Danshita, Hanada, and Tezuka, 2017; Wei and Sedrakyan, 2021), and quantum simulation (García-Álvarez *et al.*, 2017; Luo *et al.*, 2019). These works keep N finite, and therefore differ from the models in Sec. X, which take the $N \to \infty$ first. In Secs. VI–VIII, our interest was in dynamical mean-field theories of lattice systems in the thermodynamic limit, so it was appropriate to take the $N \to \infty$ limit first.

APPENDIX A: TIME REPARAMETRIZATION AND GAUGE SYMMETRIES OF THE SYK MODEL

In this appendix, we elaborate on the origin of Eq. (5.22) from a more fundamental basis and generalize it to the particle-hole asymmetric case. We return to the original equations (5.2a) and (5.2b) and simplify them in the low-energy limit. As we saw in Eq. (5.13), at frequencies $\ll U$ the $i\omega + \mu$ term can be dropped because $\mu - \Sigma(0) = 0$ and the $i\omega_n$ term is smaller than the singular frequency dependence in $\Sigma(i\omega_n)$. After Fourier transforming to the time domain, we can rewrite the original saddle-point equations as

$$\int_0^\beta d\tau_2 \Sigma_{\text{sing}}(\tau_1, \tau_2) G(\tau_2, \tau_3) = -\delta(\tau_1 - \tau_3), \quad \text{(A1a)}$$

$$\Sigma_{\text{sing}}(\tau_1, \tau_2) = -U^2 G^2(\tau_1, \tau_2) G(\tau_2, \tau_1), \quad \text{(A1b)}$$

where Σ_{sing} is the singular part of Σ. In addition, the saddle-point Green's functions and self-energies are functions only of time differences, like $\tau_1 - \tau_2$. Nevertheless, we have written them as a function of two independent times because the fluctuations about the saddle point will involve the bilocal fields, as we later see. Moreover, the symmetries are more transparent in the bilocal formulation.

It is now not difficult to verify that Eqs. (A1a) and (A1b) are invariant under the following transformation:

$$\tau = f(\sigma), \tag{A2a}$$

$$G(\tau_1, \tau_2) = [f'(\sigma_1)f'(\sigma_2)]^{-1/4} \frac{g(\sigma_1)}{g(\sigma_2)} \tilde{G}(\sigma_1, \sigma_2), \tag{A2b}$$

$$\Sigma(\tau_1, \tau_2) = [f'(\sigma_1)f'(\sigma_2)]^{-3/4} \frac{g(\sigma_1)}{g(\sigma_2)} \tilde{\Sigma}(\sigma_1, \sigma_2), \tag{A2c}$$

where $f(\sigma)$ and $g(\sigma)$ are arbitrary functions. In Eqs. (A2a)–(A2c) $f(\sigma)$ is a time reparametrization and $g(\sigma)$ is a U(1) gauge transformation in imaginary time. These are emergent symmetries because the form of the equations obeyed by $\tilde{G}(\sigma_1, \sigma_2)$ and $\tilde{\Sigma}(\sigma_1, \sigma_2)$ is the same as Eqs. (A1a) and (A1b) obeyed by $G(\tau_1, \tau_2)$ and $\Sigma(\tau_1, \tau_2)$.

We obtain the nonzero temperature solution by choosing the time reparametrization in Eq. (A2a) as the conformal map

$$\tau = \frac{1}{\pi T} \tan(\pi T \sigma), \tag{A3}$$

where σ is the periodic imaginary time coordinate with period $1/T$. Applying this map to Eq. (5.7), we obtain

$$G(\pm\sigma) = \mp C g(\pm\sigma) \sin(\pi/4 + \theta) \left(\frac{T}{\sin(\pi T \sigma)}\right)^{1/2} \tag{A4}$$

for $0 < \pm\sigma < 1/T$. The function $g(\sigma)$ is currently undetermined apart from a normalization choice $g(0) = 1$. We can now determine $g(\sigma)$ by imposing the KMS condition

$$G(\sigma + 1/T) = -G(\sigma), \tag{A5}$$

which implies

$$g(\sigma) = \tan(\pi/4 + \theta)g(\sigma + 1/T). \tag{A6}$$

The solution is

$$g(\sigma) = e^{-2\pi\mathcal{E}T\sigma}, \tag{A7}$$

where the new parameter $\mathcal{E}$ and the angle θ are related as in Eq. (5.10). This yields the final expression for $G(\sigma)$ in Eq. (5.25).

APPENDIX B: SYMMETRIES OF THE SYK SADDLE POINT

We showed in Appendix A that the low-energy limit of the saddle-point equations (A1a) and (A1b) have a large set of symmetries when expressed in terms of bilocal correlators of 2 times. However, the actual solution of the saddle-point equations (5.25) is a function only of time differences. Here we ask a somewhat different question: What subgroup of the symmetries in Appendix A applies to the thermal solution in Eq. (5.25)? In other words, how are the emergent low-energy time reparametrization and gauge symmetries broken by the low-T thermal state?

We first consider the simplest case with particle-hole symmetry at $T = 0$, when we can schematically represent the large-N solutions in Sec. V.A as

$$G_c(\tau_1 - \tau_2) \sim (\tau_1 - \tau_2)^{-1/2},$$

$$\Sigma_c(\tau_1 - \tau_2) \sim (\tau_1 - \tau_2)^{-3/2}.$$

The saddle point will be invariant under a reparametrization $f(\tau)$ when choosing $G(\tau_1, \tau_2) = G_c(\tau_1 - \tau_2)$ leads to a transformed $\tilde{G}(\sigma_1, \sigma_2) = G_c(\sigma_1 - \sigma_2)$ (and a similar process for Σ). It turns out that this is true only for the SL(2, R) transformations under which

$$f(\tau) = \frac{a\tau + b}{c\tau + d}, \qquad ad - bc = 1. \tag{B1}$$

Therefore, the approximate reparametrization symmetry is spontaneously broken down to SL(2, R) by the saddle point.

We now consider the most general case with $T > 0$ and no particle-hole symmetry. We write Eq. (A2c) as

$$G(\tau_1, \tau_2) = [f'(\tau_1)f'(\tau_2)]^{1/4}$$
$$\times G_c[f(\tau_1) - f(\tau_2)]e^{i\phi(\tau_1) - i\phi(\tau_2)}, \tag{B2}$$

where $G_c(\tau)$ is the conformal saddle-point solution given in Eq. (5.25). Here we have parametrized $g(\tau) = e^{-i\phi(\tau)}$ in terms of a phase field ϕ; we soon see that the derivative of ϕ is conjugate to density fluctuations.

It can now be checked that the $G(\tau_1, \tau_2)$ obtained from Eq. (B2) equals $G_c(\tau_1 - \tau_2)$ only if the transformations $f(\tau)$ and $\phi(\tau)$ satisfy

$$\frac{\tan[\pi T f(\tau)]}{\pi T} = \frac{a[\tan(\pi T\tau)/\pi T] + b}{c[\tan(\pi T\tau)/\pi T] + d}, \qquad ad - bc = 1,$$
$$-i\phi(\tau) = -i\phi_0 + 2\pi\mathcal{E}T[\tau - f(\tau)]. \tag{B3}$$

The transformation of $f(\tau)$ looks mysterious, but we can simplify it. We define

$$z = e^{2\pi i T\tau}, \qquad z_f = e^{2\pi i T f(\tau)} \tag{B4}$$

and the transformation in Eq. (B3) is then between unimodular complex numbers representing the thermal circle

$$z_f = \frac{w_1 z + w_2}{w_2^* z + w_1^*}, \qquad |w_1|^2 - |w_2|^2 = 1, \tag{B5}$$

where $w_{1,2}$ are complex numbers. In this form, we have an SU(1, 1) transformation, a group that is isomorphic to SL(2, R).

The symmetries in Eqs. (B3) and (B5) are crucial to determining the structure of the low-energy action for fluctuations.

APPENDIX C: SYMMETRIES OF AdS$_2$

This appendix notes that the AdS$_2$ metric

$$ds^2 = \frac{d\tau^2 + d\zeta^2}{\zeta^2} \qquad \text{(C1)}$$

is invariant under isometries that are $\mathrm{SL}(2,\mathrm{R})$ transformations, as in Eq. (B1). It is easy to verify that the coordinate change

$$\tau' + i\zeta' = \frac{a(\tau + i\zeta) + b}{c(\tau + i\zeta) + d}, \qquad ad - bc = 1, \qquad \text{(C2)}$$

with a, b, c, and d real, leaves the metric (C1) invariant.

APPENDIX D: SCHWARZIAN DETERMINANT

This appendix evaluates a quadratic fluctuation correction to the free energy of the SYK model in Eq. (5.76) arising from the time reparametrization mode in Eq. (5.74). The formal expression for this correction is

$$\mathcal{I} = \frac{1}{2} \sum_{n \neq 0, \pm 1} \ln\left[2\pi^2 N\gamma T n^2(n^2 - 1)\right]. \qquad \text{(D1)}$$

Equation (D1) is divergent, and we have to regulate it by finding the proper measure over the path integral of the ϵ_n in Eq. (5.74) (Maldacena, Stanford, and Yang, 2016; Stanford and Witten, 2017). For simplicity, we consider only the particle-hole symmetric case $\mu = 0$ in the forthcoming discussion, but the final result is more general.

We regulate the divergence in Eq. (D1) by returning to the original G-Σ path integral in Eq. (5.56), to which the Schwarzian path integral in Eq. (5.73) is a low-energy approximation. The saddle-point equations (5.56) are simply the original SYK equations (5.2a) and (5.2b). Denoting the exact saddle-point solution of the latter as $\bar{G}$ and $\bar{\Sigma}$, we can write the fluctuations as

$$G = \bar{G} + \delta G, \qquad \Sigma = \bar{\Sigma} + \delta\Sigma. \qquad \text{(D2)}$$

We then expand the action in Eq. (5.56) to quadratic order and find that the needed eigenmodes of the quadratic fluctuations are eigenmodes of the kernels (Gu *et al.*, 2020; Tikhanovskaya *et al.*, 2021a) that generalize the action in Eq. (5.48) as

$$K_{\mathrm{A/S}}(\tau_1, \tau_2; \tau_3, \tau_4)$$
$$= -\left[\frac{q}{2} \pm \left(\frac{q}{2} - 1\right)\right] U^2 \bar{G}(\tau_{13})\bar{G}(\tau_{24})\bar{G}(\tau_{34})^{q-2}. \qquad \text{(D3)}$$

We are considering the general case of SYK model with q fermion terms and $\tau_{ij} \equiv \tau_i - \tau_j$. The eigenmodes are defined by the following equations [which generalize Eq. (5.47)]:

$$k_{\mathrm{A/S}}(h) v_h^{\mathrm{A/S}}(\tau_1, \tau_2, \tau_0)$$
$$= \int d\tau_3 d\tau_4 K_{\mathrm{A/S}}(\tau_1, \tau_2; \tau_3, \tau_4) v_h^{\mathrm{A/S}}(\tau_3, \tau_4, \tau_0), \qquad \text{(D4)}$$

with dimensionless eigenvalue $k_{\mathrm{A/S}}(h)$. For $k_{\mathrm{A/S}}(h) = 1$ we obtain the scaling dimension h of composite operators associated with the fermion bilinears in the conformal limit theory. Our overall task is to expand δG and $\delta\Sigma$ in terms of the eigenmodes of $K_{A/S}$, each of which will also be eigenmodes of the quadratic fluctuation of the action in Eq. (5.56).

The Schwarzian fluctuation focuses on a specific eigenmode v_2^A, which is associated with time reparametrization symmetry. The infinitesimal version of the time reparametrizaton in Eq. (B2), using Eq. (5.68), is

$$\delta G(\tau_1, \tau_2) = [\Delta\epsilon'(\tau_1) + \Delta\epsilon'(\tau_2) + \epsilon(\tau_1)\partial_{\tau_1}$$
$$+ \epsilon(\tau_2)\partial_{\tau_2}]\bar{G}(\tau_1 - \tau_2). \qquad \text{(D5)}$$

For the conformal limit result $\bar{G} = G_c$ in Eq. (5.25), and also for the conformal Green's functions in Eq. (D3), δG in Eq. (D5) is indeed an eigenmode v_2^A of Eq. (D4) with $k_A(2) = 1$, as can be verified by explicit evaluation.

We now have all the ingredients necessary to expand the time reparametrization eigenmode of K_A in terms of the eigenmodes ϵ_n in Eq. (5.74). One needed technical step is that we multiply the K_A eigenmode by $G_c^{(q-2)/2}$ to make the kernel in Eq. (D3) a Hermitian operator. We then write

$$[G_c(\tau_1, \tau_2)]^{(q-2)/2}\delta G(\tau_1, \tau_2)$$
$$= \sum_n \epsilon_n f_n(2\pi T[\tau_1 - \tau_2])e^{-i\pi n T(\tau_1 + \tau_2)}. \qquad \text{(D6)}$$

We can easily obtain the explicit form of the coefficients $f_n(\theta)$ in Eq. (D6) as follows using Eqs. (5.25), (5.74), and (D5):

$$f_n(\theta) = \frac{\sin(n\theta/2)\cos(\theta/2)}{\sin^2(\theta/2)} - n\frac{\cos(n\theta/2)}{\sin(\theta/2)}. \qquad \text{(D7)}$$

Recall that we are working at $\mu = \mathcal{E} = 0$, and we have dropped an unimportant n-independent prefactor in Eq. (D7). The functions $f_n(\theta)$ are analogs for $\mathrm{SL}(2,\mathrm{R})$ of the Legendre polynomials for $\mathrm{SO}(3)$. As expected, they vanish identically for $n = 0, \pm 1$ because G_c is invariant under $\mathrm{SL}(2,\mathrm{R})$ transformations. The property that we need here is the n dependence of their normalization,

$$\int_0^{2\pi} \frac{d\theta}{2\pi}[f_n(\theta)]^2 = \frac{|n|(n^2 - 1)}{3}. \qquad \text{(D8)}$$

When one uses the eigenmodes of Eq. (D3), the Gaussian fluctuation contribution to the free energy from the G-Σ path integral in Eq. (5.56) can be written schematically as (Maldacena, Stanford, and Yang, 2016)

$$\mathcal{I}_{G\text{-}\Sigma} = \frac{1}{2} \sum \ln\left(\frac{1}{k_{A/S}(h)} - 1\right). \qquad \text{(D9)}$$

We now compare this G-Σ form of the fluctuation contribution to the ϵ_n fluctuation contribution in Eq. (D1). Given the transformation between the eigenmodes in Eq. (D6) and the normalization in Eq. (D8), we conclude that the $n^2(n^2 - 1)$ factor in Eq. (D1) should be identified with the product of an

$|n|(n^2-1)$ factor from Eq. (D8) and a $1 - k_A(2) \sim T|n|/U$ factor. The deviation of $k_A(2)$ from unity arises from conformal corrections to the saddle point $\bar{G} - G_c$, and arguments have been made (Maldacena, Stanford, and Yang, 2016) for their $|n|$ dependence.

With this corrected measure for ϵ_n fluctuations, we conclude that the properly regulated form of Eq. (D1) is that deduced from Eq. (D9) (Maldacena, Stanford, and Yang, 2016),

$$\tilde{\mathcal{I}} = \frac{1}{2} \sum_{\substack{|n| \neq 0, \pm 1}}^{|n| < c_1 U/T} \ln\left(\frac{T|n|}{U}\right), \qquad (D10)$$

where we have dropped T-independent constants and c_1 is a nonuniversal number determining the high-energy cutoff. We can now apply the ζ function theory result

$$\sum_{n=1}^{m} \ln(an) = m \ln(am) - m + \frac{\ln(2\pi m)}{2} + \mathcal{O}\left(\frac{1}{m}\right) \qquad (D11)$$

to Eq. (D10), and we obtain Eq. (5.77). Note that the $3/2$ coefficient of the logarithm in Eq. (5.77) is independent of c_1; it is the sum of the $1/2$ coefficient in Eq. (D11) and the omitted $n = \pm 1$ contributions in Eq. (D10).

APPENDIX E: GENERALIZATION TO THE SYK$_q$ MODEL

Much of our discussion of the SYK model has focused on the physically motivated problem with four-fermion interactions. However, the model can be readily generalized to $q \geq 4$ fermion interactions (Gross and Rosenhaus, 2017), otherwise referred to as the SYK$_q$ model. We review here the low-energy properties of a local SYK$_q$ model and the effect of perturbing it by a quadratic hopping term. The interaction Hamiltonian for electrons occupying orbitals labeled $i_\ell = 1, \ldots, N$ is given by

$$H_q = \frac{(q/2)!}{N^{(q-1)/2}} \sum_{\{i_\ell\}} U_{i_1 i_2 \ldots i_q} [c_{i_1}^\dagger c_{i_2}^\dagger \cdots c_{i_{q/2}}^\dagger c_{i_{q/2+1}} \cdots c_{i_{q-1}} c_{i_q}]$$
$$- \mu \sum_{i_\ell} c_{i_\ell}^\dagger c_{i_\ell}, \qquad (E1)$$

where as before we choose the couplings $U_{i_1 i_2 \ldots i_q}$ to be independent random variables with $\overline{U_{i_1 i_2 \ldots i_q}} = 0$ and $\overline{(U_{i_1 i_2 \ldots i_q})^2} = U^2$. The density $\mathcal{Q}$ can be tuned by an external chemical potential μ.

In the large-N limit, once again only the melon graphs survive, but the number of internal legs is now $q - 1$. The on-site Green's function reduces to the solution of the following equations:

$$G(i\omega_n) = \frac{1}{i\omega_n + \mu - \Sigma(i\omega_n)}, \qquad (E2a)$$

$$\Sigma(\tau) = -U^2 [G(\tau)]^{q/2} [G(-\tau)]^{q/2-1}, \qquad (E2b)$$

$$G(\tau = 0^-) = \mathcal{Q}. \qquad (E2c)$$

Following the analysis in Sec. V.A, we can obtain the low-energy solution at $T = 0$ for the electron Green's function. The power-law singularity at low frequencies is now determined by the dimension $\Delta = 1/q$ such that the Green's function has the form

$$G(\tau) \sim \frac{\text{sgn}(\tau)}{(U|\tau|)^{2/q}}, \qquad |\tau| \gg 1/U, \qquad (E3a)$$

$$G(i\omega) \sim \frac{i\,\text{sgn}(\omega)}{U^{2/q}|\omega|^{1-2/q}}, \qquad |\omega| \ll U. \qquad (E3b)$$

For simplicity, we chose the density to be at half filling, where the spectral asymmetry vanishes. In spite of the different scaling dimensions, the finite compressibility and residual entropy (including the T-linear correction) have the same qualitative behavior as the model with $q = 4$. Generalizations to two-band models involving distinct q-body interactions have also been studied (Haldar and Shenoy, 2018).

We now consider a lattice generalization of the model similar to that in Sec. X, where the local interaction at every site is given by H_q and the sites are coupled together via uniform translationally invariant hopping terms H_{kin}; see Eq. (10.1a). The hopping term is a relevant perturbation, and the gapless scale invariant solutions cannot survive down to the lowest energies. Starting with the decoupled limit, one finds that the coherence scale is given by

$$W_q^* \sim t \left(\frac{t}{U}\right)^{2/(q-2)}, \qquad (E4)$$

below which the hopping terms can no longer be treated perturbatively and the ground state is a Fermi liquid. In spite of the similarities in the thermodynamic properties with the $q = 4$ model, charge transport is dramatically different for $T \gg W_q^*$. The electrical resistivity in the incoherent regime is now given by

$$\rho_{\text{dc}} \sim \frac{h}{Ne^2} \left(\frac{T}{W_q^*}\right)^{2-4/q}. \qquad (E5)$$

For $q \neq 4$ the resistivity scales faster than T (but slower than T^2) with increasing temperature. The T linearity of the resistivity is tied to the electron scaling dimension of $\Delta = 1/4$ for $q = 4$.

REFERENCES

Abanov, Artem, and Andrey V. Chubukov, 2020, "Interplay between superconductivity and non-Fermi liquid at a quantum critical point in a metal. I. The γ model and its phase diagram at $T = 0$: The case $0 < \gamma < 1$," Phys. Rev. B **102**, 024524.

Abrahams, Elihu, P. W. Anderson, P. A. Lee, and T. V. Ramakrishnan, 1981, "Quasiparticle lifetime in disordered two-dimensional metals," Phys. Rev. B **24**, 6783–6789.

Abrikosov, A. A., L. P. Gorkov, and I. E. Dzyaloshinskii, 1963, *Methods of Quantum Field Theory in Statistical Physics* (Prentice-Hall, Englewood Cliffs, NJ).

Afkhami-Jeddi, Nima, Henry Cohn, Thomas Hartman, and Amirhossein Tajdini, 2020, "Free partition functions and an averaged holographic duality," arXiv:2006.04839.

Aharony, Ofer, Oren Bergman, Daniel Louis Jafferis, and Juan Maldacena, **2008**, "$N = 6$ superconformal Chern-Simons-matter theories, M2-branes and their gravity duals," J. High Energy Phys. 10, 091.

Aldape, Erik E., Taylor Cookmeyer, Aavishkar A. Patel, and Ehud Altman, 2020, "Solvable theory of a strange metal at the breakdown of a heavy Fermi liquid," arXiv:2012.00763.

Alhassid, Y., 2000, "The statistical theory of quantum dots," Rev. Mod. Phys. 72, 895–968.

Allen, P. B., H. Berger, O. Chauvet, L. Forro, T. Jarlborg, A. Junod, B. Revaz, and G. Santi, 1996, "Transport properties, thermodynamic properties, and electronic structure of $SrRuO_3$," Phys. Rev. B 53, 4393–4398.

Almheiri, Ahmed, Thomas Hartman, Juan Maldacena, Edgar Shaghoulian, and Amirhossein Tajdini, **2020**, "Replica wormholes and the entropy of Hawking radiation," J. High Energy Phys. 05, 013.

Almheiri, Ahmed, Thomas Hartman, Juan Maldacena, Edgar Shaghoulian, and Amirhossein Tajdini, 2021, "The entropy of Hawking radiation," Rev. Mod. Phys. 93, 035002.

Almheiri, Ahmed, Alexey Milekhin, and Brian Swingle, 2019, "Universal constraints on energy flow and SYK thermalization," arXiv:1912.04912.

Almheiri, Ahmed, and Joseph Polchinski, **2015**, "Models of AdS_2 backreaction and holography," J. High Energy Phys. 11, 014.

Altland, Alexander, and Dmitry Bagrets, 2018, "Quantum ergodicity in the SYK model," Nucl. Phys. B930, 45–68.

Altland, Alexander, Dmitry Bagrets, and Alex Kamenev, 2019a, "Quantum Criticality of Granular Sachdev-Ye-Kitaev Matter," Phys. Rev. Lett. 123, 106601.

Altland, Alexander, Dmitry Bagrets, and Alex Kamenev, 2019b, "Sachdev-Ye-Kitaev Non-Fermi-Liquid Correlations in Nanoscopic Quantum Transport," Phys. Rev. Lett. 123, 226801.

Altland, Alexander, Dmitry Bagrets, Pranjal Nayak, Julian Sonner, and Manuel Vielma, 2021, "From operator statistics to wormholes," Phys. Rev. Research 3, 033259.

Altshuler, B. L., L. B. Ioffe, and A. J. Millis, 1994, "Low-energy properties of fermions with singular interactions," Phys. Rev. B 50, 14048–14064.

Altshuler, B. L., and B. I. Shklovskii, 1986, "Repulsion of energy levels and conductivity of small metal samples," Sov. Phys. JETP 64, 127–135, http://www.jetp.ras.ru/cgi-bin/e/index/e/64/1/p127?a=list.

Anantharaman, Nalini, and Fabricio Macia, 2011, "The dynamics of the Schrödinger flow from the point of view of semiclassical measures," arXiv:1102.0970.

Anderson, Rhys, Fudong Wang, Peihang Xu, Vijin Venu, Stefan Trotzky, Frédéric Chevy, and Joseph H. Thywissen, 2019, "Conductivity Spectrum of Ultracold Atoms in an Optical Lattice," Phys. Rev. Lett. 122, 153602.

Andrei, N., and P. Coleman, 1989, "Cooper Instability in the Presence of a Spin Liquid," Phys. Rev. Lett. 62, 595–598.

Aronson, M. C., R. Osborn, R. A. Robinson, J. W. Lynn, R. Chau, C. L. Seaman, and M. B. Maple, 1995, "Non-Fermi-Liquid Scaling of the Magnetic Response in $UCu_{5-x}Pd_x$ ($x = 1, 1.5$)," Phys. Rev. Lett. 75, 725–728.

Arrachea, Liliana, and Marcelo J. Rozenberg, 2002, "Infinite-range quantum random Heisenberg magnet," Phys. Rev. B 65, 224430.

Azeyanagi, Tatsuo, Frank Ferrari, and Fidel I. Schaposnik Massolo, 2018, "Phase Diagram of Planar Matrix Quantum Mechanics, Tensor, and Sachdev-Ye-Kitaev Models," Phys. Rev. Lett. 120, 061602.

Bagrets, Dmitry, Alexander Altland, and Alex Kamenev, 2016, "Sachdev-Ye-Kitaev model as Liouville quantum mechanics," Nucl. Phys. B911, 191–205.

Bagrets, Dmitry, Alexander Altland, and Alex Kamenev, 2017, "Power-law out of time order correlation functions in the SYK model," Nucl. Phys. B921, 727–752.

Bandyopadhyay, Soumik, Philipp Uhrich, Alessio Paviglianiti, and Philipp Hauke, 2021, "Universal equilibration dynamics of the Sachdev-Ye-Kitaev model," arXiv:2108.01718.

Baraduc, Claire, Abdellatif Azrak, and Nicole Bontemps, 1996, "Infrared conductivity in the normal state of cuprate thin films," J. Supercond. 9, 3–6.

Basov, D. N., Richard D. Averitt, Dirk van der Marel, Martin Dressel, and Kristjan Haule, 2011, "Electrodynamics of correlated electron materials," Rev. Mod. Phys. 83, 471–541.

Beccaria, Matteo, Simone Giombi, and Arkady A. Tseytlin, 2022, "Wilson loop in general representation and RG flow in 1D defect QFT," arXiv:2202.00028.

Ben-Zion, Daniel, and John McGreevy, 2018, "Strange metal from local quantum chaos," Phys. Rev. B 97, 155117.

Berg, Erez, Samuel Lederer, Yoni Schattner, and Simon Trebst, 2019, "Monte Carlo studies of quantum critical metals," Annu. Rev. Condens. Matter Phys. 10, 63–84.

Bhattacharya, Ritabrata, Dileep P. Jatkar, and Nilakash Sorokhaibam, **2019**, "Quantum quenches and thermalization in SYK models," J. High Energy Phys. 07, 66.

Bi, Zhen, Chao-Ming Jian, Yi-Zhuang You, Kelly Ann Pawlak, and Cenke Xu, 2017, "Instability of the non-Fermi-liquid state of the Sachdev-Ye-Kitaev model," Phys. Rev. B 95, 205105.

Biroli, Giulio, and Olivier Parcollet, 2002, "Out-of-equilibrium dynamics of a quantum Heisenberg spin glass," Phys. Rev. B 65, 094414.

Blake, Mike, 2016, "Universal Charge Diffusion and the Butterfly Effect in Holographic Theories," Phys. Rev. Lett. 117, 091601.

Blake, Mike, Richard A. Davison, and Subir Sachdev, 2017, "Thermal diffusivity and chaos in metals without quasiparticles," Phys. Rev. D 96, 106008.

Blake, Mike, Hyunseok Lee, and Hong Liu, **2018**, "A quantum hydrodynamical description for scrambling and many-body chaos," J. High Energy Phys. 10, 127.

Blake, Mike, and Hong Liu, 2021, "On systems of maximal quantum chaos," J. High Energy Phys. 05, 229.

Bloch, Felix, 1929, "On the quantum mechanics of electrons in crystal lattices," Z. Phys. 52, 555–600.

Bohigas, O., and J. Flores, 1971, "Two-body random Hamiltonian and level density," Phys. Lett. 34B, 261–263.

Bohigas, O., M. J. Giannoni, and C. Schmit, 1984, "Characterization of Chaotic Quantum Spectra and Universality of Level Fluctuation Laws," Phys. Rev. Lett. 52, 1–4.

Bohrdt, A., C. B. Mendl, M. Endres, and M. Knap, 2017, "Scrambling and thermalization in a diffusive quantum many-body system," New J. Phys. 19, 063001.

Boltzmann, Ludwig, 1872, "Further studies about the heat balance among gas molecules," Wien. Ber. 66, 275–370.

Bonderson, Parsa, Meng Cheng, Kaushal Patel, and Eugeniu Plamadeala, 2016, "Topological enrichment of Luttinger's theorem," arXiv:1601.07902.

Boruch, Jan, Matthew T. Heydeman, Luca V. Iliesiu, and Gustavo J. Turiaci, 2022, "BPS and near-BPS black holes in AdS_5 and their spectrum in $\mathcal{N} = 4$ SYM," arXiv:2203.01331.

Bousso, Raphael, Xi Dong, Netta Engelhardt, Thomas Faulkner, Thomas Hartman, Stephen H. Shenker, and Douglas Stanford, 2022, "Snowmass white paper: Quantum aspects of black holes and the emergence of spacetime," arXiv:2201.03096.

Bozovic, I., D. Kirillov, A. Kapitulnik, K. Char, M. R. Hahn, M. R. Beasley, T. H. Geballe, Y. H. Kim, and A. J. Heeger, 1987, "Optical Measurements on Oriented Thin $YBa_2Cu_3O_{7-\delta}$ Films: Lack of Evidence for Excitonic Superconductivity," Phys. Rev. Lett. **59**, 2219–2221.

Bray, A. J., and M. A. Moore, 1980, "Replica theory of quantum spin glasses," J. Phys. C **13**, L655–L660.

Brinkman, W. F., and T. M. Rice, 1970, "Application of Gutzwiller's variational method to the metal-insulator transition," Phys. Rev. B **2**, 4302–4304.

Brody, T. A., J. Flores, J. B. French, P. A. Mello, A. Pandey, and S. S. M. Wong, 1981, "Random-matrix physics: Spectrum and strength fluctuations," Rev. Mod. Phys. **53**, 385–479.

Broholm, C., R. J. Cava, S. A. Kivelson, D. G. Nocera, M. R. Norman, and T. Senthil, 2020, "Quantum spin liquids," Science **367**, 263.

Brown, Peter T., *et al.*, 2019, "Bad metallic transport in a cold atom Fermi-Hubbard system," Science **363**, 379–382.

Brühwiler, M., B. Batlogg, S. M. Kazakov, Ch. Niedermayer, and J. Karpinski, 2006, "Na_xCoO_2: Enhanced low-energy excitations of electrons on a 2D triangular lattice," Physica (Amsterdam) **378B–380B**, 630–631.

Bruin, J. A. N., H. Sakai, R. S. Perry, and A. P. Mackenzie, 2013, "Similarity of scattering rates in metals showing T-linear resistivity," Science **339**, 804–807.

Burdin, S., A. Georges, and D. R. Grempel, 2000, "Coherence Scale of the Kondo Lattice," Phys. Rev. Lett. **85**, 1048–1051.

Burdin, S., D. R. Grempel, and A. Georges, 2002, "Heavy-fermion and spin-liquid behavior in a Kondo lattice with magnetic frustration," Phys. Rev. B **66**, 045111.

Cai, Ang, Zuodong Yu, Haoyu Hu, Stefan Kirchner, and Qimiao Si, 2020, "Dynamical Scaling of Charge and Spin Responses at a Kondo Destruction Quantum Critical Point," Phys. Rev. Lett. **124**, 027205.

Cao, Yuan, Debanjan Chowdhury, Daniel Rodan-Legrain, Oriol Rubies-Bigorda, Kenji Watanabe, Takashi Taniguchi, T. Senthil, and Pablo Jarillo-Herrero, 2020, "Strange Metal in Magic-Angle Graphene with Near Planckian Dissipation," Phys. Rev. Lett. **124**, 076801.

Carullo, Gregorio, Danny Laghi, John Veitch, and Walter Del Pozzo, 2021, "Bekenstein-Hod Universal Bound on Information Emission Rate Is Obeyed by LIGO-Virgo Binary Black Hole Remnants," Phys. Rev. Lett. **126**, 161102.

Cha, Peter, Aavishkar A. Patel, Emanuel Gull, and Eun-Ah Kim, 2020, "Slope invariant T-linear resistivity from local self-energy," Phys. Rev. Research **2**, 033434.

Cha, Peter, Nils Wentzell, Olivier Parcollet, Antoine Georges, and Eun-Ah Kim, 2020, "Linear resistivity and Sachdev-Ye-Kitaev (SYK) spin liquid behavior in a quantum critical metal with spin-1/2 fermions," Proc. Natl. Acad. Sci. U.S.A. **117**, 18341–18346.

Chamblin, Andrew, Roberto Emparan, Clifford V. Johnson, and Robert C. Myers, 1999, "Charged AdS black holes and catastrophic holography," Phys. Rev. D **60**, 064018.

Cheipesh, Y., A. I. Pavlov, V. Ohanesjan, K. Schalm, and N. V. Gnezdilov, 2021, "Quantum tunneling dynamics in a complex-valued Sachdev-Ye-Kitaev model quench-coupled to a cool bath," Phys. Rev. B **104**, 115134.

Chen, Anffany, R. Ilan, F. de Juan, D. I. Pikulin, and M. Franz, 2018, "Quantum Holography in a Graphene Flake with an Irregular Boundary," Phys. Rev. Lett. **121**, 036403.

Chen, Bowen, Bartlomiej Czech, and Zi-zhi Wang, 2021, "Quantum information in holographic duality," arXiv:2108.09188.

Chen, Yiming, Xiao-Liang Qi, and Pengfei Zhang, **2020**, "Replica wormhole and information retrieval in the SYK model coupled to Majorana chains," J. High Energy Phys. 06, 121.

Chew, Aaron, Andrew Essin, and Jason Alicea, 2017, "Approximating the Sachdev-Ye-Kitaev model with Majorana wires," Phys. Rev. B **96**, 121119.

Chitra, R., and G. Kotliar, 2000, "Effect of Long Range Coulomb Interactions on the Mott Transition," Phys. Rev. Lett. **84**, 3678–3681.

Chowdhury, Debanjan, and Erez Berg, 2020a, "Intrinsic superconducting instabilities of a solvable model for an incoherent metal," Phys. Rev. Research **2**, 013301.

Chowdhury, Debanjan, and Erez Berg, 2020b, "The unreasonable effectiveness of Eliashberg theory for pairing of non-Fermi liquids," Ann. Phys. (N.Y.) **417**, 168125.

Chowdhury, Debanjan, Inti Sodemann, and T. Senthil, 2018, "Mixed-valence insulators with neutral Fermi surfaces," Nat. Commun. **9**, 1766.

Chowdhury, Debanjan, and Brian Swingle, 2017, "Onset of many-body chaos in the $O(N)$ model," Phys. Rev. D **96**, 065005.

Chowdhury, Debanjan, Yochai Werman, Erez Berg, and T. Senthil, 2018, "Translationally Invariant Non-Fermi-Liquid Metals with Critical Fermi Surfaces: Solvable Models," Phys. Rev. X **8**, 031024.

Christos, Maine, Felix M. Haehl, and Subir Sachdev, 2022, "Spin liquid to spin glass crossover in the random quantum Heisenberg magnet," Phys. Rev. B **105**, 085120.

Christos, Maine, Darshan G. Joshi, Subir Sachdev, and Maria Tikhanovskaya, 2022, "Critical metallic phase in the overdoped random t-J model," Proc. Natl. Acad. Sci. U.S.A. **119**, e2206921119.

Chubukov, A. V., and A. Abanov, 2021, "Pairing by a dynamical interaction in a metal," J. Exp. Theor. Phys. **132**, 606–617.

Chubukov, Andrey V., and Dmitrii L. Maslov, 2017, "Optical conductivity of a two-dimensional metal near a quantum critical point: The status of the extended Drude formula," Phys. Rev. B **96**, 205136.

Classen, Laura, and Andrey Chubukov, 2021, "Superconductivity of incoherent electrons in the Yukawa Sachdev-Ye-Kitaev model," Phys. Rev. B **104**, 125120.

Cohen, Guy, Emanuel Gull, David R. Reichman, and Andrew J. Millis, 2015, "Taming the Dynamical Sign Problem in Real-Time Evolution of Quantum Many-Body Problems," Phys. Rev. Lett. **115**, 266802.

Coleman, P., J. B. Marston, and A. J. Schofield, 2005, "Transport anomalies in a simplified model for a heavy-electron quantum critical point," Phys. Rev. B **72**, 245111.

Coleman, P., I. Paul, and J. Rech, 2005, "Sum rules and Ward identities in the Kondo lattice," Phys. Rev. B **72**, 094430.

Coleman, P., C. Pépin, Qimiao Si, and R. Ramazashvili, 2001, "How do Fermi liquids get heavy and die?," J. Phys. Condens. Matter **13**, R723.

Collignon, Clément, Phillipe Bourges, Benoît Fauqué, and Kamran Behnia, 2020, "Heavy Nondegenerate Electrons in Doped Strontium Titanate," Phys. Rev. X **10**, 031025.

Collignon, Clément, Xiao Lin, Carl Willem Rischau, Benoît Fauqué, and Kamran Behnia, 2019, "Metallicity and superconductivity in doped strontium titanate," Annu. Rev. Condens. Matter Phys. **10**, 25–44.

Cotler, Jordan, and Kristan Jensen, 2021, "AdS$_3$ gravity and random CFT," J. High Energy Phys. 04, 033.

Cotler, Jordan S., Guy Gur-Ari, Masanori Hanada, Joseph Polchinski, Phil Saad, Stephen H. Shenker, Douglas Stanford, Alexandre Streicher, and Masaki Tezuka, 2017, "Black holes and random matrices," J. High Energy Phys. 05, 118.

Cubrovic, Mihailo, Jan Zaanen, and Koenraad Schalm, 2009, "String theory, quantum phase transitions and the emergent Fermi liquid," Science 325, 439–444.

Cubrovic, Mihailo, Jan Zaanen, and Koenraad Schalm, 2011, "Constructing the AdS dual of a Fermi liquid: AdS black holes with Dirac hair," J. High Energy Phys. 10, 017.

Cugliandolo, Leticia F., D. R. Grempel, and Constantino A. da Silva Santos, 2001, "Imaginary-time replica formalism study of a quantum spherical p-spin-glass model," Phys. Rev. B 64, 014403.

Cuomo, Gabriel, Zohar Komargodski, Márk Mezei, and Avia Raviv-Moshe, 2022, "Spin impurities, Wilson lines and semiclassics," arXiv:2202.00040.

Custers, J., P. Gegenwart, C. Geibel, F. Steglich, P. Coleman, and S. Paschen, 2010, "Evidence for a Non-Fermi-Liquid Phase in Ge-Substituted YbRh$_2$Si$_2$," Phys. Rev. Lett. 104, 186402.

Custers, J., P. Gegenwart, H. Wilhelm, K. Neumaier, Y. Tokiwa, O. Trovarelli, C. Geibel, F. Steglich, C. Pépin, and P. Coleman, 2003, "The break-up of heavy electrons at a quantum critical point," Nature (London) 424, 524–527.

Damascelli, Andrea, Zahid Hussain, and Zhi-Xun Shen, 2003, "Angle-resolved photoemission studies of the cuprate superconductors," Rev. Mod. Phys. 75, 473–541.

Damia, Jeremias Aguilera, Shamit Kachru, Srinivas Raghu, and Gonzalo Torroba, 2019, "Two-Dimensional Non-Fermi-Liquid Metals: A Solvable Large-N Limit," Phys. Rev. Lett. 123, 096402.

Danshita, Ippei, Masanori Hanada, and Masaki Tezuka, 2017, "Creating and probing the Sachdev-Ye-Kitaev model with ultracold gases: Towards experimental studies of quantum gravity," Prog. Theor. Exp. Phys. 083I01.

Darius Shi, Zhengyan, Hart Goldman, Dominic V. Else, and T. Senthil, 2022, "Gifts from anomalies: Exact results for Landau phase transitions in metals," arXiv:2204.07585.

Datta, Shouvik, Sarthak Duary, Per Kraus, Pronobesh Maity, and Alexander Maloney, 2022, "Adding flavor to the Narain ensemble," J. High Energy Phys. 05, 090.

Davison, Richard A., Wenbo Fu, Antoine Georges, Yingfei Gu, Kristan Jensen, and Subir Sachdev, 2017, "Thermoelectric transport in disordered metals without quasiparticles: The Sachdev-Ye-Kitaev models and holography," Phys. Rev. B 95, 155131.

Deng, Xiaoyu, Jernej Mravlje, Rok Žitko, Michel Ferrero, Gabriel Kotliar, and Antoine Georges, 2013, "How Bad Metals Turn Good: Spectroscopic Signatures of Resilient Quasiparticles," Phys. Rev. Lett. 110, 086401.

Deng, Xiaoyu, Aaron Sternbach, Kristjan Haule, D. N. Basov, and Gabriel Kotliar, 2014, "Shining Light on Transition-Metal Oxides: Unveiling the Hidden Fermi Liquid," Phys. Rev. Lett. 113, 246404.

Dhar, Avinash, Adwait Gaikwad, Lata Kh. Joshi, Gautam Mandal, and Spenta R. Wadia, 2019, "Gravitational collapse in SYK models and Choptuik-like phenomenon," J. High Energy Phys. 11, 067.

Dobrosavljević, V., and G. Kotliar, 1997, "Mean Field Theory of the Mott-Anderson Transition," Phys. Rev. Lett. 78, 3943–3946.

Dodge, J. S., C. P. Weber, J. Corson, J. Orenstein, Z. Schlesinger, J. W. Reiner, and M. R. Beasley, 2000, "Low-Frequency Crossover of the Fractional Power-Law Conductivity in SrRuO$_3$," Phys. Rev. Lett. 85, 4932–4935.

Doiron-Leyraud, Nicolas, Cyril Proust, David LeBoeuf, Julien Levallois, Jean-Baptiste Bonnemaison, Ruixing Liang, D. A. Bonn, W. N. Hardy, and Louis Taillefer, 2007, "Quantum oscillations and the Fermi surface in an underdoped high-T_c superconductor," Nature (London) 447, 565–568.

Dray, Tevian, and Gerard 't Hooft, 1985, "The gravitational shock wave of a massless particle," Nucl. Phys. B253, 173–188.

Dumitrescu, Philipp T., Nils Wentzell, Antoine Georges, and Olivier Parcollet, 2022, "Planckian metal at a doping-induced quantum critical point," Phys. Rev. B 105, L180404.

Eberlein, Andreas, Valentin Kasper, Subir Sachdev, and Julia Steinberg, 2017, "Quantum quench of the Sachdev-Ye-Kitaev model," Phys. Rev. B 96, 205123.

Eberlein, Andreas, Ipsita Mandal, and Subir Sachdev, 2016, "Hyperscaling violation at the Ising-nematic quantum critical point in two dimensional metals," Phys. Rev. B 94, 045133.

Eberlein, Andreas, Aavishkar A. Patel, and Subir Sachdev, 2017, "Shear viscosity at the Ising-nematic quantum critical point in two dimensional metals," Phys. Rev. B 95, 075127.

El Azrak, A., R. Nahoum, N. Bontemps, M. Guilloux-Viry, C. Thivet, A. Perrin, S. Labdi, Z. Z. Li, and H. Raffy, 1994, "Infrared properties of YBa$_2$Cu$_3$O$_7$ and Bi$_2$Sr$_2$Ca$_{n-1}$Cu$_n$O$_{2n+4}$ thin films," Phys. Rev. B 49, 9846–9856.

Else, Dominic V., and T. Senthil, 2021, "Strange Metals as Ersatz Fermi Liquids," Phys. Rev. Lett. 127, 086601.

Else, Dominic V., Ryan Thorngren, and T. Senthil, 2021, "Non-Fermi Liquids as Ersatz Fermi Liquids: General Constraints on Compressible Metals," Phys. Rev. X 11, 021005.

Emery, V. J., and S. A. Kivelson, 1995, "Superconductivity in Bad Metals," Phys. Rev. Lett. 74, 3253–3256.

Engelhardt, Netta, Sebastian Fischetti, and Alexander Maloney, 2021, "Free energy from replica wormholes," Phys. Rev. D 103, 046021.

Esterlis, Ilya, Haoyu Guo, Aavishkar A. Patel, and Subir Sachdev, 2021, "Large-N theory of critical Fermi surfaces," Phys. Rev. B 103, 235129.

Esterlis, Ilya, and Jörg Schmalian, 2019, "Cooper pairing of incoherent electrons: An electron-phonon version of the Sachdev-Ye-Kitaev model," Phys. Rev. B 100, 115132.

Fang, Yawen, *et al.*, 2022, "Fermi surface transformation at the pseudogap critical point of a cuprate superconductor," Nat. Phys. 18, 558–564.

Faulkner, Thomas, and Nabil Iqbal, 2013, "Friedel oscillations and horizon charge in 1D holographic liquids," J. High Energy Phys. 07, 060.

Faulkner, Thomas, Nabil Iqbal, Hong Liu, John McGreevy, and David Vegh, 2011, "Holographic non-Fermi liquid fixed points," Phil. Trans. R. Soc. A 369, 1640.

Faulkner, Thomas, Hong Liu, John McGreevy, and David Vegh, 2011, "Emergent quantum criticality, Fermi surfaces, and AdS$_2$," Phys. Rev. D 83, 125002.

Fiete, Gregory A., 2007, "Colloquium: The spin-incoherent Luttinger liquid," Rev. Mod. Phys. 79, 801–820.

Fisk, Z., and G. W. Webb, 1976, "Saturation of the High-Temperature Normal-State Electrical Resistivity of Superconductors," Phys. Rev. Lett. 36, 1084–1086.

Fitzpatrick, A. Liam, Shamit Kachru, Jared Kaplan, and S. Raghu, 2013, "Non-Fermi liquid fixed point in a Wilsonian theory of quantum critical metals," Phys. Rev. B 88, 125116.

Fitzpatrick, A. Liam, Shamit Kachru, Jared Kaplan, and S. Raghu, 2014, "Non-Fermi-liquid behavior of large-N_B quantum critical metals," Phys. Rev. B 89, 165114.

Florens, Serge, and Antoine Georges, 2004, "Slave-rotor mean-field theories of strongly correlated systems and the Mott transition in finite dimensions," Phys. Rev. B **70**, 035114.

Florens, Serge, Priyanka Mohan, C. Janani, T. Gupta, and R. Narayanan, 2013, "Magnetic fluctuations near the Mott transition towards a spin liquid state," Europhys. Lett. **103**, 17002.

Frachet, Mehdi, *et al.*, 2020, "Hidden magnetism at the pseudogap critical point of a cuprate superconductor," Nat. Phys. **16**, 1064–1068.

Franz, Marcel, and Moshe Rozali, 2018, "Mimicking black hole event horizons in atomic and solid-state systems," Nat. Rev. Mater. **3**, 491–501.

Fritz, Lars, and Matthias Vojta, 2004, "Phase transitions in the pseudogap Anderson and Kondo models: Critical dimensions, renormalization group, and local-moment criticality," Phys. Rev. B **70**, 214427.

Fu, Wenbo, Davide Gaiotto, Juan Maldacena, and Subir Sachdev, 2017, "Supersymmetric Sachdev-Ye-Kitaev models," Phys. Rev. D **95**, 026009.

Fu, Wenbo, and Subir Sachdev, 2016, "Numerical study of fermion and boson models with infinite-range random interactions," Phys. Rev. B **94**, 035135.

Gaikwad, Adwait, Lata Kh Joshi, Gautam Mandal, and Spenta R. Wadia, **2020**, "Holographic dual to charged SYK from 3D gravity and Chern-Simons," J. High Energy Phys. 02, 033.

Gannon, W. J., L. S. Wu, I. A. Zaliznyak, W. H. Xu, A. M. Tsvelik, Y. Qiu, J. A. Rodriguez-Rivera, and M. C. Aronson, 2018, "Local quantum phase transition in YFe_2Al_{10}," Proc. Natl. Acad. Sci. U.S.A. **115**, 6995–6999.

Gao, Ping, and Daniel Louis Jafferis, **2021**, "A traversable wormhole teleportation protocol in the SYK model," J. High Energy Phys. 07, 097.

García-Álvarez, L., I. L. Egusquiza, L. Lamata, A. del Campo, J. Sonner, and E. Solano, 2017, "Digital Quantum Simulation of Minimal AdS/CFT," Phys. Rev. Lett. **119**, 040501.

García-García, Antonio M., Tomoki Nosaka, Dario Rosa, and Jacobus J. M. Verbaarschot, 2019, "Quantum chaos transition in a two-site Sachdev-Ye-Kitaev model dual to an eternal traversable wormhole," Phys. Rev. D **100**, 026002.

García-García, Antonio M., and Jacobus J. M. Verbaarschot, 2017, "Analytical spectral density of the Sachdev-Ye-Kitaev model at finite N," Phys. Rev. D **96**, 066012.

Georges, Antoine, Gabriel Kotliar, Werner Krauth, and Marcelo J. Rozenberg, 1996, "Dynamical mean-field theory of strongly correlated fermion systems and the limit of infinite dimensions," Rev. Mod. Phys. **68**, 13–125.

Georges, Antoine, and Jernej Mravlje, 2021, "Skewed non-Fermi liquids and the Seebeck effect," arXiv:2102.13224.

Georges, Antoine, Olivier Parcollet, and Subir Sachdev, 2000, "Mean Field Theory of a Quantum Heisenberg Spin Glass," Phys. Rev. Lett. **85**, 840–843.

Georges, Antoine, Olivier Parcollet, and Subir Sachdev, 2001, "Quantum fluctuations of a nearly critical Heisenberg spin glass," Phys. Rev. B **63**, 134406.

Gharibyan, Hrant, Masanori Hanada, Stephen H. Shenker, and Masaki Tezuka, **2018**, "Onset of random matrix behavior in scrambling systems," J. High Energy Phys. 07, 124.

Ghiotto, Augusto, *et al.*, 2021, "Quantum criticality in twisted transition metal dichalcogenides," Nature (London) **597**, 345–349.

Giamarchi, Thierry, 2003, *Quantum Physics in One Dimension*, International Series of Monographs on Physics Vol. 121 (Clarendon Press, Oxford).

Gibbons, G. W., and S. W. Hawking, 1977, "Action integrals and partition functions in quantum gravity," Phys. Rev. D **15**, 2752–2756.

Giraldo-Gallo, P., *et al.*, 2018, "Scale-invariant magnetoresistance in a cuprate superconductor," Science **361**, 479–481.

Glossop, Matthew T., and Kevin Ingersent, 2007, "Magnetic Quantum Phase Transition in an Anisotropic Kondo Lattice," Phys. Rev. Lett. **99**, 227203.

Gnezdilov, N. V., J. A. Hutasoit, and C. W. J. Beenakker, 2018, "Low-high voltage duality in tunneling spectroscopy of the Sachdev-Ye-Kitaev model," Phys. Rev. B **98**, 081413.

Gourgout, A., *et al.*, 2021, "Out-of-plane Seebeck coefficient of the cuprate $La_{1.6-x}Nd_{0.4}Sr_xCuO_4$ across the pseudogap critical point: Particle-hole asymmetry and Fermi surface transformation," arXiv:2106.05959.

Grempel, D. R., and M. J. Rozenberg, 1998, "Fluctuations in a Quantum Random Heisenberg Paramagnet," Phys. Rev. Lett. **80**, 389–392.

Grempel, D. R., and Qimiao Si, 2003, "Locally Critical Point in an Anisotropic Kondo Lattice," Phys. Rev. Lett. **91**, 026401.

Grissonnanche, G., *et al.*, 2021, "Linear-in temperature resistivity from an isotropic Planckian scattering rate," Nature (London) **595**, 667.

Gross, David J., and Vladimir Rosenhaus, **2017**, "A generalization of Sachdev-Ye-Kitaev," J. High Energy Phys. 02, 093.

Grozdanov, Sašo, Koenraad Schalm, and Vincenzo Scopelliti, 2019, "Kinetic theory for classical and quantum many-body chaos," Phys. Rev. E **99**, 012206.

Gu, Yingfei, and Alexei Kitaev, **2019**, "On the relation between the magnitude and exponent of OTOCs," J. High Energy Phys. 02, 075.

Gu, Yingfei, Alexei Kitaev, Subir Sachdev, and Grigory Tarnopolsky, 2020, "Notes on the complex Sachdev-Ye-Kitaev model," J. High Energy Phys. 02, 157.

Gu, Yingfei, Andrew Lucas, and Xiao-Liang Qi, 2017, "Energy diffusion and the butterfly effect in inhomogeneous Sachdev-Ye-Kitaev chains," SciPost Phys. **2**, 018.

Gu, Yingfei, Xiao-Liang Qi, and Douglas Stanford, **2017**, "Local criticality, diffusion and chaos in generalized Sachdev-Ye-Kitaev models," J. High Energy Phys. 05, 125.

Gull, E., P. Werner, O. Parcollet, and M. Troyer, 2008, "Continuous-time auxiliary-field Monte Carlo for quantum impurity models," Europhys. Lett. **82**, 57003.

Gull, Emanuel, Andrew J. Millis, Alexander I. Lichtenstein, Alexey N. Rubtsov, Matthias Troyer, and Philipp Werner, 2011, "Continuous-time Monte Carlo methods for quantum impurity models," Rev. Mod. Phys. **83**, 349–404.

Gunnarsson, O., M. Calandra, and J. E. Han, 2003, "Colloquium: Saturation of electrical resistivity," Rev. Mod. Phys. **75**, 1085–1099.

Guo, Haoyu, Yingfei Gu, and Subir Sachdev, 2019, "Transport and chaos in lattice Sachdev-Ye-Kitaev models," Phys. Rev. B **100**, 045140.

Guo, Haoyu, Yingfei Gu, and Subir Sachdev, 2020, "Linear in temperature resistivity in the limit of zero temperature from the time reparametrization soft mode," Ann. Phys. (N.Y.) **418**, 168202.

Guo, Haoyu, Aavishkar A. Patel, Ilya Esterlis, and Subir Sachdev, 2022, "Large N theory of critical Fermi surfaces II: Conductivity," arXiv:2207.08841.

Haldar, Arijit, Sumilan Banerjee, and Vijay B. Shenoy, 2018, "Higher-dimensional Sachdev-Ye-Kitaev non-Fermi liquids at Lifshitz transitions," Phys. Rev. B **97**, 241106.

Haldar, Arijit, Prosenjit Haldar, Surajit Bera, Ipsita Mandal, and Sumilan Banerjee, 2020, "Quench, thermalization, and residual

entropy across a non-Fermi liquid to Fermi liquid transition," Phys. Rev. Research **2**, 013307.

Haldar, Arijit, and Vijay B. Shenoy, 2018, "Strange half-metals and Mott insulators in Sachdev-Ye-Kitaev models," Phys. Rev. B **98**, 165135.

Halperin, B. I., Patrick A. Lee, and Nicholas Read, 1993, "Theory of the half-filled Landau level," Phys. Rev. B **47**, 7312–7343.

Haque, Masudul, and P. A. McClarty, 2019, "Eigenstate thermalization scaling in Majorana clusters: From chaotic to integrable Sachdev-Ye-Kitaev models," Phys. Rev. B **100**, 115122.

Hartnoll, Sean A., 2015, "Theory of universal incoherent metallic transport," Nat. Phys. **11**, 54–61.

Hartnoll, Sean A., Pavel K. Kovtun, Markus Muller, and Subir Sachdev, 2007, "Theory of the Nernst effect near quantum phase transitions in condensed matter, and in dyonic black holes," Phys. Rev. B **76**, 144502.

Hartnoll, Sean A., Andrew Lucas, and Subir Sachdev, 2016, *Holographic Quantum Matter* (MIT Press, Cambridge, MA).

Hartnoll, Sean A., and Andrew P. MacKenzie, 2021, "Planckian dissipation in metals," arXiv:2107.07802.

Hartnoll, Sean A., Raghu Mahajan, Matthias Punk, and Subir Sachdev, 2014, "Transport near the Ising-nematic quantum critical point of metals in two dimensions," Phys. Rev. B **89**, 155130.

Hauck, Daniel, Markus J. Klug, Ilya Esterlis, and Jörg Schmalian, 2020, "Eliashberg equations for an electron-phonon version of the Sachdev-Ye-Kitaev model: Pair breaking in non-Fermi liquid superconductors," Ann. Phys. (N.Y.) **417**, 168120.

Haule, K., A. Rosch, J. Kroha, and P. Wölfle, 2002, "Pseudogaps in an Incoherent Metal," Phys. Rev. Lett. **89**, 236402.

Held, K., R. Peters, and A. Toschi, 2013, "Poor Man's Understanding of Kinks Originating from Strong Electronic Correlations," Phys. Rev. Lett. **110**, 246402.

Hewson, A. C., 1997, *The Kondo Problem to Heavy Fermions* (Cambridge University Press, Cambridge, England).

Heydeman, Matthew, Luca V. Iliesiu, Gustavo J. Turiaci, and Wenli Zhao, 2020, "The statistical mechanics of near-BPS black holes," arXiv:2011.01953.

Hicks, Clifford W., Alexandra S. Gibbs, Andrew P. Mackenzie, Hiroshi Takatsu, Yoshiteru Maeno, and Edward A. Yelland, 2012, "Quantum Oscillations and High Carrier Mobility in the Delafossite PdCoO$_2$," Phys. Rev. Lett. **109**, 116401.

Hirsch, J. E., and R. M. Fye, 1986, "Monte Carlo Method for Magnetic Impurities in Metals," Phys. Rev. Lett. **56**, 2521–2524.

Hod, Shahar, 2007, "Universal bound on dynamical relaxation times and black-hole quasinormal ringing," Phys. Rev. D **75**, 064013.

Homes, C. C., *et al.*, 2004, "A universal scaling relation in high-temperature superconductors," Nature (London) **430**, 539–541.

't Hooft, Gerard, 2001, "The Holographic principle: Opening lecture," Subnucl. Ser. **37**, 72–100.

Hu, H., A. Cai, and Q. Si, 2020, "Quantum criticality and dynamical Kondo effect in an SU(2) Anderson lattice model," arXiv:2004.04679.

Huang, Edwin W., Ryan Sheppard, Brian Moritz, and Thomas P. Devereaux, 2019, "Strange metallicity in the doped Hubbard model," Science **366**, 987–990.

Huijse, Liza, and Subir Sachdev, 2011, "Fermi surfaces and gauge-gravity duality," Phys. Rev. D **84**, 026001.

Huijse, Liza, Subir Sachdev, and Brian Swingle, 2012, "Hidden Fermi surfaces in compressible states of gauge-gravity duality," Phys. Rev. B **85**, 035121.

Husain, A. A., *et al.*, 2020, "Observation of Pines' demon in Sr$_2$RuO$_4$," arXiv:2007.06670.

Husain, Ali A., *et al.*, 2019, "Crossover of Charge Fluctuations across the Strange Metal Phase Diagram," Phys. Rev. X **9**, 041062.

Hussey, N. E., 2008, "Phenomenology of the normal state in-plane transport properties of high-T_c cuprates," J. Phys. Condens. Matter **20**, 123201.

Hussey, N. E., K. Takenaka, and H. Takagi, 2004, "Universality of the Mott-Ioffe-Regel limit in metals," Philos. Mag. **84**, 2847–2864.

Hwang, J., T. Timusk, and G. D. Gu, 2007, "Doping dependent optical properties of Bi$_2$Sr$_2$CaCu$_2$O$_{8+\delta}$," J. Phys. Condens. Matter **19**, 125208.

Iliesiu, Luca V., and Gustavo J. Turiaci, 2020, "The statistical mechanics of near-extremal black holes," arXiv:2003.02860.

Ioffe, A. F., and A. R. Regel, 1960, "Non-crystalline, amorphous and liquid electronic semiconductors," in *Progress in Semiconductors*, Vol. 4, edited by A. F. Gibson (John Wiley & Sons, New York), pp. 237–291.

Iqbal, Nabil, Hong Liu, and Mark Mezei, 2011, "Lectures on holographic non-Fermi liquids and quantum phase transitions," in *Proceedings of the Theoretical Advanced Study Institute in Elementary Particle Physics: String Theory and Its Applications— From meV to the Planck Scale, Boulder, CO, 2010*, edited by Michael Dine, Thomas Banks, and Subir Sachdev (World Scientific, Singapore), pp. 707–816.

Iqbal, Nabil, Hong Liu, and Mark Mezei, **2012**, "Semi-local quantum liquids," J. High Energy Phys. 04, 086.

Jackiw, Roman, 1985, "Lower dimensional gravity," Nucl. Phys. **B252**, 343–356.

Jain, Jainendra K., 2007, *Composite Fermions* (Cambridge University Press, Cambridge, England).

Jaoui, Alexandre, Ipsita Das, Giorgio Di Battista, Jaime Díez-Mérida, Xiaobo Lu, Kenji Watanabe, Takashi Taniguchi, Hiroaki Ishizuka, Leonid Levitov, and Dmitri K. Efetov, 2022, "Quantum critical behaviour in magic-angle twisted bilayer graphene," Nat. Phys. **18**, 633–638.

Jian, Chao-Ming, Zhen Bi, and Cenke Xu, 2017, "Model for continuous thermal metal to insulator transition," Phys. Rev. B **96**, 115122.

Jian, Shao-Kai, and Hong Yao, 2017, "Solvable Sachdev-Ye-Kitaev Models in Higher Dimensions: From Diffusion to Many-Body Localization," Phys. Rev. Lett. **119**, 206602.

Jiang, Hong-Chen, Matthew S. Block, Ryan V. Mishmash, James R. Garrison, D. N. Sheng, Olexei I. Motrunich, and Matthew P. A. Fisher, 2013, "Non-Fermi-liquid *d*-wave metal phase of strongly interacting electrons," Nature (London) **493**, 39.

Joshi, Darshan G., Chenyuan Li, Grigory Tarnopolsky, Antoine Georges, and Subir Sachdev, 2020, "Deconfined Critical Point in a Doped Random Quantum Heisenberg Magnet," Phys. Rev. X **10**, 021033.

Joshi, Darshan G., and Subir Sachdev, 2020, "Anomalous density fluctuations in a random *t-J* model," Phys. Rev. B **102**, 165146.

Kadowaki, K., and S. B. Woods, 1986, "Universal relationship of the resistivity and specific heat in heavy-fermion compounds," Solid State Commun. **58**, 507–509.

Keselman, Anna, Laimei Nie, and Erez Berg, 2021, "Scrambling and Lyapunov exponent in spatially extended systems," Phys. Rev. B **103**, L121111.

Khemani, Vedika, David A. Huse, and Adam Nahum, 2018, "Velocity-dependent Lyapunov exponents in many-body quantum, semiclassical, and classical chaos," Phys. Rev. B **98**, 144304.

Khemani, Vedika, Ashvin Vishwanath, and David A. Huse, 2018, "Operator Spreading and the Emergence of Dissipative Hydrodynamics under Unitary Evolution with Conservation Laws," Phys. Rev. X **8**, 031057.

Khurana, Anil, 1990, "Electrical Conductivity in the Infinite-Dimensional Hubbard Model," Phys. Rev. Lett. **64**, 1990.

Khveshchenko, D. V., 2018a, "Seeking to develop global SYK-ness," Condens. Matter **3**, 40.

Khveshchenko, D. V., 2018b, "Thickening and sickening the SYK model," SciPost Phys. **5**, 12.

Khveshchenko, D. V., 2020a, "One SYK single electron transistor," Lith. J. Phys. **60**, 185.

Khveshchenko, D. V., 2020b, "Connecting the SYK dots," Condens. Matter **5**, 37.

Khveshchenko, D. V., 2022, "SYK does not *transit gloria mundi* just yet," arXiv:2205.11478.

Kim, Jaewon, Ehud Altman, and Xiangyu Cao, 2021, "Dirac fast scramblers," Phys. Rev. B **103**, L081113.

Kim, Jaewon, Igor R. Klebanov, Grigory Tarnopolsky, and Wenli Zhao, 2019, "Symmetry Breaking in Coupled SYK or Tensor Models," Phys. Rev. X **9**, 021043.

Kim, Yong Baek, Akira Furusaki, Xiao-Gang Wen, and Patrick A. Lee, 1994, "Gauge-invariant response functions of fermions coupled to a gauge field," Phys. Rev. B **50**, 17917–17932.

Kim, Yong Baek, Patrick A. Lee, and Xiao-Gang Wen, 1995, "Quantum Boltzmann equation of composite fermions interacting with a gauge field," Phys. Rev. B **52**, 17275–17292.

Kirchner, Stefan, Silke Paschen, Qiuyun Chen, Steffen Wirth, Donglai Feng, Joe D. Thompson, and Qimiao Si, 2020, "Colloquium: Heavy-electron quantum criticality and single-particle spectroscopy," Rev. Mod. Phys. **92**, 011002.

Kitaev, Alexei, 2015, "A simple model of quantum holography," lecture, KITP Program: Entanglement in Strongly-Correlated Quantum Matter, Santa Barbara, 2015.

Kitaev, Alexei, and S. Josephine Suh, **2018**, "The soft mode in the Sachdev-Ye-Kitaev model and its gravity dual," J. High Energy Phys. 05, 183.

Klebanov, Igor R., Alexey Milekhin, Grigory Tarnopolsky, and Wenli Zhao, 2020, "Spontaneous breaking of U(1) symmetry in coupled complex SYK models," J. High Energy Phys. 11, 162.

Klebanov, Igor R., Fedor Popov, and Grigory Tarnopolsky, 2018, "TASI lectures on large N tensor models," Proc. Sci. TASI2017, 004 [arXiv:1808.09434].

Klebanov, Igor R., and Grigory Tarnopolsky, 2017, "Uncolored random tensors, melon diagrams, and the Sachdev-Ye-Kitaev models," Phys. Rev. D **95**, 046004.

Kobrin, Bryce, Zhenbin Yang, Gregory D. Kahanamoku-Meyer, Christopher T. Olund, Joel E. Moore, Douglas Stanford, and Norman Y. Yao, 2021, "Many-Body Chaos in the Sachdev-Ye-Kitaev Model," Phys. Rev. Lett. **126**, 030602.

Kohn, W., and J. M. Luttinger, 1965, "New Mechanism for Superconductivity," Phys. Rev. Lett. **15**, 524–526.

Kostic, P., Y. Okada, N. C. Collins, Z. Schlesinger, J. W. Reiner, L. Klein, A. Kapitulnik, T. H. Geballe, and M. R. Beasley, 1998, "Non-Fermi-Liquid Behavior of SrRuO₃: Evidence from Infrared Conductivity," Phys. Rev. Lett. **81**, 2498–2501.

Kotliar, G., 1995, "The large N expansion and the strong correlation problem," in *Strongly Interacting Fermions and High-T_c superconductivity*, Proceedings of the Les Houches Summer School, Session LVI, edited by B. Doucot and J. Zinn-Justin (Elsevier, New York), p. 197.

Kourkoulou, Ioanna, and Juan Maldacena, 2017, "Pure states in the SYK model and nearly-AdS₂ gravity," arXiv:1707.02325.

Kovtun, P., Dan T. Son, and Andrei O. Starinets, 2005, "Viscosity in Strongly Interacting Quantum Field Theories from Black Hole Physics," Phys. Rev. Lett. **94**, 111601.

Kruchkov, Alexander, Aavishkar A. Patel, Philip Kim, and Subir Sachdev, 2020, "Thermoelectric power of Sachdev-Ye-Kitaev islands: Probing Bekenstein-Hawking entropy in quantum matter experiments," Phys. Rev. B **101**, 205148.

Kuhlenkamp, Clemens, and Michael Knap, 2020, "Periodically Driven Sachdev-Ye-Kitaev Models," Phys. Rev. Lett. **124**, 106401.

Kumar, Aman, Subir Sachdev, and Vikram Tripathi, 2021, "Quasiparticle metamorphosis in the random t-J model," arXiv:2112.01760.

Landau, Lev Davidovich, 1957, "The theory of a Fermi liquid," Sov. Phys. JETP **3**, 920–925, http://www.jetp.ras.ru/cgi-bin/dn/e_003_06_0920.pdf.

Larkin, A. I., and Yu. N. Ovchinnikov, 1969, "Quasiclassical method in the theory of superconductivity," J. Exp. Theor. Phys. **28**, 1200, http://jetp.ras.ru/cgi-bin/e/index/e/28/6/p1200?a=list.

Larzul, Ancel, and Marco Schiró, 2021, "Quenches and (pre)thermalisation in a mixed Sachdev-Ye-Kitaev model," arXiv:2107.07781.

Lee, Patrick A., 1989, "Gauge Field, Aharonov-Bohm Flux, and High-T_c Superconductivity," Phys. Rev. Lett. **63**, 680–683.

Lee, Patrick A., 2021, "Low-temperature T-linear resistivity due to umklapp scattering from a critical mode," Phys. Rev. B **104**, 035140.

Lee, Patrick A., Naoto Nagaosa, and Xiao-Gang Wen, 2006, "Doping a Mott insulator: Physics of high-temperature superconductivity," Rev. Mod. Phys. **78**, 17–85.

Lee, Patrick A., and T. V. Ramakrishnan, 1985, "Disordered electronic systems," Rev. Mod. Phys. **57**, 287–337.

Lee, Sung-Sik, 2009, "Low-energy effective theory of Fermi surface coupled with U(1) gauge field in $2+1$ dimensions," Phys. Rev. B **80**, 165102.

Lee, Sung-Sik, 2018, "Recent developments in non-Fermi liquid theory," Annu. Rev. Condens. Matter Phys. **9**, 227–244.

Lee, Y. S., Jaejun Yu, J. S. Lee, T. W. Noh, T.-H. Gimm, Han-Yong Choi, and C. B. Eom, 2002, "Non-Fermi liquid behavior and scaling of the low-frequency suppression in the optical conductivity spectra of CaRuO₃," Phys. Rev. B **66**, 041104.

Legros, A., *et al.*, 2019, "Universal T-linear resistivity and Planckian dissipation in overdoped cuprates," Nat. Phys. **15**, 142–147.

Lensky, Yuri D., and Xiao-Liang Qi, **2021**, "Rescuing a black hole in the large-q coupled SYK model," J. High Energy Phys. 04, 116.

Liao, Yunxiang, and Victor Galitski, 2021, "Emergence of many-body quantum chaos via spontaneous breaking of unitarity," arXiv:2104.05721.

Liao, Yunxiang, Amit Vikram, and Victor Galitski, 2020, "Many-Body Level Statistics of Single-Particle Quantum Chaos," Phys. Rev. Lett. **125**, 250601.

Limelette, P., V. Ta Phuoc, F. Gervais, and R. Frésard, 2013, "ω/T scaling of the optical conductivity in strongly correlated layered cobalt oxide," Phys. Rev. B **87**, 035102.

Lindner, Netanel H., and Assa Auerbach, 2010, "Conductivity of hard core bosons: A paradigm of a bad metal," Phys. Rev. B **81**, 054512.

Liu, Hong, John McGreevy, and David Vegh, 2011, "Non-Fermi liquids from holography," Phys. Rev. D **83**, 065029.

Liu, Hong, and Julian Sonner, 2020, "Quantum many-body physics from a gravitational lens," Nat. Rev. Phys. **2**, 615–633.

Löhneysen, Hilbert v., Achim Rosch, Matthias Vojta, and Peter Wölfle, 2007, "Fermi-liquid instabilities at magnetic quantum phase transitions," Rev. Mod. Phys. **79**, 1015–1075.

Loram, J. W., K. A. Mirza, J. M. Wade, J. R. Cooper, and W. Y. Liang, 1994, "The electronic specific heat of cuprate superconductors," Physica (Amsterdam) **235C–240C**, 134–137.

Lucas, Andrew, **2015**, "Conductivity of a strange metal: From holography to memory functions," J. High Energy Phys. 03, 071.

Lucas, Andrew, and Subir Sachdev, 2015, "Memory matrix theory of magnetotransport in strange metals," Phys. Rev. B **91**, 195122.

Lucas, Andrew, and Julia Steinberg, **2016**, "Charge diffusion and the butterfly effect in striped holographic matter," J. High Energy Phys. 10, 143.

Luitz, David J., and Yevgeny Bar Lev, 2017, "Information propagation in isolated quantum systems," Phys. Rev. B **96**, 020406.

Luo, Zhihuang, Yi-Zhuang You, Jun Li, Chao-Ming Jian, Dawei Lu, Cenke Xu, Bei Zeng, and Raymond Laflamme, 2019, "Quantum simulation of the non-Fermi-liquid state of Sachdev-Ye-Kitaev model," npj Quantum Inf. **5**, 53.

Luttinger, J. M., and J. C. Ward, 1960, "Ground-state energy of a many-fermion system. II," Phys. Rev. **118**, 1417–1427.

Maček, Marjan, Philipp T. Dumitrescu, Corentin Bertrand, Bill Triggs, Olivier Parcollet, and Xavier Waintal, 2020, "Quantum Quasi–Monte Carlo Technique for Many-Body Perturbative Expansions," Phys. Rev. Lett. **125**, 047702.

Maksimovic, Nikola, *et al.*, 2022, "Evidence for a delocalization quantum phase transition without symmetry breaking in $CeCoIn_5$," Science **375**, 76–81.

Maldacena, Juan, and Xiao-Liang Qi, 2018, "Eternal traversable wormhole," arXiv:1804.00491.

Maldacena, Juan, Stephen H. Shenker, and Douglas Stanford, **2016**, "A bound on chaos," J. High Energy Phys. 08, 106.

Maldacena, Juan, and Douglas Stanford, 2016, "Remarks on the Sachdev-Ye-Kitaev model," Phys. Rev. D **94**, 106002.

Maldacena, Juan, Douglas Stanford, and Zhenbin Yang, **2016**, "Conformal symmetry and its breaking in two dimensional nearly anti–de Sitter space," Prog. Theor. Exp. Phys. 12C104.

Maldacena, Juan Martin, 1998, "The large N limit of superconformal field theories and supergravity," Adv. Theor. Math. Phys. **2**, 231–252.

Maloney, Alexander, and Edward Witten, **2020**, "Averaging over Narain moduli space," J. High Energy Phys. 10, 187.

Marcus, Eric, and Stefan Vandoren, 2019, "A new class of SYK-like models with maximal chaos," J. High Energy Phys. 01, 166.

Maslov, Dmitrii L., Vladimir I. Yudson, and Andrey V. Chubukov, 2011, "Resistivity of a Non-Galilean-Invariant Fermi Liquid near Pomeranchuk Quantum Criticality," Phys. Rev. Lett. **106**, 106403.

Mehta, Madan Lal, 2004, *Random Matrices* (Elsevier, New York).

Mena, F. P., D. van der Marel, A. Damascelli, M. Fäth, A. A. Menovsky, and J. A. Mydosh, 2003, "Heavy carriers and non-Drude optical conductivity in MnSi," Phys. Rev. B **67**, 241101.

Metlitski, M. A., and S. Sachdev, 2010, "Quantum phase transitions of metals in two spatial dimensions. I. Ising-nematic order," Phys. Rev. B **82**, 075127.

Metlitski, Max A., David F. Mross, Subir Sachdev, and T. Senthil, 2015, "Cooper pairing in non-Fermi liquids," Phys. Rev. B **91**, 115111.

Mézard, M., G. Parisi, and M. A. Virasoro, 1987, *Spin Glass Theory and Beyond: An Introduction to the Replica Method and Its Applications*, World Scientific Lecture Notes In Physics Vol. 9 (World Scientific, Singapore).

Michon, B., C. Berthod, C. W. Rischau, A. Ataei, L. Chen, S. Komiya, S. Ono, L. Taillefer, D. van der Marel, and A. Georges, 2022, "Planckian behavior of cuprate superconductors: Reconciling the scaling of optical conductivity with resistivity and specific heat," arXiv:2205.04030.

Michon, B., *et al.*, 2019, "Thermodynamic signatures of quantum criticality in cuprate superconductors," Nature (London) **567**, 218–222.

Micklitz, T., Felipe Monteiro, and Alexander Altland, 2019, "Non-ergodic Extended States in the Sachdev-Ye-Kitaev Model," Phys. Rev. Lett. **123**, 125701.

Milekhin, Alexey, **2021**, "Non-local reparametrization action in coupled Sachdev-Ye-Kitaev models," J. High Energy Phys. 12, 114.

Millis, A. J., 1993, "Effect of a nonzero temperature on quantum critical points in itinerant fermion systems," Phys. Rev. B **48**, 7183–7196.

Mitrano, M., *et al.*, 2018, "Anomalous density fluctuations in a strange metal," Proc. Natl. Acad. Sci. U.S.A. **115**, 5392–5396.

Moitra, Upamanyu, Sandip P. Trivedi, and V. Vishal, **2019**, "Extremal and near-extremal black holes and near-CFT_1," J. High Energy Phys. 07, 055.

Moon, Eun-Gook, and Andrey Chubukov, 2010, "Quantum-critical pairing with varying exponents," J. Low Temp. Phys. **161**, 263–281.

Moriya, T., 1985, in *Spin Fluctuations in Itinerant Electron Magnetism*, edited by M. Cardona, P. Fulde, and H.-J. Queisser (Springer-Verlag, Berlin).

Mott, N., 1974, *Metal-Insulator Transitions* (Taylor & Francis, London).

Mousatov, Connie H., and Sean A. Hartnoll, 2020, "On the Planckian bound for heat diffusion in insulators," Nat. Phys. **16**, 579–584.

Mross, David F., John McGreevy, Hong Liu, and T. Senthil, 2010, "Controlled expansion for certain non-Fermi-liquid metals," Phys. Rev. B **82**, 045121.

Mukerjee, Subroto, Vadim Oganesyan, and David Huse, 2006, "Statistical theory of transport by strongly interacting lattice fermions," Phys. Rev. B **73**, 035113.

Müller, Sebastian, Stefan Heusler, Alexander Altland, Petr Braun, and Fritz Haake, 2009, "Periodic-orbit theory of universal level correlations in quantum chaos," New J. Phys. **11**, 103025.

Murthy, Chaitanya, and Mark Srednicki, 2019, "Bounds on Chaos from the Eigenstate Thermalization Hypothesis," Phys. Rev. Lett. **123**, 230606.

Murugan, Jeff, Douglas Stanford, and Edward Witten, **2017**, "More on supersymmetric and 2D analogs of the SYK model," J. High Energy Phys. 08, 146.

Nahum, Adam, 2022, "Fixed point annihilation for a spin in a fluctuating field," arXiv:2202.08431.

Nahum, Adam, Sagar Vijay, and Jeongwan Haah, 2018, "Operator Spreading in Random Unitary Circuits," Phys. Rev. X **8**, 021014.

Nakajima, Yasuyuki, *et al.*, 2020, "Quantum-critical scale invariance in a transition metal alloy," Commun. Phys. **3**, 181.

Nayak, Pranjal, Ashish Shukla, Ronak M. Soni, Sandip P. Trivedi, and V. Vishal, **2018**, "On the dynamics of near-extremal black holes," J. High Energy Phys. 09, 048.

Nikolaenko, Alexander, Maria Tikhanovskaya, Subir Sachdev, and Ya-Hui Zhang, 2021, "Small to large Fermi surface transition in a single-band model, using randomly coupled ancillas," Phys. Rev. B **103**, 235138.

Otsuki, Junya, 2013, "Spin-boson coupling in continuous-time quantum Monte Carlo," Phys. Rev. B **87**, 125102.

Otsuki, Junya, and Dieter Vollhardt, 2013, "Numerical Solution of the t-J Model with Random Exchange Couplings in $d = \infty$ Dimensions," Phys. Rev. Lett. **110**, 196407.

Pálsson, Gunnar, and Gabriel Kotliar, 1998, "Thermoelectric Response near the Density Driven Mott Transition," Phys. Rev. Lett. **80**, 4775–4778.

Pankov, Sergey, Gabriel Kotliar, and Yukitoshi Motome, 2002, "Semiclassical analysis of extended dynamical mean-field equations," Phys. Rev. B **66**, 045117.

Paramekanti, Arun, and Ashvin Vishwanath, 2004, "Extending Luttinger's theorem to Z_2 fractionalized phases of matter," Phys. Rev. B **70**, 245118.

Parcollet, Olivier, and Antoine Georges, 1999, "Non-Fermi-liquid regime of a doped Mott insulator," Phys. Rev. B **59**, 5341–5360.

Parcollet, Olivier, Antoine Georges, Gabriel Kotliar, and Anirvan Sengupta, 1998, "Overscreened multichannel SU(N) Kondo model: Large-N solution and conformal field theory," Phys. Rev. B **58**, 3794–3813.

Park, Jeong Min, Yuan Cao, Kenji Watanabe, Takashi Taniguchi, and Pablo Jarillo-Herrero, 2021, "Flavour Hund's coupling, Chern gaps and charge diffusivity in moiré graphene," Nature (London) **592**, 43–48.

Parker, Daniel E., Xiangyu Cao, Alexander Avdoshkin, Thomas Scaffidi, and Ehud Altman, 2019, "A Universal Operator Growth Hypothesis," Phys. Rev. X **9**, 041017.

Paschen, Silke, and Qimiao Si, 2021, "Quantum phases driven by strong correlations," Nat. Rev. Phys. **3**, 9–26.

Patel, Aavishkar A., and Hitesh J. Changlani, 2022, "Many-body energy invariant for T-linear resistivity," Phys. Rev. B **105**, L201108.

Patel, Aavishkar A., Debanjan Chowdhury, Subir Sachdev, and Brian Swingle, 2017, "Quantum Butterfly Effect in Weakly Interacting Diffusive Metals," Phys. Rev. X **7**, 031047.

Patel, Aavishkar A., Haoyu Guo, Ilya Esterlis, and Subir Sachdev, 2022, "Universal, low temperature, T-linear resistivity in two-dimensional quantum-critical metals from spatially random interactions," arXiv:2203.04990.

Patel, Aavishkar A., Michael J. Lawler, and Eun-Ah Kim, 2018, "Coherent Superconductivity with a Large Gap Ratio from Incoherent Metals," Phys. Rev. Lett. **121**, 187001.

Patel, Aavishkar A., John McGreevy, Daniel P. Arovas, and Subir Sachdev, 2018, "Magnetotransport in a Model of a Disordered Strange Metal," Phys. Rev. X **8**, 021049.

Patel, Aavishkar A., and Subir Sachdev, 2014, "dc resistivity at the onset of spin density wave order in two-dimensional metals," Phys. Rev. B **90**, 165146.

Patel, Aavishkar A., and Subir Sachdev, 2017, "Quantum chaos on a critical Fermi surface," Proc. Natl. Acad. Sci. U.S.A. **114**, 1844–1849.

Patel, Aavishkar A., and Subir Sachdev, 2018, "Critical strange metal from fluctuating gauge fields in a solvable random model," Phys. Rev. B **98**, 125134.

Patel, Aavishkar A., and Subir Sachdev, 2019, "Theory of a Planckian Metal," Phys. Rev. Lett. **123**, 066601.

Paul, I., C. Pépin, and M. R. Norman, 2007, "Kondo Breakdown and Hybridization Fluctuations in the Kondo-Heisenberg Lattice," Phys. Rev. Lett. **98**, 026402.

Paul, I., C. Pépin, and M. R. Norman, 2008, "Multiscale fluctuations near a Kondo breakdown quantum critical point," Phys. Rev. B **78**, 035109.

Paul, I., C. Pépin, and M. R. Norman, 2013, "Equivalence of Single-Particle and Transport Lifetimes from Hybridization Fluctuations," Phys. Rev. Lett. **110**, 066402.

Pavlov, Andrei I., and Mikhail N. Kiselev, 2021, "Quantum thermal transport in the charged Sachdev-Ye-Kitaev model: Thermoelectric Coulomb blockade," Phys. Rev. B **103**, L201107.

Peierls, R., 1930, "On the theory of electrical and thermal conductivity of metals," Ann. Phys. (Berlin) **396**, 121–148.

Peierls, R., 1932, "On the question of the law of electrical resistance for low temperatures," Ann. Phys. (Berlin) **404**, 154–168.

Penington, Geoff, Stephen H. Shenker, Douglas Stanford, and Zhenbin Yang, 2019, "Replica wormholes and the black hole interior," arXiv:1911.11977.

Perepelitsky, Edward, Andrew Galatas, Jernej Mravlje, and Rok Žitko, Ehsan Khatami, B. Sriram Shastry, and Antoine Georges, 2016, "Transport and optical conductivity in the Hubbard model: A high-temperature expansion perspective," Phys. Rev. B **94**, 235115.

Pérez, Alfredo, and Ricardo Troncoso, **2020**, "Gravitational dual of averaged free CFT's over the Narain lattice," J. High Energy Phys. 11, 015.

Phanindra, V. Eswara, Piyush Agarwal, and D. S. Rana, 2018, "Terahertz spectroscopic evidence of non-Fermi-liquid-like behavior in structurally modulated PrNiO$_3$ thin films," Phys. Rev. Mater. **2**, 015001.

Pikulin, D. I., and M. Franz, 2017, "Black Hole on a Chip: Proposal for a Physical Realization of the Sachdev-Ye-Kitaev Model in a Solid-State System," Phys. Rev. X **7**, 031006.

Pixley, J. H., Rong Yu, and Qimiao Si, 2014, "Quantum Phases of the Shastry-Sutherland Kondo Lattice: Implications for the Global Phase Diagram of Heavy-Fermion Metals," Phys. Rev. Lett. **113**, 176402.

Plugge, Stephan, Étienne Lantagne-Hurtubise, and Marcel Franz, 2020, "Revival Dynamics in a Traversable Wormhole," Phys. Rev. Lett. **124**, 221601.

Polchinski, Joseph, 1994, "Low-energy dynamics of the spinon gauge system," Nucl. Phys. **B422**, 617–633.

Polshyn, Hryhoriy, Matthew Yankowitz, Shaowen Chen, Yuxuan Zhang, K. Watanabe, T. Taniguchi, Cory R. Dean, and Andrea F. Young, 2019, "Large linear-in-temperature resistivity in twisted bilayer graphene," Nat. Phys. **15**, 1011–1016.

Powell, S., S. Sachdev, and H. P. Büchler, 2005, "Depletion of the Bose-Einstein condensate in Bose-Fermi mixtures," Phys. Rev. B **72**, 024534.

Prange, Richard E., and Leo P. Kadanoff, 1964, "Transport theory for electron-phonon interactions in metals," Phys. Rev. **134**, A566–A580.

Profumo, Rosario E. V., Christoph Groth, Laura Messio, Olivier Parcollet, and Xavier Waintal, 2015, "Quantum Monte Carlo for correlated out-of-equilibrium nanoelectronic devices," Phys. Rev. B **91**, 245154.

Proust, Cyril, and Louis Taillefer, 2019, "The remarkable underlying ground states of cuprate superconductors," Annu. Rev. Condens. Matter Phys. **10**, 409–429.

Read, N., Subir Sachdev, and J. Ye, 1995, "Landau theory of quantum spin glasses of rotors and Ising spins," Phys. Rev. B **52**, 384–410.

Reber, T. J., *et al.*, 2019, "A unified form of low-energy nodal electronic interactions in hole-doped cuprate superconductors," Nat. Commun. **10**, 5737.

Ross, Simon F., 2005, "Black hole thermodynamics," arXiv:hep-th/0502195.

Rossini, Davide, Gian Marcello Andolina, Dario Rosa, Matteo Carrega, and Marco Polini, 2020, "Quantum Advantage in the Charging Process of Sachdev-Ye-Kitaev Batteries," Phys. Rev. Lett. **125**, 236402.

Rozenberg, M. J., G. Kotliar, and H. Kajueter, 1996, "Transfer of spectral weight in spectroscopies of correlated electron systems," Phys. Rev. B **54**, 8452–8468.

Rubtsov, A. N., V. V. Savkin, and A. I. Lichtenstein, 2005, "Continuous-time quantum Monte Carlo method for fermions," Phys. Rev. B **72**, 035122.

Saad, Phil, Stephen H. Shenker, and Douglas Stanford, 2018, "A semiclassical ramp in SYK and in gravity," arXiv:1806.06840.

Saad, Phil, Stephen H. Shenker, and Douglas Stanford, 2019, "JT gravity as a matrix integral," arXiv:1903.11115.

Sachdev, Subir, 1999, *Quantum Phase Transitions* (Cambridge University Press, Cambridge, England).

Sachdev, Subir, 2001, "Static hole in a critical antiferromagnet: Field-theoretic renormalization group," Physica (Amsterdam) 357C–360C, 78–81.

Sachdev, Subir, 2010, "Holographic Metals and the Fractionalized Fermi Liquid," Phys. Rev. Lett. 105, 151602.

Sachdev, Subir, 2012, "Compressible quantum phases from conformal field theories in $2 + 1$ dimensions," Phys. Rev. D 86, 126003.

Sachdev, Subir, 2015, "Bekenstein-Hawking Entropy and Strange Metals," Phys. Rev. X 5, 041025.

Sachdev, Subir, 2019, "Universal low temperature theory of charged black holes with AdS_2 horizons," J. Math. Phys. (N.Y.) 60, 052303.

Sachdev, Subir, 2022, "Statistical mechanics of strange metals and black holes," arXiv:2205.02285.

Sachdev, Subir, Chiranjeeb Buragohain, and Matthias Vojta, 1999, "Quantum impurity in a nearly critical two-dimensional antiferromagnet," Science 286, 2479–2482.

Sachdev, Subir, N. Read, and R. Oppermann, 1995, "Quantum field theory of metallic spin glasses," Phys. Rev. B 52, 10286–10294.

Sachdev, Subir, and Jinwu Ye, 1993, "Gapless Spin-Fluid Ground State in a Random Quantum Heisenberg Magnet," Phys. Rev. Lett. 70, 3339–3342.

Sadovskii, M. V., 2020, "On the Planckian limit for inelastic relaxation in metals," JETP Lett. 111, 188–192.

Sadovskii, M. V., 2021, "Planckian relaxation delusion in metals," Phys. Usp. 64, 175–190.

Sahoo, Sharmistha, Étienne Lantagne-Hurtubise, Stephan Plugge, and Marcel Franz, 2020, "Traversable wormhole and Hawking-Page transition in coupled complex SYK models," Phys. Rev. Research 2, 043049.

Samui, Tousik, and Nilakash Sorokhaibam, 2021, "Thermalization in different phases of charged SYK model," J. High Energy Phys. 04, 157.

Schlenker, Jean-Marc, and Edward Witten, 2022, "No ensemble averaging below the black hole threshold," arXiv:2202.01372.

Schlesinger, Z., R. T. Collins, F. Holtzberg, C. Feild, S. H. Blanton, U. Welp, G. W. Crabtree, Y. Fang, and J. Z. Liu, 1990, "Superconducting Energy Gap and Normal-State Conductivity of a Single-Domain $YBa_2Cu_3O_7$ Crystal," Phys. Rev. Lett. 65, 801–804.

Schröder, A., G. Aeppli, E. Bucher, R. Ramazashvili, and P. Coleman, 1998, "Scaling of Magnetic Fluctuations near a Quantum Phase Transition," Phys. Rev. Lett. 80, 5623–5626.

Schröder, A., G. Aeppli, R. Coldea, M. Adams, O. Stockert, H. v. Löhneysen, E. Bucher, R. Ramazashvili, and P. Coleman, 2000, "Onset of antiferromagnetism in heavy-fermion metals," Nature (London) 407, 351.

Schwartz, A., M. Dressel, G. Grüner, V. Vescoli, L. Degiorgi, and T. Giamarchi, 1998, "On-chain electrodynamics of metallic $(TMTSF)_2X$ salts: Observation of Tomonaga-Luttinger liquid response," Phys. Rev. B 58, 1261–1271.

Seaman, C. L., M. B. Maple, B. W. Lee, S. Ghamaty, M. S. Torikachvili, J.-S. Kang, L. Z. Liu, J. W. Allen, and D. L. Cox, 1991, "Evidence for Non-Fermi Liquid Behavior in the Kondo Alloy $Y_{1-x}U_xPd_3$," Phys. Rev. Lett. 67, 2882–2885.

Sen, Ashoke, 2005, "Black hole entropy function and the attractor mechanism in higher derivative gravity," J. High Energy Phys. 09, 038.

Sen, Ashoke, 2008, "Entropy function and AdS_2/CFT_1 correspondence," J. High Energy Phys. 11, 075.

Sengupta, Anirvan M., 2000, "Spin in a fluctuating field: The Bose (+Fermi) Kondo models," Phys. Rev. B 61, 4041–4043.

Sengupta, Anirvan M., and Antoine Georges, 1995, "Non-Fermi-liquid behavior near a $T = 0$ spin-glass transition," Phys. Rev. B 52, 10295–10302.

Senthil, T., 2008a, "Critical Fermi surfaces and non-Fermi liquid metals," Phys. Rev. B 78, 035103.

Senthil, T., 2008b, "Theory of a continuous Mott transition in two dimensions," Phys. Rev. B 78, 045109.

Senthil, T., Subir Sachdev, and Matthias Vojta, 2003, "Fractionalized Fermi Liquids," Phys. Rev. Lett. 90, 216403.

Senthil, T., Matthias Vojta, and Subir Sachdev, 2004, "Weak magnetism and non-Fermi liquids near heavy-fermion critical points," Phys. Rev. B 69, 035111.

Setty, Chandan, 2020, "Pairing instability on a Luttinger surface: A non-Fermi liquid to superconductor transition and its Sachdev-Ye-Kitaev dual," Phys. Rev. B 101, 184506.

Setty, Chandan, 2021, "Superconductivity from Luttinger surfaces: Emergent Sachdev-Ye-Kitaev physics with infinite-body interactions," Phys. Rev. B 103, 014501.

Shackleton, Henry, Alexander Wietek, Antoine Georges, and Subir Sachdev, 2021, "Quantum Phase Transition at Nonzero Doping in a Random $t − J$ Model," Phys. Rev. Lett. 126, 136602.

Shenker, Stephen H., and Douglas Stanford, 2014, "Black holes and the butterfly effect," J. High Energy Phys. 03, 067.

Shimizu, Yasuhiro, Hikaru Takeda, Moe Tanaka, Masayuki Itoh, Seiji Niitaka, and Hidenori Takagi, 2012, "An orbital-selective spin liquid in a frustrated heavy fermion spinel LiV_2O_4," Nat. Commun. 3, 981.

Si, Qimiao, 2010, "Quantum criticality and global phase diagram of magnetic heavy fermions," Phys. Status Solidi B 247, 476–484.

Si, Qimiao, and J. Lleweilun Smith, 1996, "Kosterlitz-Thouless Transition and Short Range Spatial Correlations in an Extended Hubbard Model," Phys. Rev. Lett. 77, 3391–3394.

Si, Qimiao, Silvio Rabello, Kevin Ingersent, and J. Lleweilun Smith, 2001, "Locally critical quantum phase transitions in strongly correlated metals," Nature (London) 413, 804–808.

Si, Qimiao, Silvio Rabello, Kevin Ingersent, and J. Lleweilun Smith, 2003, "Local fluctuations in quantum critical metals," Phys. Rev. B 68, 115103.

Slakey, F., M. V. Klein, J. P. Rice, and D. M. Ginsberg, 1991, "Raman investigation of the $YBa_2Cu_3O_7$ imaginary response function," Phys. Rev. B 43, 3764–3767.

Smith, J. L., and Q. Si, 1999, "Non-Fermi liquids in the two-band extended Hubbard model," Europhys. Lett. 45, 228–234.

Smith, J. Lleweilun, and Qimiao Si, 2000, "Spatial correlations in dynamical mean-field theory," Phys. Rev. B 61, 5184–5193.

Soldevilla, J. García, J. C. Gómez Sal, J. A. Blanco, J. I. Espeso, and J. Rodríguez Fernández, 2000, "Phase diagram of the $CeNi_{1-x}Cu_x$ Kondo system with spin-glass-like behavior favored by hybridization," Phys. Rev. B 61, 6821–6825.

Son, Dam Thanh, 2015, "Is the Composite Fermion a Dirac Particle?," Phys. Rev. X 5, 031027.

Song, Xue-Yang, Chao-Ming Jian, and Leon Balents, 2017, "Strongly Correlated Metal Built from Sachdev-Ye-Kitaev Models," Phys. Rev. Lett. 119, 216601.

Sonner, Julian, and Manuel Vielma, 2017, "Eigenstate thermalization in the Sachdev-Ye-Kitaev model," J. High Energy Phys. 11, 149.

Stanford, Douglas, 2016, "Many-body chaos at weak coupling," J. High Energy Phys. 10, 009.

Stanford, Douglas, and Edward Witten, 2017, "Fermionic localization of the Schwarzian theory," J. High Energy Phys. 10, 008.

Stanford, Douglas, and Edward Witten, 2019, "JT gravity and the ensembles of random matrix theory," arXiv:1907.03363.

Steinberg, Julia, and Brian Swingle, 2019, "Thermalization and chaos in QED$_3$," Phys. Rev. D **99**, 076007.

Stewart, G. R., 2001, "Non-Fermi-liquid behavior in *d*- and *f*-electron metals," Rev. Mod. Phys. **73**, 797–855.

Su, Kaixiang, Pengfei Zhang, and Hui Zhai, **2021**, "Page curve from non-Markovianity," J. High Energy Phys. 06, 156.

Swingle, Brian, and Debanjan Chowdhury, 2017, "Slow scrambling in disordered quantum systems," Phys. Rev. B **95**, 060201.

Tarnopolsky, Grigory, Chenyuan Li, Darshan G. Joshi, and Subir Sachdev, 2020, "Metal-insulator transition in a random Hubbard model," Phys. Rev. B **101**, 205106.

Taupin, Mathieu, and Silke Paschen, 2022, "Are heavy fermion strange metals Planckian?," arXiv:2201.02820.

Teitelboim, Claudio, 1983, "Gravitation and Hamiltonian structure in two spacetime dimensions," Phys. Lett. **126B**, 41–45.

Theumann, Alba, and B. Coqblin, 2004, "Quantum critical point in the spin glass Kondo transition in heavy-fermion systems," Phys. Rev. B **69**, 214418.

Tikhanovskaya, Maria, Haoyu Guo, Subir Sachdev, and Grigory Tarnopolsky, 2021a, "Excitation spectra of quantum matter without quasiparticles. I. Sachdev-Ye-Kitaev models," Phys. Rev. B **103**, 075141.

Tikhanovskaya, Maria, Haoyu Guo, Subir Sachdev, and Grigory Tarnopolsky, 2021b, "Excitation spectra of quantum matter without quasiparticles. II. Random *t-J* models," Phys. Rev. B **103**, 075142.

Tikhanovskaya, Maria, Subir Sachdev, and Aavishkar A. Patel, 2022, "Maximal quantum chaos of the critical Fermi surface," arXiv:2202.01845.

Tsuji, Naoto, and Philipp Werner, 2019, "Out-of-time-ordered correlators of the Hubbard model: Sachdev-Ye-Kitaev strange metal in the spin-freezing crossover region," Phys. Rev. B **99**, 115132.

Tulipman, Evyatar, and Erez Berg, 2021, "Strongly coupled phonon fluid and Goldstone modes in an anharmonic quantum solid: Transport and chaos," Phys. Rev. B **104**, 195113.

Tyler, A. W., A. P. Mackenzie, S. NishiZaki, and Y. Maeno, 1998, "High-temperature resistivity of Sr_2RuO_4: Bad metallic transport in a good metal," Phys. Rev. B **58**, R10107–R10110.

Valla, T., A. V. Fedorov, P. D. Johnson, B. O. Wells, S. L. Hulbert, Q. Li, G. D. Gu, and N. Koshizuka, 1999, "Evidence for quantum critical behavior in the optimally doped cuprate $Bi_2Sr_2CaCu_2O_{8+\delta}$," Science **285**, 2110–2113.

van der Marel, D., F. Carbone, A. B. Kuzmenko, and E. Giannini, 2006, "Scaling properties of the optical conductivity of Bi-based cuprates," Ann. Phys. (N.Y.) **321**, 1716–1729.

van der Marel, D., H. J. A. Molegraaf, J. Zaanen, Z. Nussinov, F. Carbone, A. Damascelli, H. Eisaki, M. Greven, P. H. Kes, and M. Li, 2003, "Quantum critical behaviour in a high-T_c superconductor," Nature (London) **425**, 271.

van Heumen, E., X. Feng, S. Cassanelli, L. Neubrand, L. de Jager, M. Berben, Y. Huang, T. Kondo, T. Takeuchi, and J. Zaanen, 2022, "Strange metal dynamics across the phase diagram of $Bi_2Sr_2CuO_{6+\delta}$ cuprates," arXiv:2205.00899.

Varma, C. M., P. B. Littlewood, S. Schmitt-Rink, E. Abrahams, and A. E. Ruckenstein, 1989, "Phenomenology of the Normal State of Cu-O High-Temperature Superconductors," Phys. Rev. Lett. **63**, 1996–1999.

Varma, Chandra M., 2016, "Quantum-critical fluctuations in 2D metals: Strange metals and superconductivity in antiferromagnets and in cuprates," Rep. Prog. Phys. **79**, 082501.

Varma, Chandra M., 2020, "Colloquium: Linear in temperature resistivity and associated mysteries including high temperature superconductivity," Rev. Mod. Phys. **92**, 031001.

Vishveshwara, C. V., 1970, "Scattering of gravitational radiation by a Schwarzschild black-hole," Nature (London) **227**, 936.

Vojta, Matthias, Chiranjeeb Buragohain, and Subir Sachdev, 2000, "Quantum impurity dynamics in two-dimensional antiferromagnets and superconductors," Phys. Rev. B **61**, 15152–15184.

Vojta, Matthias, and Lars Fritz, 2004, "Upper critical dimension in a quantum impurity model: Critical theory of the asymmetric pseudogap Kondo problem," Phys. Rev. B **70**, 094502.

Vollmer, R., T. Pietrus, H. v. Löhneysen, R. Chau, and M. B. Maple, 2000, "Phase transitions and non-Fermi-liquid behavior in $UCu_{5-x}Pd_x$ at low temperatures," Phys. Rev. B **61**, 1218–1222.

von Keyserlingk, C. W., Tibor Rakovszky, Frank Pollmann, and S. L. Sondhi, 2018, "Operator Hydrodynamics, OTOCs, and Entanglement Growth in Systems without Conservation Laws," Phys. Rev. X **8**, 021013.

Vranić, A., J. Vučičević, J. Kokalj, J. Skolimowski, R. Žitko, J. Mravlje, and D. Tanasković, 2020, "Charge transport in the Hubbard model at high temperatures: Triangular versus square lattice," Phys. Rev. B **102**, 115142.

Vučičević, J., J. Kokalj, R. Žitko, N. Wentzell, D. Tanasković, and J. Mravlje, 2019, "Conductivity in the Square Lattice Hubbard Model at High Temperatures: Importance of Vertex Corrections," Phys. Rev. Lett. **123**, 036601.

Wang, Hanteng, A. L. Chudnovskiy, Alexander Gorsky, and Alex Kamenev, 2020, "Sachdev-Ye-Kitaev superconductivity: Quantum Kuramoto and generalized Richardson models," Phys. Rev. Research **2**, 033025.

Wang, S.-C., *et al.*, 2004, "Quasiparticle Line Shape of Sr_2RuO_4 and Its Relation to Anisotropic Transport," Phys. Rev. Lett. **92**, 137002.

Wang, Wei, Andrew Davis, Gaopei Pan, Yuxuan Wang, and Zi Yang Meng, 2021, "Phase diagram of the spin-1/2 Yukawa-Sachdev-Ye-Kitaev model: Non-Fermi liquid, insulator, and superconductor," Phys. Rev. B **103**, 195108.

Wang, Xiaoyu, and Erez Berg, 2019, "Scattering mechanisms and electrical transport near an Ising nematic quantum critical point," Phys. Rev. B **99**, 235136.

Wang, Yuxuan, 2020, "Solvable Strong-Coupling Quantum-Dot Model with a Non-Fermi-Liquid Pairing Transition," Phys. Rev. Lett. **124**, 017002.

Wang, Yuxuan, Artem Abanov, Boris L. Altshuler, Emil A. Yuzbashyan, and Andrey V. Chubukov, 2016, "Superconductivity near a Quantum-Critical Point: The Special Role of the First Matsubara Frequency," Phys. Rev. Lett. **117**, 157001.

Wang, Yuxuan, and Andrey V. Chubukov, 2020, "Quantum phase transition in the Yukawa-SYK model," Phys. Rev. Research **2**, 033084.

Weber, Manuel, and Matthias Vojta, 2022, "SU(2)-symmetric spin-boson model: Quantum criticality, fixed-point annihilation, and duality," arXiv:2203.02518.

Wei, Chenan, and Tigran A. Sedrakyan, 2021, "Optical lattice platform for the Sachdev-Ye-Kitaev model," Phys. Rev. A **103**, 013323.

Wen, Xiao-Gang, 2017, "Colloquium: Zoo of quantum-topological phases of matter," Rev. Mod. Phys. **89**, 041004.

Werman, Yochai, and Erez Berg, 2016, "Mott-Ioffe-Regel limit and resistivity crossover in a tractable electron-phonon model," Phys. Rev. B **93**, 075109.

Werman, Yochai, Steven A. Kivelson, and Erez Berg, 2017, "Non-quasiparticle transport and resistivity saturation: A view from the large-*N* limit," npj Quantum Mater. **2**, 7.

Werner, Philipp, Armin Comanac, Luca de' Medici, Matthias Troyer, and Andrew J. Millis, 2006, "Continuous-Time Solver for Quantum Impurity Models," Phys. Rev. Lett. **97**, 076405.

Werner, Philipp, Aaram J. Kim, and Shintaro Hoshino, 2018, "Spin-freezing and the Sachdev-Ye model," Europhys. Lett. **124**, 57002.

Winer, Michael, Shao-Kai Jian, and Brian Swingle, 2020, "Exponential Ramp in the Quadratic Sachdev-Ye-Kitaev Model," Phys. Rev. Lett. **125**, 250602.

Witten, Edward, 1998, "Anti–de Sitter space and holography," Adv. Theor. Math. Phys. **2**, 253–291.

Wu, Wei, Xiang Wang, and A. M. S. Tremblay, 2021, "Non-Fermi liquid phase and linear-in-temperature scattering rate in overdoped two dimensional Hubbard model," arXiv:2109.02635.

Wu, Xiaochuan, Xiao Chen, Chao-Ming Jian, Yi-Zhuang You, and Cenke Xu, 2018, "Candidate theory for the strange metal phase at a finite-energy window," Phys. Rev. B **98**, 165117.

Wu, Yi-Ming, Artem Abanov, Yuxuan Wang, and Andrey V. Chubukov, 2020, "Interplay between superconductivity and non-Fermi liquid at a quantum critical point in a metal. II. The γ model at a finite T for $0 < \gamma < 1$," Phys. Rev. B **102**, 024525.

Xu, Shenglong, and Brian Swingle, 2019, "Locality, Quantum Fluctuations, and Scrambling," Phys. Rev. X **9**, 031048.

Xu, Shenglong, and Brian Swingle, 2020, "Accessing scrambling using matrix product operators," Nat. Phys. **16**, 199–204.

Xu, W., W. R. McGehee, W. N. Morong, and B. DeMarco, 2019, "Bad-metal relaxation dynamics in a Fermi lattice gas," Nat. Commun. **10**, 1588.

Zaanen, Jan, 2004, "Superconductivity: Why the temperature is high," Nature (London) **430**, 512–513.

Zapf, V. S., R. P. Dickey, E. J. Freeman, C. Sirvent, and M. B. Maple, 2001, "Magnetic and non-Fermi-liquid properties of $U_{1-x}La_xPd_2Al_3$," Phys. Rev. B **65**, 024437.

Zhang, Jiecheng, Erik D. Kountz, Kamran Behnia, and Aharon Kapitulnik, 2019, "Thermalization and possible signatures of quantum chaos in complex crystalline materials," Proc. Natl. Acad. Sci. U.S.A. **116**, 19869–19874.

Zhang, Pengfei, 2017, "Dispersive Sachdev-Ye-Kitaev model: Band structure and quantum chaos," Phys. Rev. B **96**, 205138.

Zhang, Pengfei, 2019, "Evaporation dynamics of the Sachdev-Ye-Kitaev model," Phys. Rev. B **100**, 245104.

Zhang, Pengfei, **2021**, "More on complex Sachdev-Ye-Kitaev eternal wormholes," J. High Energy Phys. 03, 087.

Zhang, Pengfei, 2022, "Quantum entanglement in the Sachdev-Ye-Kitaev model and its generalizations," arXiv:2203.01513.

Zhang, Ya-Hui, and Subir Sachdev, 2020, "Deconfined criticality and ghost Fermi surfaces at the onset of antiferromagnetism in a metal," Phys. Rev. B **102**, 155124.

Zhao, Hengcan, *et al.*, 2019, "Quantum-critical phase from frustrated magnetism in a strongly correlated metal," Nat. Phys. **15**, 1261–1266.

Zhou, Tian-Gang, Lei Pan, Yu Chen, Pengfei Zhang, and Hui Zhai, 2021, "Disconnecting a traversable wormhole: Universal quench dynamics in random spin models," Phys. Rev. Research **3**, L022024.

Zhou, Tian-Gang, and Pengfei Zhang, 2020, "Tunneling through an eternal traversable wormhole," Phys. Rev. B **102**, 224305.

Zhu, Jian-Xin, D. R. Grempel, and Qimiao Si, 2003, "Continuous Quantum Phase Transition in a Kondo Lattice Model," Phys. Rev. Lett. **91**, 156404.

Zhu, Jian-Xin, Stefan Kirchner, Ralf Bulla, and Qimiao Si, 2007, "Zero-Temperature Magnetic Transition in an Easy-Axis Kondo Lattice Model," Phys. Rev. Lett. **99**, 227204.

Zhu, Lijun, and Qimiao Si, 2002, "Critical local-moment fluctuations in the Bose-Fermi Kondo model," Phys. Rev. B **66**, 024426.

Ziman, John M., 1960, *Electrons and Phonons: The Theory of Transport Phenomena in Solids* (Oxford University Press, New York).

Zondiner, U., *et al.*, 2020, "Cascade of phase transitions and Dirac revivals in magic-angle graphene," Nature (London) **582**, 203–208.

Zou, Liujun, and Debanjan Chowdhury, 2020, "Deconfined metallic quantum criticality: A U(2) gauge-theoretic approach," Phys. Rev. Research **2**, 023344.